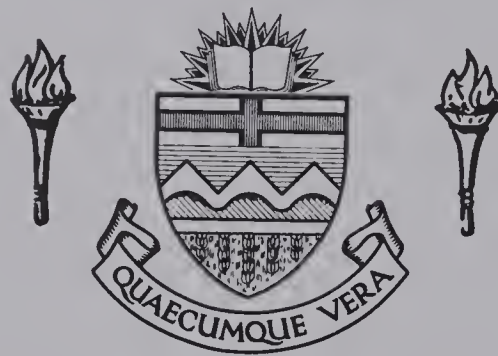


For Reference

NOT TO BE TAKEN FROM THIS ROOM

Ex libris
UNIVERSITATIS
ALBERTAENSIS



THE UNIVERSITY OF ALBERTA

SOME PROBLEMS IN NON-HOMOGENEOUS SEEPAGE

by



HARVEY GUTHER

A THESIS

SUBMITTED TO THE FACULTY OF GRADUATE STUDIES AND RESEARCH
IN PARTIAL FULFILMENT OF THE REQUIREMENTS FOR THE DEGREE OF
MASTER OF SCIENCE

DEPARTMENT OF CIVIL ENGINEERING

EDMONTON, ALBERTA

Spring, 1972

UNIVERSITY OF ALBERTA
FACULTY OF GRADUATE STUDIES AND RESEARCH

The undersigned certify that they have read, and recommend to the Faculty of Graduate Studies and Research for acceptance, a thesis entitled SOME PROBLEMS IN NON-HOMOGENEOUS SEEPAGE submitted by Harvey Guther in partial fulfilment of the requirements for the degree of Master of Science.

ABSTRACT

This thesis deals with two closely related aspects of the study of non-homogeneous seepage. Part I undertakes the calculation of pressure distributions using the finite element method and Part II describes attempts to measure water pressures with a new piezometer system.

In Part I a technique is developed and utilized which takes into account the effects of stress dependant permeability in a rock material upon the pressure distribution in unconfined flow situations. Finite element seepage theory is reviewed and the finite element seepage method is coupled with the finite element elastic stress analysis to perform the subsequent computations. A study of permeability measurements has been undertaken and a function relating permeability to stress has been derived. This function is used in the analyses.

A configuration of a steep-walled excavation is studied with variations in initial stress conditions and permeability functions. Equipotential plots, selected contours of isotropic permeability and contours of average principal effective stress are presented and discussed. The factors that affect the pressure distributions are noted.

Part II deals with the field installation of the University of Alberta multistage piezometer system in the Upper Cretaceous Edmonton Formation. Installation and

measurement procedures are discussed. Perched water tables are shown to exist. Recommendations and conclusions are formed.

ACKNOWLEDGMENTS

The author wishes to thank Dr. N.R. Morgenstern for his assistance, guidance and encouragement throughout the course of the study.

The helpful insights provided by Dr. Z. Eisenstein, Dr. D.W. Murray and other staff during the study have been fully appreciated.

The financial aid provided by the National Research Council of Canada is gratefully acknowledged.

The help of O. Wood and company with part of the fieldwork has been appreciated.

Thanks are extended to L. Stahl who typed the thesis and G. Ciere who drafted the figures.

The author has appreciated his colleagues in the Department of Civil Engineering who were always ready to help.

The author also wishes to include thanks to his Father who in the past has instilled in the author patience and perseverance.

TABLE OF CONTENTS

	Page
Title Page	i
Approval Sheet	ii
Abstract	iii
Acknowledgments	v
Table of Contents	vi
List of Figures	viii
Chapter	
I INTRODUCTION	1
1.1 General	1
1.2 The nature of non-homogeneous flow in the field	1
1.3 Statement of the problems	4
PART ONE	
II ANALYSIS	8
2.1 Introduction	8
2.2 Derivation of the seepage equation	9
2.3 Finite element formulation	11
2.4 Free surface location determination	18
2.5 Validity of the results using varying permeability	27
2.6 Method of analysis	28
III RELATION BETWEEN PERMEABILITY AND STRESS	40
3.1 General	40
3.2 Development of a relation between permeability and stress	41
3.3 Stress dependent permeability data	47

3.4	Sensitivity of permeability to stress	55
3.5	Limitations	73
IV	RESULTS	76
4.1	Description of cases analyzed	76
4.2	Computational procedures	80
4.3	Results of analyses	83
V	DISCUSSION AND CONCLUSIONS	102
5.1	Discussion	102
5.2	Conclusions	112
PART TWO		
VI	THE UNIVERSITY OF ALBERTA MULTISTAGE DOUBLE PACKER TRANSDUCER PIEZOMETER	114
6.1	Introduction	114
6.2	Description of the University of Alberta multistage piezometer system	123
VII	FIELD INVESTIGATION	129
7.1	Location of installation	129
7.2	Field procedures	130
7.3	Readings obtained	142
VIII	DISCUSSION AND CONCLUSIONS	153
8.1	Discussion	153
8.2	Conclusions	167
LIST OF REFERENCES		170
APPENDIX A:	Body force and stress release equations .	A1
APPENDIX B:	Computer program	B1
APPENDIX C:	Plot program listing	C1
APPENDIX D:	Details of piezometer parts	D1

LIST OF FIGURES

Figure		Page
2.1	Local and global co-ordinate systems	12
2.2	The seepage element	14
2.3	Free surface node correction procedure	20
2.4	Finite element comparison with closed form solution	22
2.5	Effects of poor element shape	25
2.6	Modification of grid configuration to prevent ill-conditioning of the finite element equations	26
2.7	Superposition of stress states for solution ...	31
2.8	Boundary pressures on element	32
2.9	Method for internal phreatic boundary	35
2.10	Internal phreatic boundary for one case of the model studied	36
2.11	Schematic presentation of solution	38
2.12	Flow diagram	39
3.1	Relation between joint parameters and permeability	43
3.2	Crack behaviour according to $b = A' / (J_1 + T)^M$..	46
3.3	Variation in permeability with stress	48
3.4	Permeability of coal	49
3.5	Decrease in coefficient of permeability of granites and gneisses with depth	50
3.6	Patching's curve no. 99 fitted to equation (3.7)	53
3.7	Field permeability data fitted to equation (3.7)	56
3.8	Field permeability data fitted to equation (3.7)	57
3.9	Field permeability data fitted to equation (3.7)	58
3.10	Field permeability data fitted to equation (3.7)	59

3.11	Field permeability data fitted to equation (3.7)	60
3.12	Field permeability data fitted to equation (3.7)	61
3.13	Field permeability data fitted to equation (3.7)	62
3.14	Field permeability data fitted to equation (3.7)	63
3.15	Field permeability data fitted to equation (3.7)	64
3.16	Field permeability data fitted to equation (3.7)	65
3.17	Field permeability data fitted to equation (3.7)	66
3.18	Field permeability data fitted to equation (3.7)	67
3.19	Field permeability data fitted to equation (3.7)	68
3.20	Field permeability data fitted to equation (3.7)	69
3.21	Comparison of permeability relations	70
3.22	Summary plot of T and N values	71
3.23	Correspondence for different pairs of T and N values	72
3.24	Effect of shear on permeability	75
4.1	Grid and dimensions used for analyses	78
4.2	Equipotentials in a homogeneous medium	84
4.3a	Equipotentials, $T = 40$ psi, $N = 2.0$, $K_O = 0.5$.	85
4.3b	Contours of isotropic permeability, $T = 40$ psi, $N = 2.0$, $K_O = 0.5$	86
4.3c	Contours of average principal effective stress, $T = 40$ psi, $N = 2.0$, $K_O = 0.5$	87
4.4a	Equipotentials, $T = 40$ psi, $N = 2.0$, $K_O = 2.0$.	88
4.4b	Contours of isotropic permeability, $T = 40$ psi, $N = 2.0$, $K_O = 2.0$	89
4.4c	Contours of average principal effective stress, $T = 40$ psi, $N = 2.0$, $K_O = 2.0$	90
4.5a	Equipotentials, $T = 20$ psi, $N = 3.0$, $K_O = 0.5$..	91
4.5b	Contours of isotropic permeability, $T = 20$ psi, $N = 3.0$, $K_O = 0.5$	92

4.5c	Contours of average principal effective stress, T = 20 psi, N = 3.0, $K_O = 0.5$	93
4.6a	Equipotentials, T = 20 psi, N = 3.0, $K_O = 2.0$..	94
4.6b	Contours of isotropic permeability, T = 20 psi, N = 3.0, $K_O = 2.0$	95
4.6c	Contours of average principal effective stress, T = 20 psi, N = 3.0, $K_O = 2.0$	96
4.7	Comparison of free surface locations	97
5.1	Mechanisms which influence the free surface location	104
5.2	Climatic-induced changes in the configuration of the water table	106
5.3	Proposed characteristic relationship between free surface exit height and slope height	108
6.1	Borehole piezometer and response characteristics	119
6.2	UA-GSC piezometer and response characteristics	121
6.3	Continuous borehole piezometer and response characteristics	122
6.4	Assembly drawing of the University of Alberta double packer transducer piezometer	124
6.5	Section showing typical installation	126
6.6	Hypothetical situation to illustrate the desired effects of bentonitic drilling mud	128
7.1	Location of installation superimposed on study area of Thomson (1970)	131
7.2	Section through location for installation	132
7.3	Borehole log, seal and well point locations	134
7.4	Pumping system utilized	137
7.5	Water-cement ratio related to specific gravity of cement grout	140
7.6	Transducer calibration	146
7.7	Response at well point no. 1	147
7.8	Response at well point no. 2	148

7.9	Response at well point no. 3	149
7.10	Response at well point no. 4	150
8.1	Proposed modified grouting system	156
8.2	Volume factor of double packer piezometer	158
8.3	Possible pressure distributions in slope	165
8.4	Piezometer arrangement using irrecoverable transducers	168

CHAPTER I

INTRODUCTION

1.1 General

The solution of non-homogeneous seepage problems is of concern in many circumstances. The prediction of flow quantities or pressure magnitudes is an important consideration in geotechnical, water resource and irrigation engineering. Due to the many combinations and variations that occur in the permeabilities of non-homogeneous media, a great diversity of flow regimes exist.

In soil and rock mechanics the knowledge of induced or natural groundwater conditions is of paramount consequence in stability analyses. A familiarity with the factors which influence these conditions is then necessary in order to properly evaluate the most critical conditions for instability to occur. The variation of permeability throughout the media is an important factor.

1.2 The Nature of Non-homogeneous Flow in the Field

In order to fully appreciate the complexities of non-homogeneous seepage problems, the overall setting in which flow takes place has to be examined. Groundwater movement can be viewed initially in the framework of the hydrological cycle that occurs in nature. It may then be

seen in the context of the topographical and geological formation of the area. With this perspective the groundwater conditions in a valley or excavation with their own unique stratigraphy and geometric configurations are more fully understood. Further complications will occur when the seepage conditions caused by draining or damming are superimposed on the "natural" flow regime.

The permeabilities of the materials in a geological formation and also on the smaller scale of an individual slope may be quite varied in terms of both non-homogeneity and anisotropy. This in turn will affect the groundwater flow characteristics of the area. Impermeable strata situated among more permeable layers often result in perched water tables. For example thin layers of bentonite of low permeability that are underlain by a draining coal seam tend to produce this condition. In other areas porous limestone resting on impermeable shale may bring about the same result. A fault in a rock slope may act as a groundwater barrier, groundwater conduit or as a subsurface drain. A slope may be comprised of a relatively homogenous rock material but irregular jointing may cause large variations in the equivalent permeabilities of the joints resulting in irregular pressure distributions in the slope. These examples coupled with a realization of the effects of regional groundwater behaviour (Toth, 1962; Freeze and Witherspoon, 1966, 1967, 1968) are sufficient to illustrate the vast differences that can occur in nature in groundwater flow.

Various workers have reported cases and situations where the consideration of non-homogeneous flow has been essential. Lyell (1969) mathematically formulates the problem where several layers drain into an open pit mine resulting from a number of perched water tables. He uses field piezometer measurements in conjunction with the analytical studies to predict future seepage patterns. With this information the effects of slope stability are evaluated. In another case, Steffen and Klingman (1966) indicate that piezometric data is invaluable for monitoring and evaluating the stability of slopes at the Nchanga open pit mine. While arriving at shear strength values in a failed slope, Eigenbrod and Morgenstern (1971) illustrate the importance of interpreting the water pressure distribution correctly at a location where several perched water tables occur. Khan (1970) attempts to show that the effects of non-uniform permeabilities aid in explaining in part the Vajont reservoir disaster. In a type of retrogressing slope failure problem, Henkel (1967) has described the effect of flow in non-homogeneous deposits and shows how under certain conditions degradation of the slope occurs due to its non-homogeneity.

Generally the effects of foundation permeability variations are an essential consideration in dam design. One case where these variations were assumed to be relatively inconsequential illustrates dramatically the importance of non-homogeneous flow. In the Malpasset dam failure (Bernaix,

1969), the effect of confining stresses imposed by the structure on the rock foundation material caused greater permeability variations than anticipated with the result that unexpected critical seepage gradients led to the catastrophe.

These examples should suffice to show the importance of predicting as well as measuring the seepage behaviour in non-homogeneous media. For a more complete and integrated understanding of non-homogeneous flow it is evident that both analysis and instrumentation will continue to play an important role in the future.

1.3 Statement of the Problems

Recently seepage and groundwater studies have received renewed interest since the digital computer has facilitated problem solving. Until recently seepage analyses of non-homogeneous media have been difficult to handle. Various attempts using theoretical, experimental and analogue methods have usually resulted in cumbersome and inflexible means of solution.

Computer applications using finite element and finite difference numerical procedures may be used in the treatment of non-homogeneous seepage problems (Zienkiewicz and Cheung, 1965; Tomlin, 1965). Finite element methods have proved to be the most flexible of these numerical analyses and it is with this method that unconfined flow problems have also been solved. Early finite element

seepage programs did not include the solution of these problems due to the boundary conditions that are present at the free surface, i.e., the velocity normal to the free surface $v_n = 0$, and the pressure at the free surface, $P = 0$. Various workers (Taylor and Brown, 1967; Finn, 1967; Neuman and Witherspoon, 1970) have incorporated these boundary conditions in conventional seepage programs through iteration techniques using mesh and nodal movement.

With the finite element method it is also possible to solve steady state free surface flow in a medium of continuously varying isotropic or anisotropic permeabilities. One important case of the latter comes about when the permeabilities are dependent on the imposed state of stress. This may occur in rock slopes where the secondary permeability (i.e. along the cracks or joints) is the major source of water conductivity. This phenomenon of permeability changes with stress has been observed in the laboratory (e.g. Patching, 1965; Bernaix, 1969) and a permeability decrease with depth which is attributed in part to increased stress has been observed in the field (e.g. Davis and Turk, 1964; Sherman and Banks, 1970). For example, from the work of Bernaix and Patching it is known that stress changes in samples of various materials such as fissured gneisses and friable coals cause changes in permeability that may be several orders of magnitude depending on the extent of the stress changes. One of the problems of concern here was to analyze the resultant pressure distribution in an

excavation where the permeability throughout the medium was a function of the stress.

When determining the flow behaviour in a slope, it is obvious that as the degree of non-homogeneity increases, the need for adequate piezometric instrumentation also increases (e.g. Steffan and Klingman, 1966). However it is desirable to make an estimate of the groundwater conditions in the most economical and efficient manner. Often a multitude of measuring elevations and locations are required (e.g. Lyell, 1969) and to facilitate measurements, it is convenient to utilize a piezometer with rapid response characteristics (Penman, 1961). Electric diaphragm piezometers incorporate such a feature (Brooker et al, 1968) and the pressure measurement itself can be determined with great ease. Unfortunately drawbacks of diaphragm piezometers in general have been their lack of dependability (Lindberg, 1965) as well as the excessive costs of electrical diaphragm tips. Hence in addition to taking into account their dependability, it is desirable to decrease these costs. As a result piezometer tips have been developed which are recoverable and initially these instruments were designed to measure the pressure at one location per borehole (Lundgren, 1966). In a second task this thesis assesses the University of Alberta multistage piezometer system. This electrical diaphragm piezometer is designed to measure pressures at various pre-selected levels in a borehole. With the pressure information obtained one might also

evaluate the effects of non-homogeneity on the seepage behaviour.

PART ONE

CHAPTER II

ANALYSIS

2.1 Introduction

This chapter discusses the finite element method of analysis of problems in steady seepage and related aspects of concern. A seepage program (Taylor and Brown, 1967) is coupled with a finite element linear elastic stress program to solve for the phreatic surface and pressure distribution in a medium with stress dependent isotropic permeability. Taylor and Brown's program is used to find the seepage body forces for the stress analysis. After the body forces, calculated from the seepage distribution, have been assigned throughout the stress grid the effective stresses are computed and used to find the permeabilities. These are taken to be a function of the effective stresses in the manner described in Chapter III. The permeabilities are assigned to the proper seepage elements and the stable position of the free surface is found by iteration. This cycle of finding the body forces, stress distribution and free surface location is repeated until the difference in the stable positions of the free surface of two successive cycles indicates that convergence is obtained. The analysis is applied to seepage into an excavation as illustrated in Chapter IV.

2.2 Derivation of the Seepage Equation

The flow of water in a porous medium is caused by a hydraulic gradient, i , which may be defined as

$$i = \text{gradient } (Y + P/\gamma_w) = \text{grad } U \quad (2.1)$$

where Y = level at the point related to some datum

P = pressure at the point

γ_w = unit weight of water

U = hydraulic potential

Darcy's law states that the apparent velocity, v , is proportional to the gradient i of the hydraulic potential.

$$v = -ki = -k \text{ grad } U \quad (2.2)$$

If the anisotropic nature of the medium is considered in two dimensions the constant of proportionality known as the permeability, k , is given by a matrix of values and may be written as,

$$\begin{bmatrix} k \end{bmatrix} = \begin{bmatrix} k_{xx} & k_{xy} \\ k_{yx} & k_{yy} \end{bmatrix} \quad (2.3)$$

and therefore the velocity v is a vector given by

$$\begin{Bmatrix} v_x \\ v_y \end{Bmatrix} = - \begin{bmatrix} k_{xx} & k_{xy} \\ k_{yx} & k_{yy} \end{bmatrix} \begin{Bmatrix} \frac{\partial U}{\partial x} \\ \frac{\partial U}{\partial y} \end{Bmatrix} \quad (2.4)$$

If x and y are the principal directions of anisotropy and k_x and k_y are the principal values of permeability, the velocities may be expressed as

$$v_x = k_x \frac{\partial U}{\partial x} \quad (2.5a)$$

$$v_y = k_y \frac{\partial U}{\partial y} \quad (2.5b)$$

Imposing the condition of continuity upon a unit volume and assuming an incompressible fluid, the following is obtained.

$$\frac{\partial v_x}{\partial x} + \frac{\partial v_y}{\partial y} = 0 \quad (2.6)$$

From (2.5) this becomes,

$$\frac{\partial}{\partial x} \left(k_x \frac{\partial U}{\partial x} \right) + \frac{\partial}{\partial y} \left(k_y \frac{\partial U}{\partial y} \right) = 0 \quad (2.7)$$

In this work,

$$k = k_x = k_y = k(x, y) \quad (2.8)$$

and hence equation (2.7) becomes,

$$\frac{\partial k}{\partial x} \frac{\partial U}{\partial x} + \frac{\partial k}{\partial y} \frac{\partial U}{\partial y} + k \frac{\partial^2 U}{\partial x^2} + k \frac{\partial^2 U}{\partial y^2} = 0 \quad (2.9)$$

2.3 Finite Element Formulation

Even though isotropic permeabilities are used in this work, anisotropy will be considered in the following formulation of the finite element analysis.

A permeability matrix in the x-y global system is defined in terms of the permeabilities which are usually determined parallel and perpendicular to the principal axis of permeability. The axes may be at an angle θ to the global x axis as shown in Figure 2.1.

Quantities in the local co-ordinate system are primed.

From equations (2.5), velocities in the local system may be expressed as

$$\begin{Bmatrix} v_{x'} \\ v_{y'} \end{Bmatrix} = \begin{bmatrix} k_{x'} & 0 \\ 0 & k_{y'} \end{bmatrix} \begin{Bmatrix} \frac{\partial U}{\partial x'} \\ \frac{\partial U}{\partial y'} \end{Bmatrix} = [k'] \begin{Bmatrix} \frac{\partial U}{\partial x'} \\ \frac{\partial U}{\partial y'} \end{Bmatrix} \quad (2.10)$$

It can easily be shown that

$$\begin{Bmatrix} v_x \\ v_y \end{Bmatrix} = \begin{bmatrix} \cos\theta & -\sin\theta \\ \sin\theta & \cos\theta \end{bmatrix} \begin{Bmatrix} v_{x'} \\ v_{y'} \end{Bmatrix} = [T_1] \begin{Bmatrix} v_{x'} \\ v_{y'} \end{Bmatrix} \quad (2.11)$$

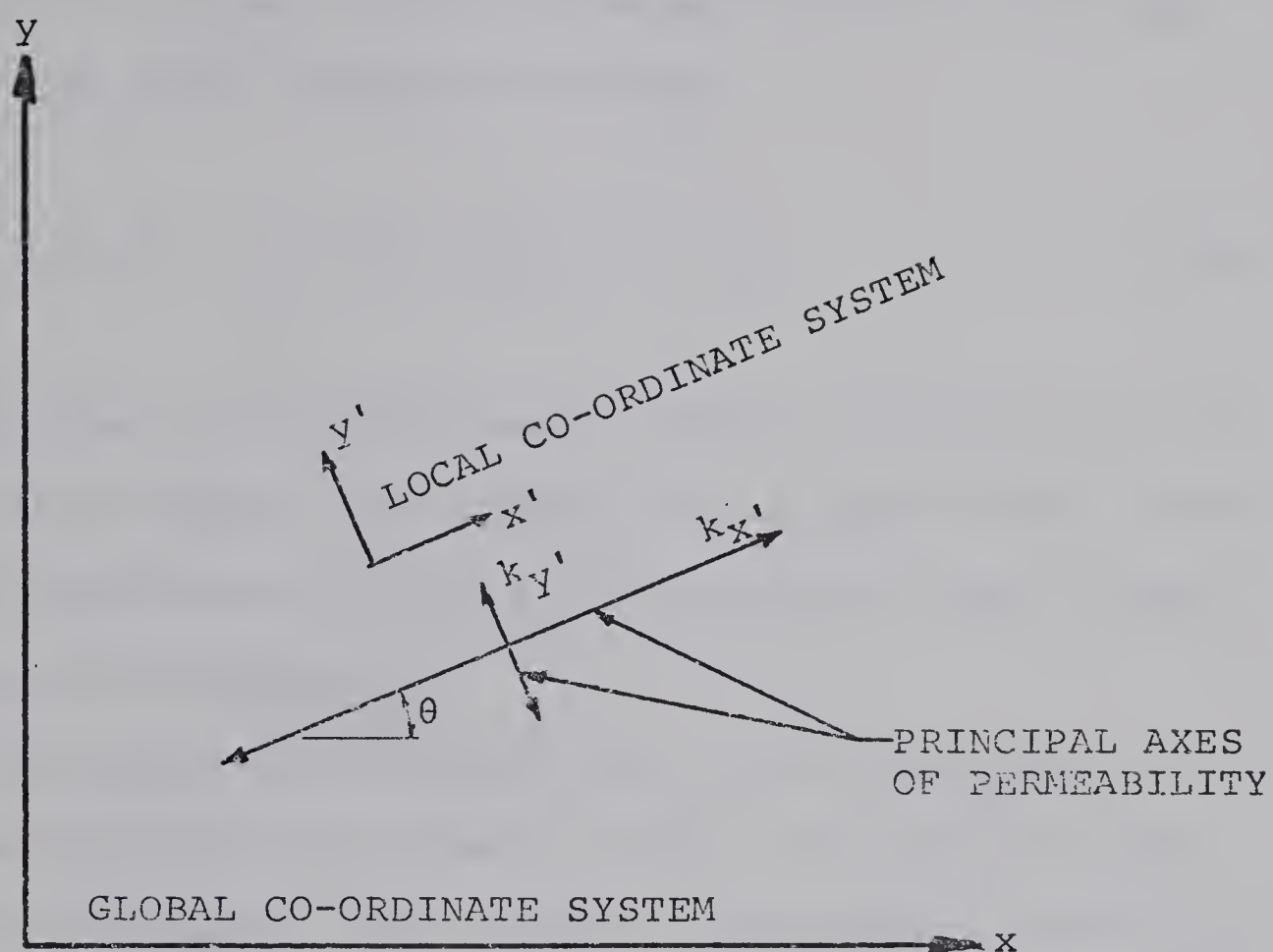


FIG. 2.1. LOCAL AND GLOBAL CO-ORDINATE SYSTEMS

and

$$\begin{Bmatrix} \frac{\partial U}{\partial x'} \\ \frac{\partial U}{\partial y'} \end{Bmatrix} = \begin{bmatrix} \cos\theta & \sin\theta \\ -\sin\theta & \cos\theta \end{bmatrix} \cdot \begin{Bmatrix} \frac{\partial U}{\partial x} \\ \frac{\partial U}{\partial y} \end{Bmatrix} = [T_2] \begin{Bmatrix} \frac{\partial U}{\partial x} \\ \frac{\partial U}{\partial y} \end{Bmatrix} \quad (2.12)$$

From these equations and equation (2.4) the permeability matrix in the global system may be related to the values in the local system as follows.

$$[k] = [T_1] [k'] [T_2] \quad (2.13)$$

To use the finite element method the properties of an individual element have firstly to be established. The following derivation will be for the element known as the constant velocity triangle.

The simplest assumption for the distribution of pressures P across the element in Fig. 2.2a is that they vary linearly between the vertices (Zienkiewicz and Cheung, 1965; Zienkiewicz, Mayer and Cheung, 1966). Hence the pressure \tilde{P} at any location throughout the triangle will be given by

$$\tilde{P} = \alpha_1 + \alpha_2 x + \alpha_3 y \quad (2.14a)$$

or

$$\tilde{P} = \begin{bmatrix} 1 & x & y \end{bmatrix} \begin{Bmatrix} \alpha_1 \\ \alpha_2 \\ \alpha_3 \end{Bmatrix} \quad (2.14b)$$

The three unknowns in equation (2.14) may be

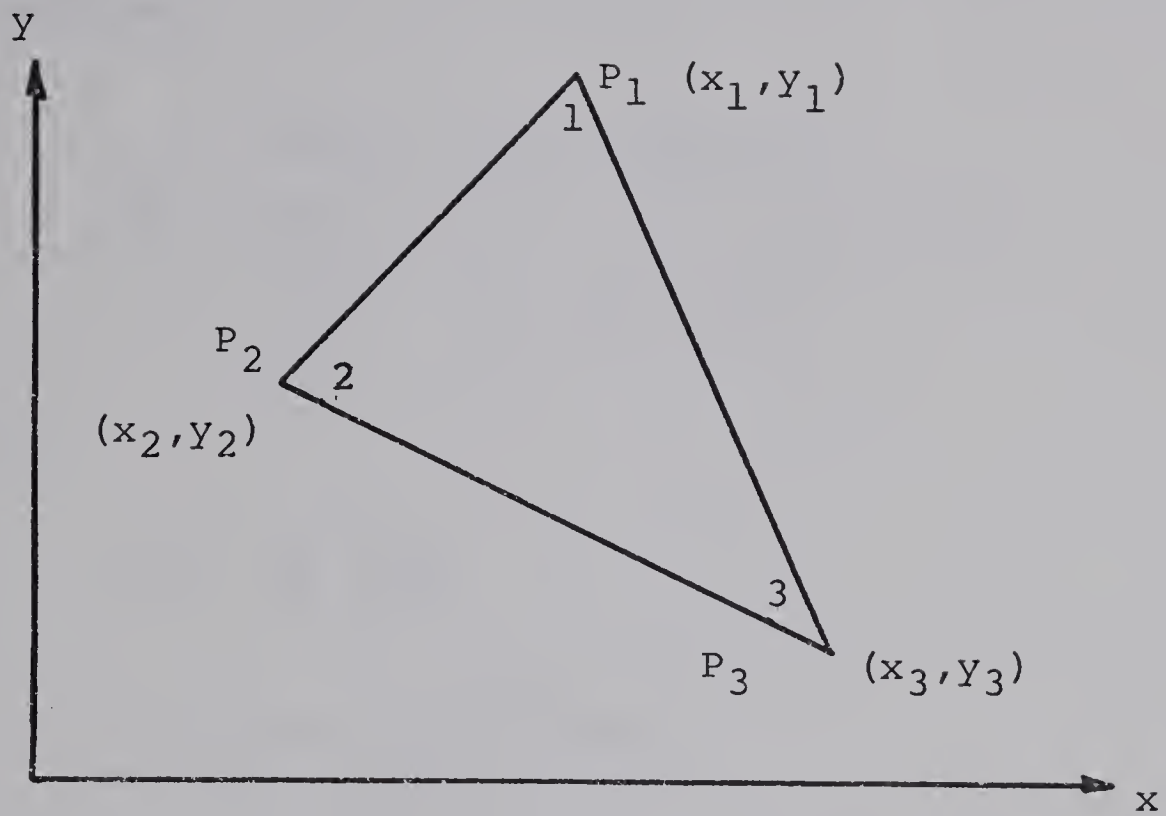


FIG. 2.2a. ELEMENT PRESSURES

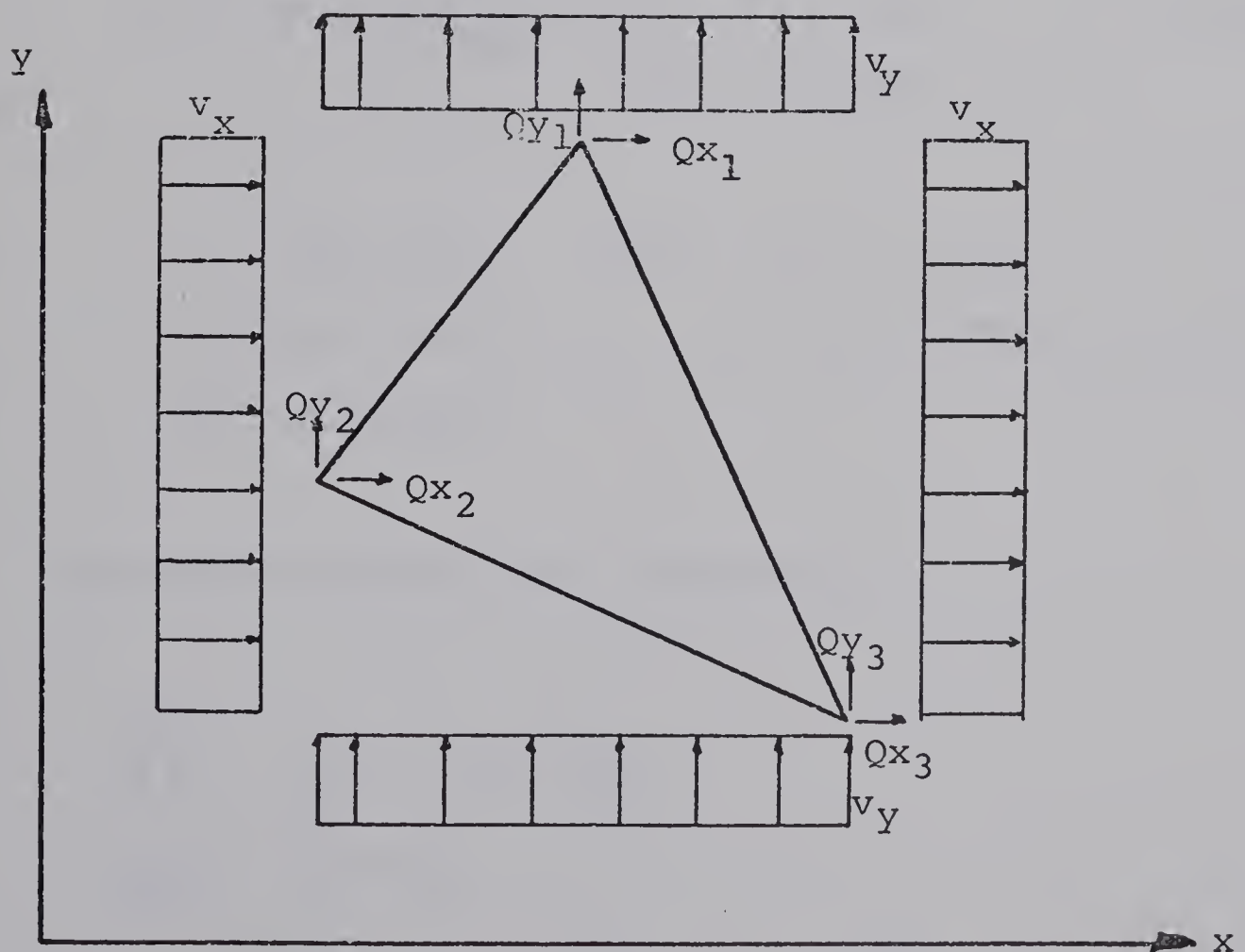


FIG. 2.2b. ELEMENT FLOWS

FIG. 2.2 THE SEEPAGE ELEMENT

evaluated by forming equations in α_1 , α_2 and α_3 at the three vertices

$$\begin{Bmatrix} P \\ P \\ P \end{Bmatrix} = \begin{Bmatrix} P_1 \\ P_2 \\ P_3 \end{Bmatrix} = \begin{bmatrix} 1 & x_1 & y_1 \\ 1 & x_2 & y_2 \\ 1 & x_3 & y_3 \end{bmatrix} \begin{Bmatrix} \alpha_1 \\ \alpha_2 \\ \alpha_3 \end{Bmatrix} = [A] \{\alpha\} \quad (2.15)$$

Therefore

$$\{\alpha\} = [A^{-1}] \{P\} \quad (2.16)$$

and
$$\tilde{P} = [1 \ x \ y] [A^{-1}] \{P\} \quad (2.17)$$

where

$$[A^{-1}] = \frac{1}{t_1 + t_2 + t_3} \begin{bmatrix} t_1 & t_2 & t_3 \\ y_{23} & y_{31} & y_{12} \\ x_{32} & x_{13} & x_{21} \end{bmatrix} \quad (2.18)$$

with
$$\begin{aligned} t_1 &= x_2 y_3 - x_3 y_2 & \text{and} & & x_{ij} &= x_i - x_j \\ t_2 &= y_1 x_3 - x_1 y_3 & & & y_{ij} &= y_i - y_j \\ t_3 &= x_1 y_2 - x_2 y_1 \end{aligned}$$

Pressure gradients are obtained as

$$\begin{aligned} \begin{Bmatrix} \frac{\partial \tilde{P}}{\partial x} \\ \frac{\partial \tilde{P}}{\partial y} \end{Bmatrix} &= \begin{bmatrix} 0 & 1 & 0 \\ 0 & 0 & 1 \end{bmatrix} [A^{-1}] \{P\} \\ &= \frac{1}{t_1 + t_2 + t_3} \begin{bmatrix} y_{23} & y_{31} & y_{12} \\ x_{32} & x_{13} & x_{21} \end{bmatrix} \{P\} \\ &= [B] \{P\} \end{aligned} \quad (2.19)$$

Using equations (2.4) and (2.19) velocities may be given as

$$\begin{aligned} \begin{Bmatrix} v_x \\ v_y \end{Bmatrix} &= \begin{bmatrix} k_{xx} & k_{xy} \\ k_{yx} & k_{yy} \end{bmatrix} \begin{Bmatrix} \frac{1}{\gamma_w} \frac{\partial \tilde{P}}{\partial x} + \frac{\partial Y}{\partial x} \\ \frac{1}{\gamma_w} \frac{\partial \tilde{P}}{\partial y} + \frac{\partial Y}{\partial y} \end{Bmatrix} \\ &= \begin{bmatrix} k \end{bmatrix} \begin{bmatrix} B \end{bmatrix} \{P\} + \begin{bmatrix} k \end{bmatrix} \left\{ \frac{\partial Y}{\partial s} \right\} \end{aligned} \quad (2.20)$$

where $\frac{\partial Y}{\partial s} = \begin{Bmatrix} 0 \\ 1 \end{Bmatrix}$
and P will have units of length

Equivalent nodal point flows may be written for each element. Then continuity of flow at node N requires that

$$\sum_{i=1}^{\ell} Q_N^i = 0 \quad (2.21)$$

where ℓ is the number of elements connected to node N

From Fig. 2.2b the horizontal flow Q_x and vertical flow Q_y for node i may be written as

$$Q_{xi} = \frac{v_x}{2} y_{jk} \quad (2.22a)$$

$$Q_{yi} = \frac{v_y}{2} x_{kj} \quad (2.22b)$$

Hence the nodal flows may be related to the velocities by

$$\{Q\} = [L]\{v\} \quad (2.23)$$

where

$$[L] = \frac{1}{2} \begin{bmatrix} y_{23} & x_{32} \\ y_{31} & x_{13} \\ y_{12} & x_{21} \end{bmatrix} \quad (2.24)$$

Using equation (2.20), (2.23) becomes

$$\{Q\} = [L][k][B]\{P\} + [L][k]\left\{\frac{\partial Y}{\partial S}\right\} \quad (2.25)$$

Equation (2.25) is used in forming equation (2.21). Computing equation (2.21) requires solving a set of simultaneous equations in terms of P_N . The nodes where the pressures are specified will have to be modified to give the known pressure as the solution. Equation (2.9) is the equation of steady state flow which is solved for the two dimensional case assuming certain boundary conditions by equation (2.21) through the assignment of the appropriate permeability to each discrete element. Equation (2.21) has been derived considering an assembly of elements while

equation (2.9) was obtained assuming a continuum. Both have been deduced by giving heed to continuity and Darcy's law.

The program of Taylor and Brown can use either triangles or quadrilaterals. When quadrilateral elements are used they are divided into four triangular elements by two diagonals. A provision is included for generation of quadrilateral elements. Additional details for the use of the program are given by Kealy and Busch (1970).

A similar derivation corresponding to the one presented above may be given for the stress analysis. Instead of pressures at the nodes displacements are used in the displacement formulation. Since displacement is a vector quantity with two components for a two dimensional analysis, the matrices are expanded but the same procedure may be followed as outlined here. Holand and Bell (1970) give details of the method.

2.4 Free Surface Location Determination

The free surface is located where the flow, v_n normal to the surface is zero and the pressure, P , at the surface is atmospheric. Due to the number of equations involved either v_n can be set to zero or P can be set to zero. The program of Taylor and Brown sets $v_n = 0$ and iterates so that $P \rightarrow 0$.

During an iteration the solution of the finite element equations yields positive or negative pressures,

P, at the free surface nodes. In the program a location correction for any free surface node M is made according to the equation

$$dx = BETA \times P \times \cos\theta/\gamma_w \quad (2.26a)$$

$$dy = BETA \times P \times \sin\theta/\gamma_w \quad (2.26b)$$

where dx and dy are the correction components,

BETA is a factor to prevent instability of the iteration procedure, and

θ is the correction direction with respect to the x axis for node M.

If the nodes are corrected to where the iteration gives zero excess pressure, then the position may be overcorrected (i.e. if BETA = 1.0) and instability may occur. To prevent this a value of BETA < 1 is assigned. Generally a value of 0.85 to 0.90 is used. Fig. 2.3 demonstrates the procedure.

The program calculates the square root of the sum of the squares of the x and y correction components for n free surface nodes and compares this to the input tolerance value TOL. If

$$TOL > \sqrt{dx_1^2 + dy_1^2 + dx_2^2 + dy_2^2 + \dots + dx_n^2 + dy_n^2} \quad (2.27)$$

the iteration process is stopped. A tolerance of 0.1% of the net head may be used. In general if the free surface is converging properly a tolerance of 0.01% will produce negligible difference in the final result compared to a

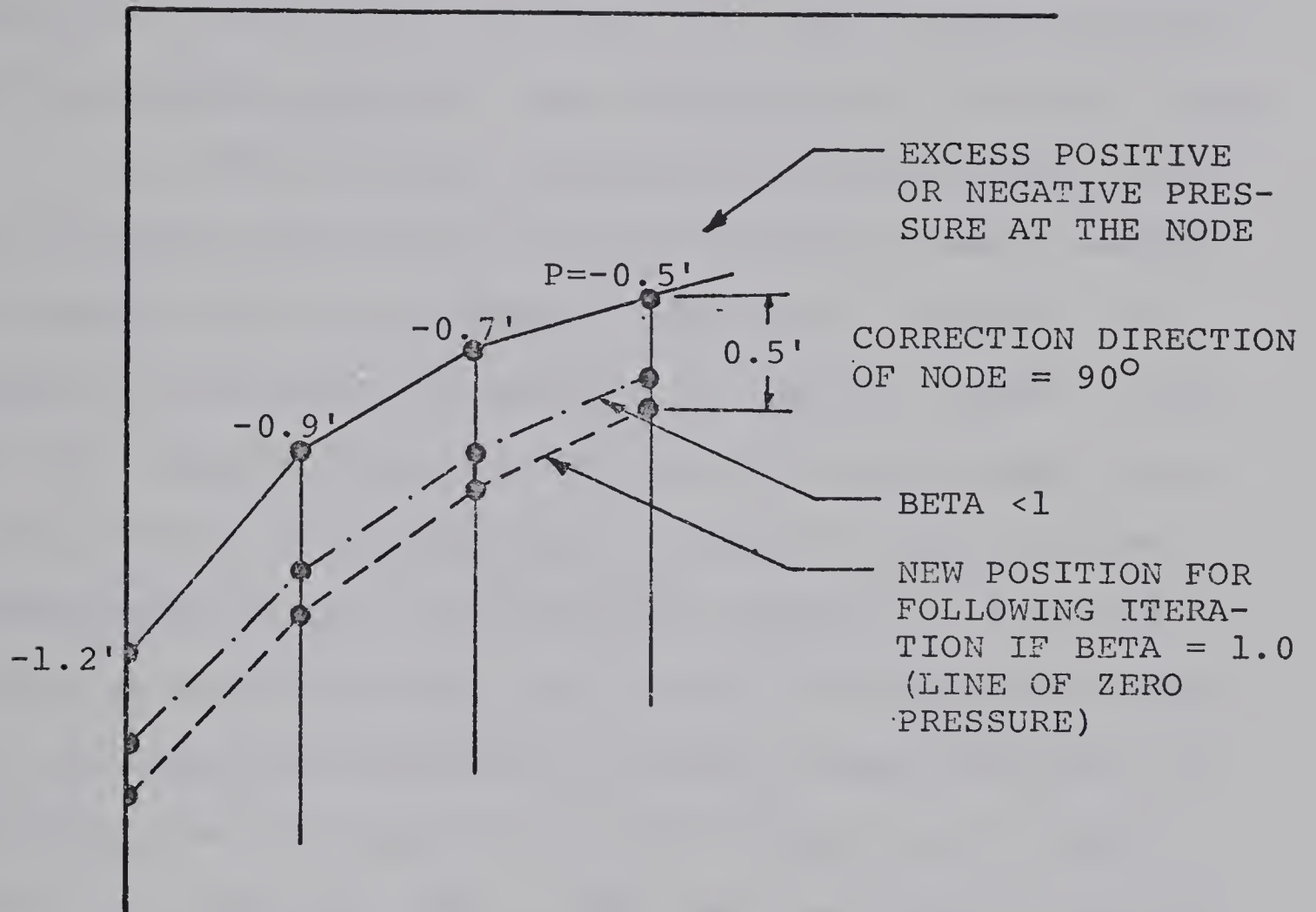


FIG. 2.3 FREE SURFACE NODE CORRECTION PROCEDURE

tolerance in the order of 0.1%.

The program generates nodal points by spacing them evenly on a straight line between any two consecutive input nodes with a nodal number difference greater than one. After adjustment of the free surface nodes the intermediate points are regenerated and hence the nodes between the free surface and the adjacent input nodes will be "strung" along.

In order to gain confidence in the procedure it is best that the discretization of the finite element method be checked with a closed form free surface solution. A closed form solution as computed by Günther (Muskat, 1946) for the phreatic line of a configuration that might occur in the core of a rockfill dam is shown as a dotted line superimposed on the finite element solution in Fig. 2.4. It may be seen that there is a close correspondence between the two solutions although the finite element solution is slightly lower for most of the free surface and slightly above it at the exit face. When the free surface location of a 30° slope was checked with the finite difference solution of Khan (1971) the same sort of behaviour occurred but the discrepancy for some parts of the free surface appeared slightly larger in terms of percentage of free surface height from the base. However, Khan's comparison with the free surface solution of Numerov (Harr, 1962) shows the finite difference solution to be somewhat higher. A close approximation to the solution at the face in Fig. 2.4 is difficult since the free surface approaches it tangentially

FINITE ELEMENT
COMPARISON WITH CLOSED FORM SOLUTION

-----GÜNTHER'S CLOSED FORM SOLUTION

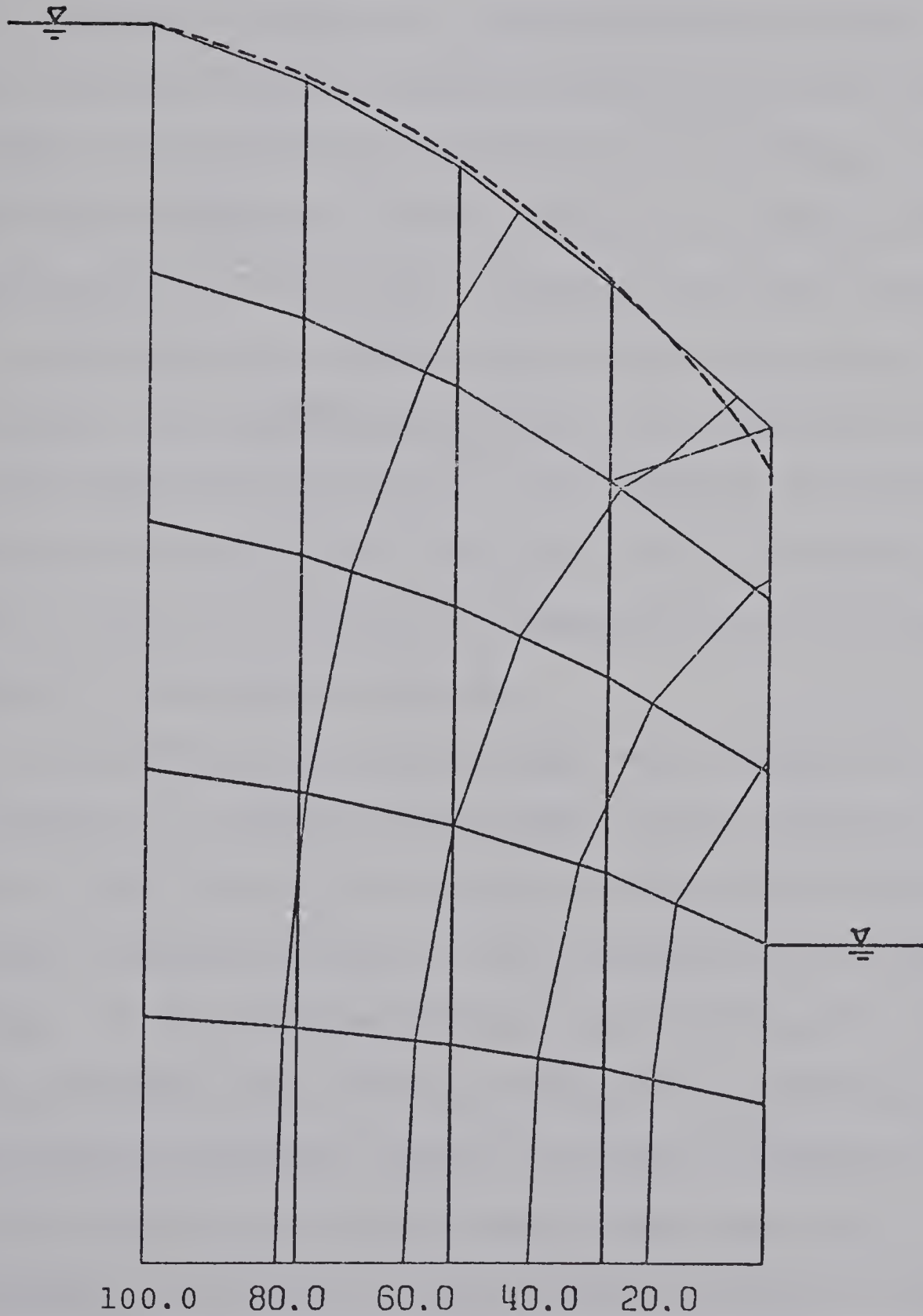


FIG. 2.4

(Casagrande, 1940). Also, Taylor and Brown (1967) state, "An ambiguity . . . must exist where the free surface intersects the geometric boundary of the body because the nodal flow at this point cannot be zero. This difficulty is minimized by reducing the mesh size adjacent to this point." In some cases a closer approximation may be obtained by taking a greater frequency of elements near the face. However this may create a second problem if in the final grid shape an abundance of thin elongate odd shaped triangular or quadrilateral elements occur. This will usually result in ill-conditioning of the finite element equations causing a lack of convergence or giving the improper location of the free surface. The second problem may be rectified by estimating the final position of the free surface and designing a grid with both triangular and quadrilateral elements if required so that the final grid configuration will contain a minimum of odd shaped elements.

Ill-conditioning occurs when small changes in the coefficients of a linear system cause large changes in the solution. Small errors will occur in the banded flow matrix during its solution because of the accumulation of round-off error. It was discovered that ill-conditioning occurred in these problems when certain triangular or quadrilateral element shapes caused one term on the main diagonal of the banded flow matrix to be much smaller than the rest. Unfortunately an attempt at using double precision computation resulted in no apparent improvement. Conte (1965) discusses

the phenomena of ill-conditioning of linear systems and may be consulted for a fuller treatment of the subject.

The results of poor element shape has been noted in the work of Kealy and Busch (1971) and Neuman and Witherspoon (1970). This is illustrated in Figure 2.5a and 2.5b. Neuman and Witherspoon compare the results of their more rapidly converging finite element solution with the results of Taylor and Brown's and attribute the divergence to an inconsistent method of nodal shifting and fail to indicate that a judicious choice of element configuration will not cause divergence.

The author had problems similar to these mentioned here. The pressure at the second free surface node from the face would not tend to zero giving the sort of effect shown in Fig. 2.5a. It was found that the ratio of the smallest to the largest term of the odd shaped element flow matrices was in the order of $1/200$ when this occurred. When the element shapes were modified in this region as shown in Fig. 2.6 this ratio was decreased to the order of $1/20$ and the pressure at the second node tended to zero accordingly. The author feels that the effect of element shape should be investigated more fully on a methodical basis. It might also be advantageous to probe the possibility of modifying the solution procedure of the banded flow matrix so that ill-conditioning of the finite element equations will be minimized.

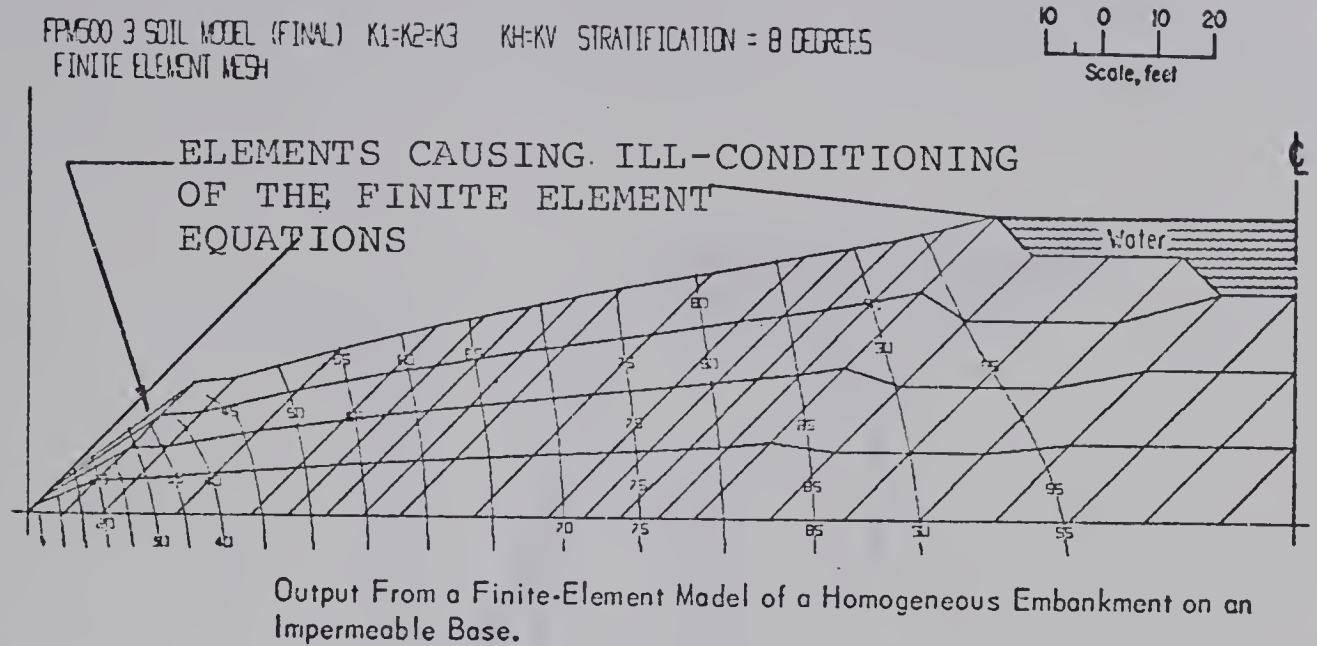


FIG. 2.5a ODD SHAPED ELEMENTS IN THE WORK OF KEALY AND BUSCH (1971)

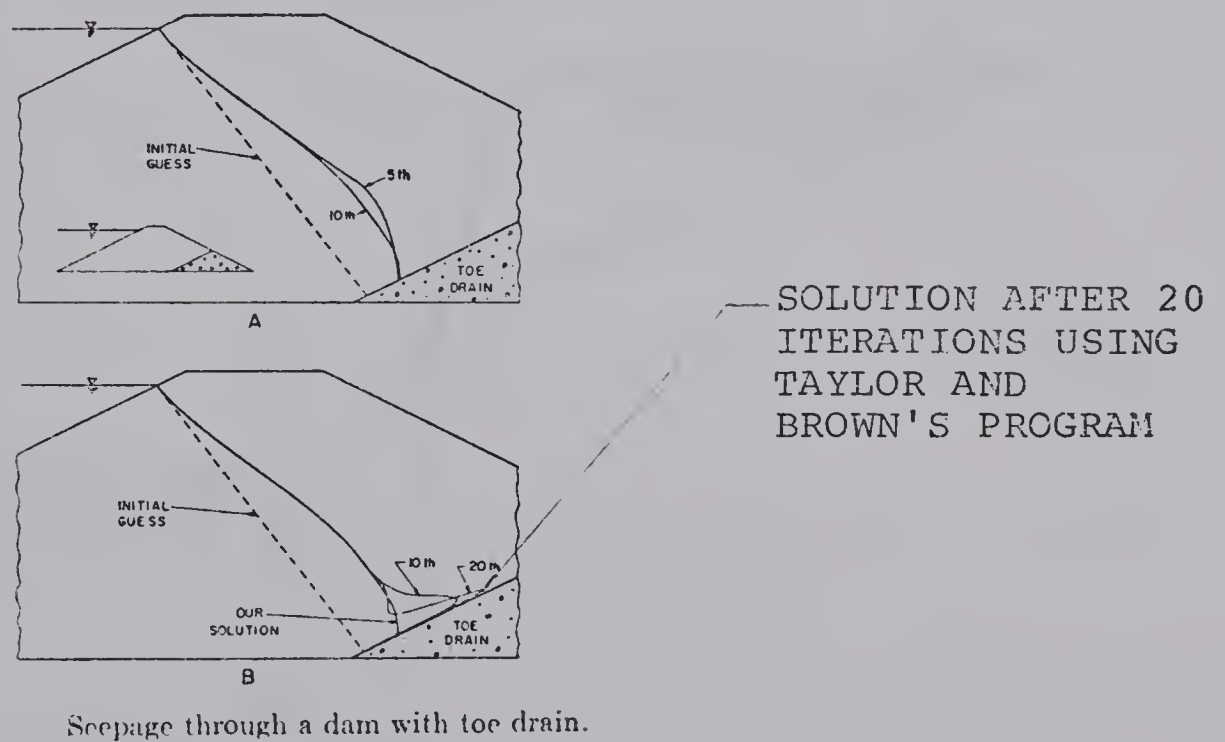


FIG. 2.5b ILLUSTRATION BY NEUMAN AND WITHERSPOON (1970) OF TAYLOR AND BROWN'S DIVERGING SOLUTION

FIG. 2.5 EFFECTS OF POOR ELEMENT SHAPE

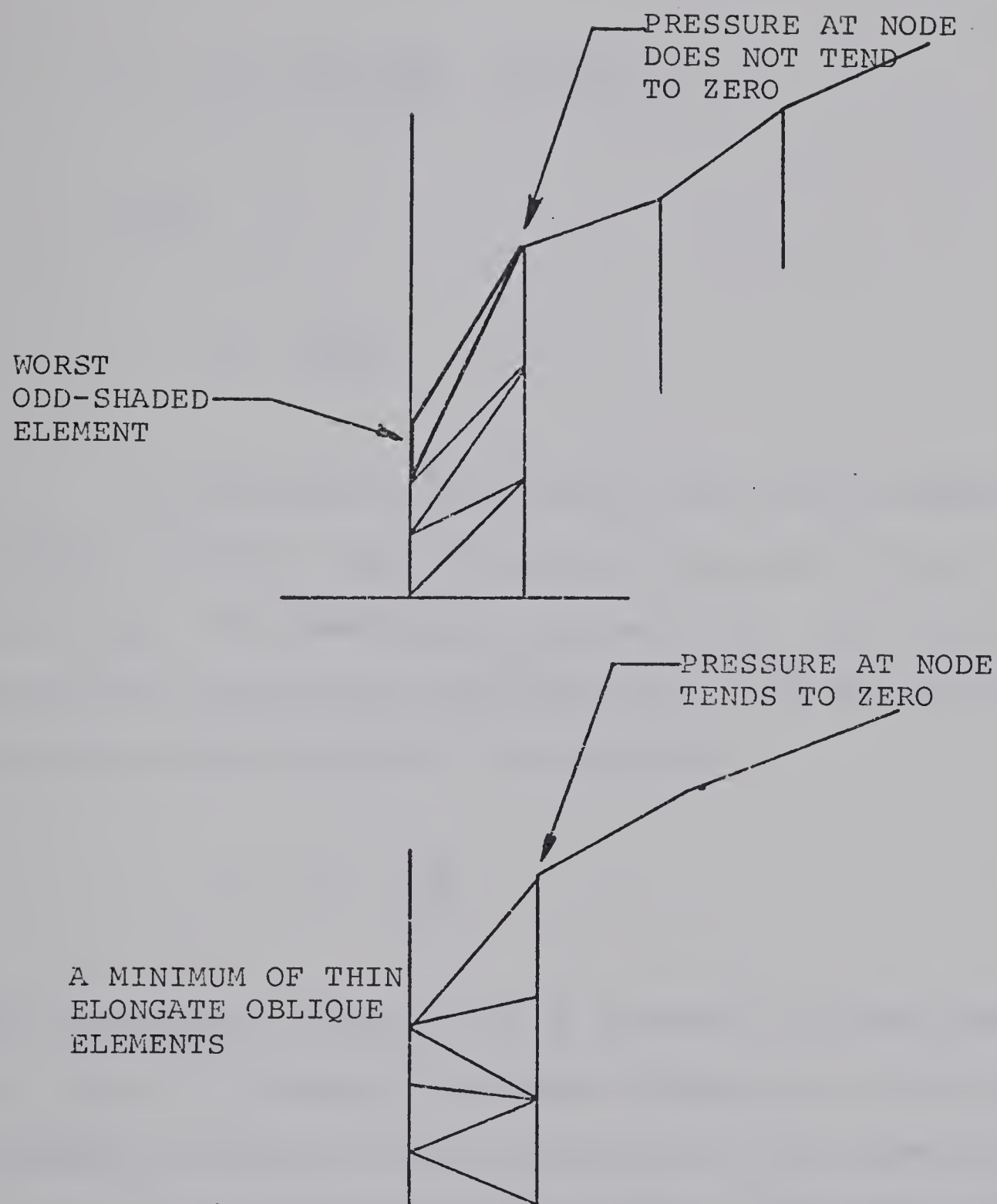


FIG. 2.6 MODIFICATION OF GRID CONFIGURATION TO PREVENT ILL-CONDITIONING OF THE FINITE ELEMENT EQUATIONS

2.5 Validity of the Results Using Varying Permeability

For the case of flow through a horizontal tube with varying permeability

$$v_x = k(x) \frac{\Delta P}{\Delta x} = \text{CONSTANT} = c \quad (2.28)$$

and

$$\Delta P = \frac{c \Delta x}{k(x)} \quad (2.29)$$

If an equal pressure drop across each element is desired $\Delta x/k(x)$ must be kept in the same ratio or $\Delta x \propto k(x)$. The smaller the permeability, the smaller Δx should be to maintain the same ratio. For the two dimensional case and assuming k is constant,

$$v = ki = k \frac{\Delta P}{\Delta s} \quad (2.30)$$

For increasing gradient and ΔP constant, Δs must decrease or $\Delta s \propto 1/i$. Hence in general element size should be reduced in areas of large gradients and low permeabilities.

For the case of flow through a tube with permeability varying linearly in the direction of flow a theoretical curve may be obtained for the pressure along the tube and compared to the result using various element sizes. However since it is difficult to evaluate a complicated two dimensional case

by extension of the results from a simple case it is best to observe the consequences with variation of element size in the actual problem.

2.6 Method of Analysis

In Chapter III a relation between the average principal stress and permeability is derived. For an excavation in plain strain the average principal effective stress may be obtained as follows:

$$\begin{aligned}\text{The first stress invariant} &= I_1 = \sigma_x + \sigma_y + \sigma_z \\ &= \sigma_I + \sigma_{II} + \sigma_{III}\end{aligned}\quad (2.31)$$

For the excavation process,

$$\begin{aligned}\Delta I_1 &= \Delta \sigma_x + \Delta \sigma_y + \Delta \sigma_z \\ &= \Delta \sigma_I + \Delta \sigma_{II} + \Delta \sigma_{III}\end{aligned}\quad (2.32)$$

The final invariant of stress,

$$\begin{aligned}I_{1f} &= I_1 + \Delta I_1 \\ &= \sigma_y + K_O \sigma_y + K_O \sigma_y + \Delta \sigma_x + \Delta \sigma_y + \Delta \sigma_z\end{aligned}\quad (2.33)$$

For plain strain

$$\sigma_z = \nu(\sigma_x + \sigma_y) \quad (2.34a)$$

and

$$\Delta \sigma_z = \nu(\Delta \sigma_x + \Delta \sigma_y) \quad (2.34b)$$

Therefore

$$I_{1f} = \sigma_y (1+2K_0) + (\Delta \sigma_x + \Delta \sigma_y) (1 + \nu) \quad (2.35)$$

The average principal effective stress will be

$$J_1 = \frac{1}{3} [\sigma_y (1+2K_0) + (\Delta \sigma_x + \Delta \sigma_y) (1 + \nu)] \quad (2.36)$$

In general for an excavation a situation as shown in Fig. 2.7a will be established. Since it was thought that the effects of stress dependent permeability would be most pronounced for a steep slope angle, it was decided to study the case of an excavation with a vertical face. The water table was chosen to be initially at the surface. This simplified the problem since this theoretically precluded a non-triangular stress release distribution on the face of the excavated slope.

Consider the following steps as shown in Fig. 2.7b-2.7e in arriving at a method of solution. Fig 2.7b shows the initial state with no excavation and the water table at the surface. The assumed insitu stress conditions are

as shown. If an excavation is made as shown in Fig. 2.7c a release of effective stresses will with a finite element program produce the correct displacements and stress changes in the slope provided that the excavation is full of water. If the water is now removed from the excavation a phreatic surface S will develop as shown in Fig. 2.7d. Considering the region above the free surface marked II and assuming the pressure to be at atmospheric above the free surface the change in body force/unit volume will be equal to the unit weight of water since the buoyant force of the water is removed from this area. In the area marked I the change in body force/unit volume will be due to the seepage force of the water. Therefore to obtain the correct change in effective stresses body forces must be considered. Then the final state of effective stress σ_f' will be given by the addition of the initial state, σ_o' the change due to stress release $\Delta\sigma_{ex}'$ and the change due to seepage $\Delta\sigma_s'$ as shown in Fig. 2.7e or

$$\sigma_f' = \sigma_o' + \Delta\sigma_{ex}' + \Delta\sigma_s' \quad (2.37)$$

The stresses induced due to seepage may be taken into account by giving heed to the water pressure distribution. Consider the triangular element shown in Fig. 2.8.

Let

\vec{u}_r = resultant vector of forces

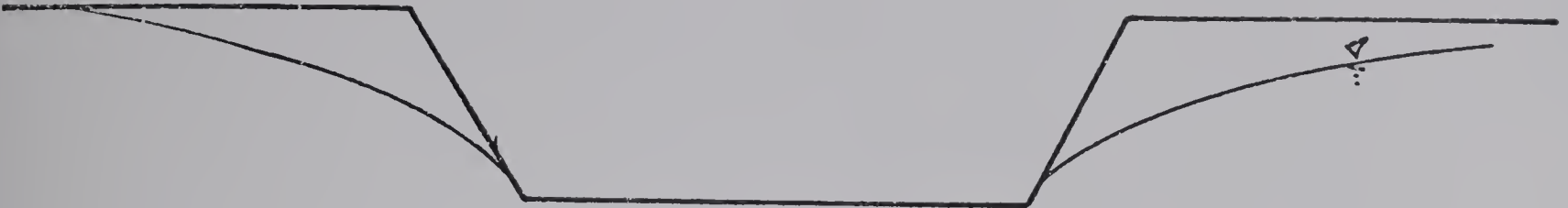


FIG. 2.7a GENERAL CASE

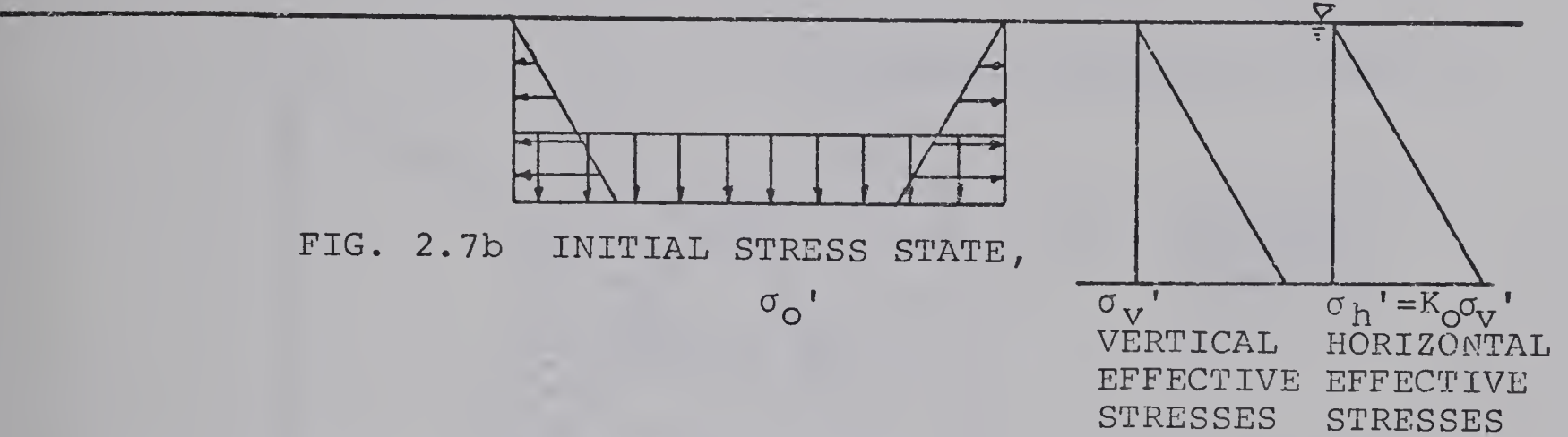


FIG. 2.7b INITIAL STRESS STATE, σ_0'

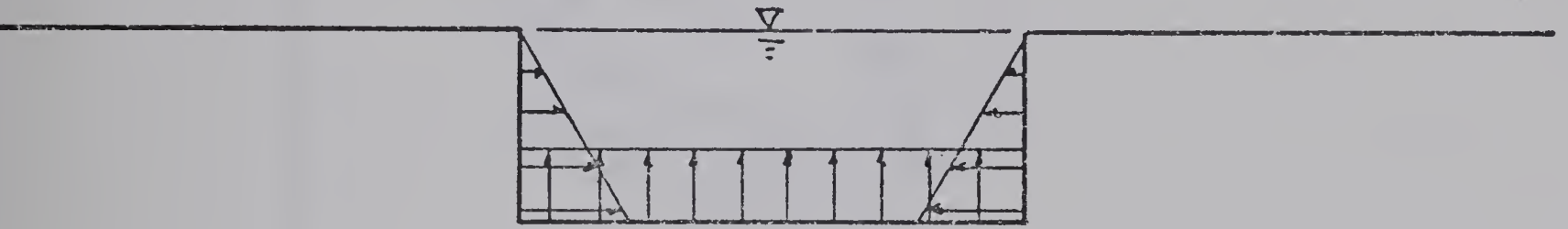


FIG. 2.7c EFFECTIVE STRESS RELEASE, $\Delta\sigma_{ex}'$

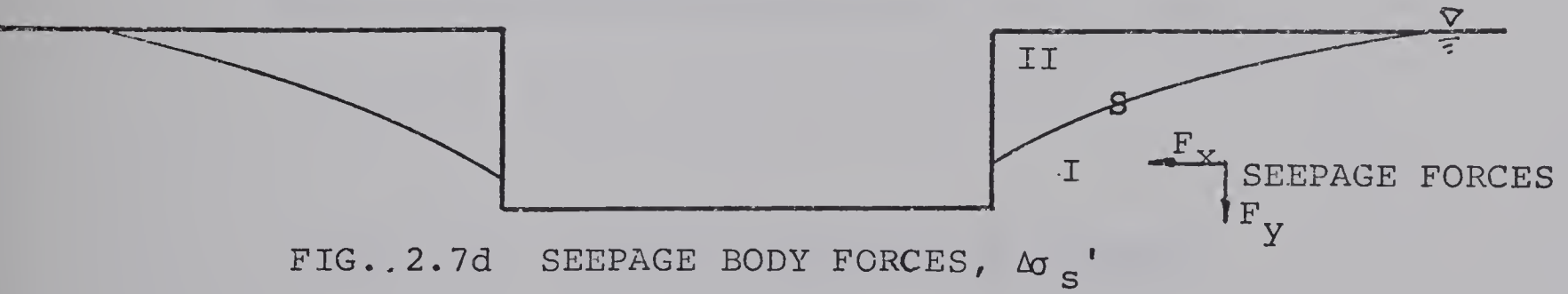


FIG. 2.7d SEEPAGE BODY FORCES, $\Delta\sigma_s'$

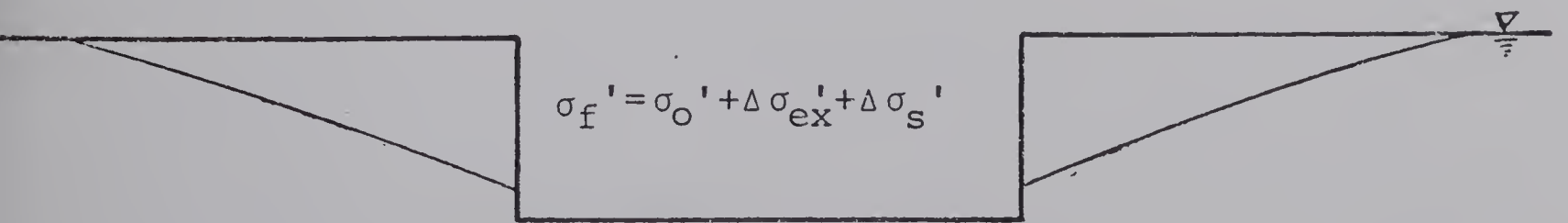


FIG. 2.7e FINAL STATE, σ_f'

FIG. 2.7 SUPERPOSITION OF STRESS STATES FOR SOLUTION

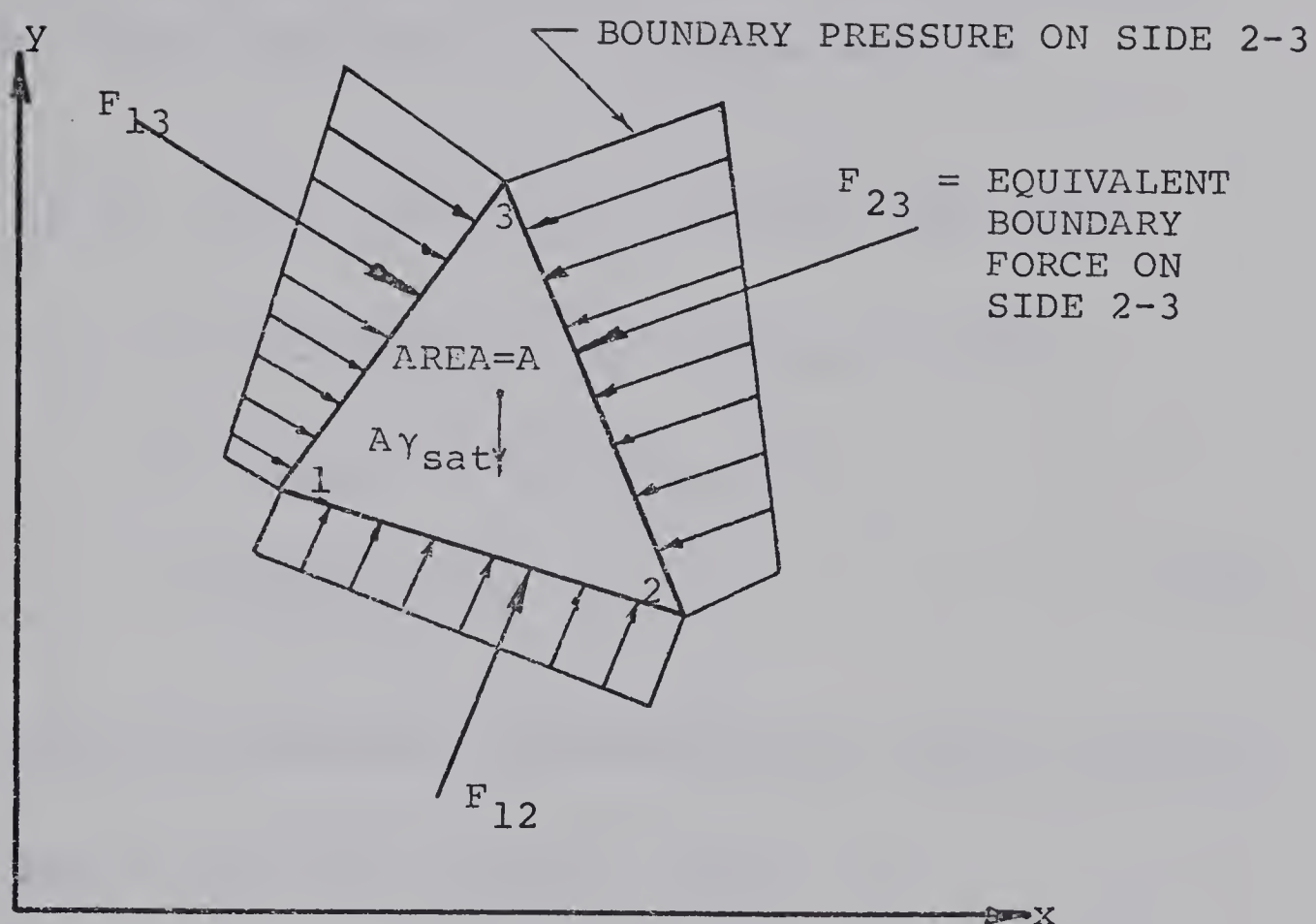


FIG. 2.8 BOUNDARY PRESSURES ON ELEMENT

γ_{sat} = saturated unit weight

γ_{sub} = submerged unit weight

A = area of element

\vec{j} = unit vector in y direction

The change in body force, $\Delta B.F.$, due to seepage, from the initial condition of no seepage will be,

$$\begin{aligned}
 \Delta B.F. &= \text{Final body force} - \text{Initial body force} \\
 &= (-A \gamma_{\text{sat}} \vec{j} + \vec{u}_r)_F - (-A \gamma_{\text{sat}} \vec{j} + \vec{u}_r)_I \\
 &= -A \gamma_{\text{sat}} \vec{j} + \vec{u}_r + A \gamma_{\text{sub}} \vec{j} \\
 &= -A \gamma_w \vec{j} + \vec{u}_r \quad (2.38)
 \end{aligned}$$

Above the phreatic surface $\vec{u}_r = 0$, $\therefore \Delta B.F. = -A \gamma_w \vec{j}$

For no flow $\vec{u}_r = +A \gamma_w \vec{j}$, $\therefore \Delta B.F. = 0$

The $\Delta B.F.$ found can be equally divided among the 3 nodes of the element. $\Delta B.F.$ is identical to the seepage force in the medium. The equations of the change in body force are developed and verified in comparison to the seepage force in Appendix A.

Both the seepage program described earlier and the stress program used were left basically unchanged. They were coupled through the use of common statements and several additional subroutines. One finite element grid was used for the stress analysis and another was used for the seepage

analysis. In order to facilitate the assignment of body forces from the seepage to the stress grid and the appointment of permeabilities from the stress to the seepage grid, the element configurations were made to correspond below the phreatic surface. Above this boundary the stress grid also possessed the additional domain II as shown in Fig. 2.7d with a unit weight of γ_w . By having the element configurations correspond exactly for both the seepage and stress grids below the free surface location the delineation of the phreatic boundary was achieved in the stress grid. Just as the nodes below the free surface in the seepage grid were "strung" along, both the nodes above and below this line in the stress grid were made to be strung along between the horizontal limits of the top and bottom of the excavation. Fig. 2.9 shows the general method and Fig. 2.10 shows the internal phreatic surface location in the stress grid for one case of the model studied. Since all the slope face nodes changed position due to the moving free surface, the release forces had to be recalculated for each stress analysis. The release force equations are given in Appendix A.

To find the correct free surface a process consisting of a double iteration technique was used. The iterations in one process are called "iterations" and in the other are called "cycles". One cycle began with a stress analysis which included the seepage body forces from the previous cycle. The stresses were then used to calculate the

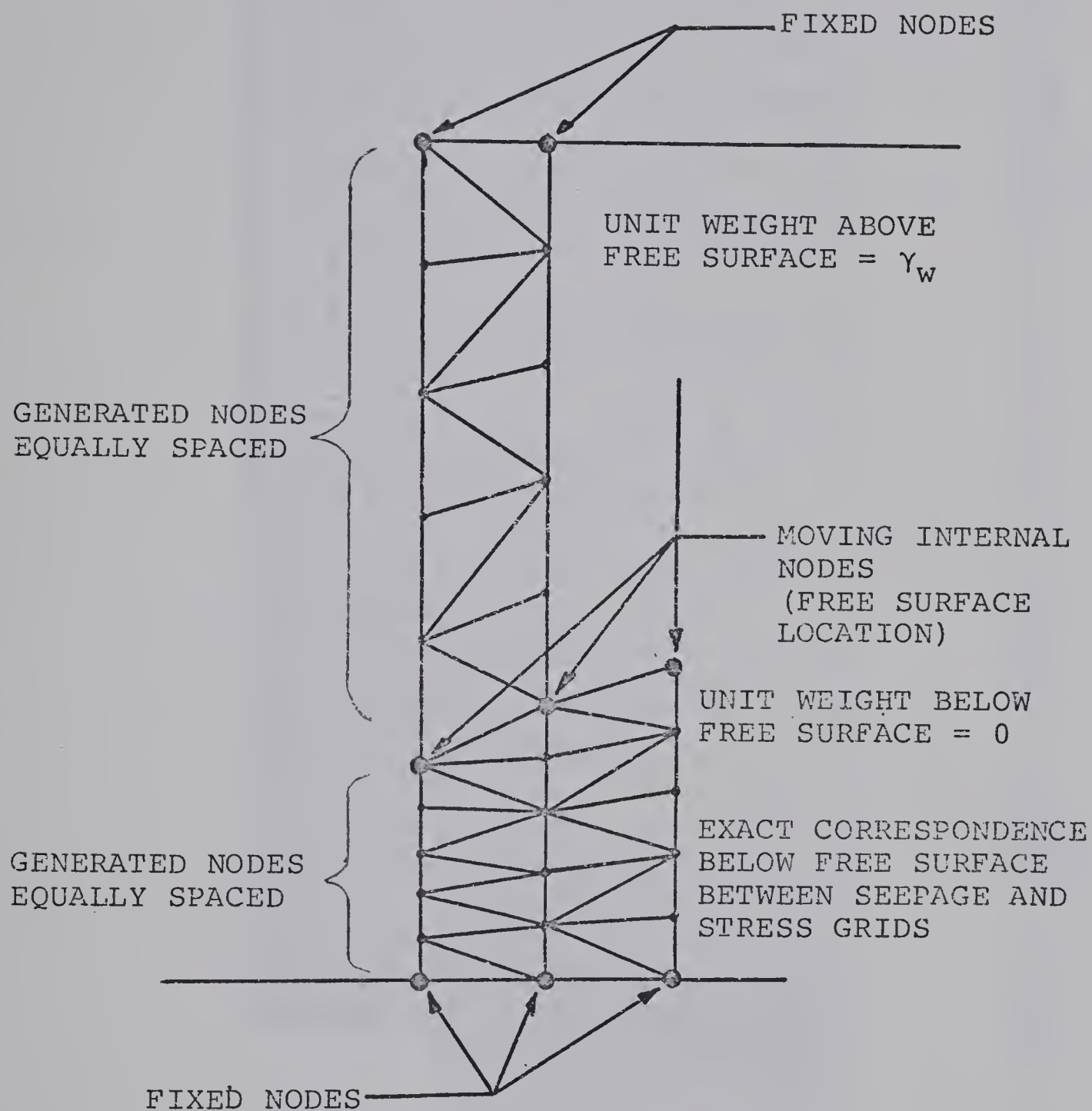


FIG. 2.9 METHOD FOR INTERNAL PHREATIC BOUNDARY

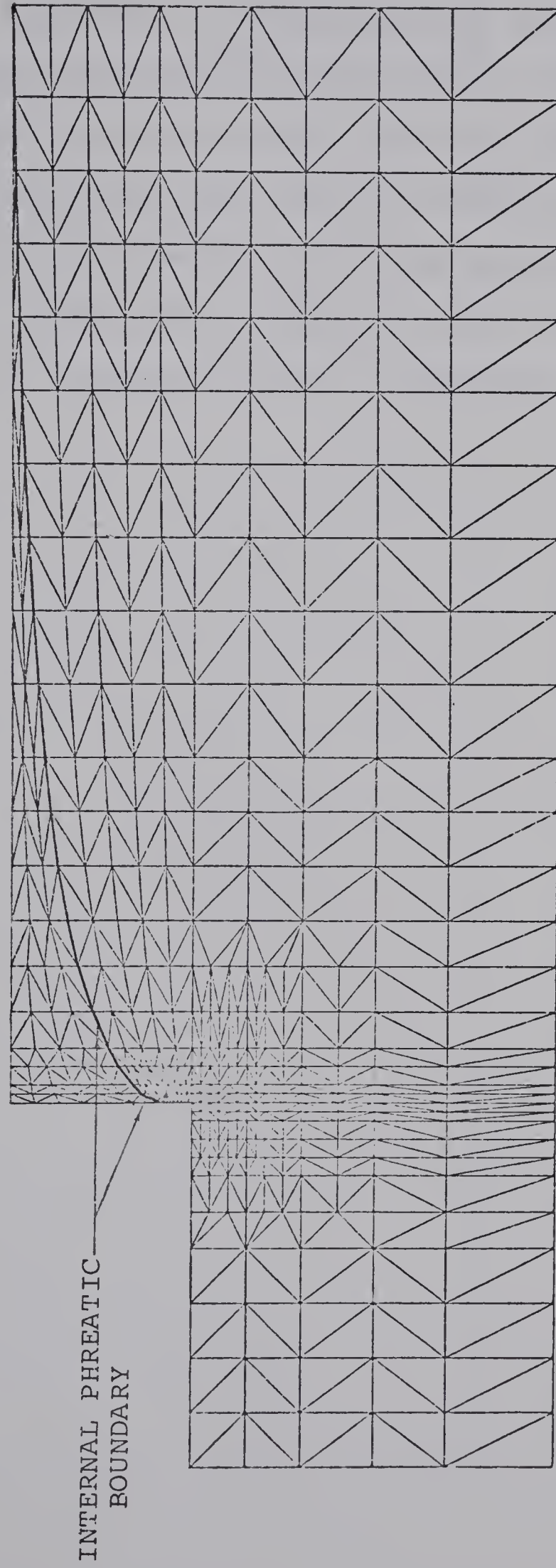


FIG. 2.10 INTERNAL PHREATIC BOUNDARY FOR ONE CASE OF THE MODEL STUDIED

permeabilities of each element. The free surface was found with these by iterating. Convergence was taken when the movement between two cycles was less than a specified amount. Seepage forces resulting from the analysis for a homogeneous medium were used for the initial cycle. Fig. 2.11 gives a schematic representation of the processes and Fig. 2.12 gives the general flow diagram for the computer program. A listing of the program is given in Appendix B.

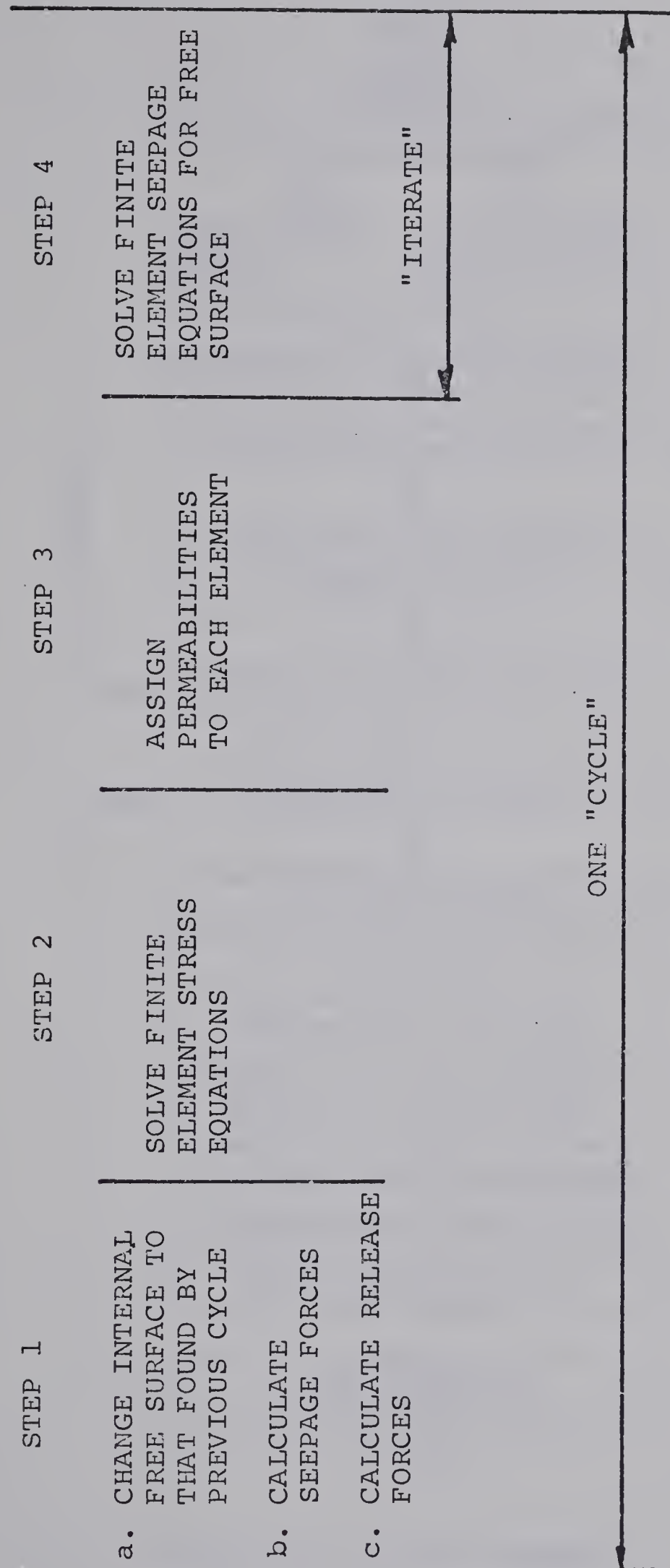


FIG. 2.11 SCHEMATIC PRESENTATION OF SOLUTION

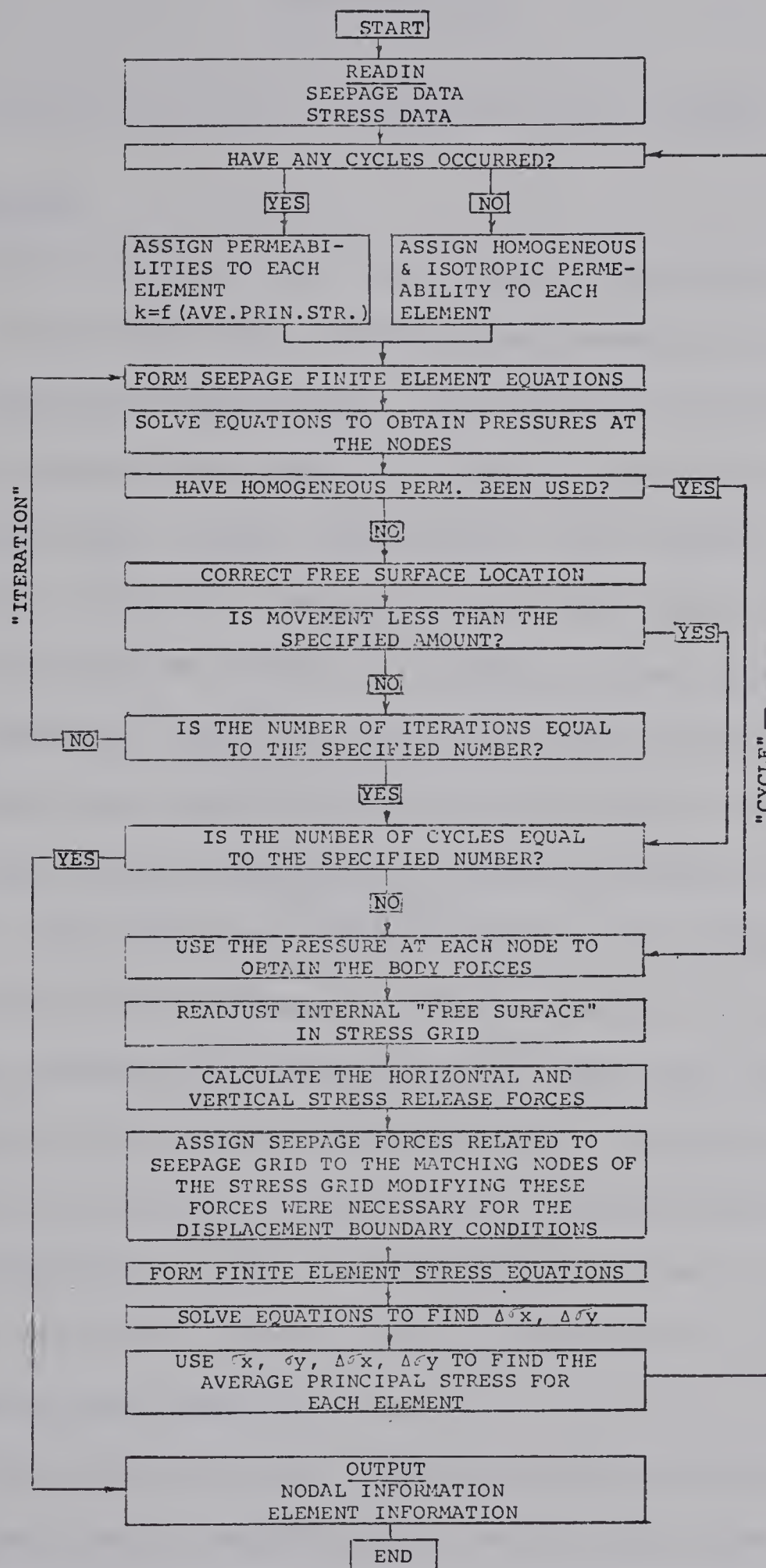


FIG. 2.12 FLOW DIAGRAM

CHAPTER III

RELATION BETWEEN PERMEABILITY AND STRESS

3.1 General

Until recently the variation of permeability with stress in rocks has been investigated mostly in the context of oil reservoir engineering. The effect of all-round confining pressure has been studied by Fatt and Davies (1952), Knutson and Bohor (1962) and others. The effect of permeability under triaxial conditions has also been studied by Mordecai and Morris (1971). In other areas Brace et al (1968), Patching (1965) and Bernaix (1969) have also demonstrated that permeability changes with stress. All workers have found reductions in permeability as loading increased. The fall was rapid at first and changed less rapidly for higher stresses. In most cases the reservoir sandstone permeability reduction was less than 50%. The coals tested by Patching, the granites investigated by Brace and the gneisses researched by Bernaix showed much larger reductions. From these studies, it was concluded that this reduction occurs due to the change in the secondary structure of the material.

The aforementioned laboratory determinations can be supplemented now by permeability values from the field. Sherman and Banks (1970) have summarized many known field permeability values obtained from packer tests. The variations in fluid conductivities also arise due to a secondary structure

in the rock. However this structure is on a different scale than that in the laboratory specimens.

In this work it is assumed that flow of water through jointed and fissured rock obeys equation (2.9) on a macroscopic scale. One intuitively feels that this is correct. There may be an analogy here with the discretization of the finite element approach where an overall result is correct but with discrepancies occurring on the element scale. Snow (1967) gives the justification for using equations based on Darcy's law for fractured media. This means that the rock is taken to conduct water everywhere and not just at the joints and fissures. It will now be assumed that this conductivity at every point is in some way related to the effective principal stresses at every point and independent of shear. However it must be remembered that the permeability of interest arises due to the secondary structure in the rock and that the primary permeability is assumed to be small in comparison. This chapter attempts to arrive at a reasonable form of equation relating permeability and stress.

3.2 Development of Relation Between Permeability and Stress

An insight into the permeability of jointed rock may be obtained using a procedure suggested by Terzaghi (1960). A model is assumed containing three similar sets of joints intersecting each other at right angles. The joint spacing is D and the width of joint is b . From the laws of laminar

flow of water between parallel plates the average velocity V , at which water flows between the plates is given by

$$V = \frac{\gamma_w}{12\mu} b^3 i \quad (3.1)$$

where μ = dynamic viscosity of water

If flow takes place through the model through two sets of joints and at right angles to the third set the quantity of seepage through a square $B \times B$ is

$$Q = V \frac{2B^2}{D} = \frac{i\gamma_w b^3}{12\mu} \times \frac{2B^2}{D} = k i B^2 \quad (3.2)$$

$$\text{where } k = \frac{\gamma_w b^3}{6 \mu D} \quad (3.3)$$

Substituting the appropriate values of μ and γ_w , k becomes

$$k (\text{cm/sec}) = 16300 \, b^3 / D \quad (3.4)$$

The relation between b , D and k is shown in Fig. 3.1. From equation (3.4) and the plot of Fig. 3.1, it is observed that if D is constant the permeability in an idealized model is dependent upon the crack opening to the third power. This opening in turn will be influenced by the state of stress in the region of the crack. Hence it is obvious that if the crack opening is in any way sensitive to stress the medium will tend to have large variations

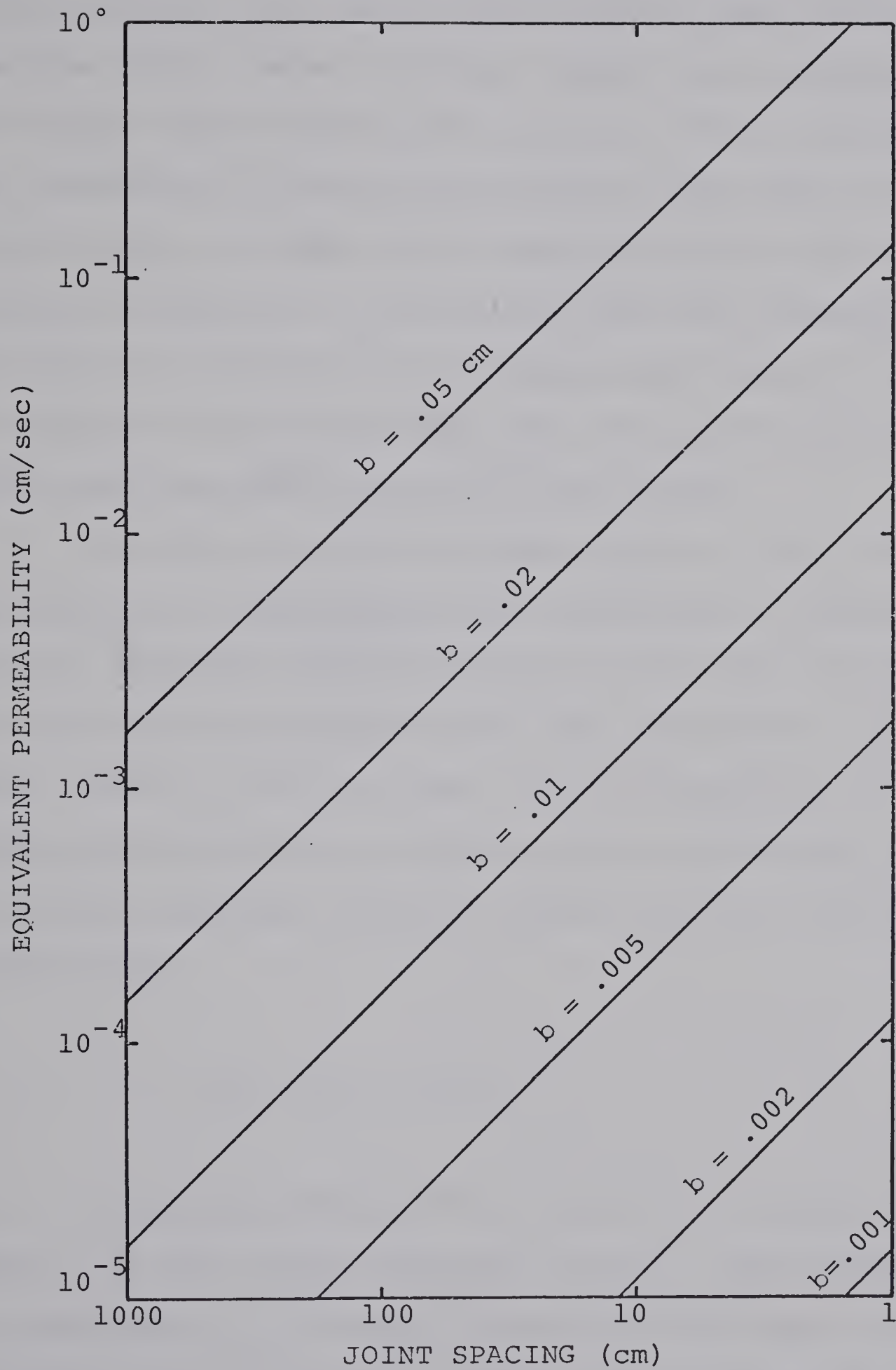


FIG. 3.1 RELATION BETWEEN JOINT PARAMETERS AND PERMEABILITY

in permeability.

Fissures in a rock material can be visualized as discontinuities with two of the dimensions much greater than the third. Walsh and Brace (1966) have estimated this aspect ratio to be in the order of 10^3 for low pressures. The orientation of these planar openings may vary in a random manner. If most of the head loss occurs due to flow through the fissures it is possible that the permeability may also be a function of an average crack width to a power although as in the joint model this too would be an idealization and oversimplification to some degree.

In order to arrive at some workable first order approximation of the permeability dependence on stress, again an isotropic jointed rock or an isotropic fissured rock material is assumed to exist for the medium. As a direct result of this isotropy and the assumption of conduction everywhere a relation may be established between an average principal effective stress J_1 and an isotropic permeability:

$$k = k_x = k_y = f(J_1) \quad (3.5)$$

It may be instructive to relate the average crack width b , to the average principal stress. The following is not presented as a rigorous formulation but only in the hope that it will lead to a clearer understanding of permeability dependence on stress. In general the joint or

crack opening will decrease with an increase in stress. Since no data was found for a relation between stress and crack opening a general function could be used to describe the typical behaviour. Fig. 3.2 shows some of the types of behaviour that might possibly occur. It is a type of decay behaviour that a simple exponential function could represent in some cases. However the property of an applied exponential function is that the rate at which the crack width changes is proportional to the width itself and this may not be general enough. It was found that a function of the form

$$b = \frac{A'}{(J_1 + T)^M} \quad (3.6)$$

where A' , T and M are constants

will approximate a great variety of decay behaviour. For example, as shown in Fig. 3.2, $T = 10$ psi and $M = 3.0$ could represent a crack closing very quickly with stress or $T = 100$ psi and $M = 1.0$ might represent a slowly closing crack having dislodged grain material in the crack.

If equation (3.6) is valid, equation (3.3) can be extended to the form

$$k_{\text{average}} = \frac{A}{(J_1 + T)^N} \quad (3.7)$$

This form will hold true where the main permeability arises

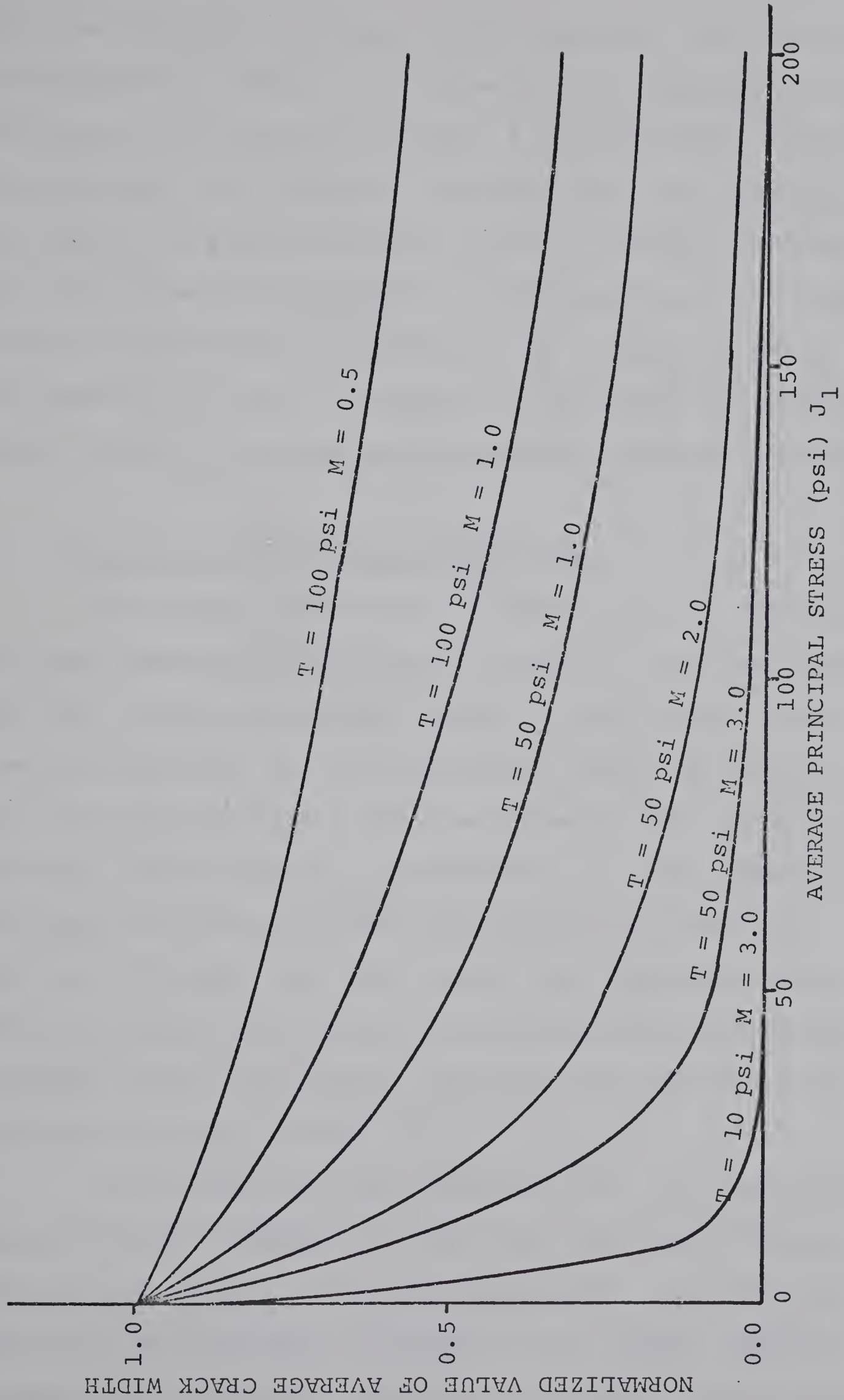


FIG. 3.2 CRACK BEHAVIOUR ACCORDING TO $b = \frac{A'}{(J_1 + T)M}$

from the secondary structure of the material and alterations in permeability result from the mechanical changes in crack width due to the applied stress. A relation that follows this equation will produce a straight line on a log-log plot when k is plotted against J_1+T . It should be noted that the pressure distribution is dependent on the relative values of permeability and hence will be independent of A . The quantity of flow is dependant on the absolute permeability and may be scaled up and down by changing A accordingly.

3.3 Stress Dependent Permeability Data

The stress dependence of permeability in some rocks has been demonstrated by various workers. The most relevant data will be reviewed here. Bernaix (1969) tested microfissured materials in an experimental set-up as shown in Fig. 3.3a with typical results as shown in Fig. 3.3b. Patching (1965) tested the permeability of coal under an all-round confining pressure with results as shown in Fig. 3.4. Sherman and Banks (1970) have tabulated data which illustrate the decrease in permeability as measured by packer tests, with depth. The data for granites and gneisses are shown in Fig. 3.5.

In the walls of the sample of Fig. 3.3a the principal effective stresses arising from fluid body forces vary in some manner across the sample wall. Bernaix has calculated the principal stresses in the sample assuming a homogeneous material. However in actuality these stresses

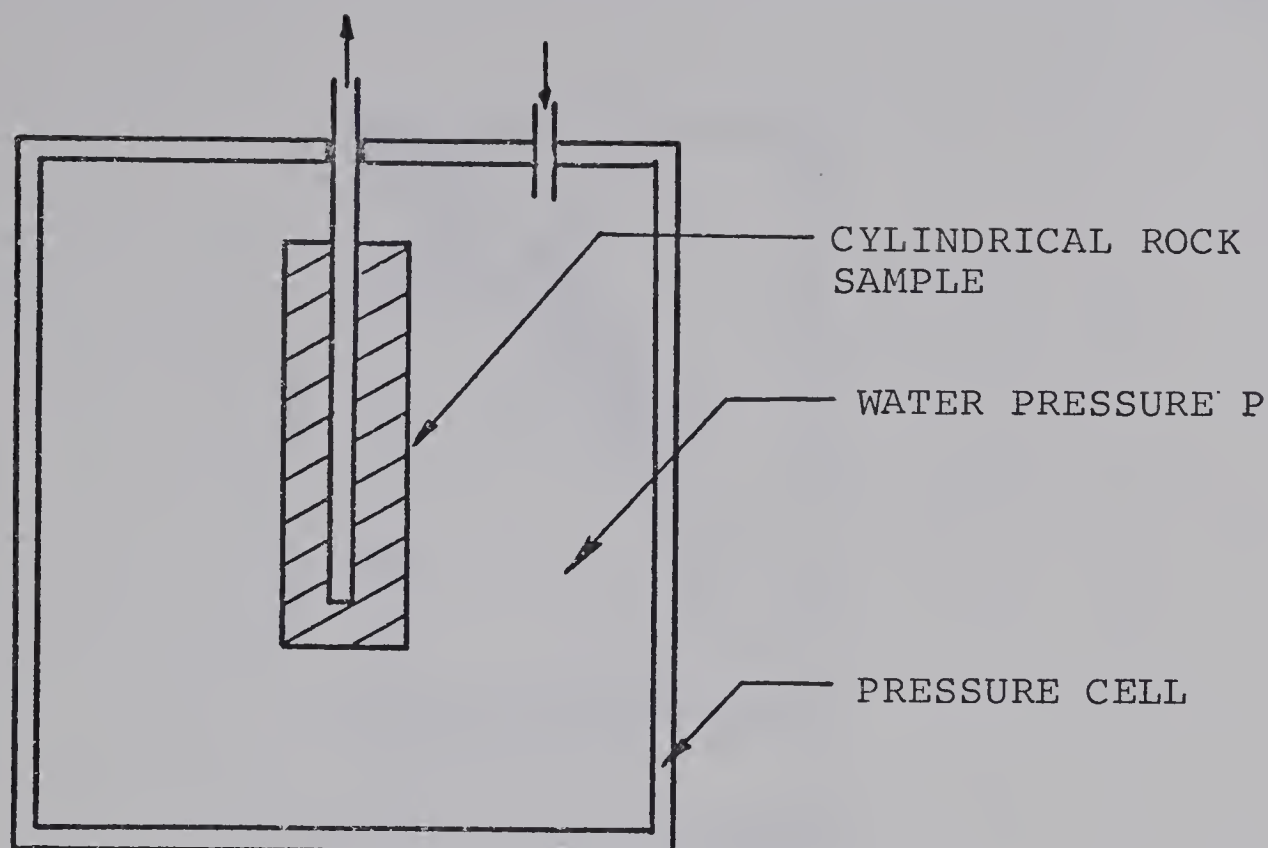


FIG. 3.3a TESTING CONFIGURATION

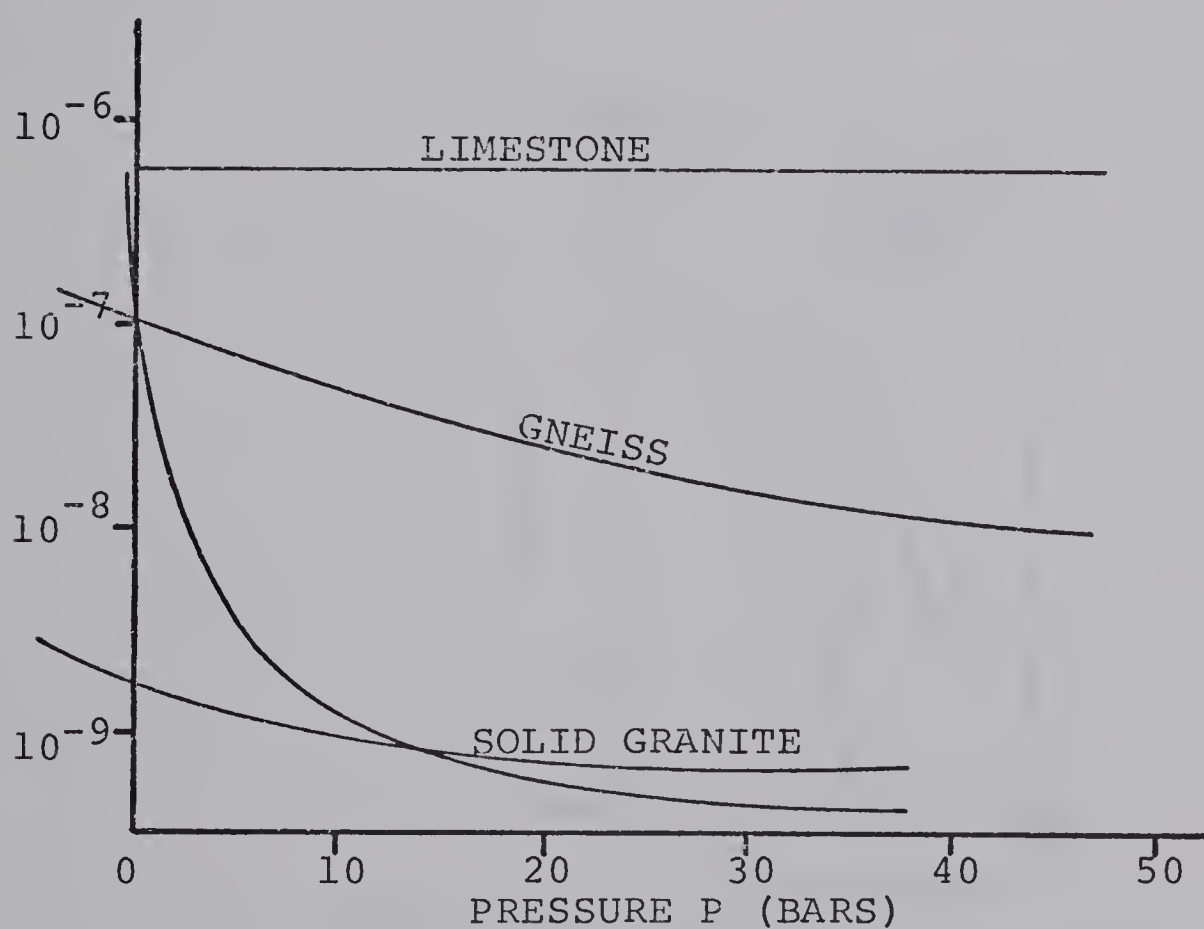


FIG. 3.3b TYPICAL RESULTS OF TEST IN FIG. 3.3a

FIG. 3.3 VARIATION IN PERMEABILITY WITH STRESS (AFTER BERNAIX, 1969)

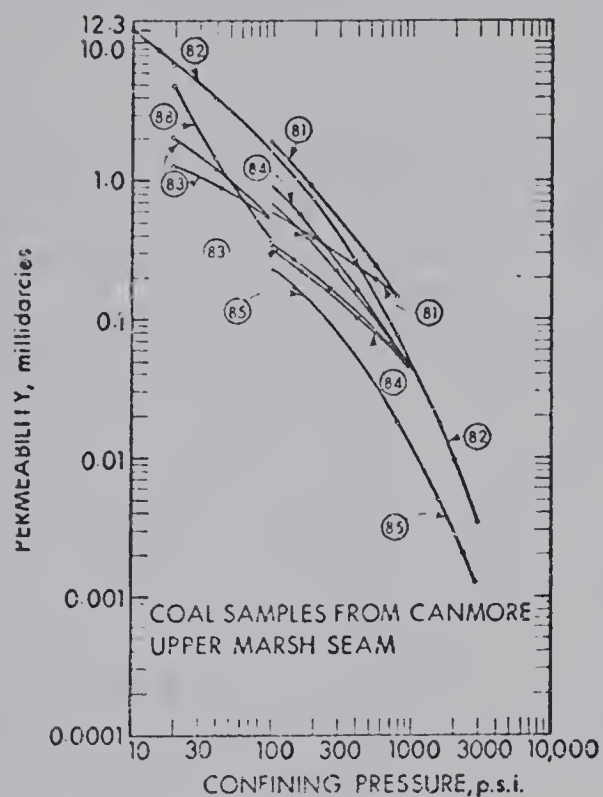


FIG. 3.4a Permeability vs confining pressure, samples from one seam.

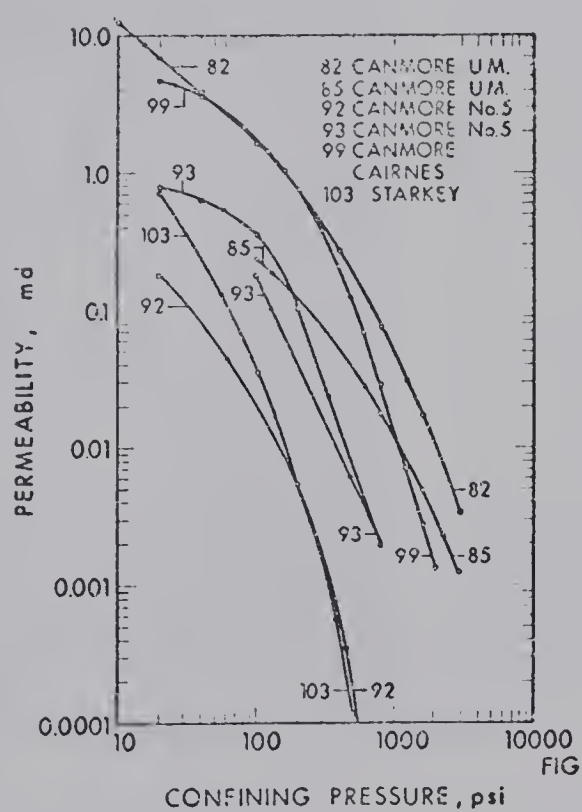


FIG. 3.4b Permeability vs confining pressure, samples from several seams.

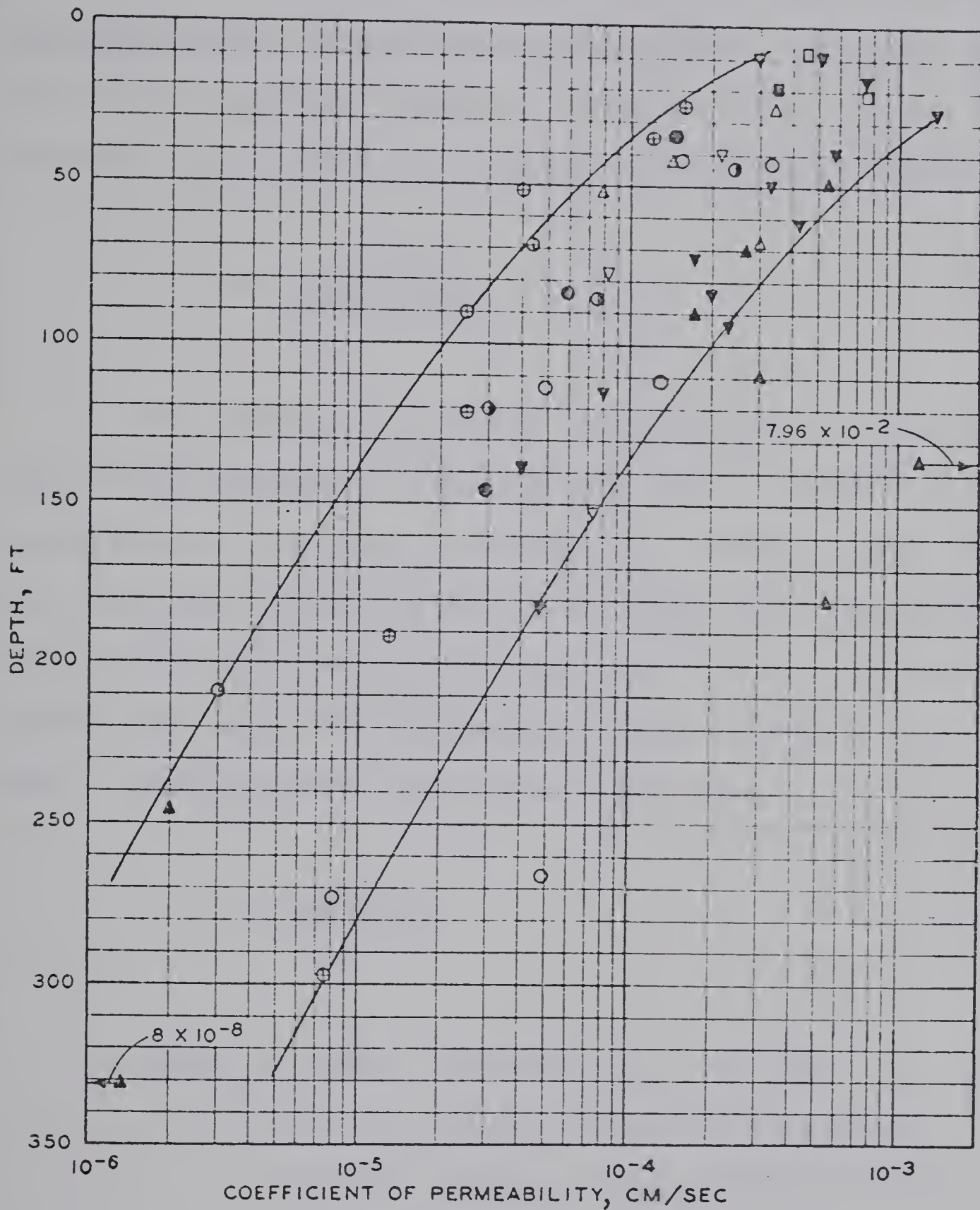


FIG. 3.5 DECREASE IN COEFFICIENT OF PERMEABILITY OF GRANITES AND GNEISSES WITH DEPTH (AFTER SHERMAN AND BANKS, 1970)

are affected by the stress dependent permeability and this makes it difficult to obtain a unique relation between permeability and average principal stress. Strictly speaking the curves should be viewed as an index in evaluating the material. The author has defined a sensitivity index as:

$$S = \frac{k(-1 \text{ bar})}{k(+50 \text{ bars})} \quad (3.8)$$

In Patching's work dry nitrogen gas was used as one of the permeants in the friable coal. He used "semi-anthracite to low volatile bituminous coals". Field samples were cut into uniform prisms, surrounded by a flexible epoxy resin and stressed isotropically in an oil filled pressurized cell. No mention of sample orientation is made. Permeabilities were calculated from

$$k = \frac{\mu L Q}{(P_1 - P_2) A} \quad (3.9)$$

where k is the permeability in Darcies

μ is the dynamic viscosity in poises

L is the length of the specimen in cm.

Q is the average flow rate in cc/sec.

$P_1 - P_2$ is the driving pressure in atmospheres

A is the cross-sectional area of the sample
in cm^2

Although a gas was used, the use of a liquid would change the viscosity and specific gravity. Also gas slippage would not occur. This latter phenomena known as the "Klinkenberg effect" is a slipping of the fluid along the pore walls which gives rise to an apparent dependence of permeability on pressure. Mordecai and Morris (1971) have found this effect to be of limited importance. In any case this results in only a small change in permeability compared to changes caused by stress variation. Hence water would give the same type of variation of permeability as the gas used.

Although the permeability is somewhat stress path and time dependent the overall behaviour is clear. In general a curve can be approximated by equation (3.7) when the initial segment at low stress is curved with the curvature decreasing for increasing stress and the curve becoming essentially linear for high stresses. It may be seen from Fig. 3.4 that this behaviour is characteristic of some of the curves although all the curves do not follow this description. Plotting curve no. 99 a straight line approximation may be made for the curve using $T = 200$ psi and giving $N = 3.36$ as shown in Fig. 3.6.

Sherman and Banks give a summary of the known field data of the permeability of jointed rock with most of it being obtained from Snow (1968a). The permeabilities were determined by water pressure tests with packers. The permeabilities are calculated on the assumption that the

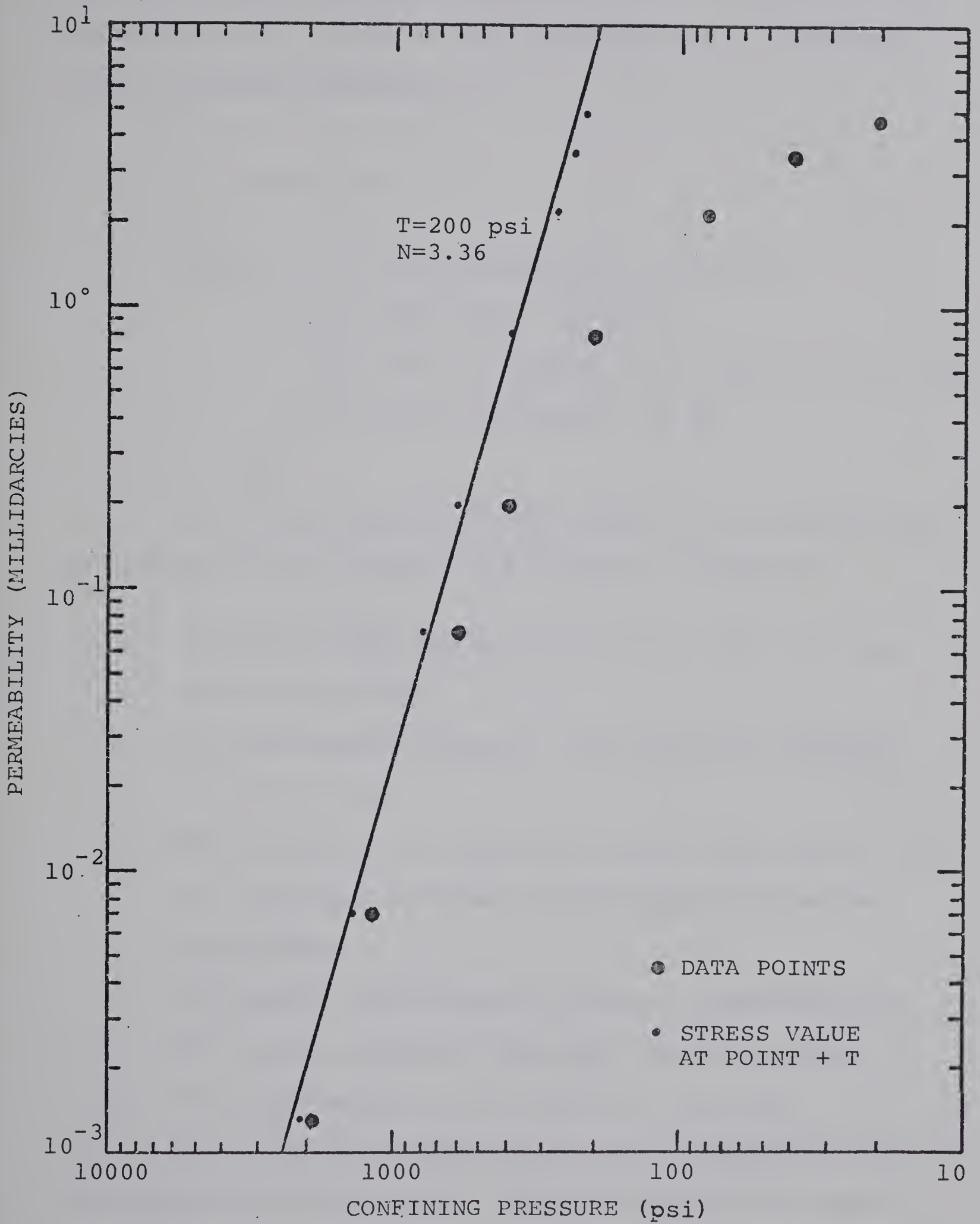


FIG. 3.6 PATCHING'S CURVE NO. 99 FITTED TO EQUATION (3.7)

flow is laminar, and that the material is homogeneous and isotropic with respect to the permeabilities. The computation is made according to:

$$Q = k H S$$

where k is the permeability in cm/sec.

Q is the flow in cm^3/sec .

H is the net head at the test section in cm

S is the shape factor in cm

The field data tabulated by Sherman and Banks may be interpreted by making the following assumptions:

- a. The water table is at the surface (the net head, H , is not given).
- b. The horizontal stresses = the vertical stresses, i.e. $K_0 = 1.0$.
- c. The tests are performed in a flat lying area, i.e., the vertical stresses can be computed from the overburden.
- d. The packer tests have no effect on permeability.
- e. The joint system is isotropic and homogeneous.
- f. The unit weight of the rock $\gamma_t = 165$ pcf.

It is probable that all of these assumptions will be violated to some degree. However they may be used in order to evaluate the existence of a first order approximation between the average principal stress and the permeability.

The results are shown for items which best fit equation (3.7) in Figures 3.7 through 3.20. From a total of 22 items of 3 points or more, greater than one half fit the equation to some extent, whereas the remaining data was too scattered to be used. In some cases the curves were fitted to a smooth fitting line passing through the data points for $T = 0$ psi. In the other cases the trial value of T was added directly to the J_1 value of the point. It may be observed that some scatter does occur but for the information shown, the data tends to follow equation (3.7) to some degree. The relations, normalized at 10 psi so that the permeabilities in the range of 10 psi to an upper limit may be compared, are plotted on Fig. 3.21. Fig. 3.22 shows T plotted against $\log N$. The occurrence of large T usually results in large N . Large values of T will occur when for $T = 0$ psi the curvature in the field relations exist at relatively high stresses on a log-log permeability-stress plot.

3.4 Sensitivity of Permeability to Stress

In an initial analysis it was noted that for a particular K_0 and depth from the top of slope to the lower boundary a certain range of effective stresses occurred. Fig. 3.23 shows log permeability versus average principal stress plotted for equation (3.7) for several values of T and N with the values of permeability again normalized at 10 psi. It may be seen that the curve for a certain

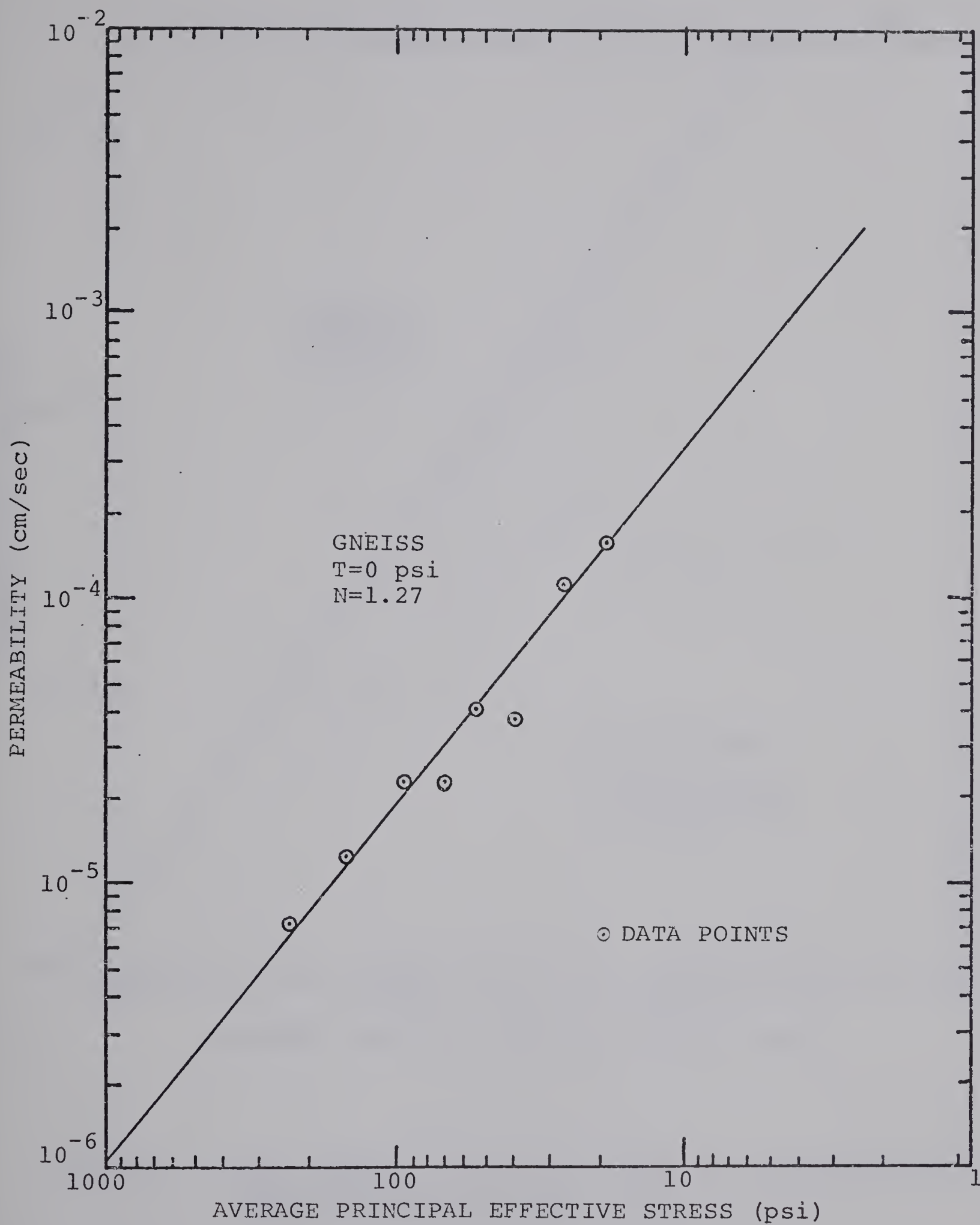


FIG. 3.7 FIELD PERMEABILITY DATA FITTED TO EQUATION (3.7)
(FROM SHERMAN AND BANKS, 1970)

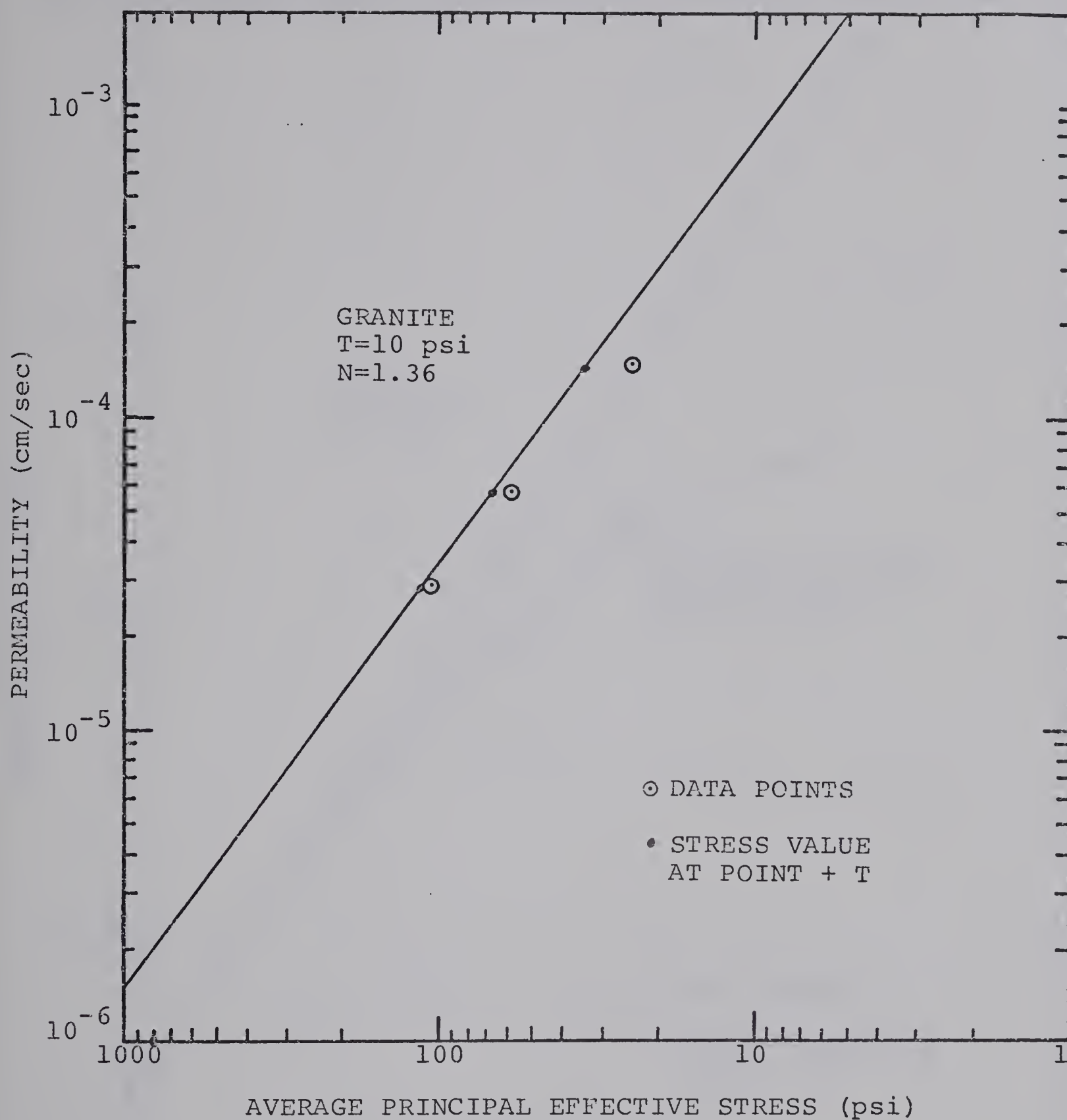


FIG. 3.8 FIELD PERMEABILITY DATA FITTED TO EQUATION (3.7)
(FROM SHERMAN AND BANKS, 1970)

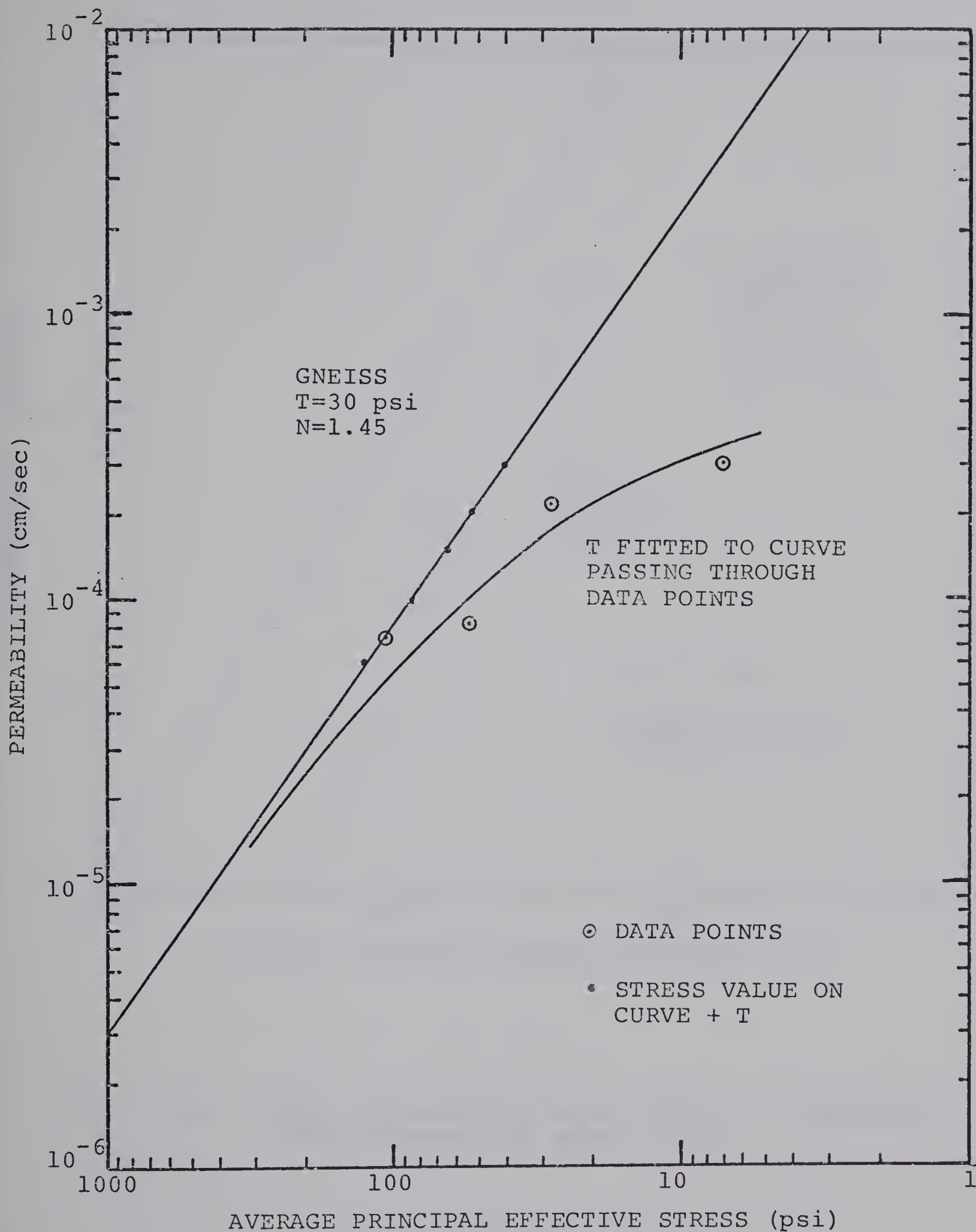


FIG. 3.9 FIELD PERMEABILITY DATA FITTED TO EQUATION (3.7)
(FROM SHERMAN AND BANKS, 1970)

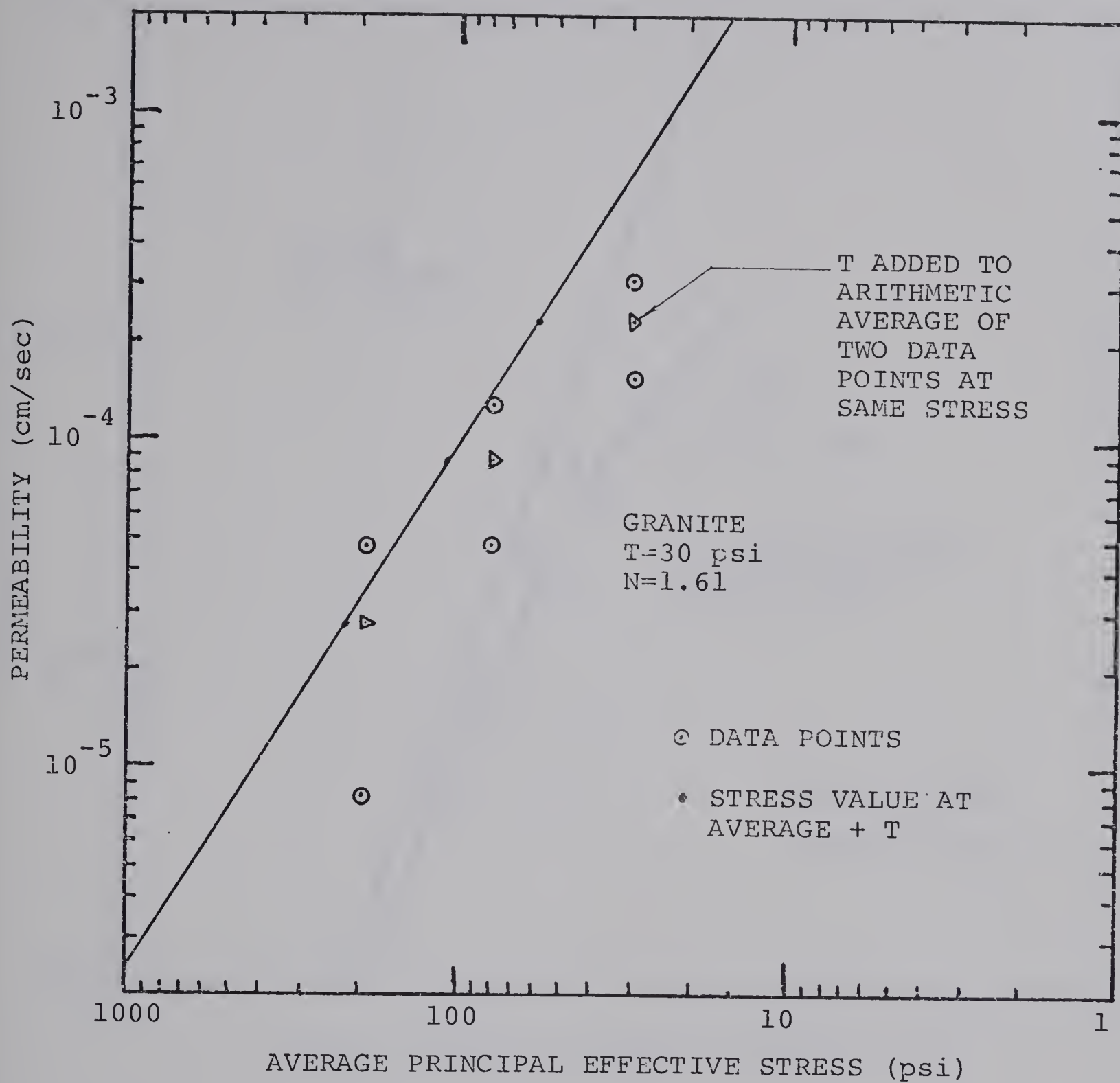


FIG. 3.10 FIELD PERMEABILITY DATA FITTED TO EQUATION (3.7)
(FROM SHERMAN AND BANKS, 1970)

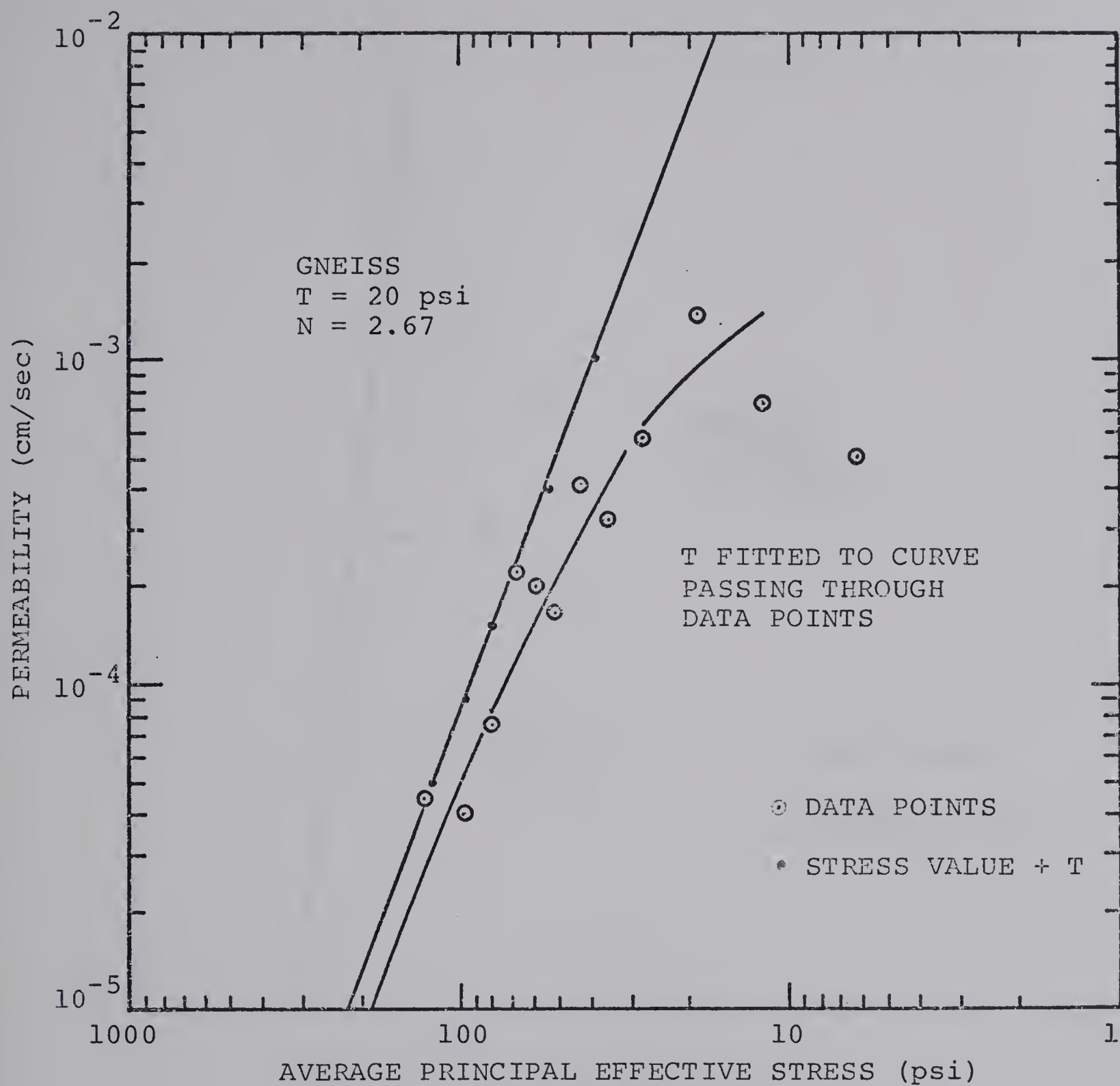


FIG. 3.11 FIELD PERMEABILITY DATA FITTED TO EQUATION (3.7)
 (FROM SHERMAN AND BANKS, 1970)

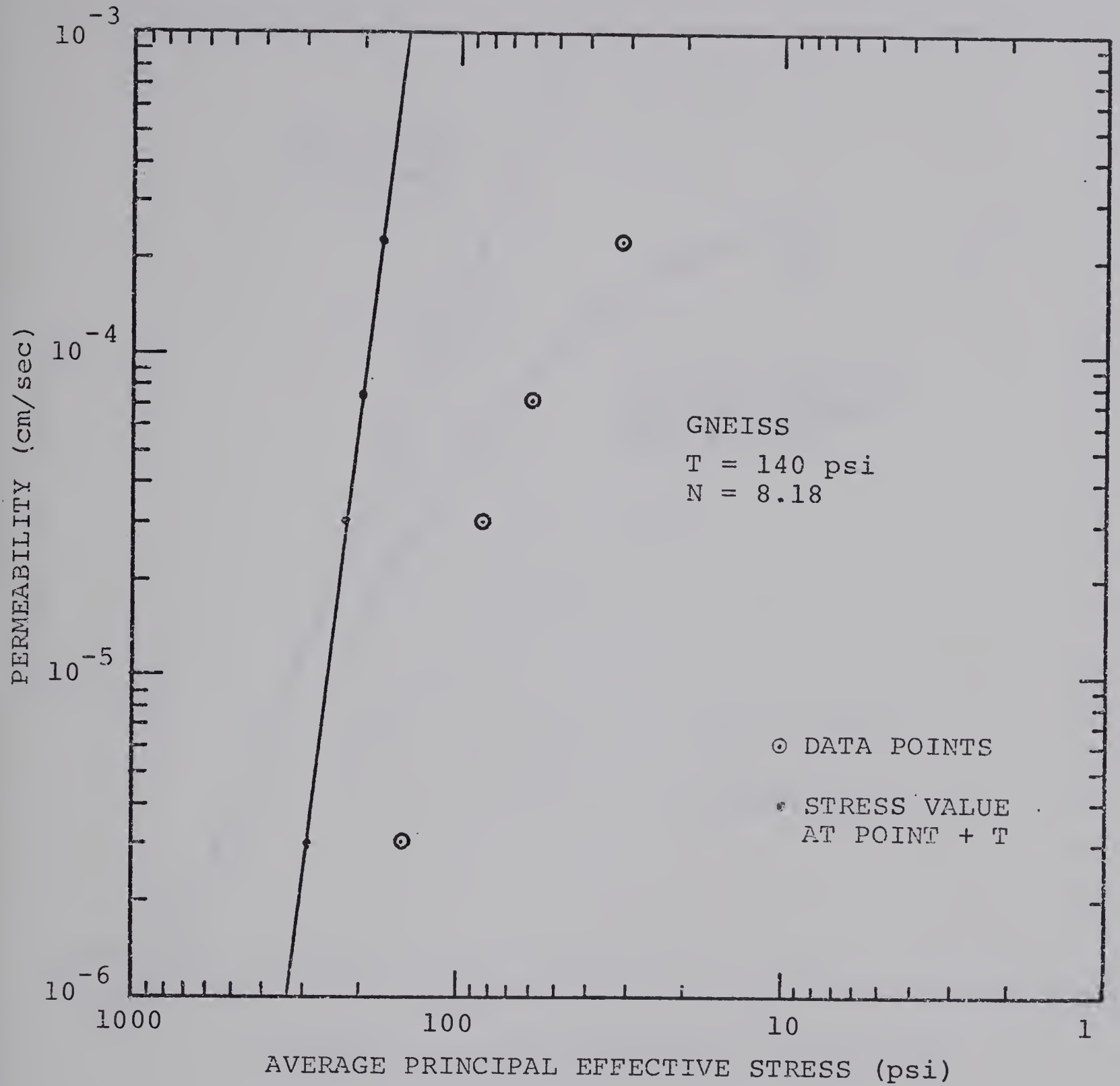


FIG. 3.12 FIELD PERMEABILITY DATA FITTED TO EQUATION (3.7)
(FROM SHERMAN AND BANKS, 1970)

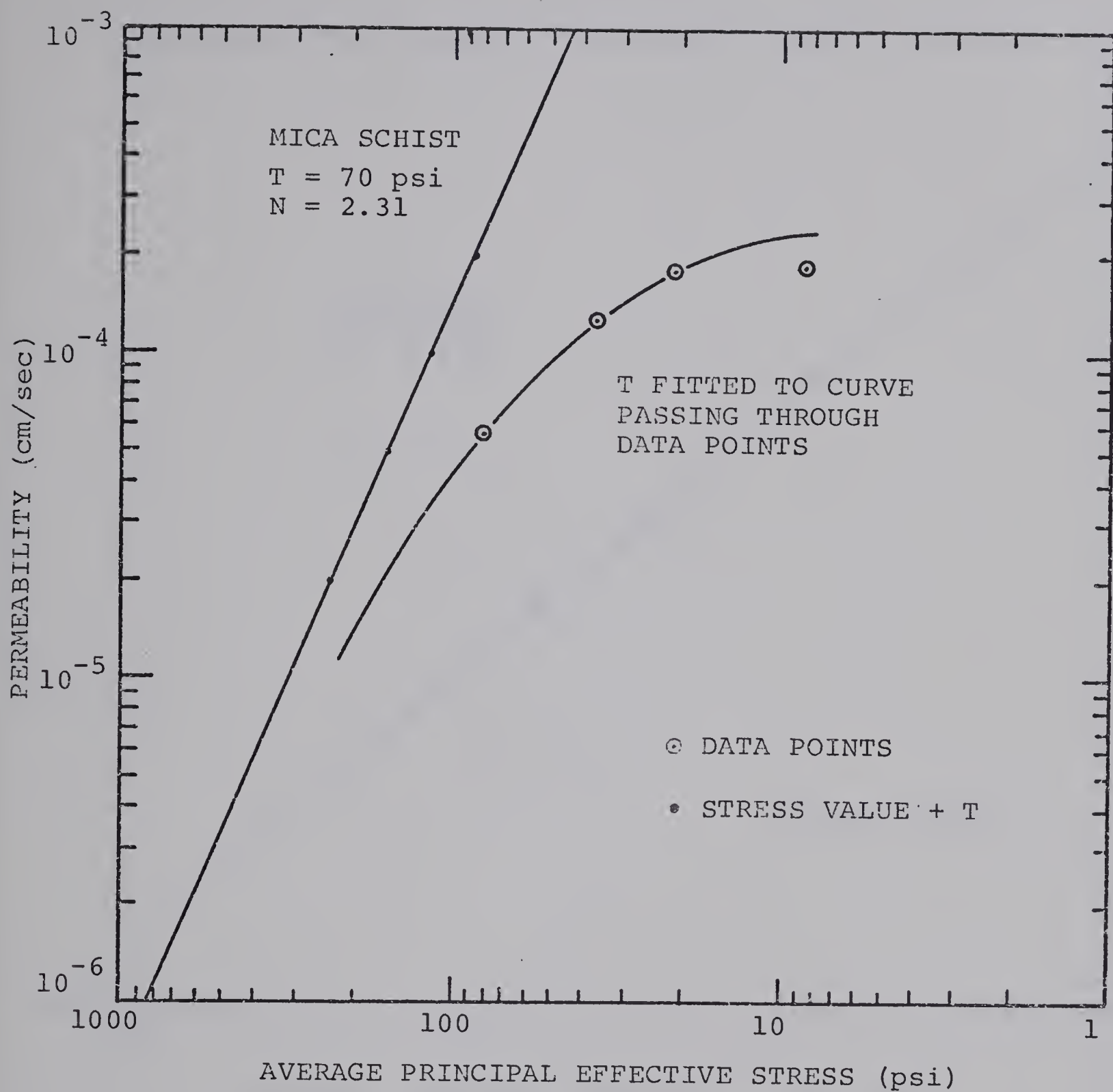


FIG. 3.13 FIELD PERMEABILITY DATA FITTED TO EQUATION (3.7)
 (FROM SHERMAN AND BANKS, 1970)

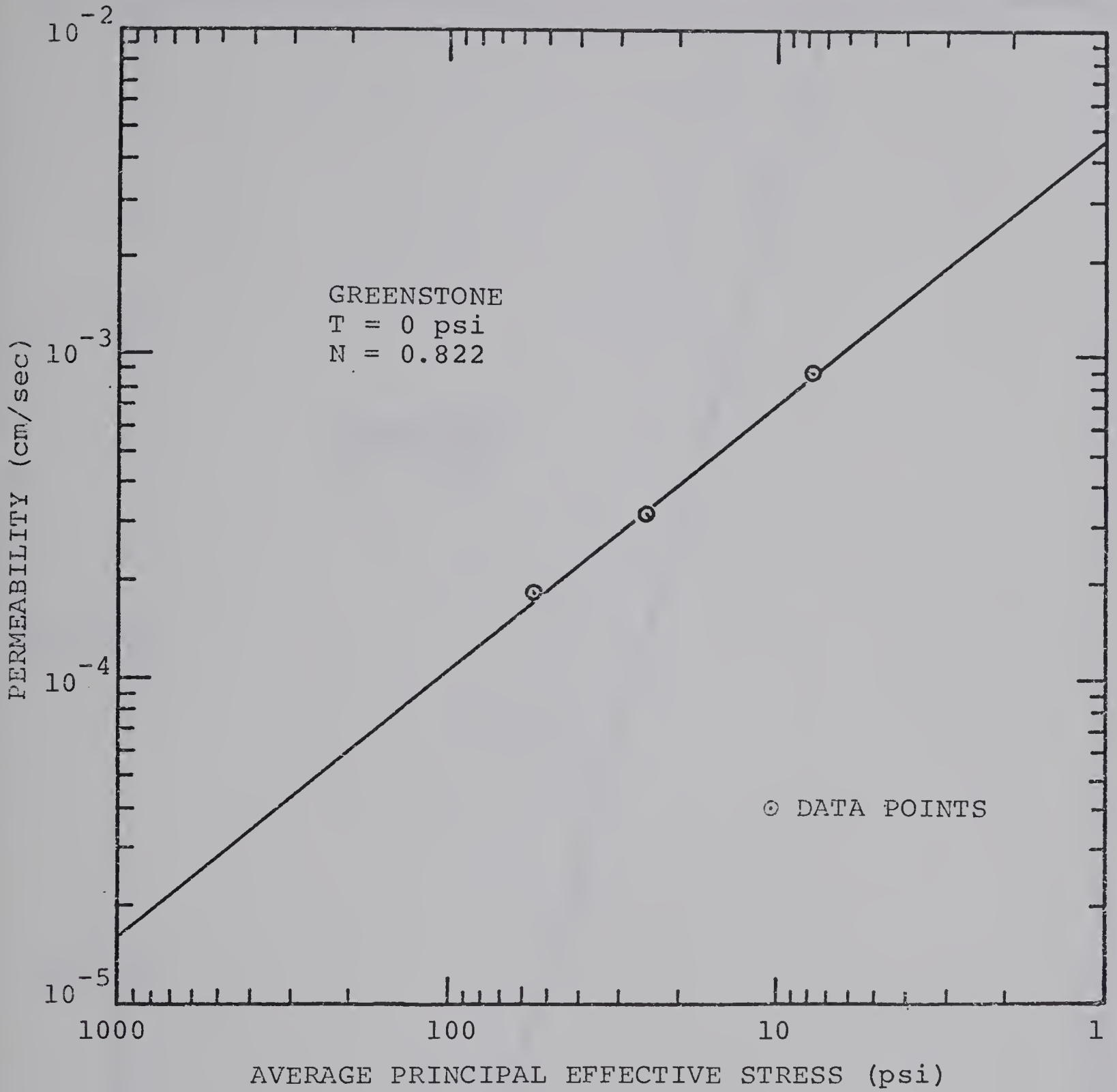


FIG. 3.14 FIELD PERMEABILITY DATA FITTED TO EQUATION (3.7)
(FROM SHERMAN AND BANKS, 1970)

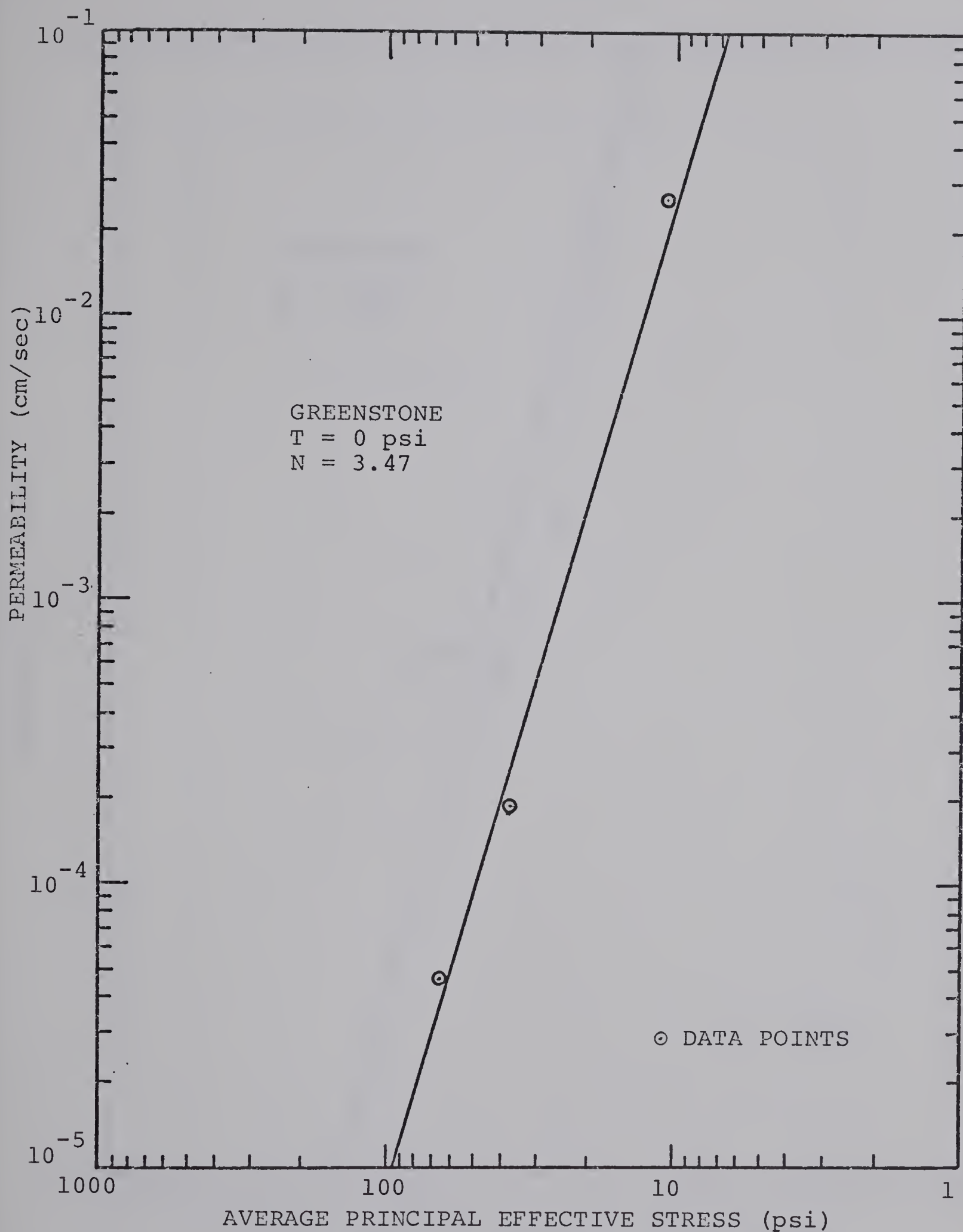


FIG. 3.15 FIELD PERMEABILITY DATA FITTED TO EQUATION (3.7)
(FROM SHERMAN AND BANKS, 1970)

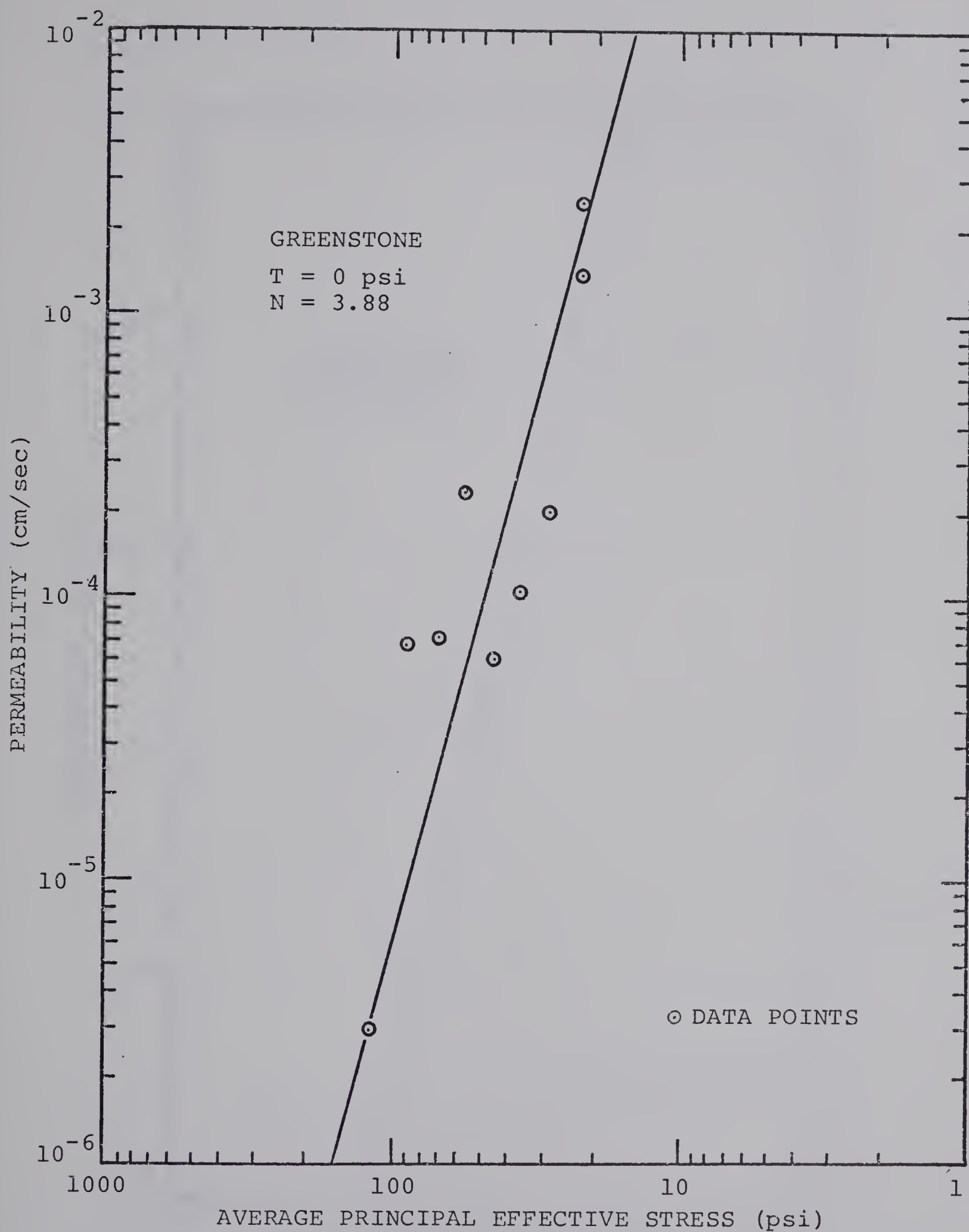


FIG. 3.16 FIELD PERMEABILITY DATA FITTED TO EQUATION (3.7)
 (FROM SHERMAN AND BANKS, 1970)

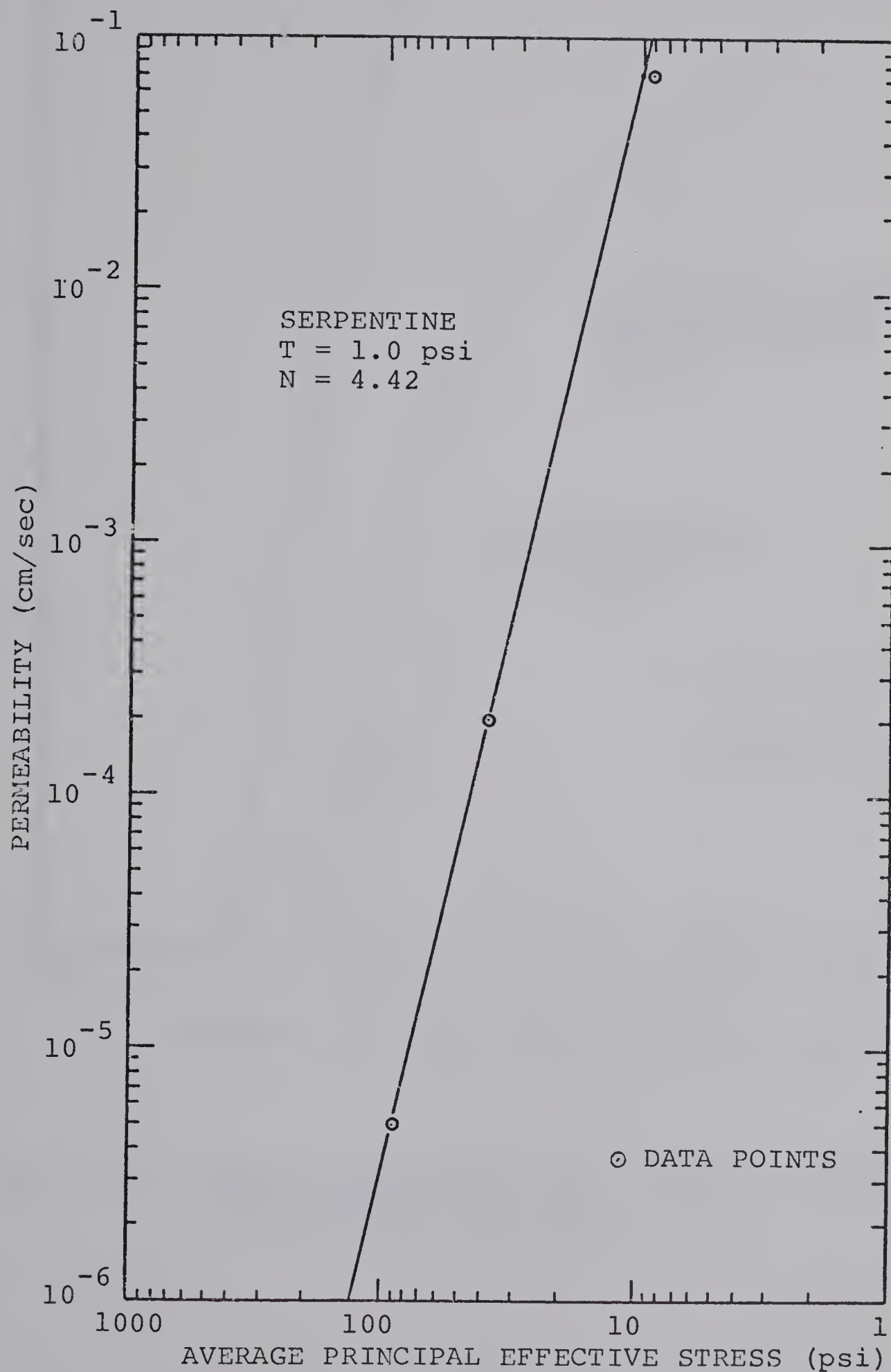


FIG. 3.17 FIELD PERMEABILITY DATA FITTED TO EQUATION (3.7)
 (FROM SHERMAN AND BANKS, 1970)

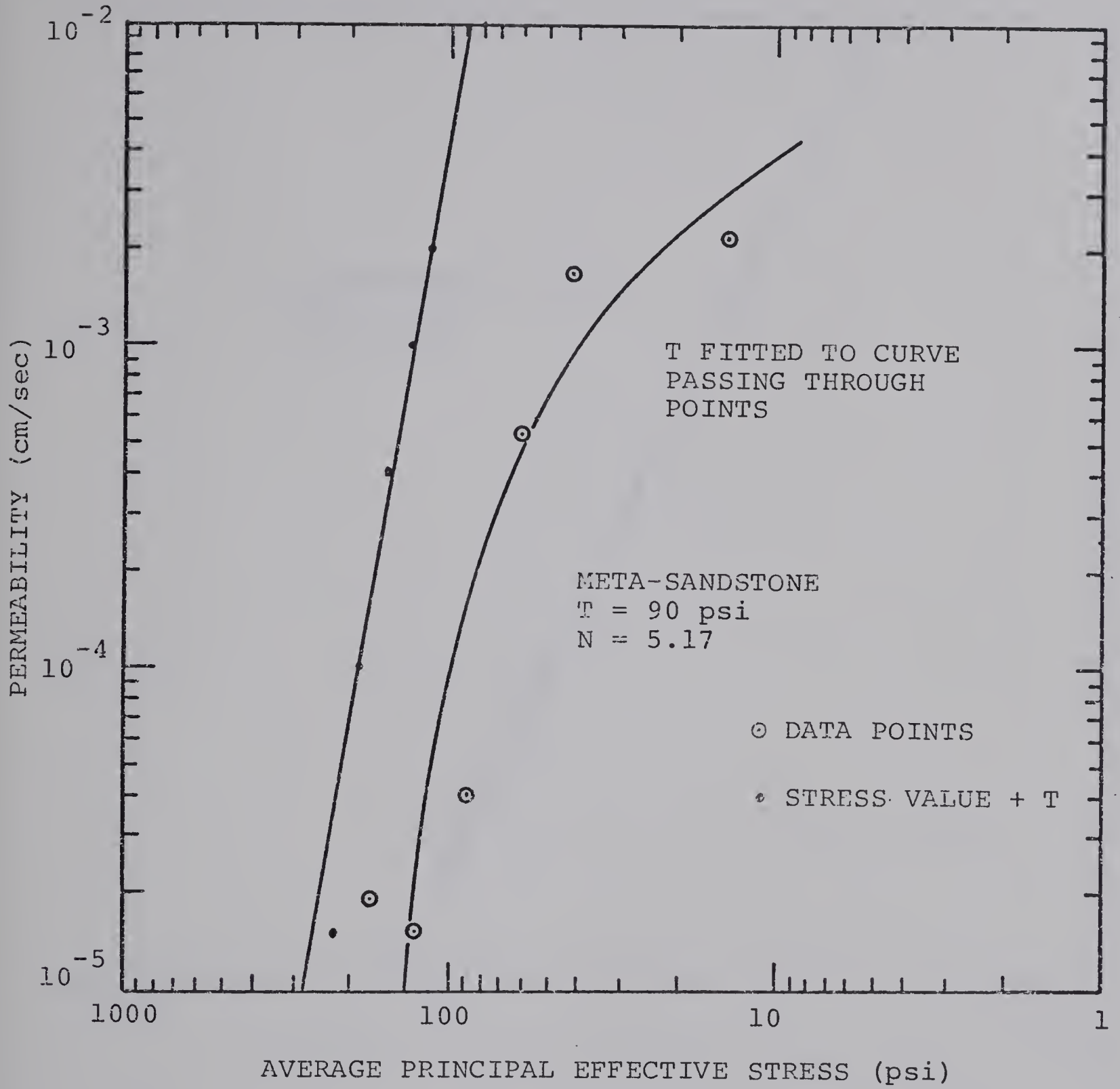


FIG. 3.18 FIELD PERMEABILITY DATA FITTED TO EQUATION (3.7)
(FROM SHERMAN AND BANKS, 1970)

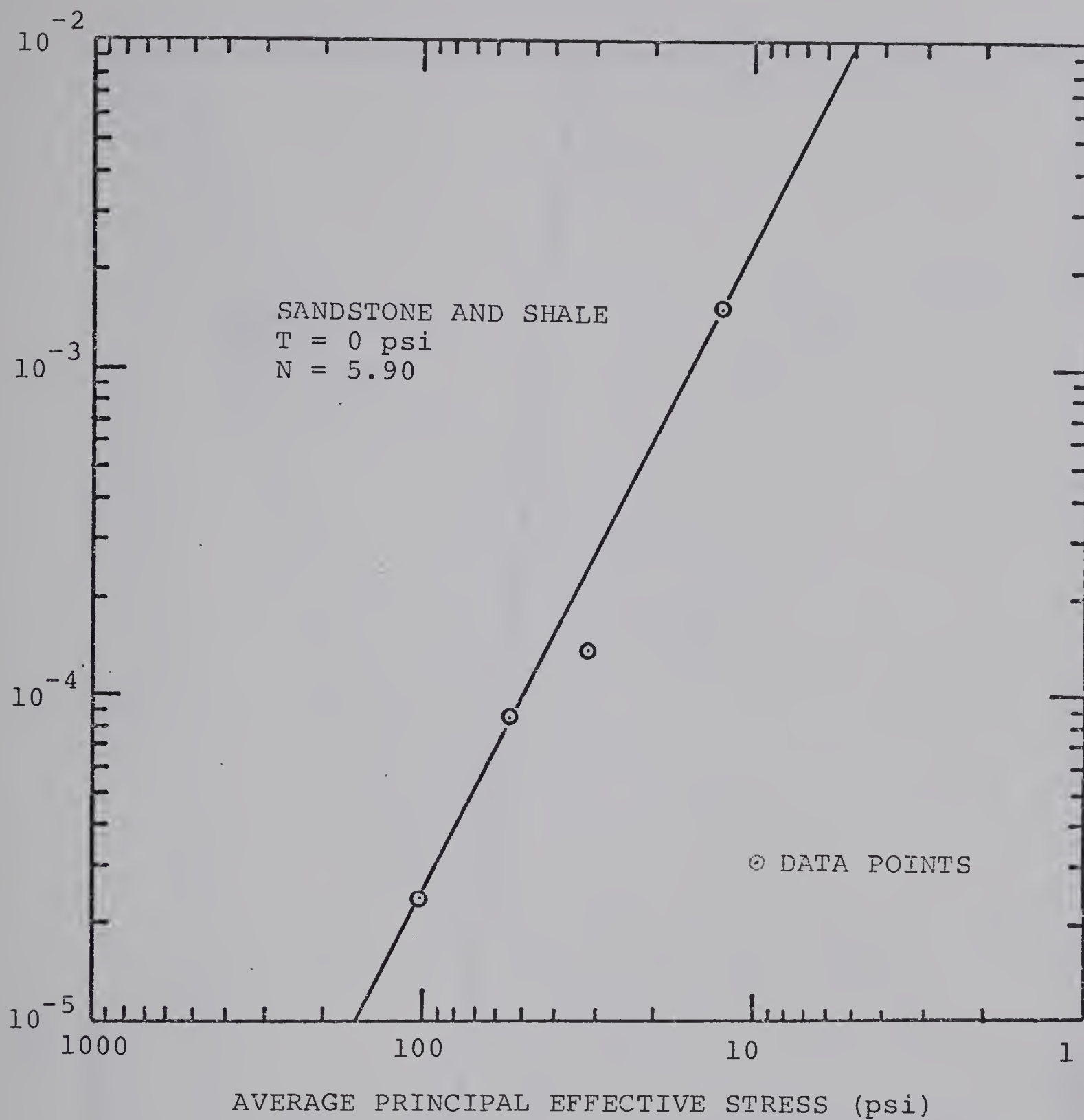


FIG. 3.19 FIELD PERMEABILITY DATA FITTED TO EQUATION (3.7)
 (FROM SHERMAN AND BANKS, 1970)

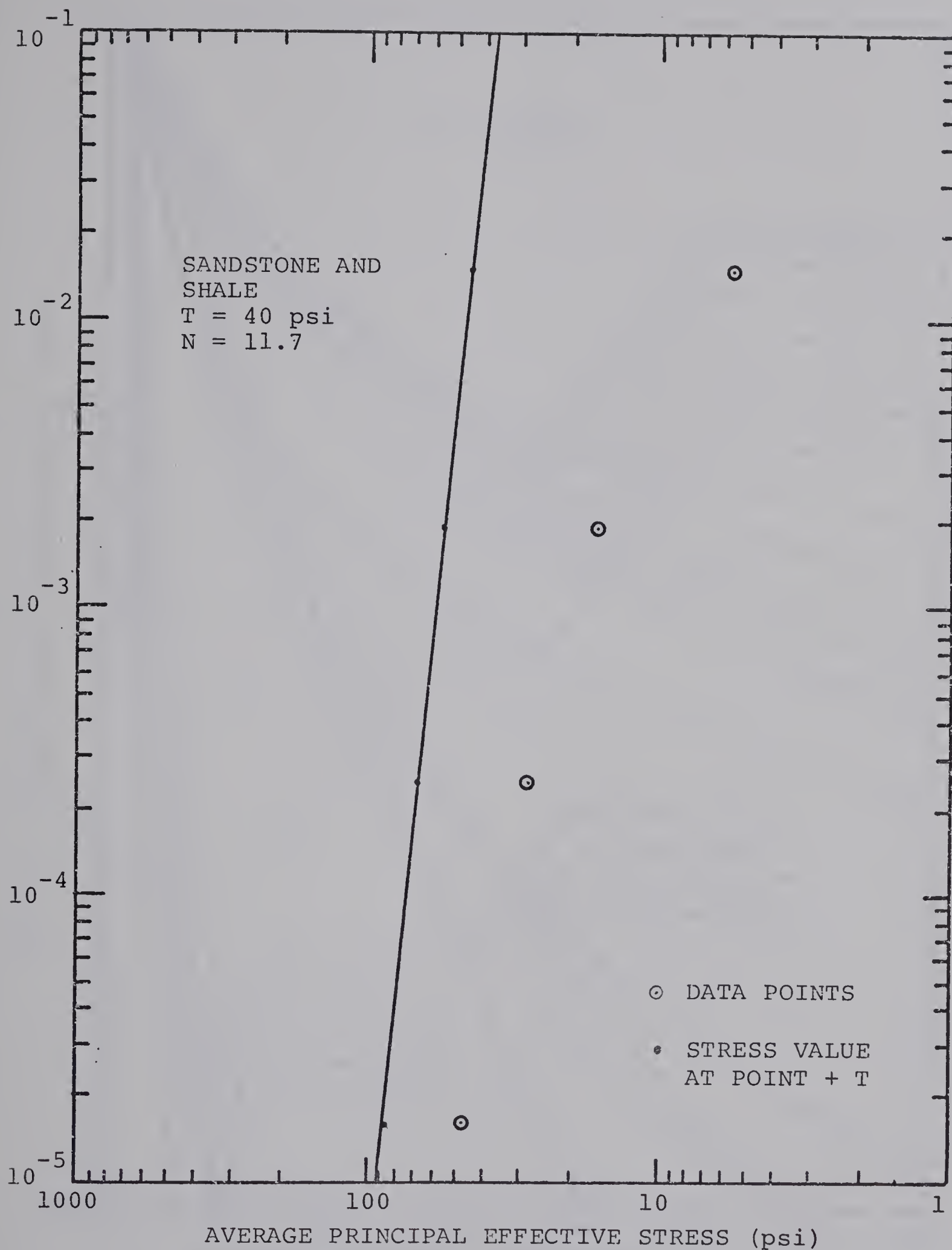


FIG. 3.20 FIELD PERMEABILITY DATA FITTED TO EQUATION (3.7)
 (FROM SHERMAN AND BANKS, 1970)

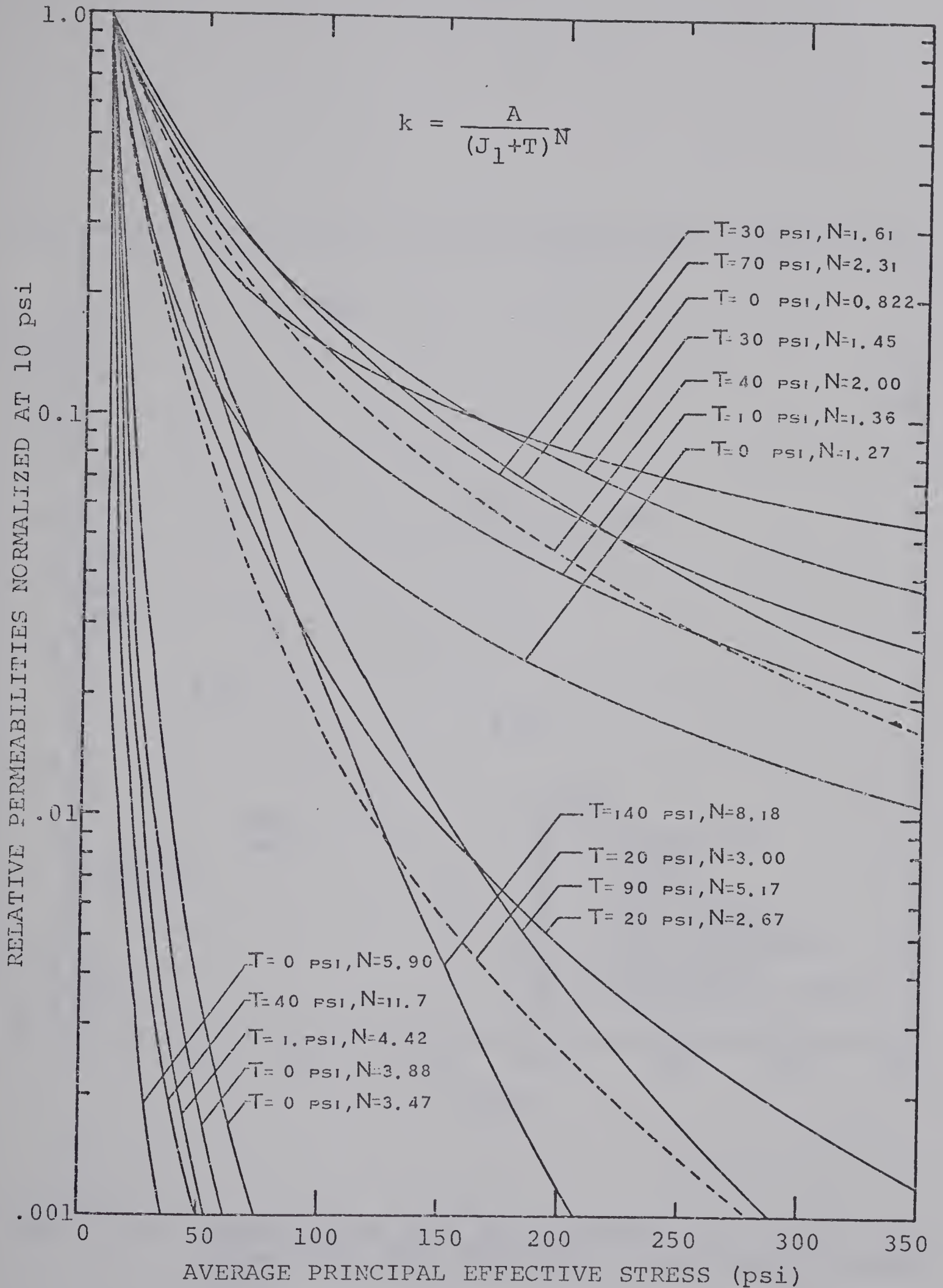


FIG. 3.21 COMPARISON OF PERMEABILITY RELATIONS

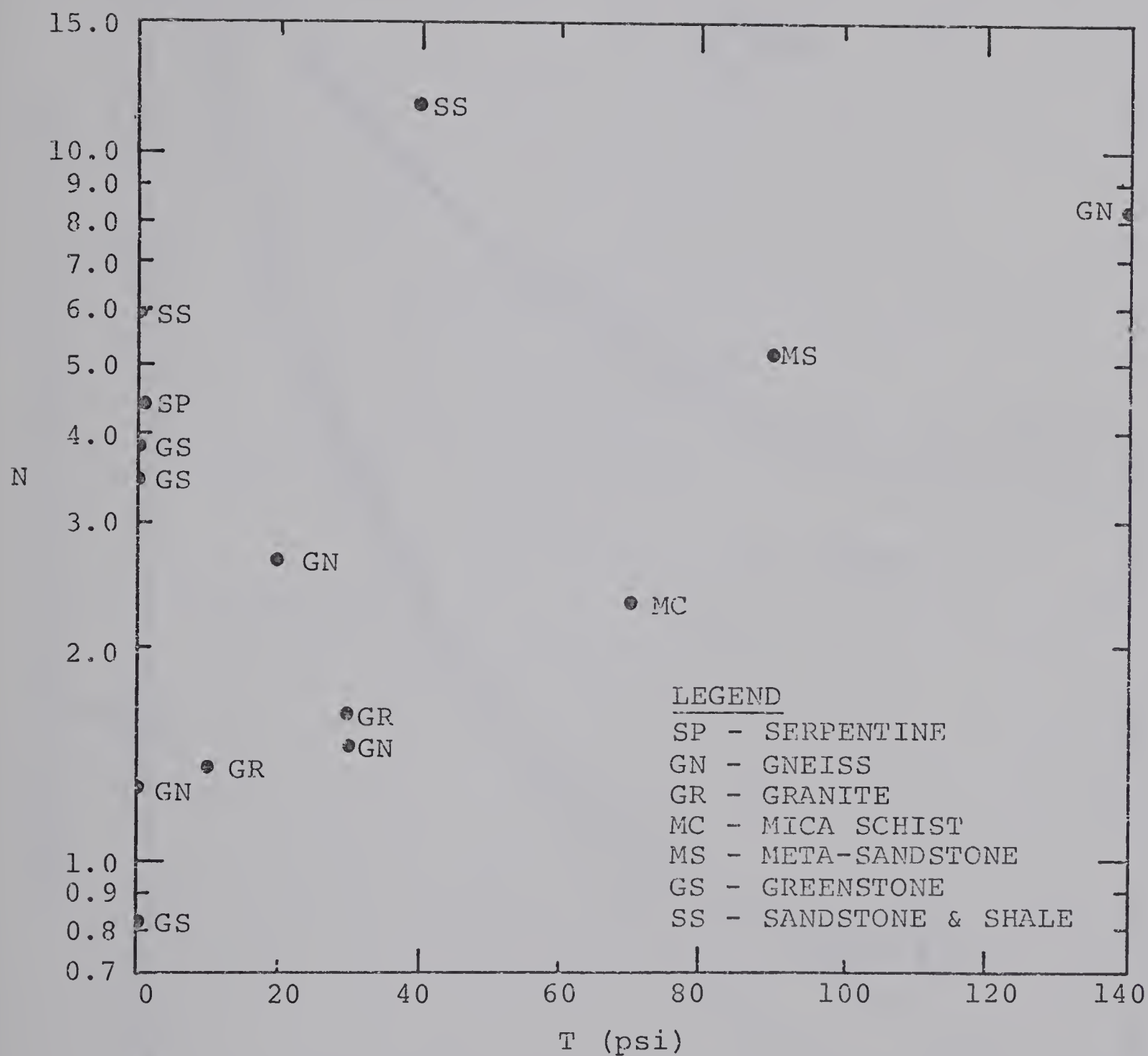


FIG. 3.22 SUMMARY PLOT OF T AND N VALUES
(FROM FIELD DATA TABULATED BY SHERMAN AND BANKS, 1970)

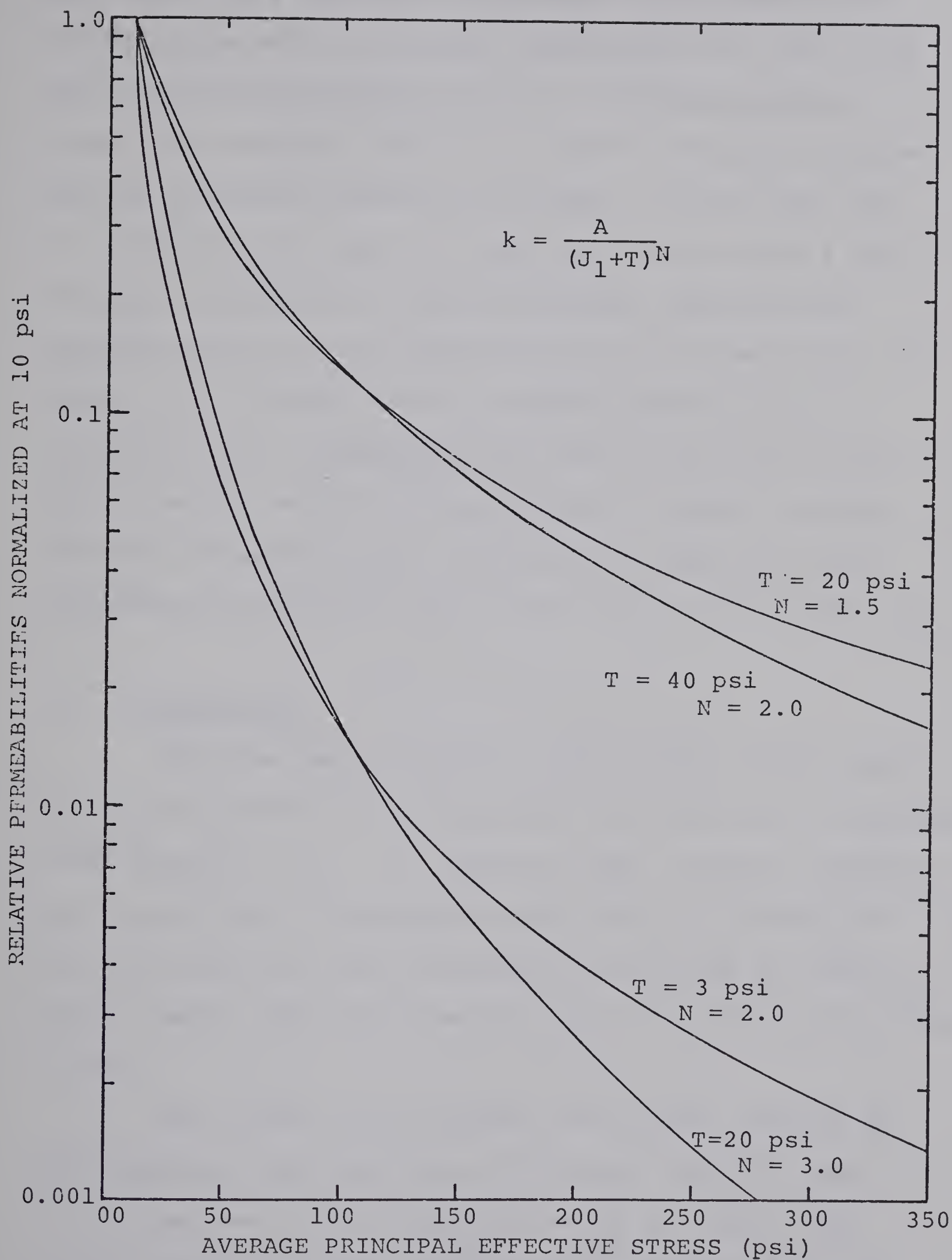


FIG. 3.23 CORRESPONDENCE FOR DIFFERENT PAIRS OF T AND N VALUES

combination of T and N will correspond approximately to another curve with a different combination of T and N and that this correspondence occurs in a certain pressure range. For example, with $N = 1.5$ and $T = 20$ psi a corresponding variation occurs in the range of 10-150 psi with $N = 2.0$ and $T = 40$ psi. It was found while doing a preliminary investigation that the pressure distribution depended mostly on the sensitivity of the permeability to stress. As a result for the seepage analysis it was decided to use a combination of T and N that would give a typical medium sensitive variation and a typical strong variation of permeability. The curves chosen are shown superimposed as dotted lines on the field data of Fig. 3.21.

3.5 Limitations

With the data at hand it would appear that a good first approximation of permeability variation can be obtained using equation (3.7). It should be kept in mind, however, that a multitude of assumptions were used in arriving at this conclusion and that alternative forms may be equally good. However this form does fit much data and is convenient to use.

Snow (1968a) has computed the minimum spacing of open fractures and found that from water pressure tests for 35 damsites from the surface to 200 ft. depth, the minimum spacing of open fracture increased from 4 to 14 ft. Setting $D = Bd+C$ in equation (3.4), the appropriate

equation to describe permeability may have the form

$$k = \frac{A}{(J_1 + T)^N (Bd + C)} \quad (3.11)$$

where d is depth

and B and C are constants

Since it was assumed that $J_1 = f(d, K_0)$, it can be seen from the form of equation (3.11) that this effect could possibly be incorporated in the values of T and N determined previously and may account for the group of very sensitive relations in Fig. 3.21. If a stress increase occurs equation (3.11) may be valid since no new fractures are formed and the existing ones become tighter. If a stress release occurs previously imperceptible and closed fractures will possibly open up so that equation (3.7) could be valid.

Although equation (3.7) was used for the analysis the form may be too compact. Besides using the average stresses shear effects have not been incorporated into the equation mostly due to the lack of data. For an area of high shear stresses where the shear strength is approached there would be a tendency of movement along the joints and fissures. A dilation effect would occur in the area of the fracture due to its roughness increasing the average width of the crack resulting in increased permeability.

Fig. 3.7 shows this effect in a sandstone (Mordecai and Morris, 1971). Therefore the results in Chapter IV would apply to materials which have no volume change with shear.

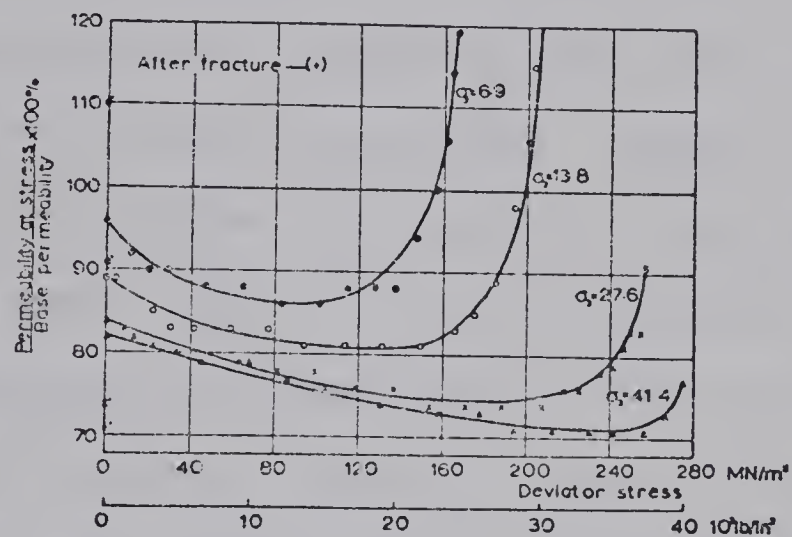


FIG. 3.24 EFFECT OF SHEAR ON PERMEABILITY
(AFTER MORDECAI AND MORRIS, 1971)

CHAPTER IV

RESULTS

4.1 Description of Cases Analyzed

As pointed out in Chapter II it was felt that the influence of stress dependent permeability would be most pronounced in a steep-walled excavation. Hence only one configuration of a 90° slope was studied. The influence of varying the slope angle may also reveal important effects.

For a configuration considered to have infinite base of depth H and infinite crest of slope of height H , Dunlop, Duncan and Seed (1968) have shown that negligible influence is felt in the area of the toe for an upslope boundary at a distance of $6H$ from the toe and a downslope boundary $3H$ from the toe. For theoretical seepage analyses in slopes, 4 times the net head or slope height from the toe to the full upstream head is a common boundary condition (Khan, 1971; Sharp, 1970). Also Kealy and Busch (1971) using their finite element seepage model have shown for a homogeneous isotropic embankment on a base with a depth approximately equal to the embankment height that a base to embankment permeability ratio of 0.1 yielded almost identical results to the case when the ratio was 0.001. Knowing that in the present case, the permeability decreases with depth in addition to having the preceding guidelines

in mind, one-half of a centre-line symmetric excavation as shown in Fig. 4.1 was chosen for the stress and seepage analyses. The 100 ft. slope height was chosen arbitrarily. This can also be a parameter to vary in future studies since unfortunately the results of this analysis cannot be normalized although they may be extended. Normalization is prevented because the permeability variation occurs in a particular stress range. However a substantial amount of the variation will occur for this slope height. As a result the effects may be magnified in order that the governing principles in these situations will be illustrated more clearly.

The stress grid shown has 483 nodes and 871 elements while the corresponding seepage grid below the free surface has 422 nodes and 755 elements. Triangular elements were utilized because a better approximation to the permeability variation can be obtained for the same number of nodes. For example, four nodes produce only one rectangular element whereas the same number produces two triangular elements. It is not the number of elements but the number of nodes that determines in large part the computation time.

The grid was designed on the basis of several considerations. In addition to a desire for detail at the toe, an adequate representation of the effect of the permeability values throughout the medium as discussed in section 2.5 is required. The grid design is also influenced by a desire to obtain a minimum value for a matrix quantity

STRESS GRID

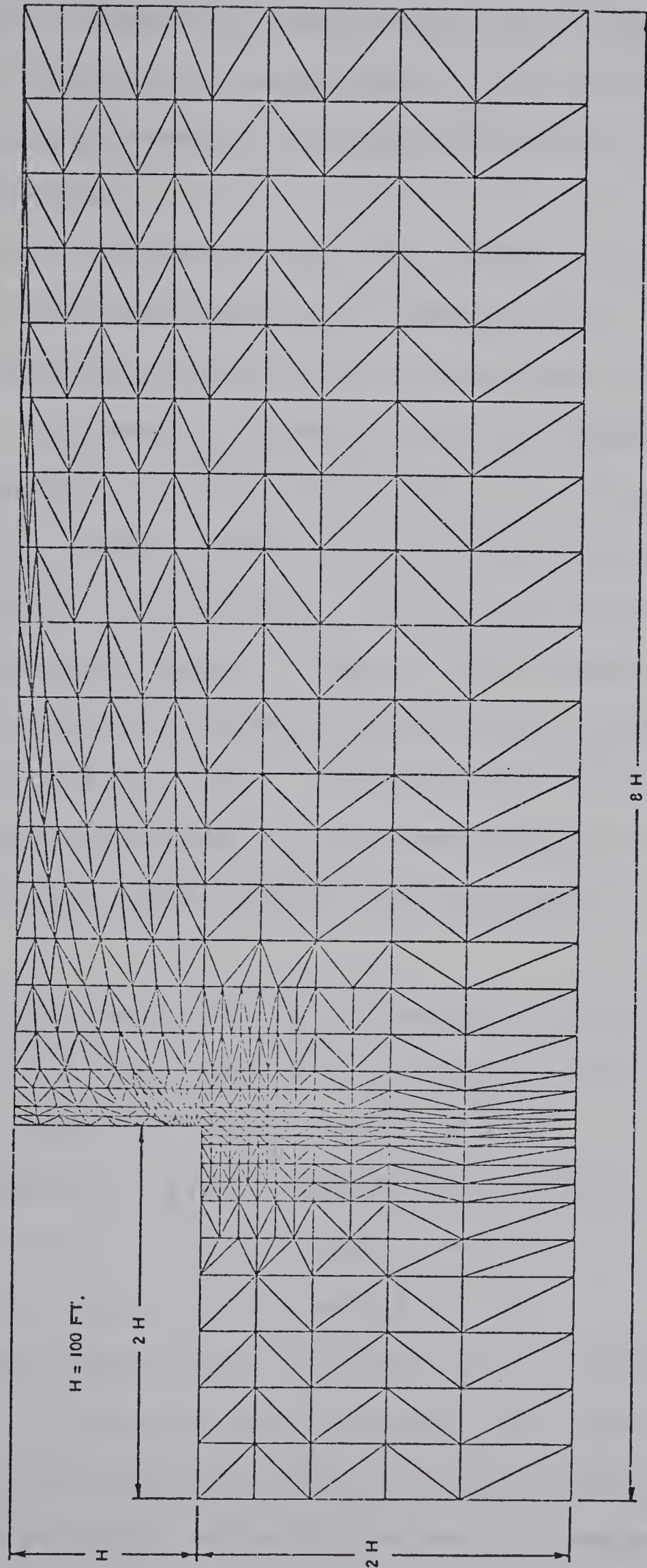


FIG. 4.1 GRID AND DIMENSIONS USED FOR ANALYSES

known as the "bandwidth" which evolves as a characteristic feature of the system of equations (2.21) and which affects the storage requirements and computation time in the finite element analysis.

It was decided to vary the initial insitu stress conditions with the variation in permeability. A simple K_0 initial effective stress condition was chosen as shown in Fig. 2.7b. In general however it must be remembered that finite horizontal stresses often occur at the surface for rock materials (Hast, 1967) and this may be another aspect to investigate in the future. It is common knowledge that changing Poisson's ratio, ν , in a finite element analysis causes only minor variations in the stress distribution. The modulus of elasticity, E , effects the displacements and has little effect on the stresses in plane strain.

The four cases studied and presented in section 4.3 are:

1. A medium sensitive field permeability relation, i.e., $T = 40$ psi, $N = 2.0$ and $K_0 = 0.5$.
2. $T = 40$ psi, $N = 2.0$ and $K_0 = 2.0$.
3. A sensitive field permeability relation, i.e., $T = 20$ psi, $N = 3.0$ and $K_0 = 0.5$.
4. $T = 20$ psi, $N = 3.0$ and $K_0 = 2.0$.

Since the pressure distribution is independent of the factor A in equation (3.7) a value was selected to yield equivalent permeabilities for both functions at 0 psi average principal effective stress for comparison

purposes. A value of 10^{-4} arbitrary permeability units (L/T) at 0 psi was chosen. This resulted in $A = 0.16$ for $T = 40$ psi and $N = 2.0$ and $A = 0.8$ for $T = 20$ psi and $N = 3.0$. Hence the two permeability functions shown in Fig. 3.21 and used for the analysis were

a. $K = 0.16 / (J_1 + 40)^2$

b. $K = 0.8 / (J_1 + 20)^3$

The seepage analysis was considered as a plane flow problem and the stress analysis was determined for plane strain conditions. The material properties were taken as
 modulus of elasticity, $E = 10^8$ psf
 Poisson's ratio, $\nu = 0.2$
 unit weight of rock material $\gamma_T = 165$ psf.

4.2 Computational Procedures

As outlined in section 2.6, to initiate the solution, one iteration of a seepage analysis was performed prior to the first complete cycle. An initial position of the free surface was chosen which would hopefully tend to accelerate the convergence of the subsequent cycle process. Homogeneous and isotropic permeabilities were used for the first iteration. The position of the free surface used for this iteration was always higher than the equilibrium value for the homogeneous and isotropic case and as a result the solution yielded negative pressures at and near the free surface nodes. The pressures throughout the medium were then used to compute the body forces for the stress analysis

of the initial cycle. The results of the stress analysis were used in turn to calculate the permeabilities. Hence these initial permeabilities were computed on the basis of an improper pressure distribution and a probable irregular location of the free surface. Even though this solution initiation procedure delayed cycle convergence it was a necessary part of the convergence process. The following cycles utilized pressure distributions which had been calculated in association with free surfaces where little excess negative or positive pressures usually existed.

A tolerance value of 0.1% of the slope height or net head was generally used to determine the free surfaces for each cycle. Since the final position of the free surface was not known the primary estimate was often far from an equilibrium value. Hence, at times for the initial cycles the tolerance value was not met since an inadequate number of iterations was occasionally specified. This tended to result in a requirement for additional cycles for cycle convergence. Because of initial difficulties due to poor element shapes and because of a lack of familiarization with cycle convergence behaviour, the specified number of iterations was not a constant and was sometimes inadequate as mentioned but in retrospect a value of 10 might have been ideal. However for cycle convergence the tolerances prescribed were always met for at least the last two cycles.

Usually the final free surfaces converged to an

equilibrium position requiring 4-8 cycles. For the initial cycles the stable free surface for each cycle tended to oscillate about the final equilibrium value. This oscillating behaviour was weak for most cases. However, strong oscillating behaviour did occur for the sensitive permeability variation coupled with $K_0 = 2.0$.

For cycle convergence a movement criteria was used. If the change between the last two cycles performed for any one of the nodes on the free surface was less than approximately 0.1% of the slope height, the final free surface location was accepted. The case described with strong oscillating effects was accepted at 0.24% of the slope height after 9 cycles.

As a result of the slow convergence in some cases, an allowance was incorporated into the program for performing several cycles, examining the state of convergence and continuing the converging process after adjusting the free surface to the value found by the previous cycle. This procedure was accomplished in part by reading and writing the permeability values on a tape file.

An IBM 360/67 digital computer was employed for the calculations. The approximate duration of central processing unit time for the stress analysis of one cycle was 50 seconds and for one seepage iteration was 10 seconds.

For each analysis the relevant data was output on punched cards. In addition to the input data, element permeabilities, element stresses and nodal potential values

were among the more important data output. This information was used to plot equipotentials, permeability contours and average principal effective stress contours.

An interpolation and plotting program was written to reduce the output seepage data and plot the equipotentials and the final grid shape. A listing is given in Appendix C.

Each equipotential plot results from characteristic permeability variations. Contours of equal permeability were initially attempted to be output using a library contouring program but it gave extremely poor results due to an uneven density of points within the grid boundary. As a result the equipotential plot program was modified to compute the average nodal permeability, calculate and plot selected contours of equal isotropic permeability. A similar procedure was used to output the contours of the average principal effective stresses.

4.3 Results of Analyses

Results are presented for the cases listed in section 4.1 in Figures 4.3 to 4.6. For each case the equipotential distribution represented by contours in percentages of the total head, selected contours of isotropic permeability and the related contours of average principal effective stress are presented. Fig. 4.2 gives the equipotentials in a homogeneous medium for comparison. A comparison of the free surface locations are presented in Fig. 4.7.

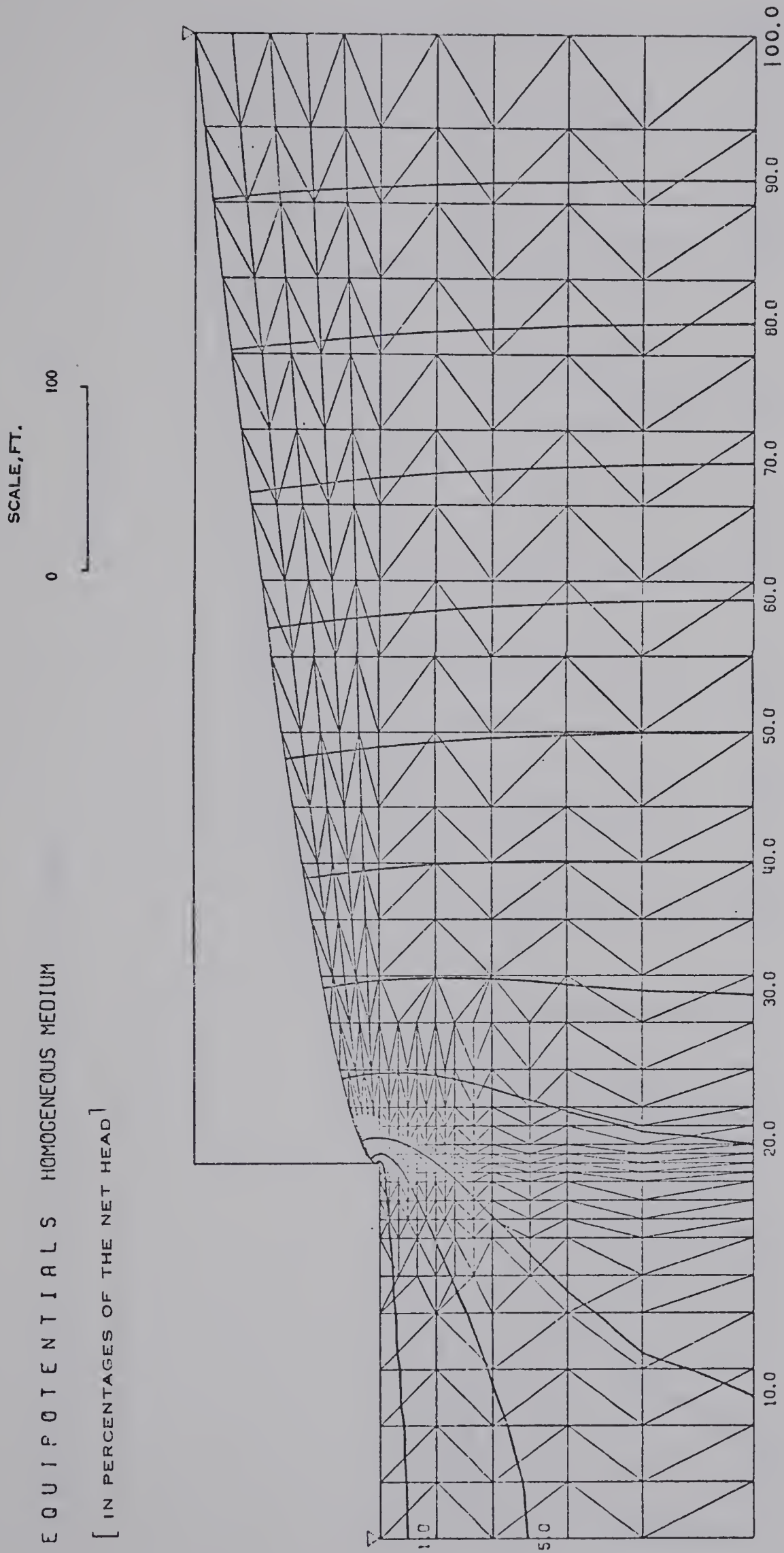


FIG. 4.2 EQUIPOTENTIALS IN A HOMOGENEOUS MEDIUM

EQUIPOTENTIALS WEAIR VARIATION $K=0.5$ 402368

[IN PERCENTAGES OF THE NET HEAD]

SCALE, FT.

0 100

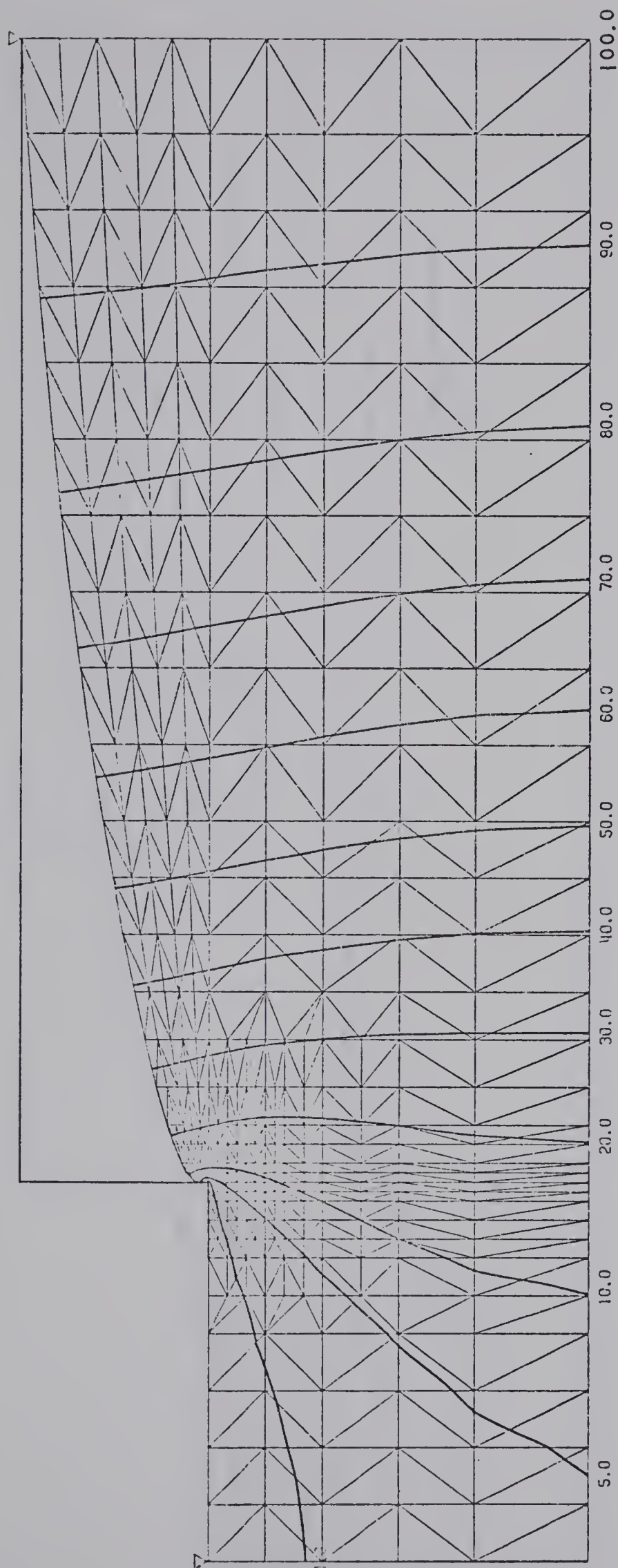


FIG. 4.3a EQUIPOTENTIALS, $T = 40$ PSI, $N = 2.0$, $K_O = 0.5$

SCALE, FT.

0 100

PERMEABILITY CONTOURS $K=0.5$ WEAVER VARIATION 402388

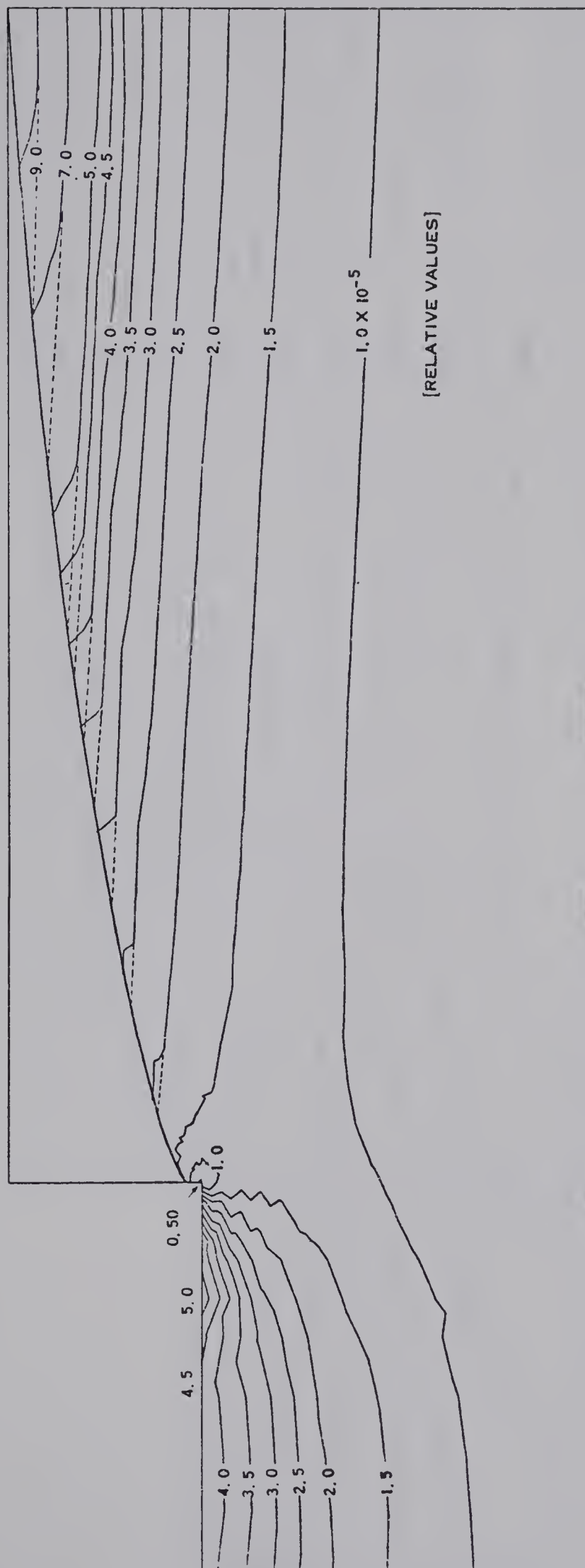


FIG. 4.3b CONTOURS OF ISOTROPIC PERMEABILITY, $T = 40$ PSI, $N = 2.0$, $K_O = 0.5$

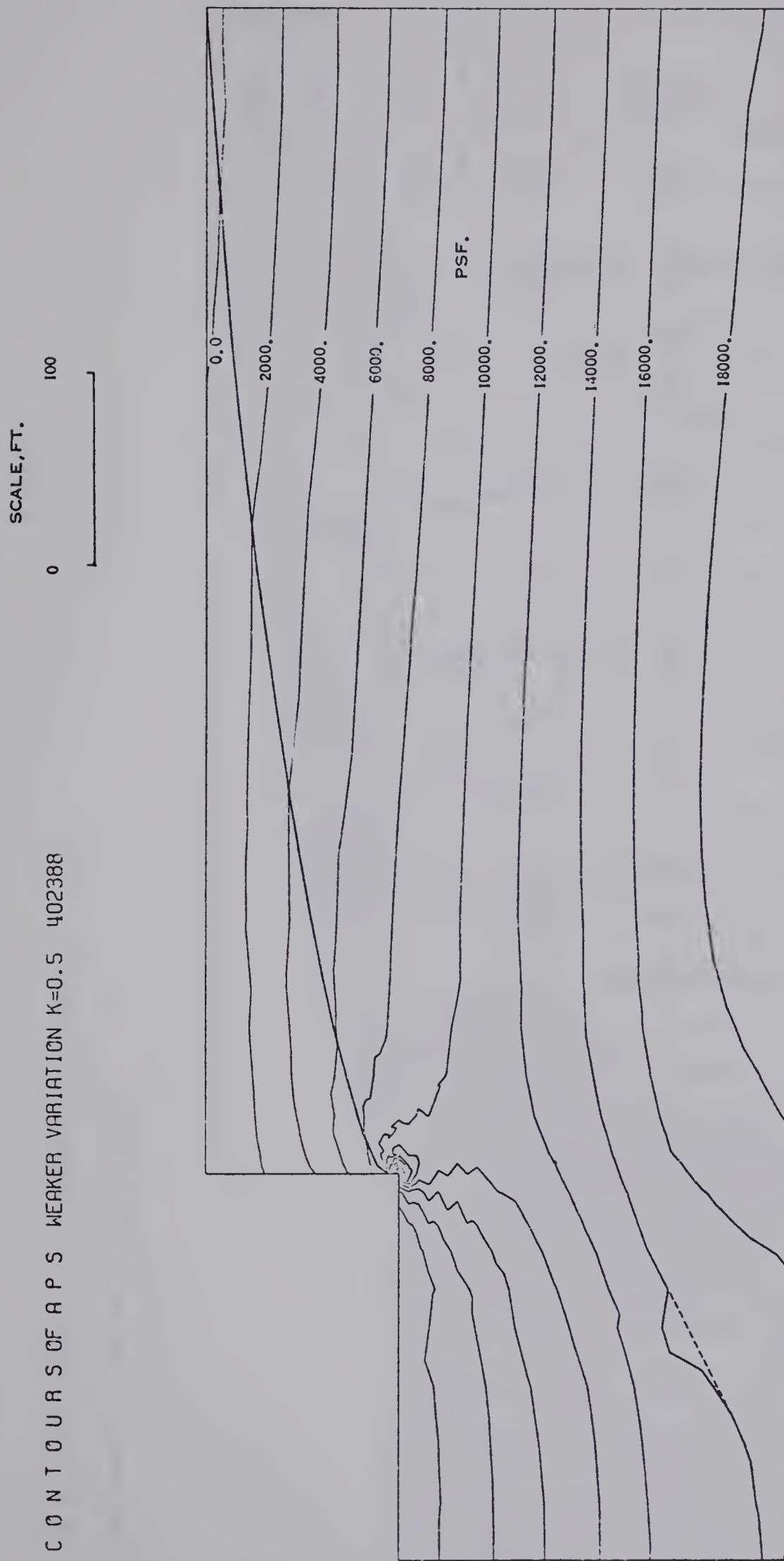


FIG. 4.3c CONTOURS OF AVERAGE PRINCIPAL EFFECTIVE STRESS, $T=40$ PSI, $N=2.0$, $K_0=0.5$

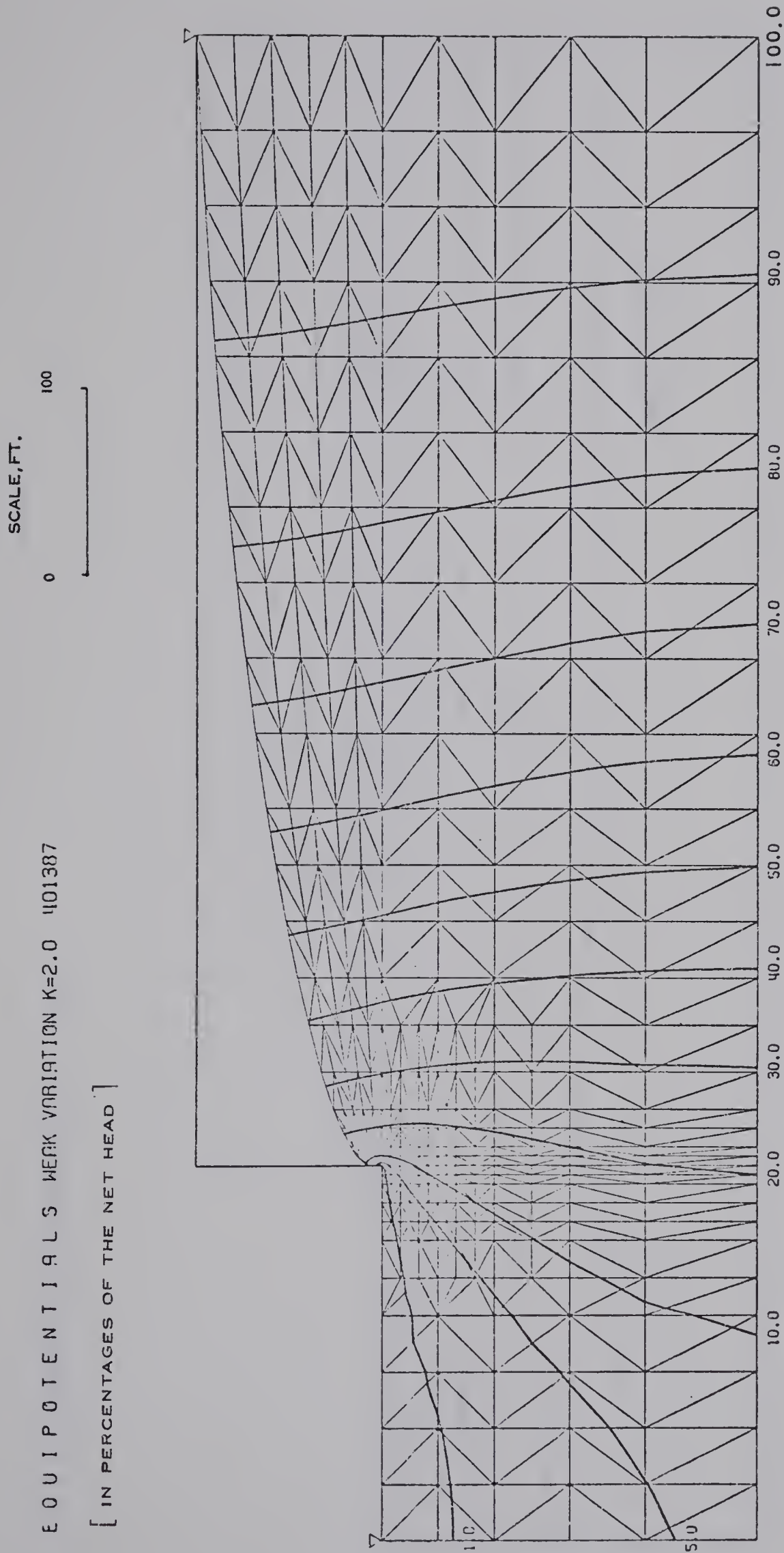


FIG. 4.4a EQUIPOTENTIALS, $T=40$ PSI, $N=2.0$, $K_O=2.0$

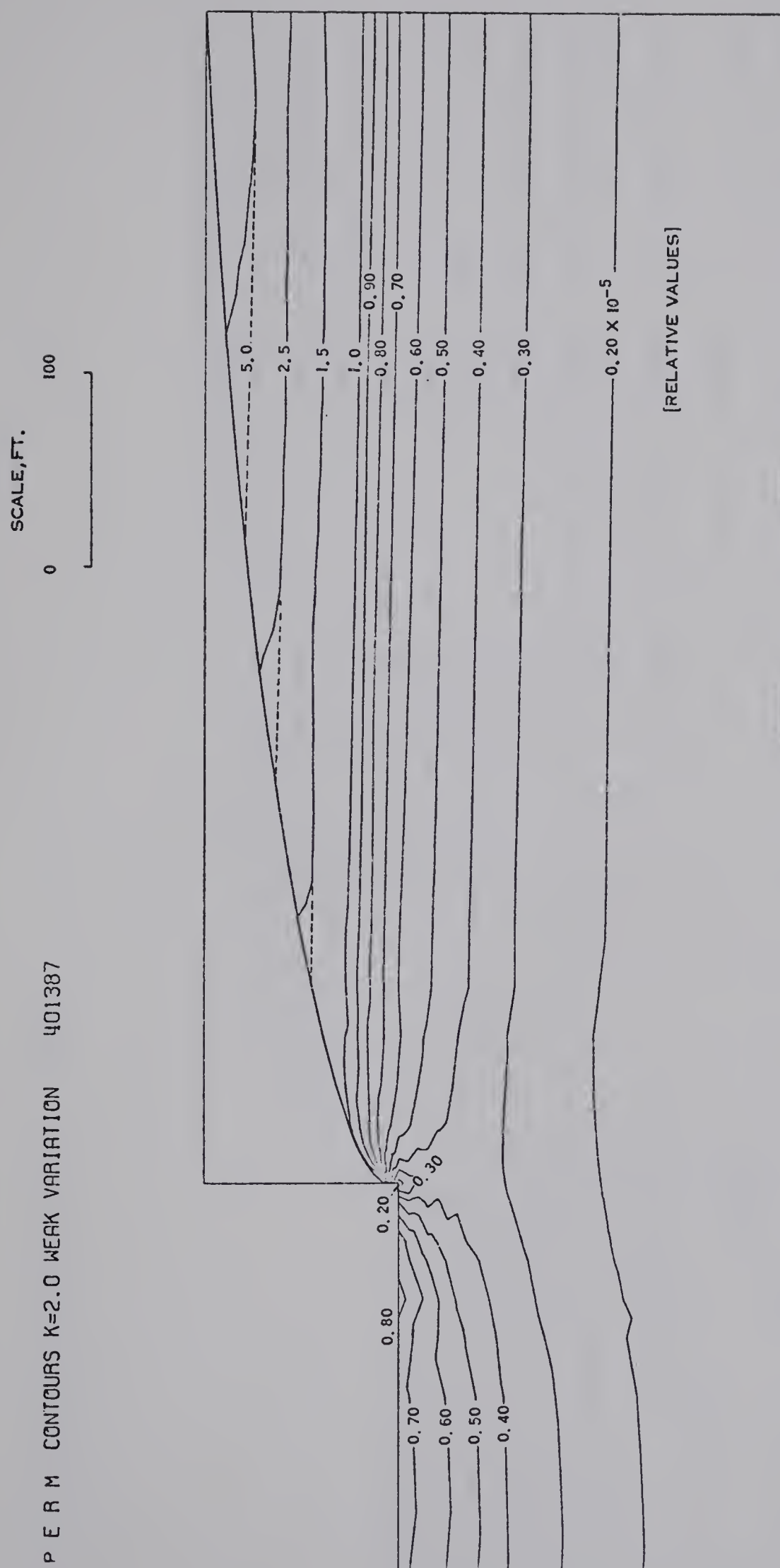


FIG. 4.4b CONTOURS OF ISOTROPIC PERMEABILITY, $T=40$ PSI, $N=2.0$, $K_O=2.0$

SCALE, FT.



A P S CONTOURS $K=2.0$ WEAK VARIATION 401387



FIG. 4.4c CONTOURS OF AVERAGE PRINCIPAL EFFECTIVE STRESS, $T=40$ PSI, $N=2.0$, $K_0=2.0$

EQUIPOTENTIALS STRONG VARIATION $K=0.5$ 404447
 [IN PERCENTAGES OF THE NET HEAD]

SCALE, FT.
 0 100

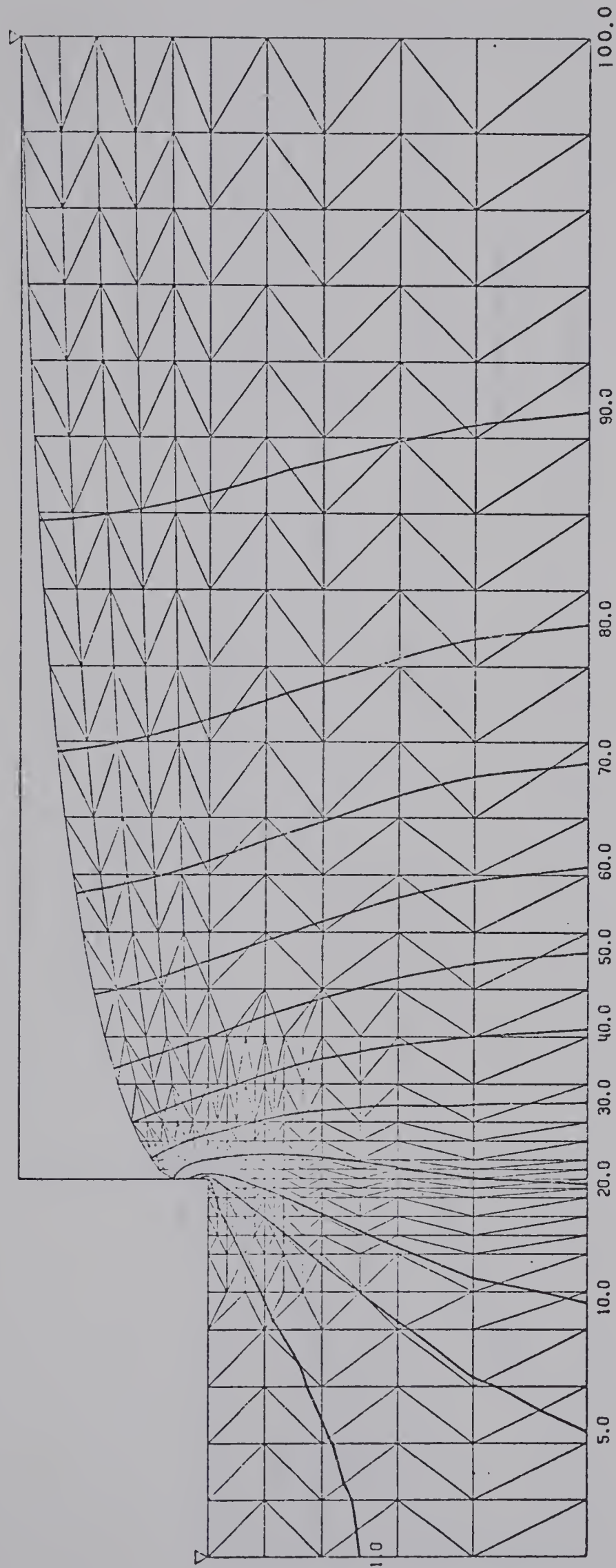


FIG. 4.5a EQUIPOTENTIALS, $T=20$ PSI, $N=3.0$, $K_O=0.5$

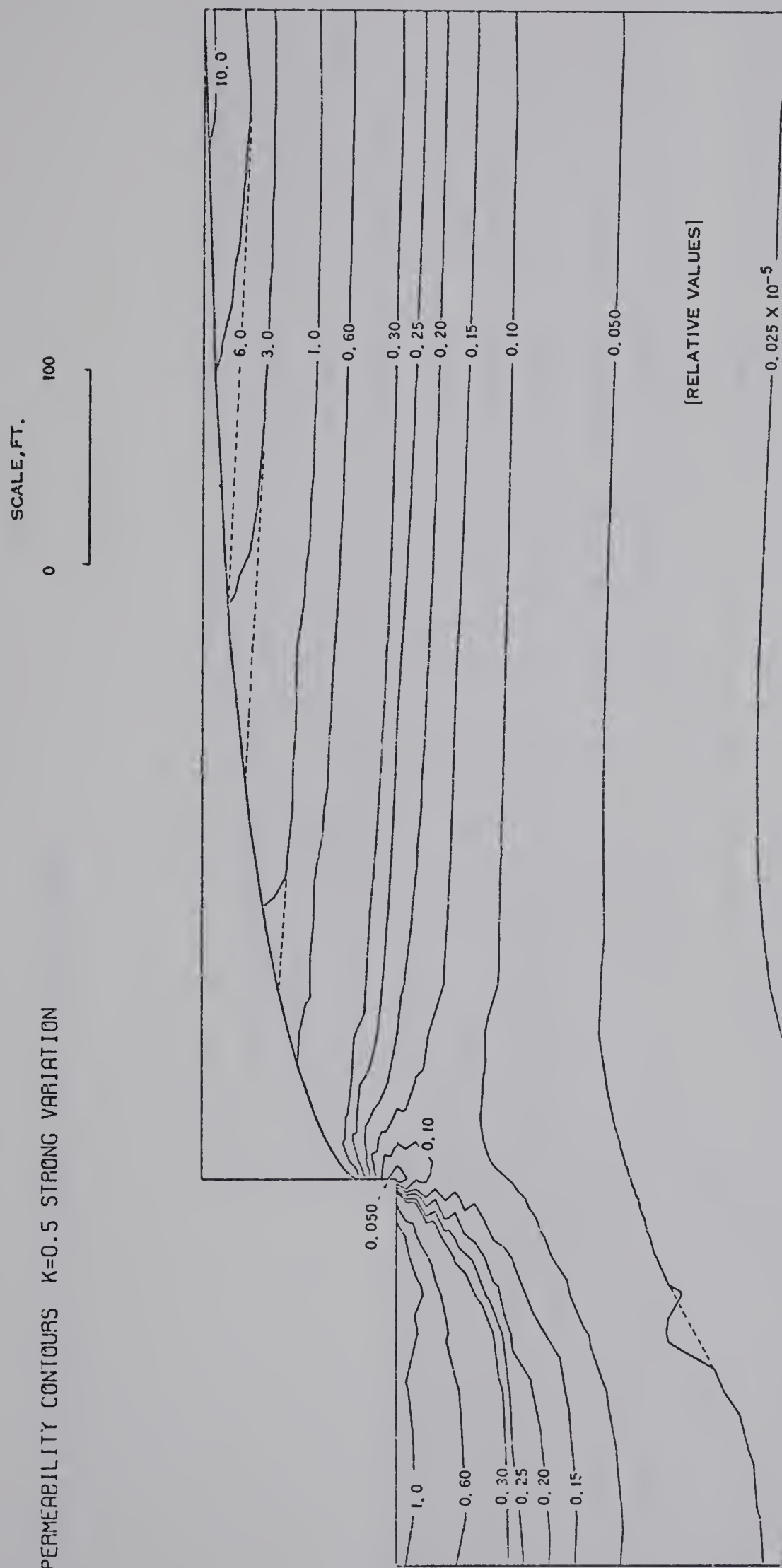


FIG. 4.5b CONTOURS OF ISOTROPIC PERMEABILITY, $T=20$ PSI, $N=3.0$, $K_O=0.5$

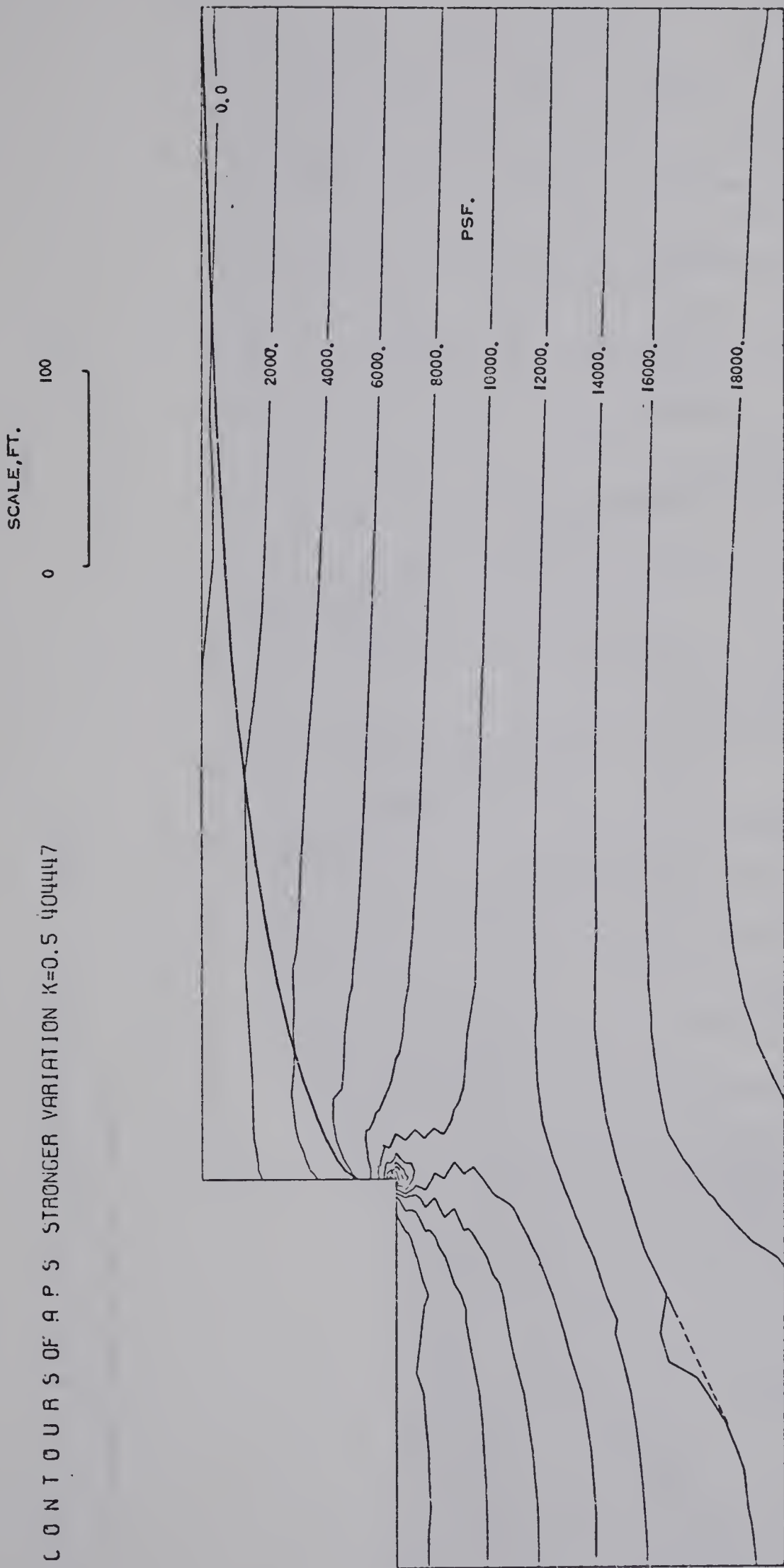


FIG. 4.5c CONTOURS OF AVERAGE PRINCIPAL EFFECTIVE STRESS, $T=20$ PSI, $N=3.0$, $K_O=0.5$

EQUIPOTENTIALS STRONG VARIATION $K=2.0$ 406634

[IN PERCENTAGES OF THE NET HEAD]

SCALE, FT.

0 100

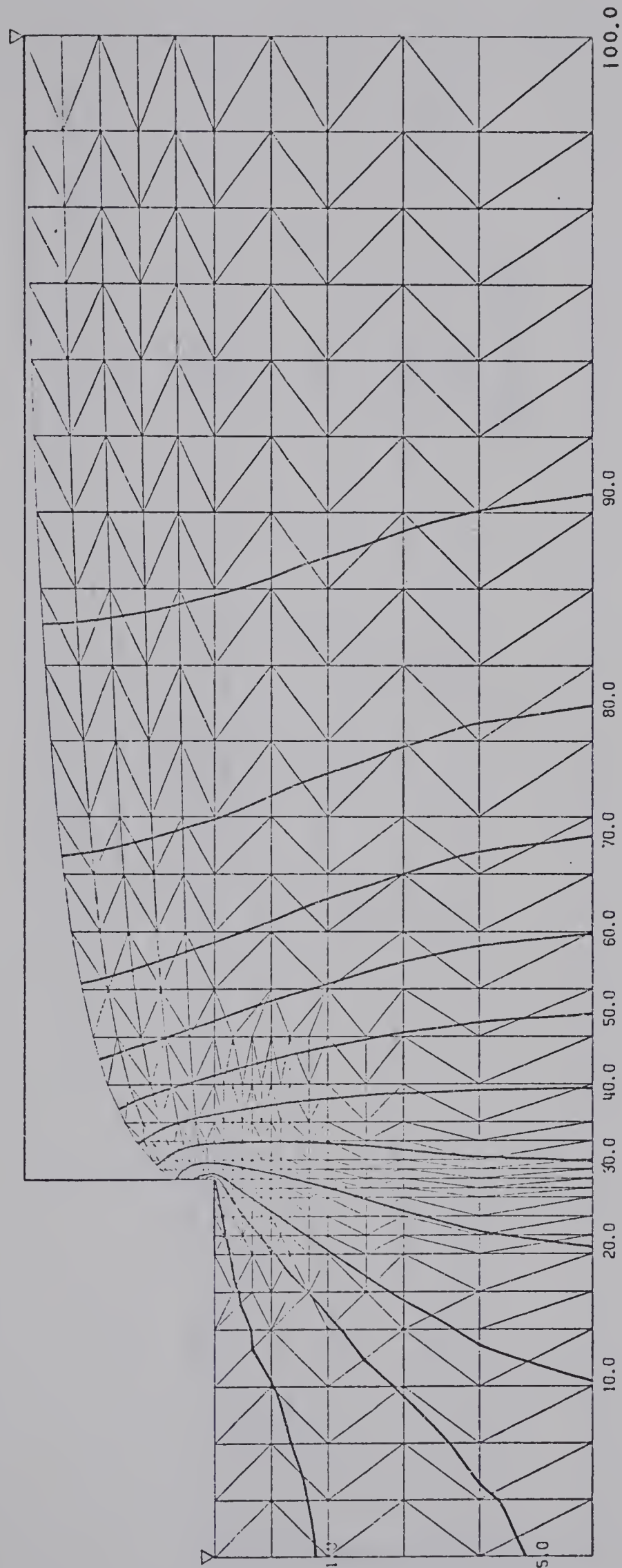


FIG. 4.6a EQUIPOTENTIALS, $T=20$ PSI, $N=3.0$, $K_O=2.0$

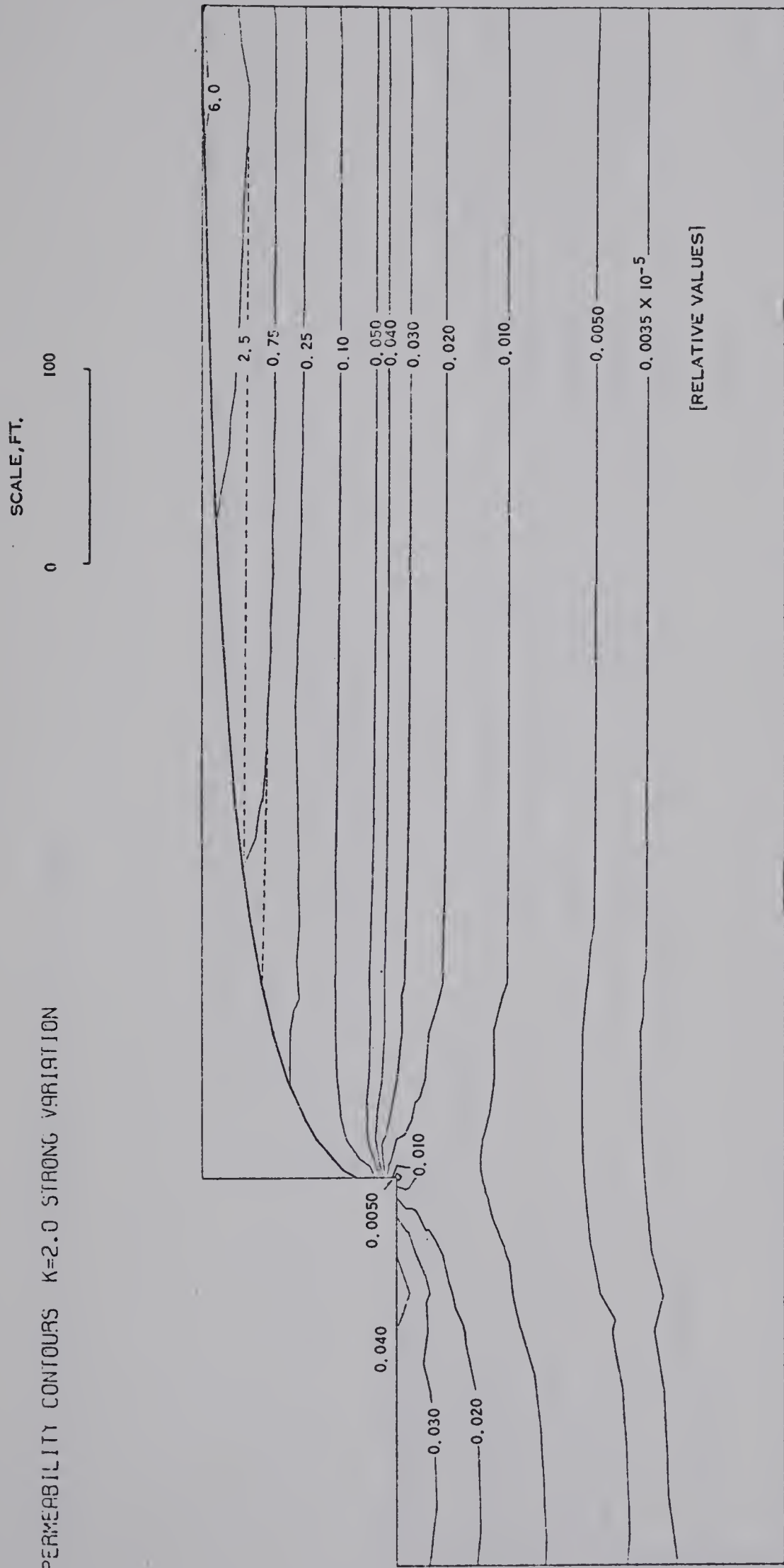


FIG. 4.6b CONTOURS OF ISOTROPIC PERMEABILITY, T=20 PSI, N=3.0, K_O=2.0

SCALE, FT.
0 100

C O N T O U R S O F A P S S T R U N G V A R I A T I O N K=2.0 406634

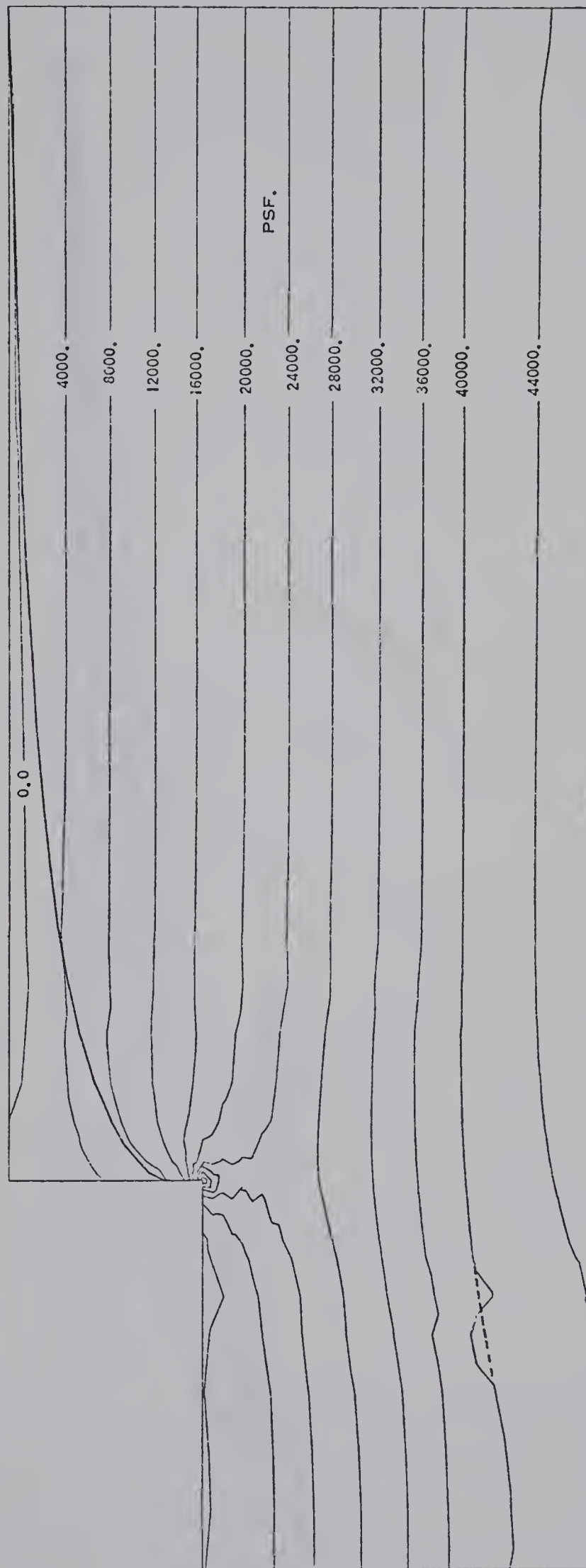


FIG. 4.6c C O N T O U R S O F A V E R A G E P R I N C I P A L E F F E C T I V E S T R E S S , T=20 P S I , N=3.0 , K_O=2.0



FIG. 4.7 COMPARISON OF FREE SURFACE LOCATIONS

To deduce the contour plots of stress and permeability, average nodal values were employed. These average values may give poor results under certain conditions. Each nodal value is computed directly by taking an average value of the surrounding elements. Cases where these averages do not give completely representative values at the nodes will occur when several of the elements attached to one node physically extend more in the direction of maximum change of quantity contoured than the other elements producing a weighted average. In other situations, an irregular number of elements may be attached to one node due to a boundary or because of grid design and may cause non-representative values. At a boundary the averaging procedure will be most affected when the contour is parallel to it and will be least affected when the contour is orthogonal to it. For example, when a contour approaches a boundary at a low angle poor results will occur yielding a type of refraction effect close to the boundaries. In contrast to these element averages, nodal potential values are derived directly from the finite element solution and have not been obtained through an averaging procedure. This will result in well defined values for the equipotentials and the free surface.

As a result of the averaging procedure somewhat improper or discontinuous values are obtained in the following areas of the contour plots:

- a. Within an element dimension from both the free

surface and the upper grid boundary in the stress plots.

- b. At the lower boundary of the stress plots and in some cases in the permeability plots where contours exist within an element dimension from the lower boundary.
- c. In the area of the toe and at an approximate location of a slope's height beneath the toe where a zig-zag feature of the contour lines occurs.

In some of these areas the proper value has been drawn in as a dotted line.

Characteristic features may be observed from the equipotential distributions. It is seen that the phreatic surface is higher for the more sensitive permeability function for both $K_0 = 0.5$ and $K_0 = 2.0$. In addition the phreatic surface is higher for $K_0 = 2.0$ than for $K_0 = 0.5$ in both cases. The fact that the permeability variations used have more influence on the free surface than the K_0 values used may also be noted. The equipotentials are more "S" shaped near the upstream boundary of the slope for both the more sensitive permeability function and the higher K_0 value.

In the contour plots of permeability and stress distinctive effects may also be noted. Since permeability contours are directly derived from the stress distribution, all observations made for the former will be applicable to the latter. For the higher value of K_0 the permeability

contours in the slope are flatter and appear almost horizontal while for the lower value the contours are at more of an angle but they too tend to become closer to horizontal towards the back of the slope. The permeability contours become straighter and more horizontal with depth in all cases although poor average nodal values may obscure this behaviour. Into the excavation, away from the face and down from the floor, the permeability contours become more horizontal for all cases.

Interesting results are observed in the region of the toe. In all cases there is an area of low permeability in this vicinity. For $K_0 = 2.0$ this area extends a distance directly beneath the toe while for $K_0 = 0.5$ the area of lower permeability extends down as well but more into the slope than for $K_0 = 2.0$. This area of low permeability is less pronounced for $K_0 = 2.0$ than for $K_0 = 0.5$. Also at the toe, away from the face, and below the floor an average principal stress decrease occurs from the original value with a greater effect occurring for the lower value of K_0 .

With the higher K_0 value, essentially a log type of decrease in permeability occurs with depth. As well as this decrease, for $K_0 = 0.5$ permeabilities also become lower when progressing in position from inside the slope to the face. Furthermore, the higher K_0 case has an area of greater permeabilities directly above the region of low permeabilities at the toe since a decrease in stress occurs here. However, for $K_0 = 0.5$ little of this effect appears

to occur above the toe. It is of interest to note that an increase in curvature of the free surface is observed in this area for $K_0 = 2.0$ compared to $K_0 = 0.5$. In addition the exit points approximately coincide for the sensitive relation and are in close proximity to each other for the medium sensitive relation.

A permeability of 10×10^{-5} arbitrary units should occur at the surface at the back of the slope if the average principal stress is zero. The program results reveal an area of tension here (which may be due to the boundary condition at the back of the slope) and consequently will cause greater permeabilities than 10×10^{-5} arbitrary units. This effect is more pronounced for the low K_0 cases but is somewhat obscured by poor nodal values at this upper boundary.

It is of merit to observe that only minor characteristic differences may be distinguished in the permeability contours between the results of the two sensitivities used for similar values of K_0 .

In the stress plots, the contours above the free surface appear more closely spaced than below it. This is a reflection of the total unit weight of material acting above the free surface and the buoyant unit weight acting beneath it.

CHAPTER V

DISCUSSION AND CONCLUSIONS

5.1 Discussion

It is somewhat unfortunate that the results presented for the iterative procedure have not or could not be compared to any existing solution, field situation or experimental setup. The solutions will have to be accepted on the merit of the following. The basic approach of the iterative method is simple and the consequent results seem entirely reasonable. Also the finite element method in general has proven itself many times and in addition the particular seepage program used was checked against a close form solution as shown in Chapter II.

The results of section 4.3 illustrate the principles or mechanisms involved in the location of the free surfaces. In conjunction with the effect of the sensitivity of the permeability function, there appear to be three major mechanisms involved in raising the free surface with different combinations being accentuated under different initial stress conditions. Firstly there is a continuous decrease in permeability with depth away from the face. In all cases as the distance into the slope from the face increases the permeability contours become increasingly more level and in the limit will be completely horizontal

with an associated uniform decrease in permeability with depth due to increased overburden stresses. Secondly, an area at the toe exists which has relatively lower permeabilities than the surrounding region due to the stress concentration. This area has a downward component from the toe under all conditions and a horizontal component into the slope under conditions of low initial stress. Thirdly a decrease in permeability occurs on a horizontal path in the slope towards the face as the contours are sloped up due to the excavation towards the toe and face. In cases of low K_0 this effect is greater than for high K_0 . All three mechanisms are dominant to some extent with all effects appearing influential for low K_0 . As the initial stresses increase the first mentioned effect becomes more dominant than the following two in influencing the pressure distribution. It would appear that any other mechanisms if they do operate are of limited importance in keeping up the free surface. Fig. 5.1 illustrates the mechanisms.

Stress release influences the pressure distribution to varying degrees in two distinct areas. Stress release occurs away from the toe and in the excavation but this has little effect since most of the head loss has occurred prior to this region. It does appear however for cases with high K_0 's that stress release may have some influence on the free surface location at and towards the face. A comparison of these areas in Fig. 4.7 shows for the two

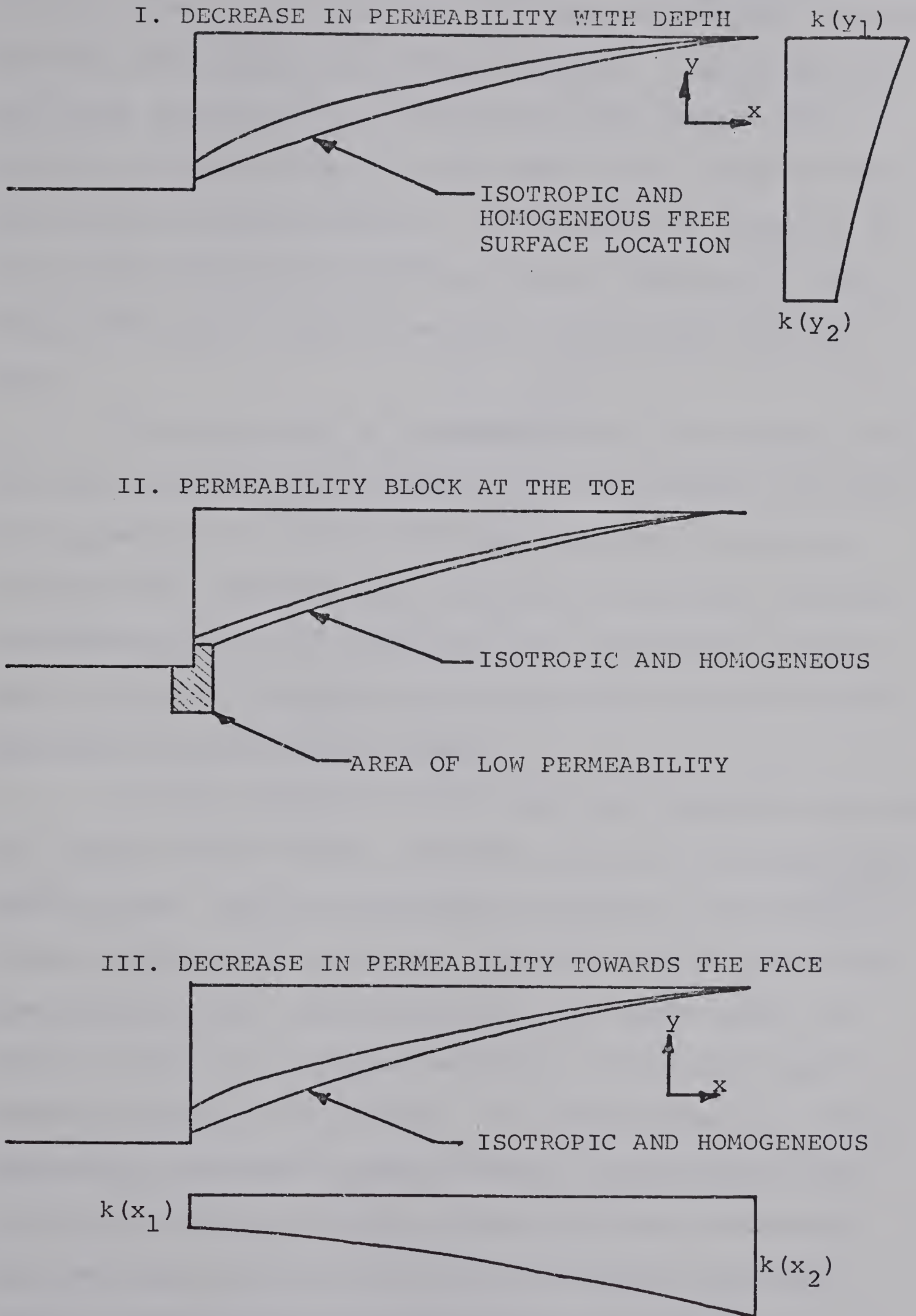


FIG. 5.1 MECHANISMS WHICH INFLUENCE THE FREE SURFACE LOCATION

initial stress conditions for the same permeability function that the exit points are almost identical. The effect for the lower sensitivity is less because the entire free surface and flow regime is lower and farther removed from this area of stress release. The release has resulted in increased curvature of the free surface towards the face with resultingly steeper gradients toward this vertical wall.

The major area of permeabilities in the slope which then may be important in determining the pressure distribution appears to be behind the face and above a position somewhat down from the toe. If this is true the variation in permeability in this area may be a controlling factor and an important variable in studying the effect of stress dependent permeability in slopes.

A fixed location for the upstream boundary condition was chosen for the study. However, climatic factors in the hydrological cycle as discussed in Chapter I will profoundly affect this condition. Terzaghi (1962) shows how precipitation and runoff may affect the water table, as shown in Fig. 5.2, in close proximity to the face due to tension cracks at the surface. An area of tension in this section of the slope is most clearly illustrated in Fig. 4.6c in an indirect fashion. This additional mechanism may then compound the effects of an already high water table in undermining the stability of the slope.

(a) Location of lowest and highest water-table in jointed rock with uniform but low coefficient of permeability;

(b) water-table in the same rock during heavy rainstorms or snow melt if permeability in space a b c is much higher than elsewhere.

Line c d represents the water-table at times when the joints drain freely, and e'd', when they are plugged with ice.

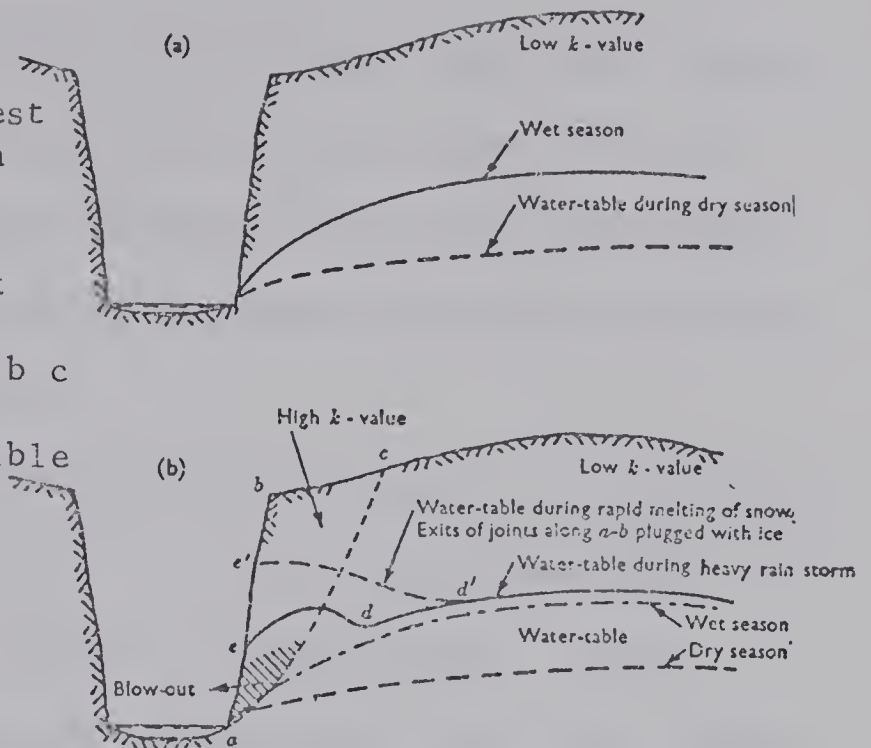


FIG. 5.2 CLIMATIC-INDUCED CHANGES IN THE CONFIGURATION OF THE WATER TABLE (AFTER TERZAGHI, 1962)

In this work an isotropic linear elastic analysis has been used and this linear isotropic property has been attributed to the rock. However, it is well known that non-linear properties occur in rocks due to the cracks and joints (e.g. Morgenstern and Phukan, 1966; Zienkiewicz and Stagg, 1967). Furthermore, from the crack behaviour shown in Fig. 3.2 it is evident that a non-linear stress-strain behaviour is also inherent in the rock material considered.

It may be argued that the non-linearity will not nullify the general principles exhibited here since this curvilinear behaviour commonly occurs in the lower stress ranges. The area surrounding the toe being the general area of concern may be considered to be out of the lower stress ranges with low range effects in other parts of the slope having minimal influence in the area of the toe.

Similarly it can be argued for consistency that the curves of Fig. 3.2 could be approximated by a straight line at higher stresses. Since many idealizations have been made in this work the inclusion of non-linear behaviour may be too much of a sophistication.

Related to the non-linearity discussed but separate from it is a possible increase in elastic modulus with depth (e.g. for soft rocks Meigh and Greenland, 1965). Again as a first approximation the modulus has been taken to be constant.

Isotropic rock properties have also been assumed in this work and it may be that anisotropic effects are important. However, Duncan and Goodman (1968) have analyzed a jointed rock representing it by an equivalent orthotropic continuum. They found that the assumed orthotropic nature did not give much different results from where the rock was assumed isotropic. Hence the assumption of isotropy appears to be very reasonable.

The results of this study are valid essentially for a slope height of 100 ft. These results may be extended however by realizing that a slope of a different height having a permeability relation that would produce the same permeabilities as for the 100 ft. slope would then be valid. Thus the results will hold for a whole series of permeability functions with the appropriate slope heights. For any slope height, h , the results will be valid for the following permeability relations:

$$k = \frac{A}{(J_1 + 0.4h)^2} \quad (5.1a)$$

$$k = \frac{A}{(J_1 + 0.2h)^3} \quad (5.1b)$$

It is seen that to arrive at the same pressure distribution in higher slopes a less sensitive relation is required and for lower slopes a more sensitive relation is required. It appears that the effect would be less for higher slopes with the sensitivities used and possibly more for lower slopes. Hence for any sensitivity there is a slope height where the effect will be a maximum since for lower slopes less relative variation occurs and it is the relative variations that cause the effects. A plot of exit point height against slope height would have the characteristic behaviour as shown in Fig. 5.3 and a family of curves could be obtained by varying either T or N or both in some manner.

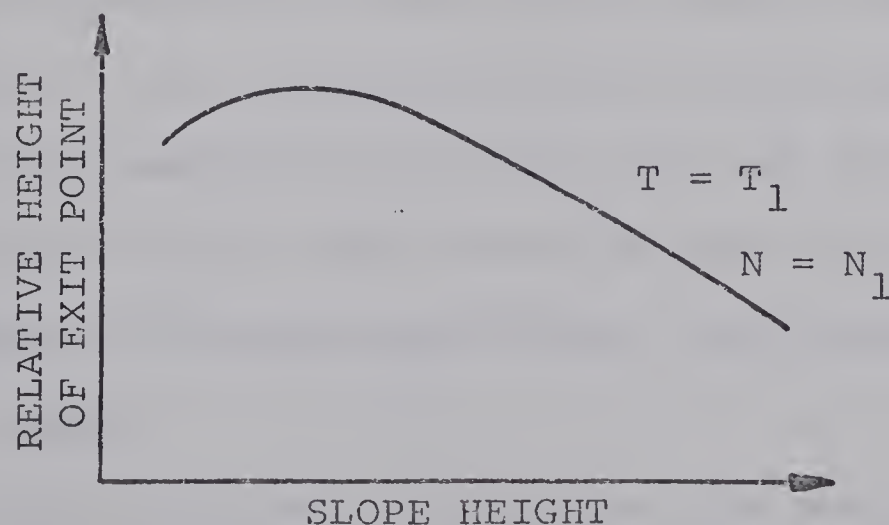


FIG. 5.3 PROPOSED CHARACTERISTIC RELATIONSHIP BETWEEN FREE SURFACE EXIT HEIGHT AND SLOPE HEIGHT

For a higher slope with a water table occurring below the surface with the same net head and upstream boundary condition as in this study and with the same permeability functions the elevating effect of the free surface would be less since all the stresses affecting the permeability will be shifted up causing the variation to be less.

The principles discussed initially will certainly be in operation for slopes with different geometric features. To assess the effect of decreased slope angle from this study is difficult, although this may possibly be facilitated by comparing the average principal effective stresses for such cases with the cases studied. It is likely that the mechanisms revealed here may predominate differently for different slope angles. This may also be the case for concave and convex shaped faces where lateral stresses will tend to become compressive or tensile. Related to the geometric configurations are the magnitude of the shearing stresses. In situations where shear affects the permeability the mechanism of low permeability at the toe may be neutralized. If the remaining mechanisms are not affected the least influence due to shear would be felt for the higher K_0 cases where this mechanism affects the pressure distribution the least.

It is of interest to note that the mechanism at the toe may be analagous to that controlling the emission of gas in coal mines (Patching, 1970). Gas is generated

in the coal due to the maturing process of the material. When coal is mined underground, the resulting hazards of fire, explosion or outbursts and suffocation are in existence. Stress concentrations in the coal near a face can be due to abutment loadings or due to the shape of the opening. These phenomena may reduce permeability so that high gas pressure gradients can exist near the faces of these areas. This damming effect in both the slope and the mine has detrimental effects on safety. A finite element analysis of the problem in this particular area of mine safety may prove fruitful.

In view of the preceding discussions it is felt that if these effects exist in rock slopes the stability of these slopes will be influenced to some extent by this behaviour. However the effect may often be obscured in the field due to the natural non-homogeneity of the material. In some cases the resultant pressure distribution may decrease the stability substantially and possibly should be considered among the factors which influence the stability of a slope. To describe the effect in a quantitative manner seems impractical in view of the typical non-homogeneity that occurs in nature. Nevertheless if such effects were to be taken into account in a stability analysis it would be required to perform an analysis similar to the one carried out in this work.

It is hoped that an extension of the simplified theory of section 3.2 to a more realistic approximation

using the individual stresses could be developed. Different joint distribution and properties should be taken into account (Parsons, 1966; Snow, 1968b) in addition to shear effects so that anisotropy as well as non-homogeneity may be considered. However lack of insitu permeability and stress data would hamper this development to some extent. In the event a more advanced theory is evolved, the program with its provision for determining the stresses at any orientation and facility for handling anisotropy could then be easily extended to encompass increasingly more realistic cases.

The inter-element configurations above and below the free surface may be seen in Fig. 2.10. This one grid was used for low free surface cases as well as high free surface cases. Low phreatic surfaces will cause an abundance of elements below the free surface at the toe and will produce a fine grid in this region. However, the coarser grid above the free surface at the face may affect the results in the finer mesh below this boundary but the effect, if any, is minimal. A comparison between the average principal stress contours of a case with a high free surface and a low free surface for a particular K_0 value show the same characteristic behaviour in the shape of the contours just above the toe. If effects do become significant however, in the present method this could easily be rectified by using a tailored mesh although the construction of a grid for this size of problem can become time consuming.

An alternative approach would be to develop a method involving a completely fixed stress grid. Pressures at the locations of the nodes in the stress grid could be found interpolating inside a seepage triangle after a search for this appropriate element. A special technique would then also have to be developed for distributing forces for the elements traversed by the free surface. The body forces would be assigned again according to equation (2.38). The search routine would be required once more for locating the centre of a seepage element in the appropriate stress element with subsequent interpolation in the stress element being necessary if average nodal stresses were used. The permeability could then be assigned and the method continued as described in Chapter II.

5.2 Conclusions

The present stage of development of the computer program was adequate to analyse the basic configuration of excavation studied. When required the program may be easily extended to encompass shear and anisotropy effects.

For the excavation, the free surface location is influenced by the state of initial ground stress and the variation of permeability. With both increasing sensitivity of the permeability function and increasing values of the initial horizontal stresses the phreatic surface rises above the location for a homogeneous isotropic medium for the cases studied. The general increase in elevation of

the free surface location is a result of three basic types of permeability variations which operate to varying degrees. Firstly a decrease in permeability occurs with depth. Secondly an area of low permeability exists at the toe and thirdly a decrease in permeability occurs on a horizontal path from inside the slope towards the face.

The influence of excavation stress release causes a decrease in the average principal stress values from the original values. Two distinctive areas influence the pressure distribution to varying degrees. These areas occur at a location in the excavation away from the toe and at a position above the toe.

If the free surface behaviour is not wholly negated by the assumptions used at arriving at it, the effects of stress dependent permeability may in some cases have significant influence in decreasing the stability of rock slopes.

PART TWO

CHAPTER VI

THE UNIVERSITY OF ALBERTA MULTISTAGE DOUBLE PACKER PIEZOMETER

6.1 Introduction

Part II now deals with the measurement of water pressures in the field while Part I has dealt with the prediction of seepage behaviour and the associated pressures. Measurements in the field continue to play an important part in estimating and monitoring the stability of soil and rock slopes.

Many types of piezometer designs are in existence today. All piezometer systems in use currently may be broadly categorized into open standpipe systems or closed systems. In addition, closed systems may be of hydraulic or diaphragm design.

Before a general description is given it should be noted that all piezometer systems must be sealed into place. The pressure measured should be comparable to the actual pressure at the location if no piezometer installation had been made. The systems may be sealed in a permeable layer or a homogeneous material which could be part of a larger stratum. Vaughan (1969) has analyzed these two situations for a single piezometer installation to determine the

effects of grout permeability on piezometer measurement.

Open standpipe systems tend to be simple in design. They often consist of a porous intake tip customarily surrounded by a sand filter. The intake section is connected to a standpipe which rises to the ground surface. A change in pressure at the tip will cause flow in or out of the system until equilibrium is reached with the column of water in the standpipe. The measured head of water above the tip gives the pressure at this point. For relatively pervious soils open standpipe piezometers tend to function adequately. Casagrande (1949) developed a system incorporating a large filter intake with a small diameter standpipe. A bentonite soil was used to seal the device in place. With soft soils, some designs can be pushed into the ground with the hope that it is self-sealing. The Geonor type (Bjerrum et al, 1965) operates in this manner.

Hydraulic piezometers commonly consist of a porous tip connected to a manometer or Bourdon gauge by one or two tubes. The flushing of air out of the system is facilitated by the use of two tubes. Because of the nature of the system and its use in partly saturated soil, air often forms in it. Where it is desired a rapid response is registered when a change in pressure at the tip occurs. A much slower response will be noted for air in the system. The pressure at the tip is obtained by the addition of the measurement at the surface to the net head of water between the tip and the gauge. This piezometer type is used mostly

in embankments and shallow foundations. Examples of these closed hydraulic systems are the United States Bureau of Reclamation plastic tip piezometer for embankments and the Bishop piezometer (Bishop et al., 1963).

Diaphragm piezometers consist essentially of a cylindrical housing with a diaphragm at one end. A porous stone separates the diaphragm from the activating water stress. The pressure is measured basically in two ways. In one system the diaphragm acts as a valve. The diaphragm is shut by external water pressure and opened by internal fluid pressure. To take a reading the internal pressure is continuously increased. A monitored quantity of either pressure or volume measured through a return tube will reveal when the valve opens. At this point the pressures on both sides of the diaphragm are balanced and the activating pressure can be read at the surface. Among others, air activated diaphragm systems have been used (Warlam, 1963). With the other method an electrical conductor is used to communicate the amount of deflection of the diaphragm to the surface. The electrical currents can be converted to pressure by a previously determined calibration curve. To sense the pressure on the diaphragm electrical piezometers may have vibrating wire mechanisms (Scott and Kilgour, 1967) or strain gauge mechanisms (Lundgren, 1966).

Upon installation of electrical instruments, measurements may often be conducted in a simple and efficient manner. Vibrating wire devices operate on the principle

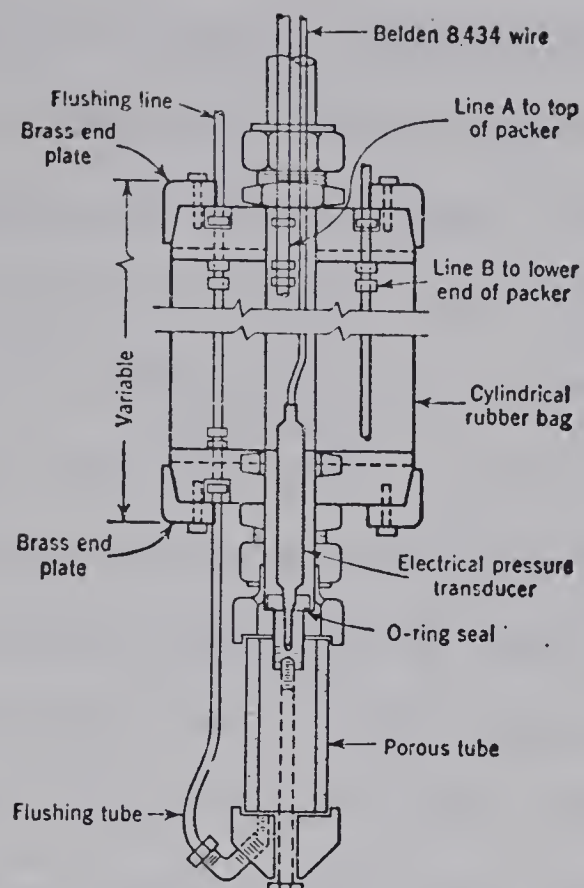
that the natural frequency of a stretched wire is dependent on the tension in the wire. To obtain a reading a stretched wire attached to the diaphragm in the instrument is activated by an electro-magnet. Sensors in the instrument then pick up the frequency. An electronic system at the surface monitors the frequency which is consequently related to pressure by a calibration curve. Transducer piezometers commonly use electrical strain indicators to gauge the pressure on the diaphragm. Upon deflection of the diaphragm an electrical resistor mounted on it changes its electrical conductivity. The resistances of the transducer and strain indicator combine in circuit so that a wheatstone bridge is developed. As a result the strain indicator resistance reading can be converted to pressure by a calibration curve.

One important factor influencing the acquisition of pore pressure data is a measurement time lag (Hvorslev, 1951). This time lag is dependent on the permeability of the soil, the shape and size of the intake and the volume factor of the system, i.e., the volume of water which must flow to or from the system for a unit change in pressure. Where quick response times are required for rapid determination of pressure or where the low permeability of a soil may cause excessively long response times it is desirable to have small volume factors. In general diaphragm piezometers have this characteristic. The most convenient diaphragm system from the standpoint of measurement is an

electrically operated piezometer. Since the costs of these electrical units in the past have been somewhat excessive as well as the fact that diaphragm systems tend to be unreliable for very long periods of time (Lindberg, 1965), many of these types have been developed to be retrievable (e.g. Brooker et al, 1968).

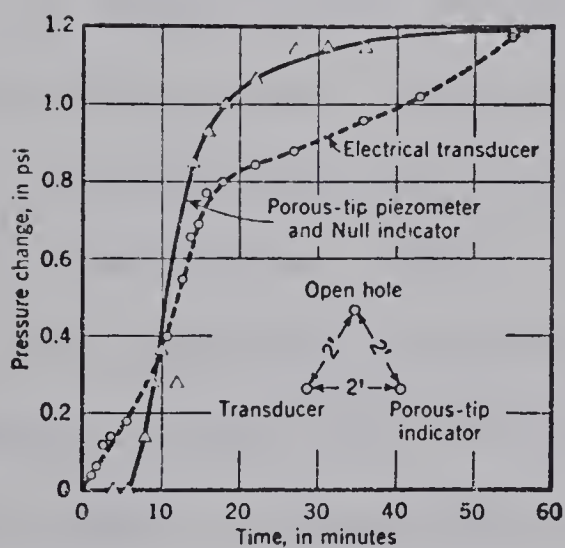
A recoverable transducer device has been designed as shown in Fig. 6.1a which is installed directly into a drilled hole (Lundgren, 1966). It is sealed by means of an inflatable rubber bag. The bag is filled with water by admitting water through line B as shown on Fig. 6.1a and allowing air to escape through line A. When the water in the bag is placed under pressure the piezometer will be sealed under proper conditions at the desired elevation. A comparison between the response times of this device and a porous-tip piezometer with a null indicator is given by Lundgren and shown in Fig. 6.1b. The two piezometer systems were installed in a clayey soil at a depth of 16.5 ft. The water table was originally 5 ft. from the surface. A third borehole had been drilled so that each of the three holes formed the corner of an equilateral triangle with 2 ft. sides. The effect measured resulted from lowering the water level 10.5 ft. in 22 minutes. The results reveal an apparently sensitive system.

A device similar to the one described previously was developed by the University of Alberta in co-operation with the Geological Survey of Canada (Brooker et al, 1968).



Recoverable electric piezometer has been developed for use in the field, to provide greater accuracy, easier installation, and more rapid response.

FIG. 6.1a BOREHOLE PIEZOMETER



Comparative sensitivity of electrical transducer versus porous-tip piezometer and null indicator is shown. Effect measured was lowering of water level in an adjacent open borehole 10.5 ft in 22 min.

FIG. 6.1b RESPONSE BEHAVIOR

FIG. 6.1 BOREHOLE PIEZOMETER AND RESPONSE CHARACTERISTICS (AFTER LUNDGREN, 1966)

Known as the UA-GSC transducer piezometer, it is shown in Fig. 6.2a-i and is intended as an instrument for measuring pressures in impermeable clay shales. In this method a 4-6 in. hole is drilled. A well point is attached to the end of a 1½ in. I.D. galvanized iron pipe of borehole length and lowered into the hole to the required depth. A sand filter is installed around the wellpoint and a cement or clay grout is placed immediately above the filter sand to provide the required seal. This installation in the borehole is shown in Fig. 6.2a-ü. The piezometer is lowered to the well point and the packers are inflated using an air reservoir. The instrument will be sealed into the desired area when the rubber packers expand against the walls of the iron pipe. A comparison of response curves between the device and an open standpipe is given by Brooker et al and is shown in Fig. 6.2b.

Another system, ingenious in design and somewhat different from the previous two models has been fabricated for use in rock (Londe, 1971). The transducer instrument is known as a continuous borehole piezometer. A borehole is permanently lined with a continuous flexible rubber membrane as shown in Fig. 6.3a, closed at the bottom and fitted at the top with a pressure lock. The membrane is filled with water so that the pressure at all points in the membrane will be greater than the surrounding pressure in the rock. This results in a seal against the rock for the entire length of the membrane. A measuring probe shown in

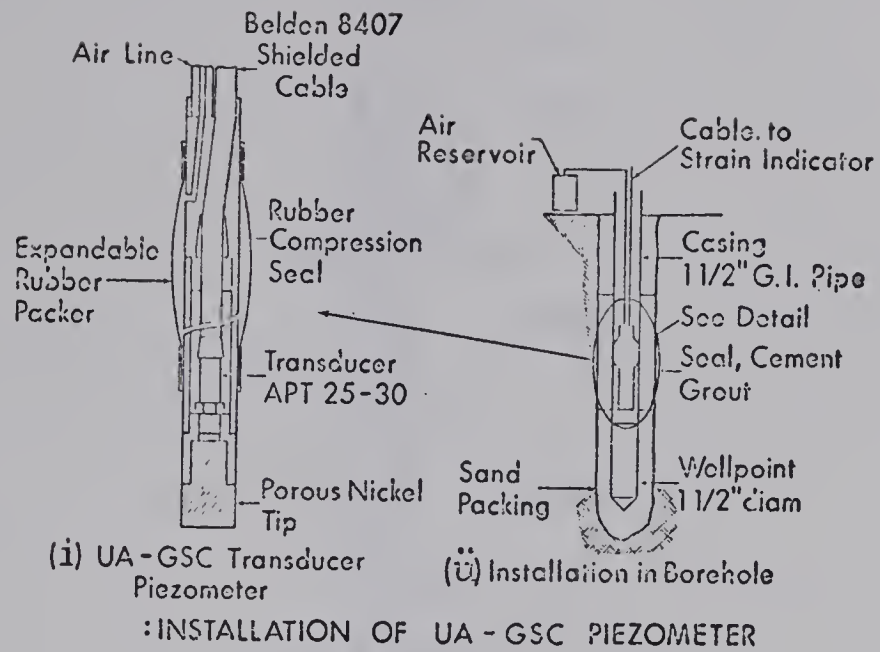


FIG. 6.2a UA-GSC PIEZOMETER SYSTEM

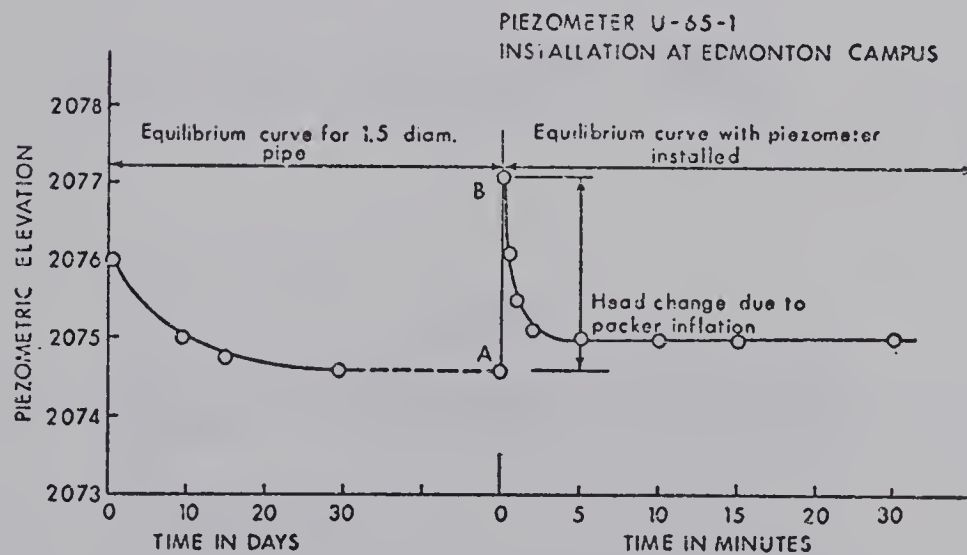


FIG. 6.2b RESPONSE BEHAVIOUR

FIG. 6.2 UA-GSC PIEZOMETER AND RESPONSE CHARACTERISTICS
(AFTER BROOKER ET AL, 1968)

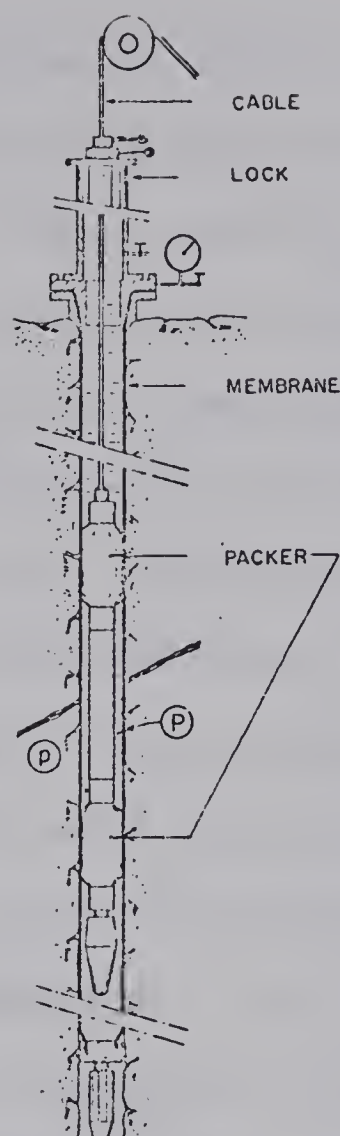


FIG. 6.3a PIEZOMETER SYSTEM

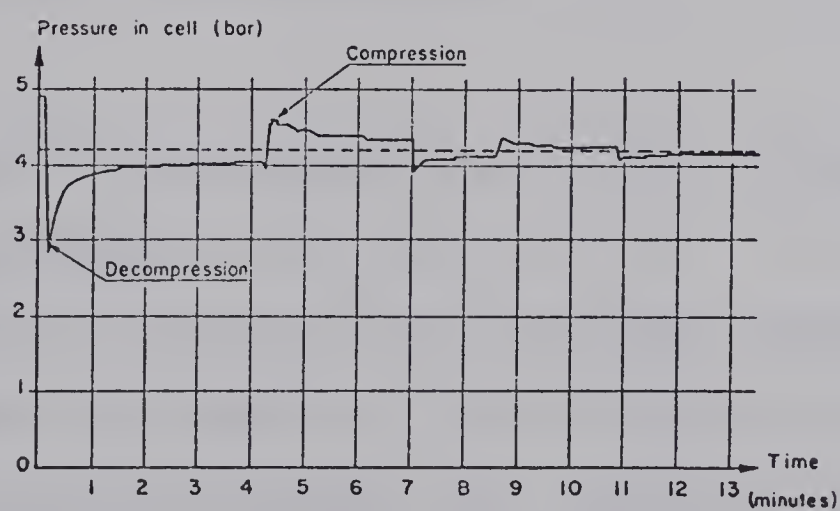


FIG. 6.3b RESPONSE BEHAVIOUR

FIG. 6.3 CONTINUOUS BOREHOLE PIEZOMETER AND RESPONSE CHARACTERISTICS (AFTER LONDE, 1971)

Fig. 6.3a carrying two packers to isolate a short section of the hole is passed through the pressure lock and lowered to any desired elevation. After activation of the packers an electrically operated piston in the probe can be engaged so that the pressure P inside the membrane at the probe will be less than the pressure p in the rock. Water will flow from the surrounding rock causing equalization of the pressures on both sides of the membrane. A pressure transducer in the probe will measure the pressure in the hole. Since the monitored pressure will tend towards the true value asymptotically, the piston is activated to bracket the magnitude of the correct pressure. Fig. 6.3b shows a response curve using this bracketing technique in quartzite. With this technique a continuous water pressure profile of the borehole can be developed. The present instrument was purported capable of being used in 86 and 116 mm boreholes at depths of "several hundred meters".

6.2 Description of the University of Alberta Multistage Piezometer System

A comparable device to the continuous borehole piezometer has been developed at the University of Alberta for use in soil and rock slopes. The instrument can be described as a borehole double packer transducer piezometer and is basically the UA-GSC piezometer with an additional packer below the transducer. The piezometer unit is shown in Fig. 6.4. The design has evolved through the efforts of

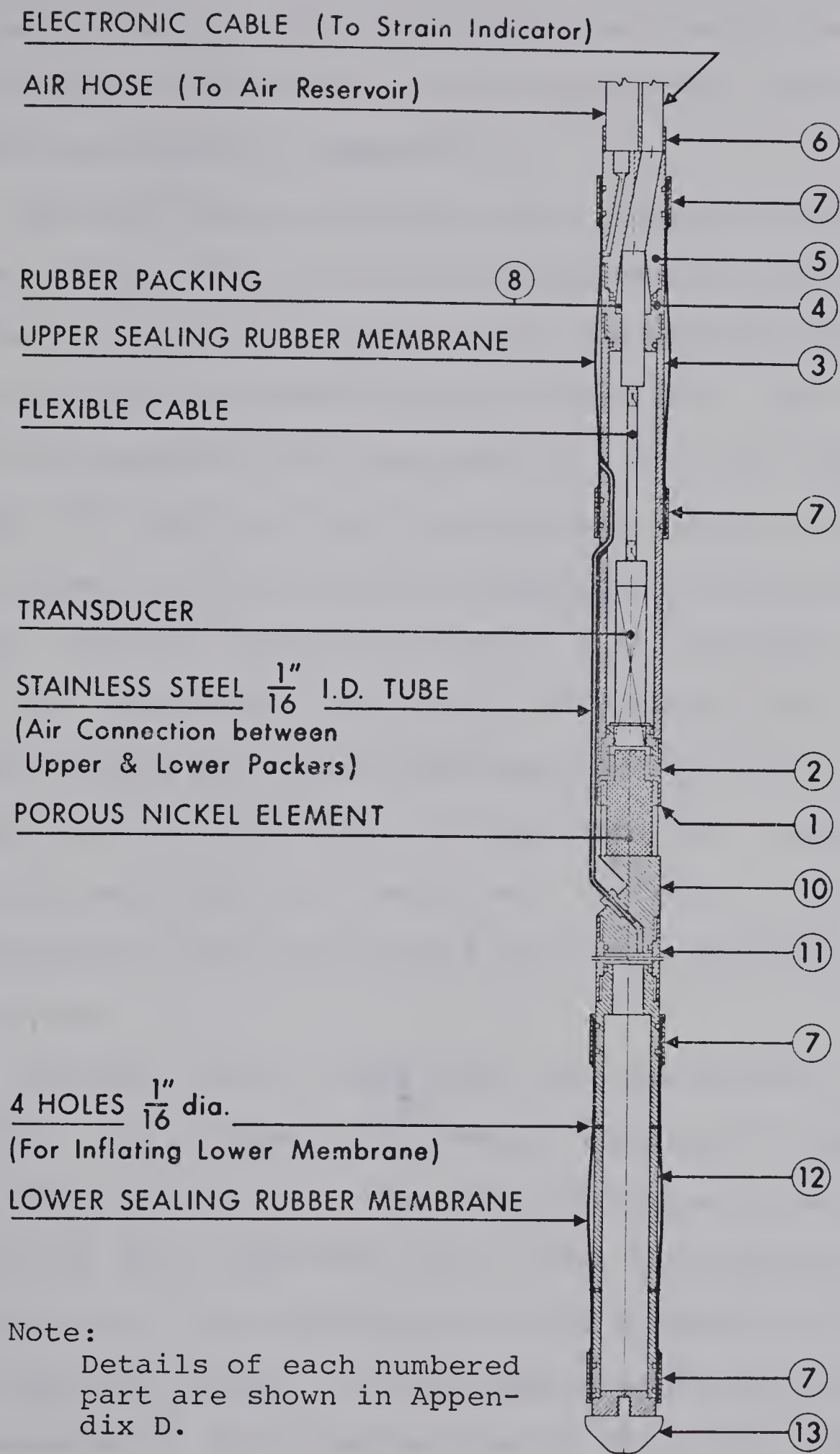


FIG. 6.4 ASSEMBLY DRAWING OF THE UNIVERSITY OF ALBERTA
DOUBLE PACKER TRANSDUCER PIEZOMETER

staff and students in the geotechnical section of the civil engineering department at the university. Piezometer components are shown in Appendix D.

The multistage system can take readings at pre-selected levels. From the stratigraphy revealed by the borehole log of a 6-8 in. drill hole, the desired locations of well points in the borehole are determined. The well points are assembled with sections of $1\frac{1}{2}$ in. I.D. polyvinyl chloride (PVC) pipe so that the measuring points will be at the proper elevations when the assembly is lowered in the hole. The well points consist of 1 ft. sections of $1\frac{1}{2}$ in. I.D. galvanized iron casing, threaded at both ends, perforated throughout with approximately $\frac{1}{4}$ in. holes and surrounded with 2 layers of fine mesh wire. Impermeable seals are placed above and below each wellpoint. Filter sand is positioned at the points and filler sand is deposited between them.

Readings can be taken after the installation is completed. The piezometer is lowered down the PVC casing to the desired wellpoint. The flexible rubber membranes are inflated with compressed air to seal the device at the desired area or layer developing in the formation of a closed measuring system. A diagrammatic representation of the piezometer in operation is given in Fig. 6.5. Readings of pressure versus time will reveal the equilibrium pressure at the point.

TO STRAIN
INDICATOR

TO AIR RESERVOIR

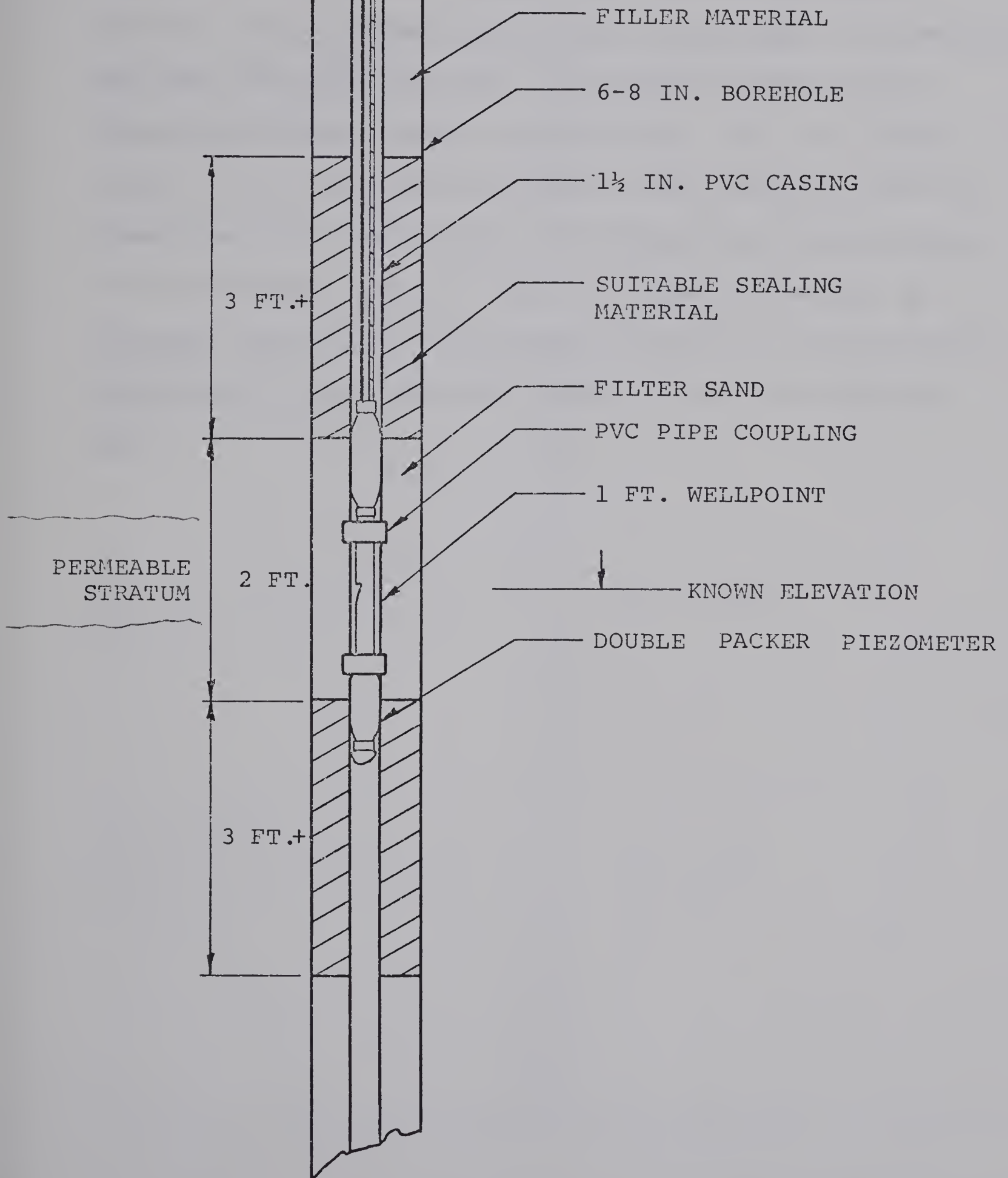


FIG. 6.5 SECTION SHOWING TYPICAL INSTALLATION

The effects of drilling mud are important in maintaining the original flow conditions in permeable water bearing strata after the installation is completed and no measurements are being taken. The use of a bentonite drilling slurry during the initial boring tends to penetrate and seal the strata so that longitudinal communication between the levels chosen is minimized. The low volume factor of the instrument develops rapid response times in areas where the sealing mud has effected low permeability in the permeable layers. Fig. 6.6 shows an example of a possible equilibrium flow regime arising in a hypothetical situation to illustrate the desired effects of drilling mud.

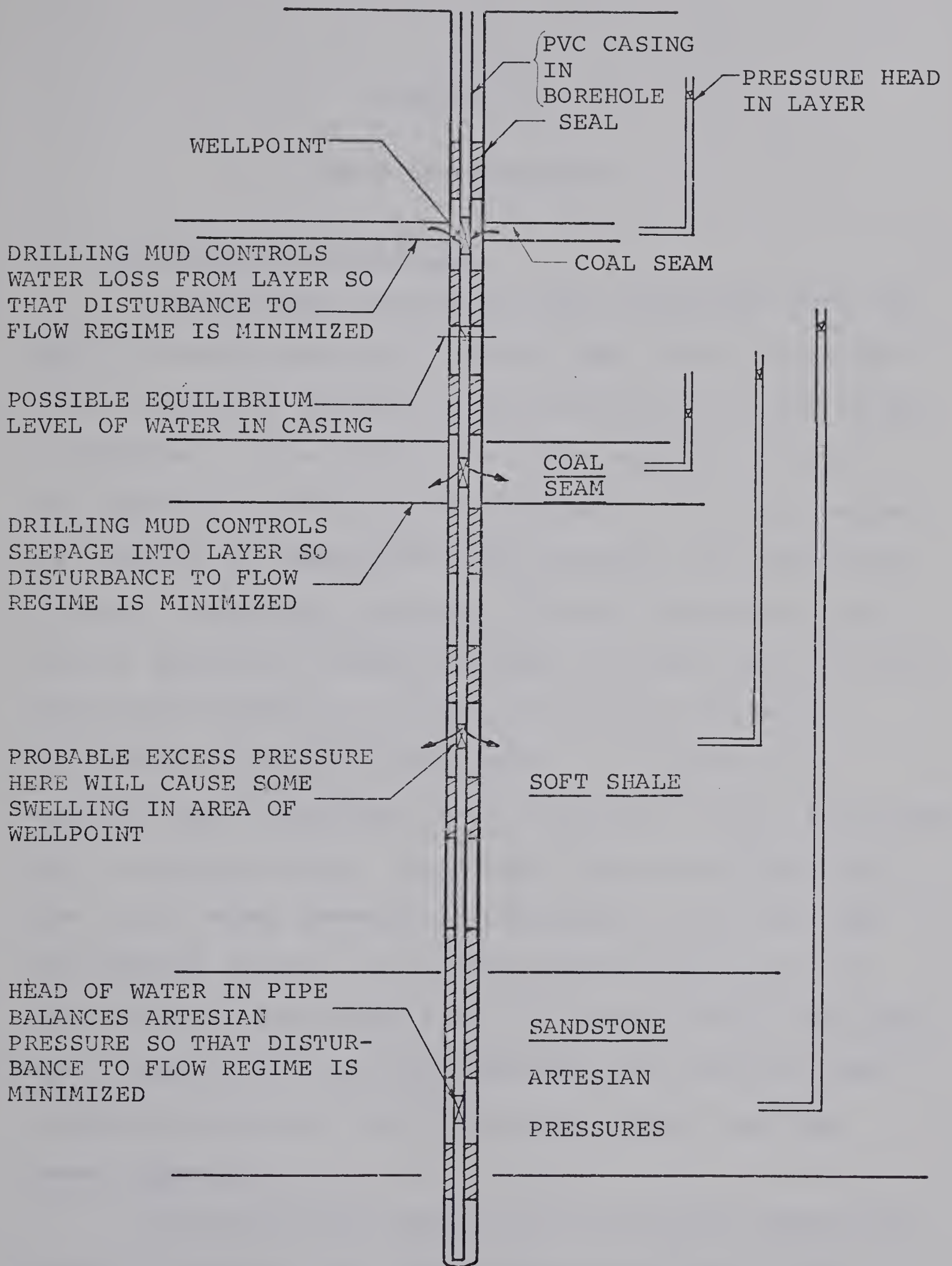


FIG. 6.6 HYPOTHETICAL SITUATION TO ILLUSTRATE THE DESIRED EFFECTS OF BENTONITIC DRILLING MUD

CHAPTER VII

FIELD INVESTIGATION

7.1 Location of Installation

Investigators working in areas associated with the Upper Cretaceous Edmonton Formation have found that information concerning possible or existing perched water tables is important. In a report on a slope stability study in the immediate vicinity of the University of Alberta campus, E.W. Brooker and Associates (1970) express the limitations of their analysis by remarking, "Perched groundwater conditions applied to failure surfaces extending deep into the (Cretaceous) bedrock can lead to an overly pessimistic indication of stability conditions". In another case, Eigenbrod and Morgenstern (1971) analyzing a slide associated with Cretaceous bedrock and perched water conditions show that if the water pressure distribution in the slide had been deduced naively, an improper interpretation of the shear strength determined from the analysis would have been made. Hence in the past the knowledge of irregular water conditions associated with Cretaceous bedrock has been deemed important.

An appropriate location with Cretaceous bedrock was sought to ascertain the working characteristics of the piezometer system, its strengths, its weaknesses and if possible a reasonable indication of the groundwater conditions.

Since no existing open boreholes were available an attempt was made to determine a convenient and suitable location. In particular it was decided to select a site where the stratigraphy was generally known and that entertained a high probability of having one or more perched water tables. As shown in Fig. 7.1 a location near the University of Alberta campus was chosen which would penetrate the Upper Cretaceous bedrock. A maximum depth of 200 ft. of hole was planned.

The geology of the area has been studied previously and the following brief description is taken from the work of Thomson (1970). Deposits of four ages are present in this area. Starting with the oldest, these are, (1) Upper Cretaceous, (2) Saskatchewan Sands and Gravels, (3) Glacial (dense till) and (4) Postglacial or recent (lacustrine deposits). The strata of the Upper Cretaceous consist of interbedded grey shale, grey sandstone, bentonitic sandstone, bentonitic shale, coal and bentonite. Approximately 20 ft. above the river a coal seam 2 to 3 ft. thick outcrops. A section through the location is given in Fig. 7.2. It is well known that the coal beds tend to be laterally extensive. Since the coal layers often drain into the valley, irregular pressure distributions abound.

7.2 Field Procedures

A Failing 1500 drilling unit was used for the work associated with the installation. The stratigraphy in the Upper Cretaceous bedrock was determined by obtaining

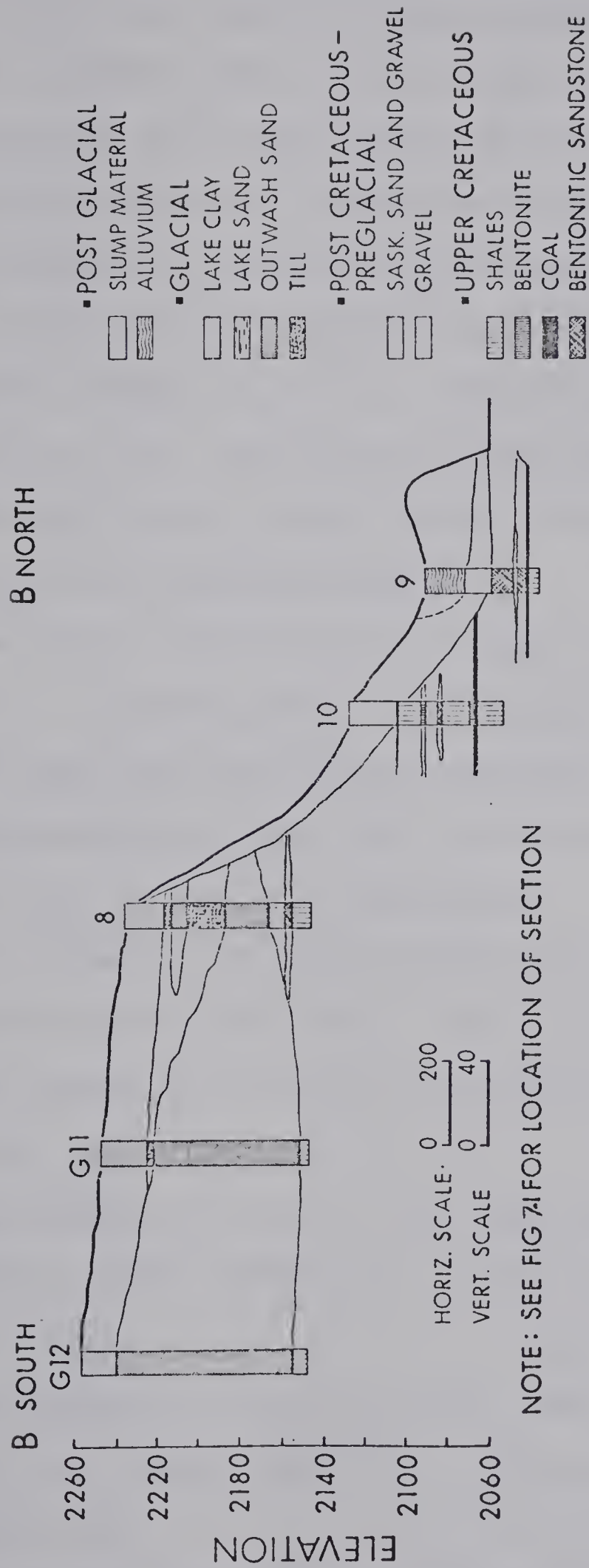


FIG. 7.2 SECTION THROUGH LOCATION FOR INSTALLATION (AFTER THOMSON, 1970)

continuous core using both a pitcher sampler and a 4 in. core barrel. Seventy feet of hole which was partly in the sands and gravels were cased with a 9½ in. steel casing since previous experience in these materials pointed to the possible collapse of the hole and to sampling difficulties caused by gravel falling to the base of the boring. Drilling was ceased at a depth of 197 ft. After the lower 127 ft. were reamed to 8 in., bentonite drilling mud was circulated in the hole until fluid losses ceased. Clear water was then circulated to clean the boring.

The log of the test hole is shown on the right side of Fig. 7.3. A possible coal layer exists at a depth of 121 ft. but core recovery was not obtained. It was decided to establish well points for the installation as shown on the left of Fig. 7.3 at four elevations:

- a. Well point no. 1 in the Saskatchewan Sands and Gravels at 59. ft. (Elev. 2177. ft.)
- b. Well point no. 2 in the clay shale at 105. ft. (Elev. 2129. ft.)
- c. Well point no. 3 in a 4 ft. coal stratum found at 156.ft. (Elev. 2080. ft.) This is 15-20 ft. above the river.
- d. Well point no. 4 in a 6-12 in. coal layer found at 187. ft. (Elev. 2049. ft.) This is 10-15 ft. below the river.

The sealing material was selected on the basis of insitu soil conditions, ease of placement and permeability

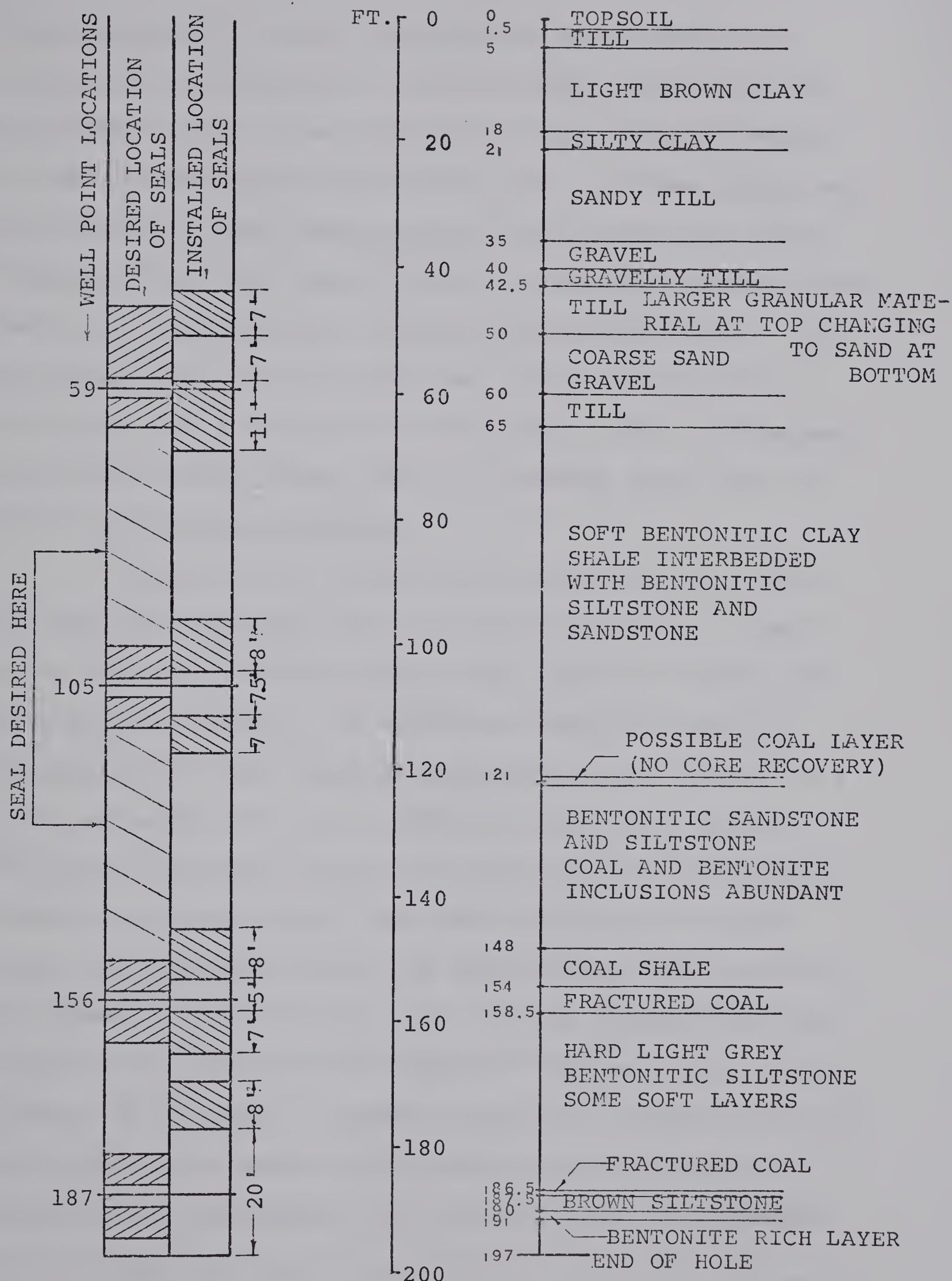


FIG. 7.3 BOREHOLE LOG, SEAL AND WELL POINT LOCATIONS

characteristics. A seal adequate for many insitu soil conditions was desirable. For the depths associated with the installation, it was essential that a pumpable grout be used since tamping a seal into place at these depths was not feasible. Past experience and laboratory tests have indicated that pure cement grouts or bentonite cement grouts have high permeabilities relative to bentonite clay. This was thought to arise in large part from cracking due to shrinkage. As a result it was decided to use a low permeability AM-9 grout (Lamb, 1960) or a cement grout with an additive to induce expansion.

Because of the highly toxic nature of AM-9 grout and because experience with its use was lacking, a cement grout with an expansive additive was used for sealing the well points in place. An economical additive known as 'Entraplast A'* was mixed with normal Portland cement in a ratio by weight of 1 part additive to 100 parts cement. This grout has been tested and used successfully by Lyell (1969) in a harder rock. For pure cement paste tested under lab conditions where the water-cement (W/C) ratio of the paste was less than 0.7 and 0.5, the permeability was found to be less than 10^{-10} and 10^{-11} cm/sec respectively (Powers et al, 1955). However increases in permeability in the cement often occur due to preferential flow paths caused during settlement (or "bleeding") and as mentioned

*Supplied by Sika Ltd., England

previously microcracking associated with shrinkage.

The pumping system on the drilling unit was used for placing the grout. The pump was a duplex reciprocating type with possible pumping rates of up to 180 gallons per minute. Since the lowest possible rate of pumping was much too high to place the grout without dispersion, the pumping system was modified with a by-pass valve to obtain minute flow rates of grout into the hole. The initial seal was placed without a bypass system resulting most likely in a poor seal. Approximately three seals were placed per day. Fig. 7.4 shows the pumping system used.

Grout was pumped down the hole using a 1 in. I.D. PVC pipe in 20 ft. sections. Additional 10 ft., 5 ft., 2 ft. and 1 ft. sections were used to obtain any length of grout pipe required. The grouting pipe was also used as a gauge for measuring the sand fill depth and the grouted length of seal. The depth measurements were facilitated by the sedimentation of a small layer of pea gravel to form a base from which measurements could be taken.

Clean uniform Ottawa sand was sedimented to form the filter material at the well points. A well graded sand was used as a filler material between well points. For the present installation the use of well graded sand by sedimentation caused segregation and a longer wait time for settlement than was necessary. Hence if sand fill is required in any future installations a well sorted coarse material should be used. Sand settling time for 200 ft. of hole was

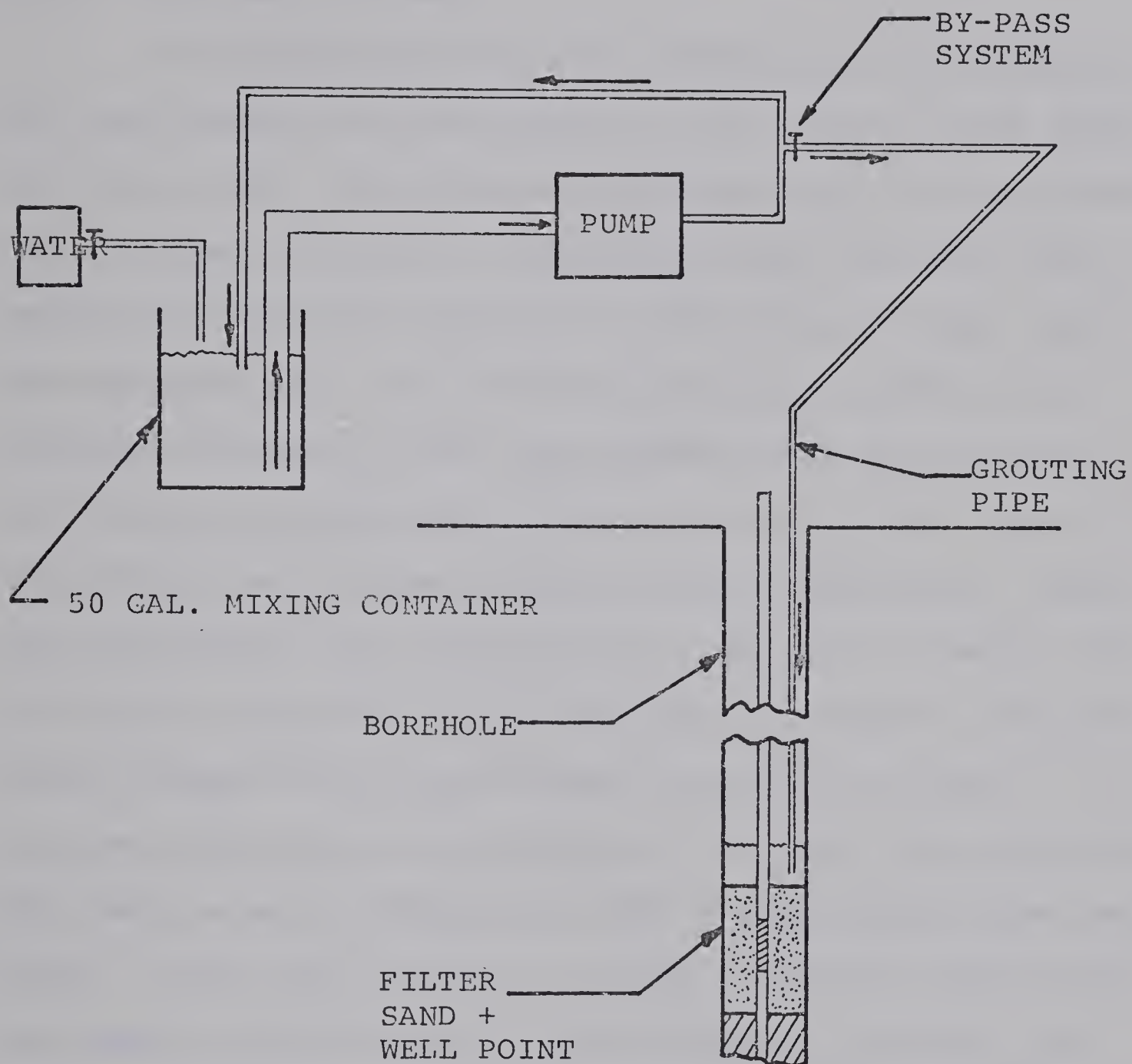


FIG. 7.4 PUMPING SYSTEM UTILIZED

such that if installations deeper than this are attempted a new method of placing the sand should be found in order to decrease stand-by time for machinery when high priced rental equipment is used.

It was decided that a set cement was not required for continuation of installation of the seals, filter sand and filler sand. This decision resulted from the consideration of several factors. Laboratory tests revealed that a minimum of "bleeding" occurred for W/C ratios of less than approximately 0.5. As a result, for larger ratios, the effective stresses in the fresh cement will be low since relatively high pore water pressures in the cement slurry are induced due to consolidation and sedimentation. Hence sand penetration for a slurry with a W/C ratio greater than 0.5 will be large due to its inability to support the sand grains because of low inter-cement particle stresses. It was also observed in the laboratory that the sand penetrated the cement a small distance so that a sand cement layer was formed. This layer acted as a filter squeezing water from the cement, consolidating it and giving it strength. Because of the confining action of the sand-cement layer, shear strength in the grout was not required to prevent penetration. The penetration pressure of the sand will also be reduced since the sand and seals were to be placed under water so that the buoyant weights of the sand and cements are only acting. In addition if sand is placed over the grout, arching in the sand against the sides of

the borehole limit penetration stresses to a large extent. Hence with these mechanisms in operation sand penetration into the fresh grout will not be excessive.

The following two procedures were consequently observed in the installation of the materials in the field. After grouting, a token wait time of 30 minutes was allowed before sand was sedimented, so that the cement had some time to settle if it was dispersed at the top of the seal. Also a thin layer of fine sand was deposited between sand and cement layers. This was necessary because the coarser fraction in the sand used settled first disturbing the seal if a fine sand supporting base was not present.

In addition to the two preceding procedures a W/C ratio of 0.5 or less was required for placing the seals. The pumping system used had a minimum circulating volume of 20-25 gallons. With this initial volume of water a minimum of six 80 lb. bags of cement had to be mixed at any one time to obtain a W/C ratio of 0.5. Cement was added to the circulating grout in the pumping system until this ratio was reached. Water-cement ratios were determined from grout samples which were taken and weighed in the field. The W/C ratio was interpreted according to Fig. 7.5.

The grout volumes pumped were calculated to give a 5-8 ft. seal. Due to the expansive nature of the grout it was desirable to use a seal as long as feasible so that the middle expanded against the upper and lower parts of the set cement. Seal lengths were gauged by monitoring the

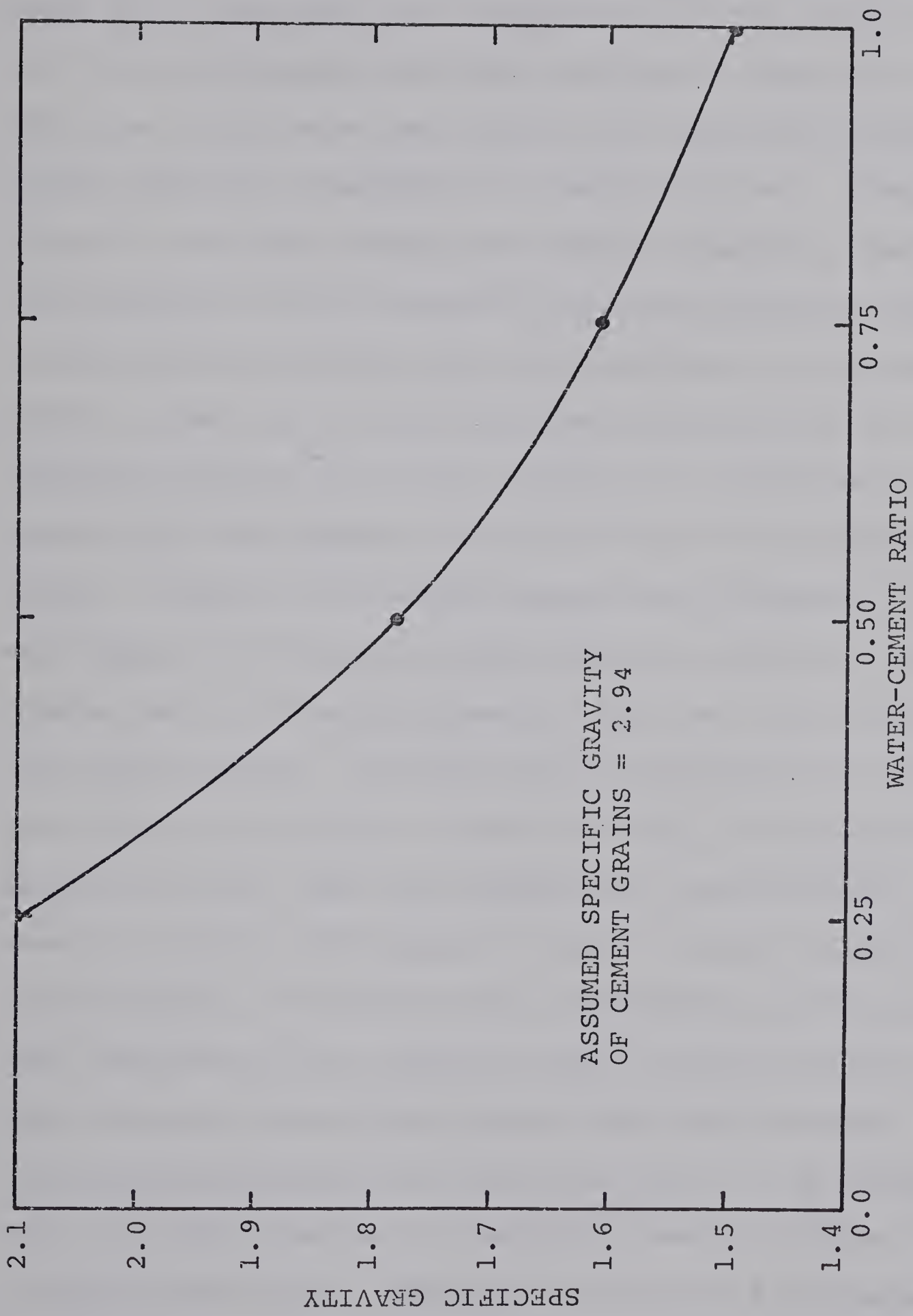


FIG. 7.5 WATER-CEMENT RATIO RELATED TO SPECIFIC GRAVITY OF CEMENT GROUT

level in the mixing drum. The estimated final locations of the seals are summarized on the left of Fig. 7.3. For well point no. 1 the hole had sloughed in to give a much longer seal than anticipated and thus grouting in the well screen. This seal could have been removed and replaced quickly with a more flexible arrangement of pumping system. However since the drilling program was behind schedule a lack of time coupled with the thought that the piezometer could quickly measure through the grout resulted in no remedial action. When dealing with perched conditions it is always desirable to seal the entire length of a relatively homogeneous and impermeable stratum if it is of considerable extent. Hence if the water pressure distribution at the well point in the shale is far from hydrostatic an incorrect reading may be obtained since the hole was not sealed for the entire length. Grouting was not performed further on both sides of the point as shown in Fig. 7.3 because initially a 5-8 ft. seal was planned for 4 well points. As a result a lack of 'Entraplast A' was on hand to grout the entire length. This and other deficiencies in foresight then resulted in the length of seal at this location. Nevertheless interesting results from the piezometer readings are obtained for well point no. 2. As shown in Fig. 7.3, the location of the bottom seal is higher than it should have been. This was a result of a misjudgment in the installation procedure of the sand. Since the permeability of the coal layer is much larger than the clay shale

the position of the bottom seal is not critical.

7.3 Readings Obtained

At the outset, difficulties were encountered in obtaining reliable measurements. The problems met, essentially fell into two main categories. Firstly a class of problems appeared which concerned lowering the instrument in the casing and thereafter finding the correct level for measurement. A second group of difficulties was related to the maintenance of packer pressure in the piezometer. A majority of the problems were overcome to obtain the readings presented below.

Even before the well points were grouted in place some difficulties were encountered in lowering the piezometer for the length of the PVC casing. It was found that the instrument would not pass the first coupling. The upper section of pipe was dismantled and it was observed that the PVC pipe ends had been pressed inward to form a circular protruding lip. This might have been due to a possible over-tightening of the coupling. After the edges were filed flush the pipe was reassembled and the instrument was lowered to the bottom without serious difficulty.

Notwithstanding the precautions described previously, during subsequent measurements similar difficulties were encountered at some locations. This was due possibly to the obstruction described, to a recessed annular ring formed at the joints on which the piezometer could catch

or to some other block mechanism. The piezometer always passed the restricted locations but often in the attempt the sleeve securing the packer membranes tended to be loosened so that the packers were unable to maintain pressure. If pressure loss was observed the piezometer was hauled to the surface for inspection.

Usually when a pressure loss occurred the membrane was immediately suspected. On one occasion however after both membranes had been replaced and firmly secured a persistent pressure loss still occurred. After the instrument was brought to the laboratory for inspection a close examination revealed a leak in the air line several inches above the connection of the hose to the piezometer. A leak in the pressurizing hose was not considered likely because the hydraulic line was of double stainless steel jacketed design with a nylon covering. After this section of hose was replaced pressure loss problems were of a minor nature.

The air and the electrical lines weighed 0.152 and 0.149 lb. per ft. respectively combining to give 0.3 lb. per ft. In addition the piezometer body weighed approximately 7 lbs. As a result for the lowest well point approximately a 60 lb. force was required to hold the assembly in place and handling became awkward for this depth. Also it was found while marking off the well point elevations on the air hose in the lab that it stretched substantially. Since the electrical cable elongated easily as well, the ability

to locate the well point levels precisely was hindered. On one occasion a membrane was damaged when it expanded into the perforations on the inside of the well point. Because of this stretching, the piezometer level had to be adjusted in small increments to find the well point level. Also to aid in the seating the distance between the packers was increased by incorporating an extending section in the body of the piezometer. Since the instrument might not have been centred properly at the well point a maximum error in measurement in the order of 1 ft. of water could have occurred due to misalignment. On the average however the error was likely smaller. After the levels were found both the air and electrical lines could be marked to give the proper elevation for future readings.

Another difficulty arose when searching for the correct level. The compressed air reservoirs with volumes of 288 cu. in. could be pressurized to only 90 psi with existing facilities instead of an allowable 400 psi. Consequently at the lower well point when packer pressures had to be in the order of 60 psi or more only one or two inflations were possible. An attempt was made to overcome this inconvenience by the use of a highly pressurized CO₂ container. Since measurements at the time were taken in sub-zero weather the temperature of the CO₂ gas as it vaporized into the system was very low. In the installation the temperature was probably in the order of 40°F and subsequently when the gas warmed a pressure increase occurred.

This had an undesirable effect on the measured response curves. In addition, a clumsy system of valves on the CO₂ container resulted in a sudden high pressure on one occasion rupturing the membranes. With this experience, the use of CO₂ as a pressure source was discontinued.

A faulty regulator on one of the air reservoirs was also responsible for pressure loss several times.

On account of the problems described previously an initial set of mostly incomplete readings were acquired. These were taken in December of 1971. The temperature in the field at this time ranged to -40°F and resulted in poor performance of the equipment on the surface and very unpleasant working conditions. A second set taken in the beginning of 1972 proved more fruitful. The level of water in the casing dropped between these two times to an equilibrium level 12 ft. above well point no. 3. When readings were desired for the upper two well points, the casing had to be filled above the level where the readings were desired.

Figures 7.7 through 7.10 show the measurements obtained at the four well points when interpreted according to the calibration curve of Fig. 7.6. Generally, packer pressures 15-20 psi in excess of the head above the well point were used to seal the piezometer in place. As discussed, difficulty was experienced in obtaining the readings so that all the curves are not complete. Since great efforts were made to obtain all of these readings, they will nevertheless be presented.

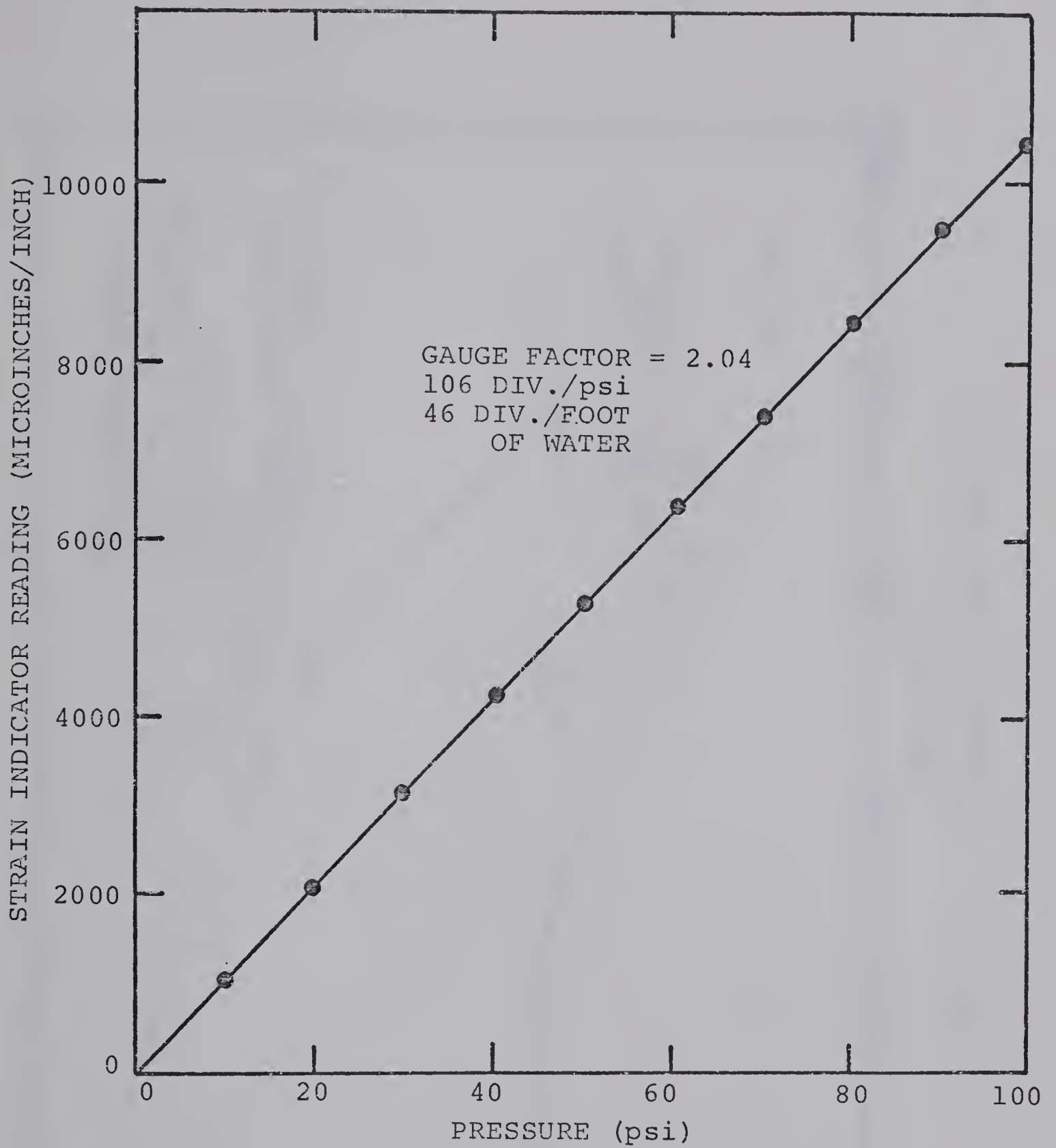


FIG. 7.6 TRANSDUCER CALIBRATION

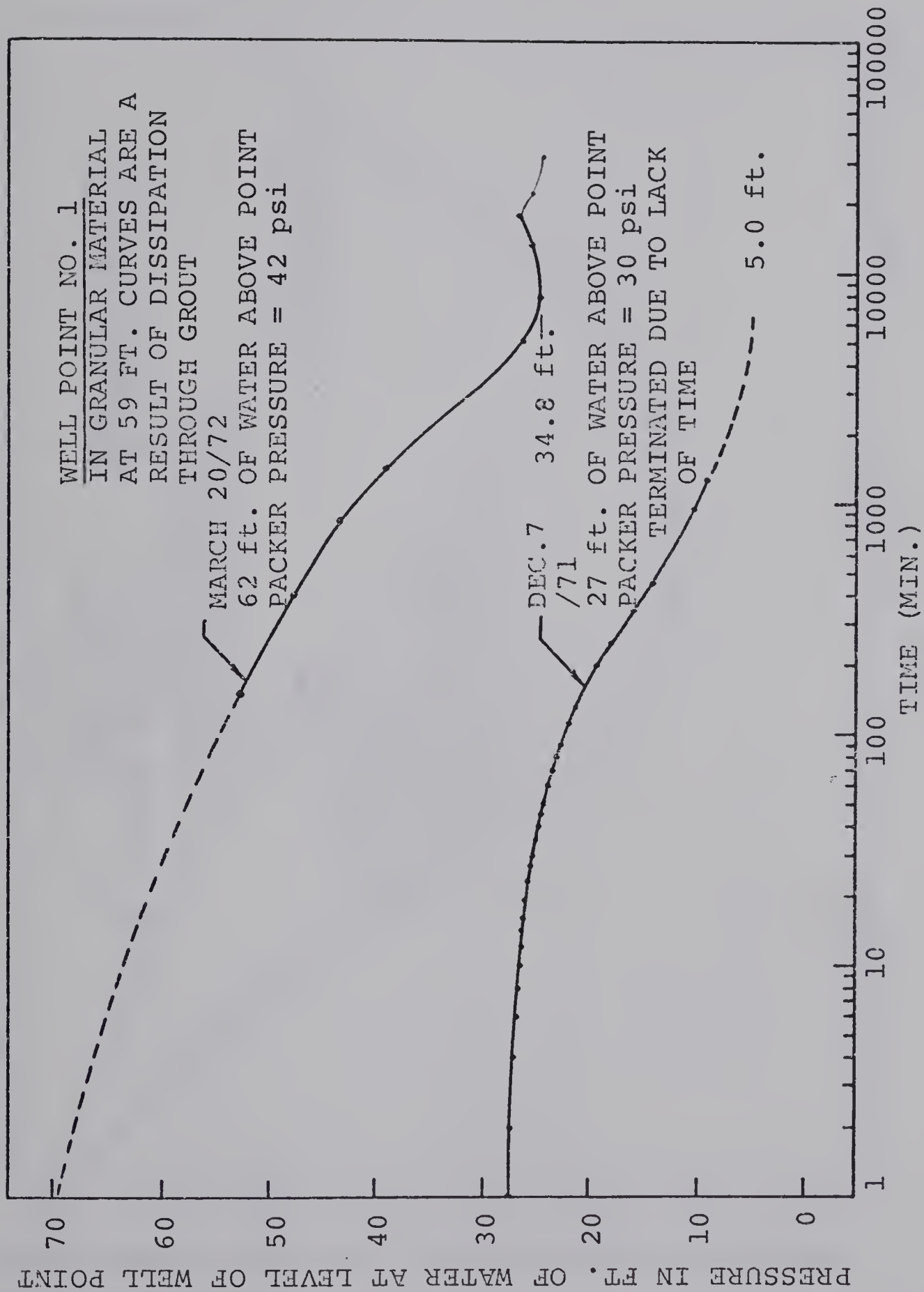


FIG. 7.7 RESPONSE AT WELL POINT NO. 1

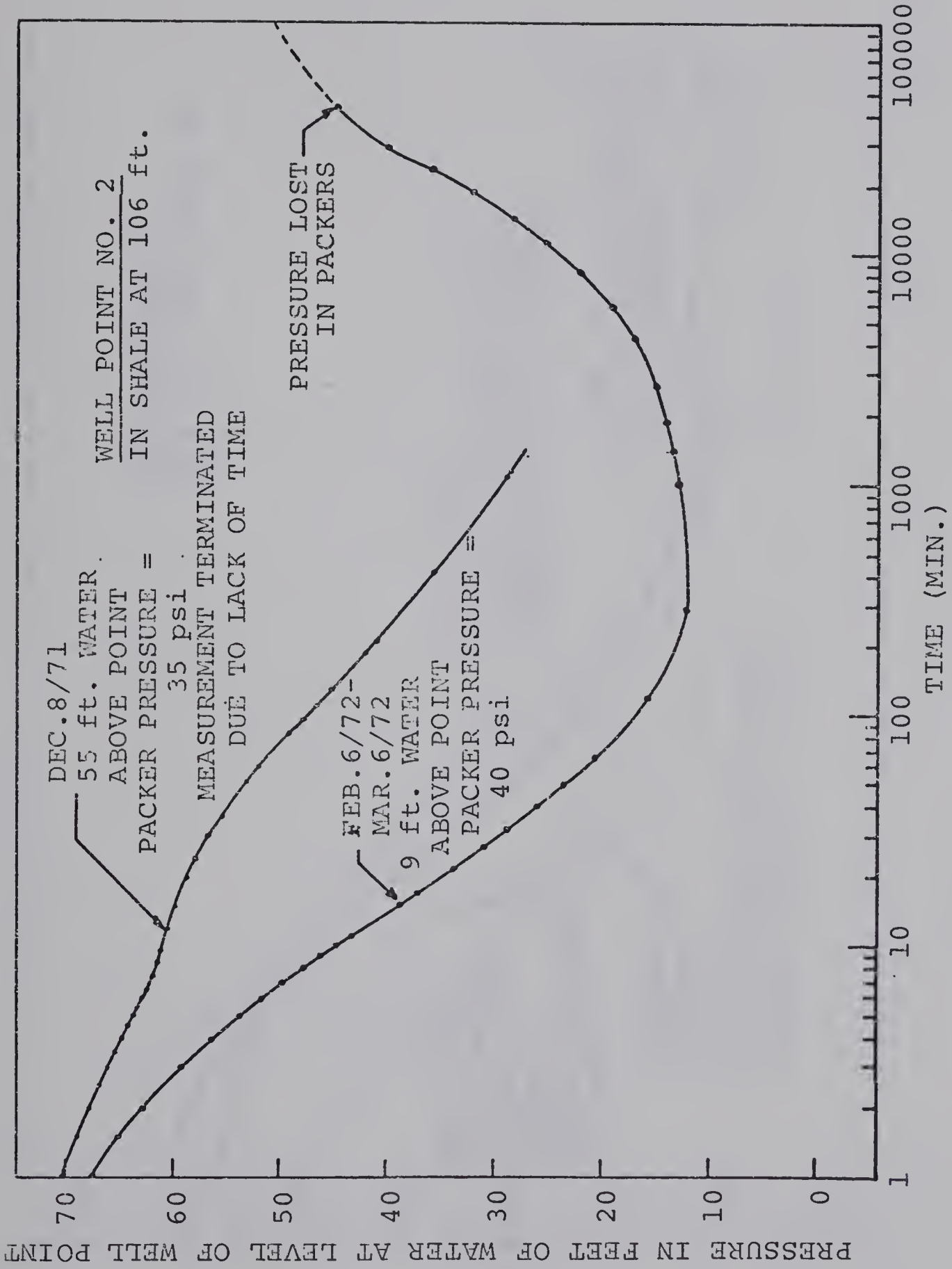


FIG. 7.8 RESPONSE AT WELL POINT NO. 2

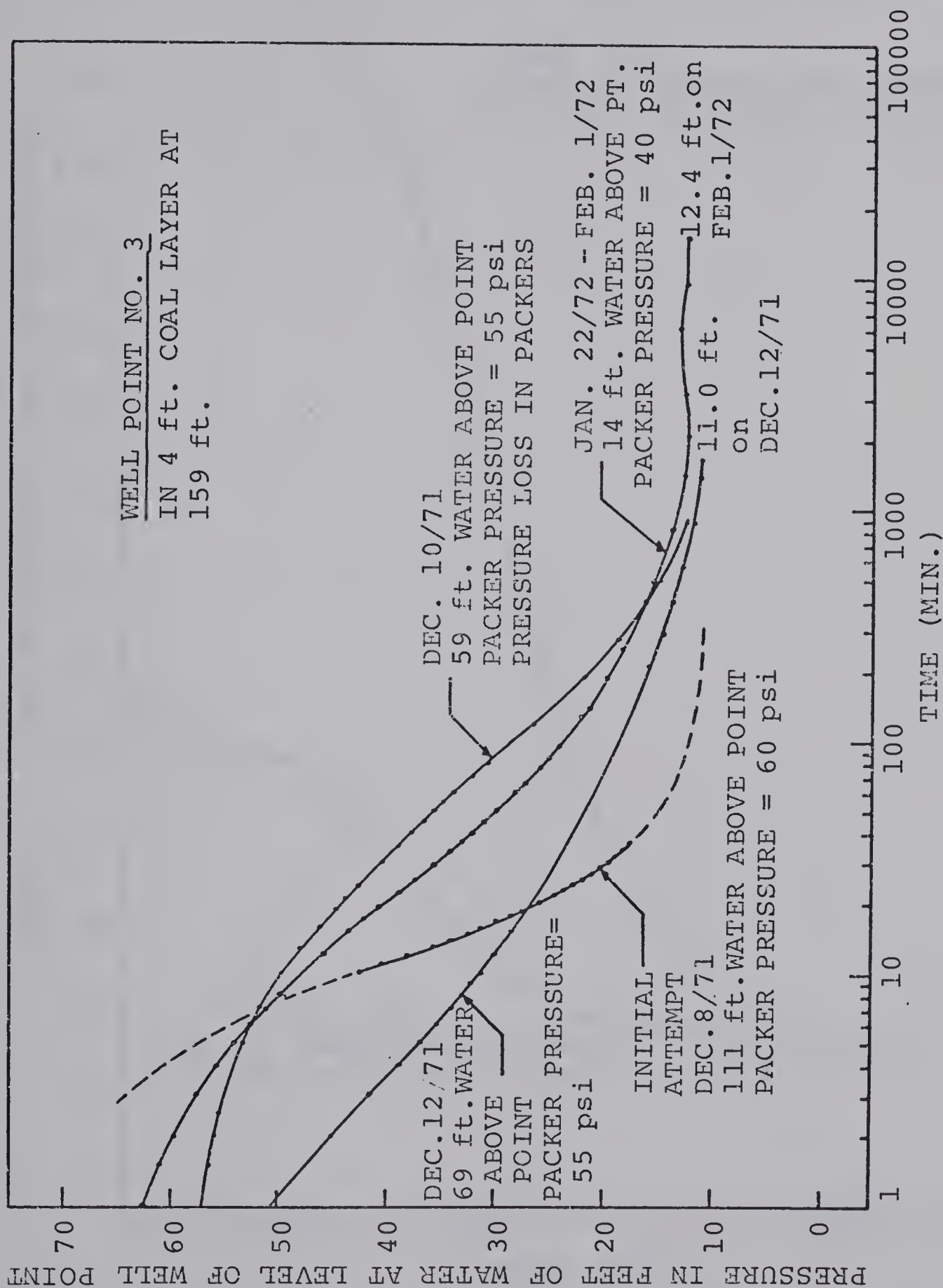


FIG. 7.9 RESPONSE AT WELL POINT NO. 3

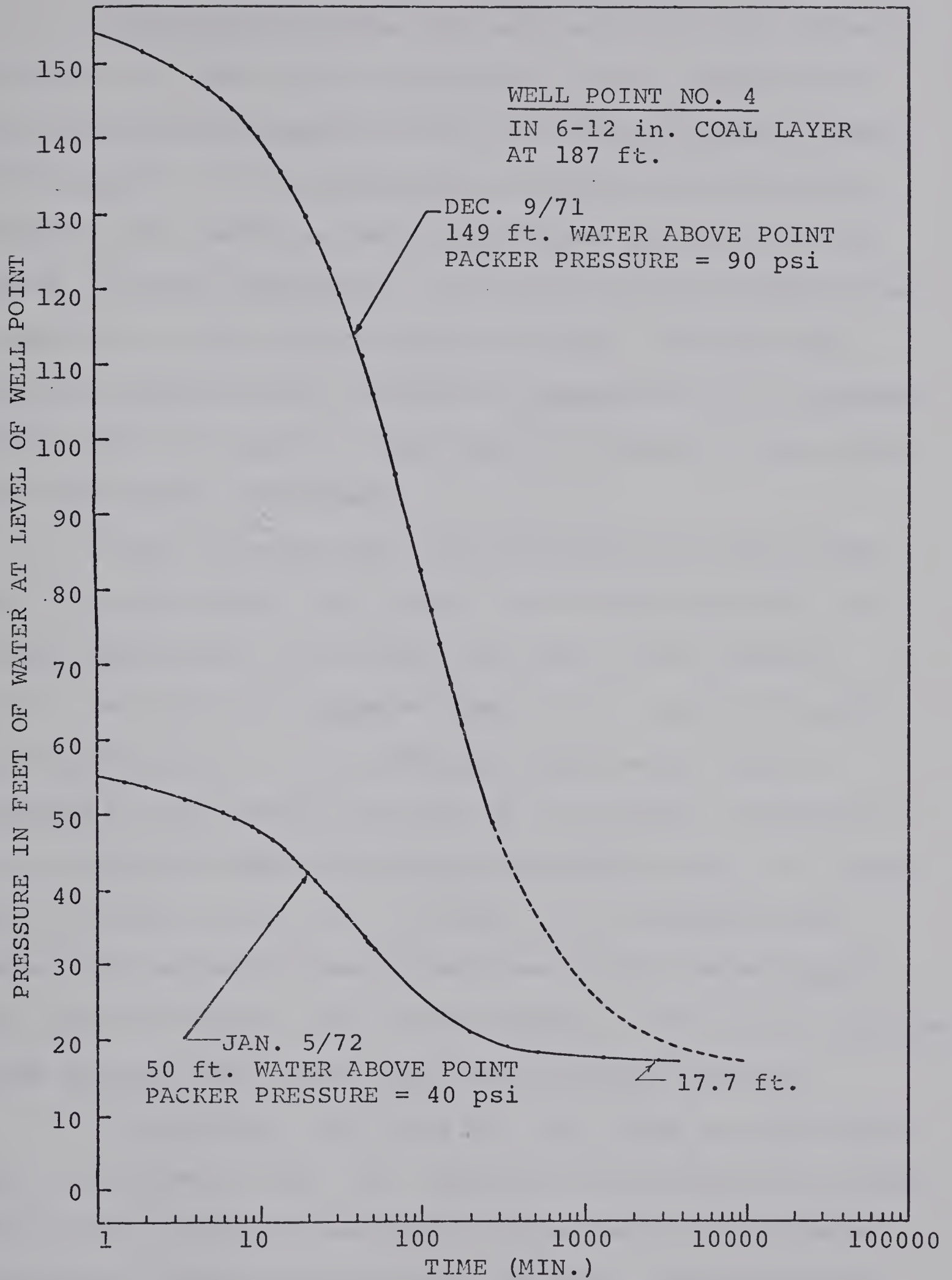


FIG. 7.10 RESPONSE AT WELL POINT NO. 4

The curves obtained for well point no.1 are shown in Fig. 7.7. The initial measurement after completion of the installation appears to show very little head of water at the point. It is interesting to note the slow initial response for the first measurement since this part of the curve is almost horizontal. The following measurement shows a head of 34.8 ft. at one period in time. Although the initial reading is not complete it appears that the response times could be similar. Water had to be added to the casing for the second measurement.

Fig. 7.8 shows the curves procured for well point no. 2 in the shale. The initial curve shows that the possible equilibrium value could have been in the order of 20 ft. or less with response times in the order of 10,000 to 20,000 minutes. The subsequent measurement shows a minimum at 300 minutes followed by an increase in pressure with increases still occurring at 40,000 minutes to a value in the order of 60-70 ft. of water. It is important to note that before this measurement was taken the well point was above the water level in the casing. The initial response time appears much slower than the following response.

The behavior for the 4 ft. coal layer at well point no. 3 is shown in Fig. 7.9. Equilibrium pressures for three trials are generally reached at approximately 2000 minutes yielding a value of 11 to 13 ft. of head. An equilibrium value of 11.0' was attained on Dec. 13/71 and a value of 12.4' on Feb. 1/72. It is of interest to note the much

more rapid response for the initial trial than for any of the other trials.

The equilibrium pressure for well point no. 4 shows 17.7' of head in Fig. 7.10. The 6-12 in. coal layer is estimated to occur 10-15 ft. below river level. Equilibrium occurs at approximately 1000 minutes for the second measurement. The reading of Dec. 9/71 was obtained soon after the completion of the installation and at the time a large head of water was still in the casing. This is the reason for the large pressure dissipation. For the two readings shown the response time for the earlier reading appears to be longer.

CHAPTER VIII

DISCUSSION AND CONCLUSIONS

8.1 Discussion

With the installation and operation of the multi-stage piezometer system insight has been obtained concerning grouting procedures, quality of the cement seals, piezometer operating characteristics and the pressure distribution in the slope. With this knowledge it is felt that decisions may be formed regarding future implementation of the system or a modified version thereof.

The grouting procedure utilized may be improved for more rapid placement of seals. The cost of the installation is in part determined by the placement rate when expensive rental equipment is used and it is desirable to keep all costs minimal. There were two main problems in positioning the seals. The lack of knowledge of the seal height placed and the absence of a facility to easily flush out seals improperly installed are the two difficulties that ideally should be overcome in future grouting operations. The following discusses features which may be incorporated in such a system.

With the setup used, only one pump was in operation. When it was necessary to circulate water through the hole during grouting operations the pump had to be cleared of slurry and replaced with water. This switchover procedure

resulted in time delays and caused dilution of the existing grout when cement was again circulated. Hence it is desirable to have an auxiliary unit for pumping water.

A controlled or accurately determined grout height is required in the case of a lower seal. A method should be included for clearing out the grout pipe so that the volume of seal applied is known more accurately. For example, in 200 ft. of 1 in. I.D. pipe approximately 1 cu. ft. of material exists. This is a substantial amount and is comparable to the volume placed for the seal. If the pipe is disconnected from the pump and raised before it is cleared out the grout will add to the seal and also become dispersed with the water in the hole. If pumped water is used in the clearing process disturbance and dilution of the seal may occur. Hence compressed air might be ideal for the procedure.

Even though attempts can be made to accurately control the seal length various factors may cause error. With the installation of seals one is always "working in the dark" as it were and hence it is desirable to incorporate a system to measure the height of grouting applied. This may possibly be performed using resistivity measurements with probes being attached to the grouting rod in some manner. Thus having the upper location under control more grout could quickly be added if desired or the entire seal could be flushed away if the length was longer than predicted and might interfere with the operation of the

well point. Also dispersion of the sealing material might be detected earlier if the grout were pumped in place too quickly.

In addition to installing the seals the pipe could also aid with the placement of the filter and filler sands. Since sedimented sand is usually in a loose state it would be advantageous to have it compacted. Vibration of the sand would assist in this. Hence the grouting pipe could be used to densify the material by attaching a vibrating source to it. It is not desirable to vibrate the PVC piezometer casing since this may disturb the previous seals which have just begun to set.

In these ways the grouting pipe could serve a multitude of functions. Besides placing the cement seals and measuring the height of sand fill, it could be used to flush out the hole quickly when required, compact the sedimented sand and measure the length of seal placed. A representation of the proposed system is given in Fig. 8.1.

It is very disappointing to note that response times measured with the multistage system are much longer than those indicated by Brooker et al (1968) in Fig. 6.2b. Brooker et al infer that the single packer piezometer has a very small volume factor with resultant rapid response times. It is true that the volume factor of a transducer alone is estimated to be in the order of 10^{-6} to 10^{-7} cm^5/gm which is almost negligible compared to that of a closed hydraulic system such as a Bishop piezometer system.

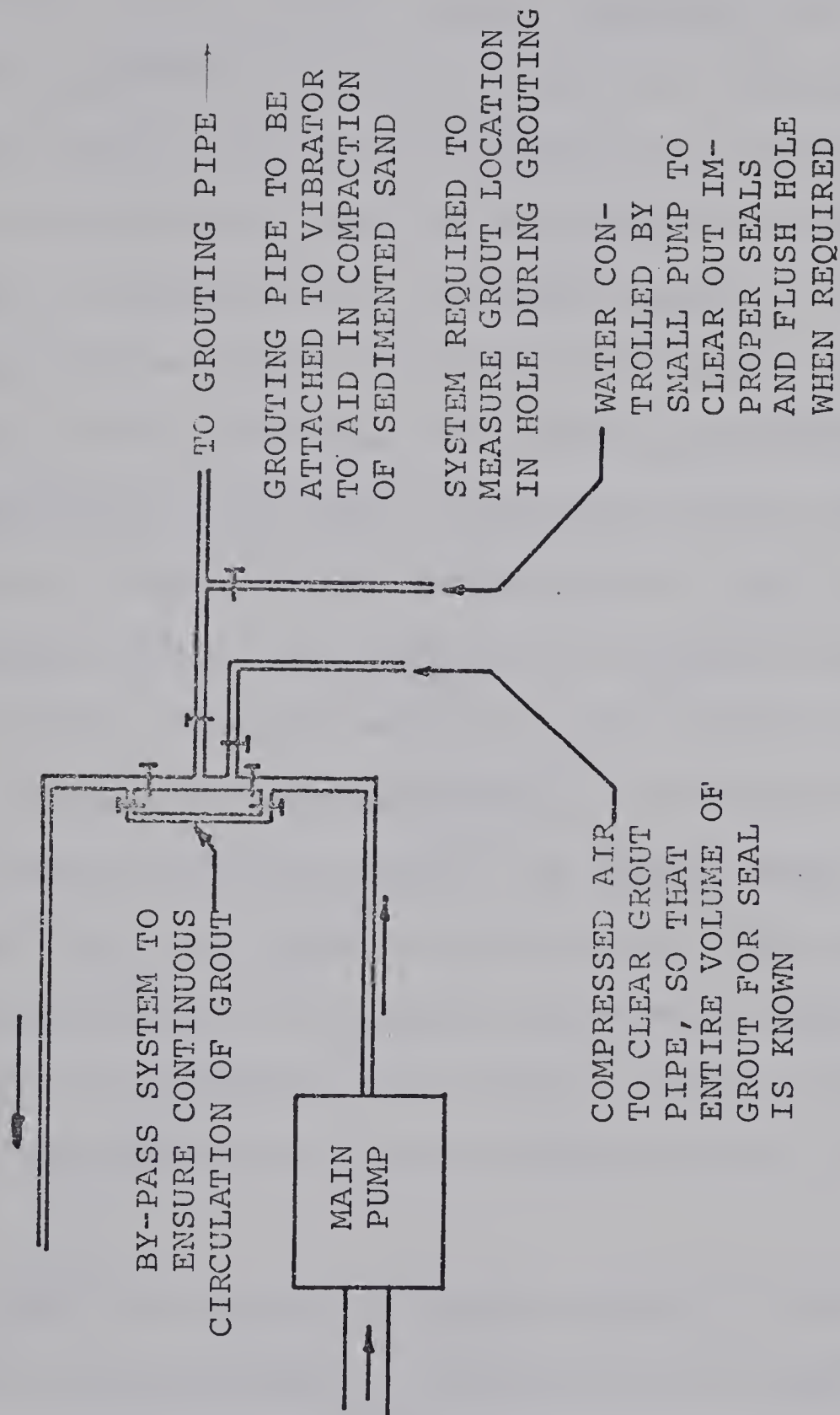


FIG. 8.1 PROPOSED MODIFIED GROUTING SYSTEM

However the flexibility of the air filled packers must also be taken into account. This will substantially increase the amount of water required to activate the system. The volume factor of the double packer piezometer was measured using the apparatus as shown on Fig. 8.2. Care was taken to exclude any air that would affect the results. From the curves on the figure it may be seen that an average volume of 0.1 cc is required for a pressure change of 1 psi giving an average volume factor of $1.42 \times 10^{-3} \text{ cm}^5/\text{gm}$ which is comparable to the stiffness of a Bishop piezometer system with approximately 200 ft. of polythene leads (Penman, 1961).

As a result of the information of Fig. 8.2 it can be concluded with a large degree of certainty that the response curve given by Brook et al as shown in Fig. 6.2b for well points in shale is actually a result of dissipation of excess pressure through the cement seals. These seals must have been full of microcracks with resultant high permeabilities. The quick response is then not a result of the purported small volume factor in conjunction with the low permeability of the shale but of a pervious seal.

From the obtained response curves in general and in view of the preceding it is felt that the expansive additive 'Entraplast A' is wholly adequate for sealing piezometers into boreholes. Its use is recommended where insitu field conditions will allow a rigid material to provide adequate sealing qualities.

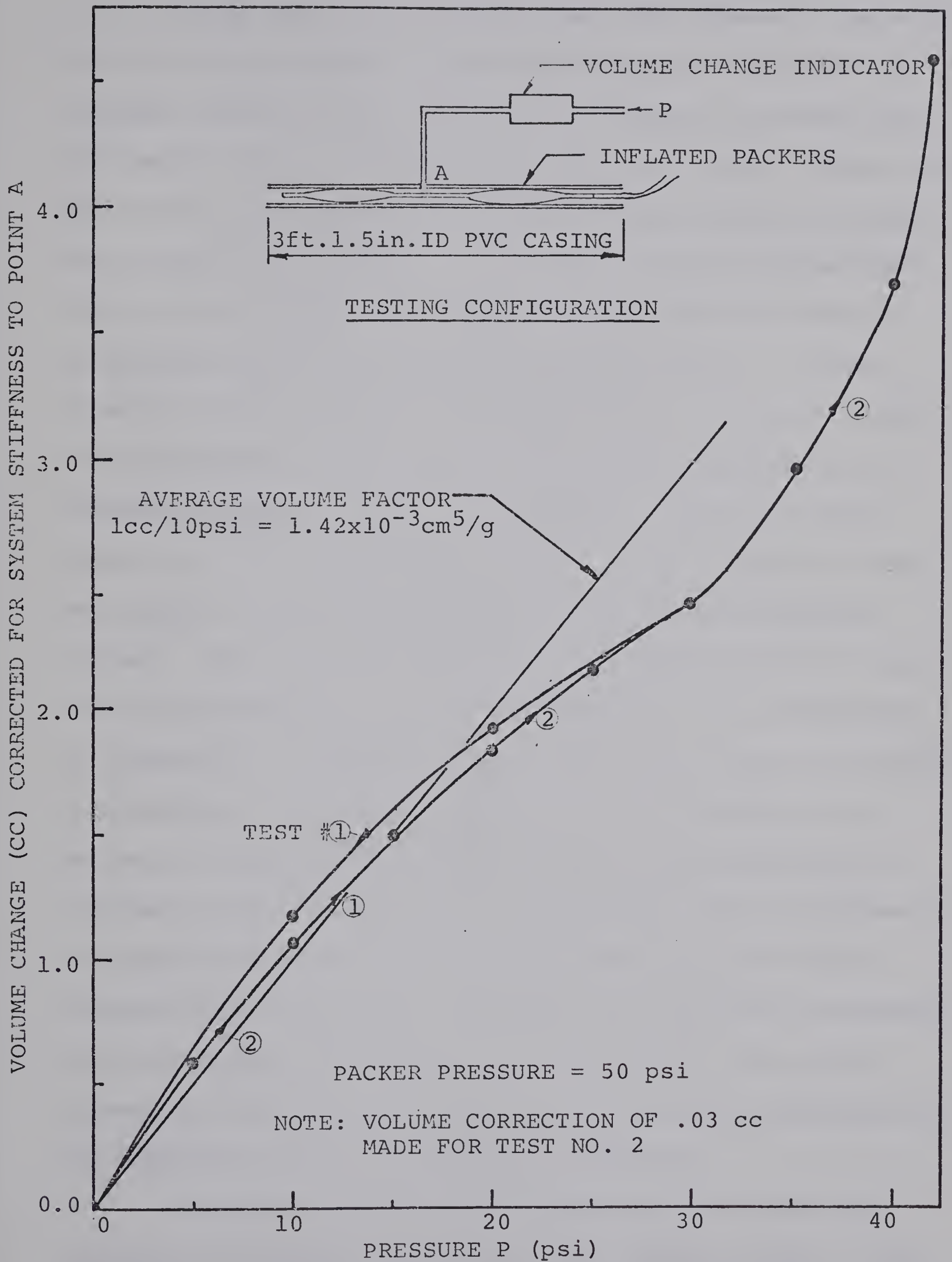


FIG. 8.2 VOLUME FACTOR OF DOUBLE PACKER PIEZOMETER

From Fig. 8.2 it may be seen that pressure increases will not occur beyond 42 psi which indicates that for the testing configuration used, 8 psi is required to seal the piezometer since the packer pressure was 50 psi. Hence this was taken as an indication of the critical packer pressure to be used in the field. In the work it was assumed that on the basis of the information of Fig. 8.2 which was determined during the field measurements that an excess pressure in the order of 20-30 psi would be enough to seal the piezometer in all cases. The curves obtained seem to indicate adequate seals. For example, curves for well point no. 3 were acquired under a variety of initial heads and appear to proceed generally to similar equilibrium values. Since criteria were not established prior to the field measurements, a fuller investigation is recommended to determine a complete set of criteria in cases of different combinations of pressures above, below and between the packers so that field conditions may be simulated and to evaluate other factors which may possibly have an influence in sealing the piezometer such as increasing the cable tension after inflation. Although the author has confidence in the results obtained, if it is found that the packer pressures used were not sufficient in general, readings may be repeated with the appropriate pressures.

Response times for piezometer systems have been studied and analyzed (Hvorslev, 1951; Gibson, 1963). Hvorslev predicted for an incompressible material that times to

a certain percentage response will be a constant for any change in pressure at the piezometer tip. Possibly this effect is brought out in the response curves of well point no. 3 in the coal. Although percentage responses will not be the same for the entire measurements, it is interesting to note the curves tend to come to equilibrium at a similar time. Readings at the other well points were too scarce or too varied to make any such observation.

Information may be determined from the equilibrium values of the response curves. For well point no. 1, assuming an initial equilibrium reading much less than the following measurement, it appears that freezing of the slope face may have effected an area of low permeability causing the water table to rise substantially. The melting effect of the sun may have some influence on determining the upper water distribution in the slope. The slope in which the multistage piezometer is situated is on the south side and removed from the effects of the sun. If this hypothesis is valid the general influence of freeze-up could possibly be determined by attempting a correlation of slide frequency with the sun-side or shade-side of the river.

The low permeability of the seal which has grouted in the screen of well point no. 1 will cause considerable time lag. Any change in groundwater conditions that do occur will be reflected with a large phase change.

Although the initial reading at well point no. 2

is incomplete as well, it is interesting to speculate that the freeze-up also effects the pressure in this area. It is possible that an installation time lag caused by stress release could have caused the low initial reading. However, low pressures occurred simultaneously at the upper two well points and a water table increase is then apparently reflected at both points as well. A large measurement time lag appears at the second well point because the pressure became zero as the equilibrium water level in the casing fell below this point. The well point acted as a drain with the result that the pressure in this area became low. The soil subsequently must have consolidated but to a very small degree since the shales are generally quite hard. When the piezometer was installed the second time, the draining was stopped and water flowed into the area again increasing the pressure. This process may be observed in Fig. 7.8 as it reached a minimum. Equilibrium was not yet attained even after one month. The initial response curve hopefully precludes a theory of a leaky cement seal. The phenomena described emphasizes one of the weaknesses of the present multistage system. Generally an increased measurement time lag will be effected in impervious and compressible material when the pressure due to the column of water in the casing at the well point is lower or higher than the pressure in the soil. A single packer piezometer in impervious material may be more practical since a large change in pressure at the point relative

to the pressure in the soil should not occur as the water in the casing should not drain out. Hence it is recommended that measuring points not be placed in impervious materials when used in conjunction with an open multistage system since measurement time lag will be large even if the volume factor is small. As pointed out in section 7.2, depending on the pressure distribution in the shale, longer seals might have resulted in different equilibrium readings. However, measurement time lag would also have occurred for that case.

The well point in the 4 ft. coal layer might also bring out some of the same effects of freezing as may have been observed with the upper two well points. According to the section of Thomson (1970), the coal layer outcrops approximately 700 ft. from the installation so that this appears to be a well draining layer.

The rapid response of the initial trial at this well point is interesting. The following is a possible explanation. With the initial high head the drilling mud penetrated to a certain extent. As the piezometer was installed and packers inflated the pressure decreased as shown on Fig. 7.9 and the effective stresses in the coal layer at the point increased. As a result the drilling mud was squeezed further into the coal fractures with the tightening of the cracks. Apparently the effect of the combination of the drilling mud and the crack tightening has affected subsequent measurements. The fact that some

fractured coals may have large changes in permeability with stress has already been brought out in Fig. 3.4. One would ordinarily expect and hopefully obtain response characteristics as shown with the initial measurement.

The bottom coal layer appears to drain freely into the river. The layer is approximately 10-15 ft. below the river level with a measured head of water of 17.4 ft. There is likely flow out of the 4 ft. layer and into the 6-12 in. layer. The flow is enough to account for the head above well point no. 3 and flow into well point no. 4. It is possible that the pressure in the lower layer may be a function of river level. This could be ascertained within the limits of the instrument by continuous measurements of pressure and river level.

It is recommended that measurements be continued on the installation for the acquisition of additional data accompanying seasonal pressure fluctuations as well as to verify the measurements already obtained.

During the drilling program a bentonite bed was not observed above the 4 ft. coal layer and may have been missed. In the work of Thomson (1970) a 6 in. bentonite layer is purportedly above this coal stratum. This may act as an impermeable barrier depending on the overall relative permeabilities of the bentonite and shale. Eigenbrod and Morgenstern (1971) also report a bentonite bed above one of the coal layers. Although geological reasons may exist for a systematical sequence of this nature,

bentonite seams will not necessarily overlies coal beds and furthermore could be below the coal as well.

A possible pressure diagram for winter conditions may exist as shown in Fig. 8.3. The effect of a possible coal seam at 121 ft. and the consequences of possible inadequate seals in the shale may cause the distribution to be considerably different but on the basis of the obtained data the interpretation is as adequate as any. Also if bentonite acts as an impermeable barrier, the pressure distribution may be as indicated by the dash-dotted lines and could appear as the dashed line if the bentonite has no effect. In terms of slope stability this perched distribution will influence analyses to give higher factors of safety if failure surfaces extend below the perched water tables.

It is apparent that the multistage piezometer system is not as practical as was first thought. The major drawback of the present system is the much longer than expected response times. This was exactly the one aspect that made the instrument appear practical. However the system may yet be useful for measuring pressures in permeable strata. If compression of air in the packers is the main cause of the magnitude of the volume factor the incorporation of an incompressible fluid in some manner may decrease this value. For example, Lundgren (1966) uses water for inflation of the packers and this may have decreased the volume factor of the instrument used. Preferably however, another packer system should be designed

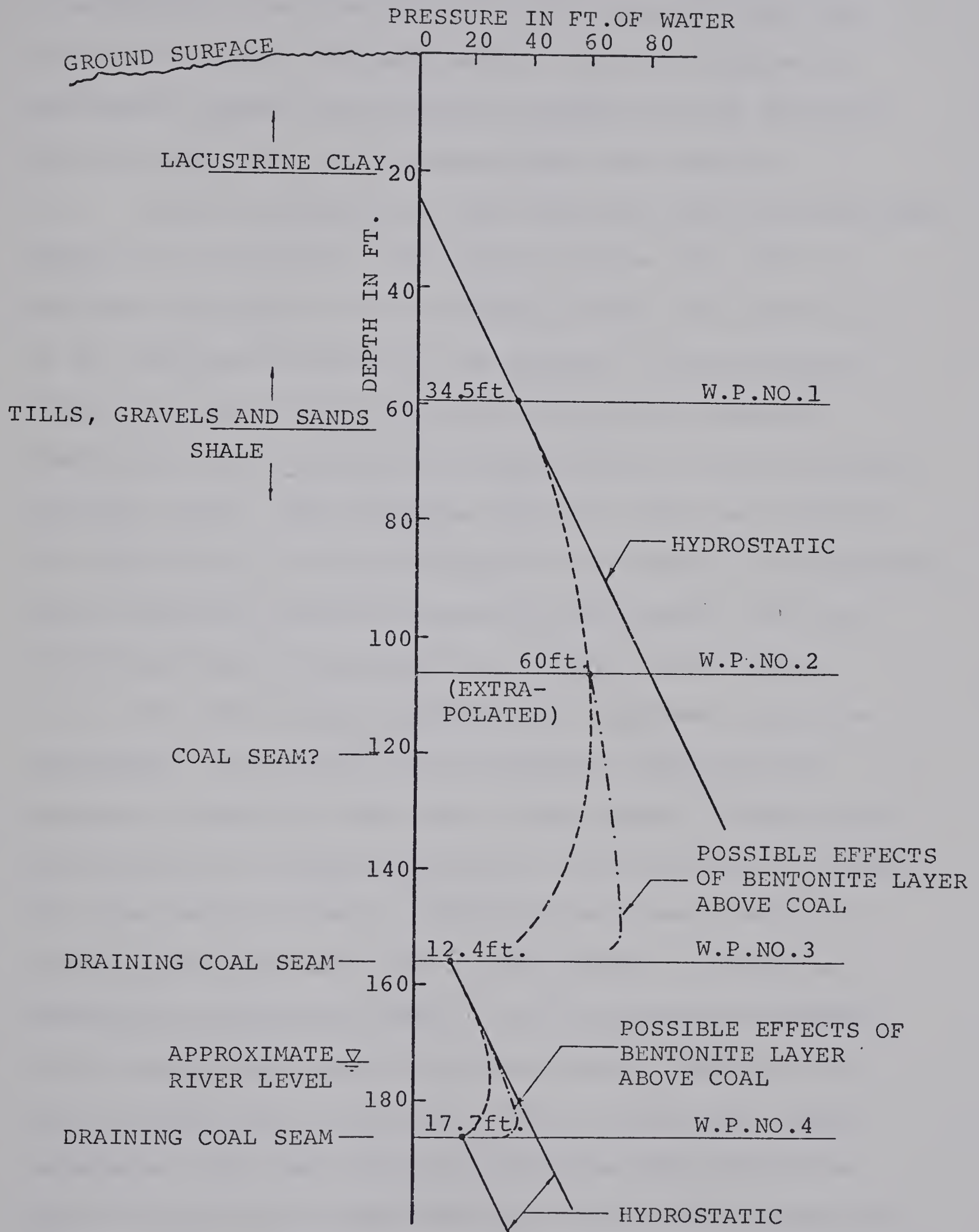


FIG. 8.3 POSSIBLE PRESSURE DISTRIBUTIONS IN SLOPE

to establish a low compliance of the instrument and yet be able to produce adequate seals. If such a system is developed, almost instantaneous response will be attained and will make the system immeasurably more useful.

Other problems have also detracted from the practical aspects of the system. For depths greater than 200 ft. problems will occur in the lowering of the instrument due to the additional weight of the cables. If the present cables are used difficulties will also be encountered finding the exact well point location due to the elasticity of these lines. Both of these problems might be overcome with the use of a relatively rigid steel cable in conjunction with a hoisting system to place the instrument. The air line could then be replaced by a lighter rubber hose.

In view of the preceding other systems should be considered. As of late very economical Japanese built pressure transducers have come on the market. These could be fitted into a proper housing tip and permanently grouted into the desired layers. Although the present devices contain some hysteresis and a small amount of creep as revealed by laboratory tests, for the pressures measured in the study these would have been ideal. However since one is always wary of burying a wholly electrical system because of their past unreliability over long periods of time, a long-term program should be initiated to reveal the true limitations of these transducers in the field, modifying them as required. A system for placing these could

be designed as shown in Fig. 8.4. The improved grouting procedure discussed could be used for installing the seals. With this piezometer system there will be negligible measurement time lags in addition to the convenient and rapid acquisition of data at all points simultaneously.

8.2 Conclusions

The grouting system used was generally adequate to install the cement seals. Some inconveniences and limitations associated with the technique have been noted and a modified method has been proposed.

The grout used was suitable. A cement slurry with 'Entraplast A' additive has proved to be a successful and workable grouting material for sealing well points into their respective locations. If properly installed a set cement is not required for continuation of placement of sand and seals.

The present piezometer system although workable is not practical in its present form. A more accurate method for situating or seating the piezometer at the well point is required. The inflatable packers give rise to a larger than expected volume factor. To make the system feasible the response time should be reduced. This could be brought about by designing a new packer system with a much lower compliance. Well points in an incompressible and impermeable material will often result in long measurement time lags. This difficulty could be overcome with a system of irrecoverable pressure transducers when these devices

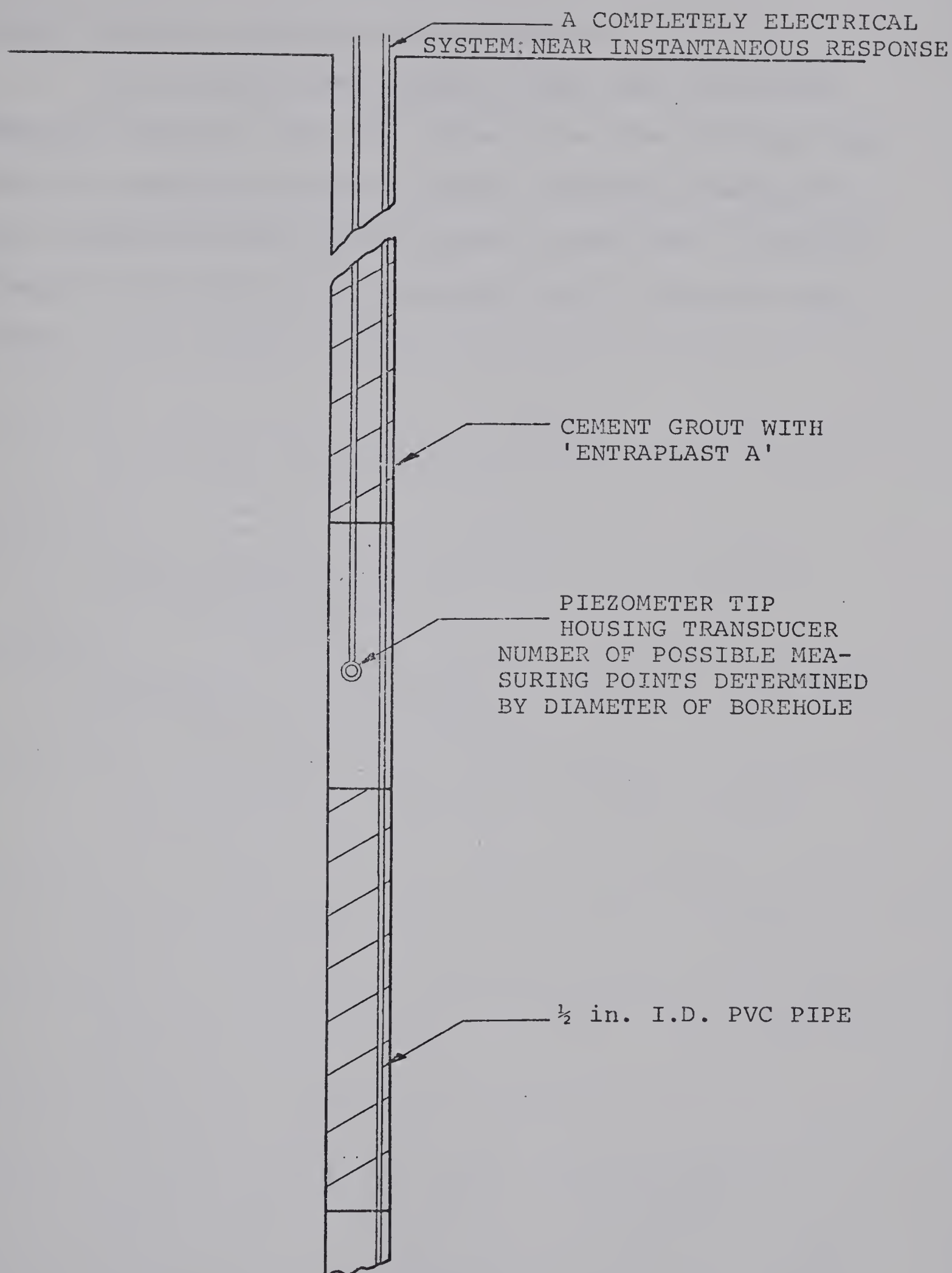


FIG. 8.4 PIEZOMETER ARRANGEMENT USING IRRECOVERABLE TRANSDUCERS

become reliable, accurate and economical.

In the past, coal layers in the Upper Cretaceous Edmonton Formation have been shown to be free draining into the North Saskatchewan River valley. Another example of this feature is shown in the present study where irregular pressure distributions are revealed due to these draining layers.

LIST OF REFERENCES

- Bernaix, J., 1969. "New laboratory methods of studying the mechanical properties of rocks". Int. J. Rock Mech. Min. Sci., 6, 43-90.
- Bishop, A. W., Kennard, M. F., and Penman, A. D. M., 1961. "Pore pressure observations at Selset Dam". Proc. Conf. on Pore Pressure and Suction in Soils, 36-47, Butterworths, London.
- Bjerrum, L., Kenney, T. C., and Kjaerresli, B., 1965. "Measuring instruments for shuttered excavations". Proc. ASCE, J. Soil Mech. and Found. Div., 91, SMI, 111-141.
- Brace, W. F., Walsh, W. B., and Frangos, W. T., 1968. "Permeability of granite under high pressure". J. Geophysical Research, 73, 6, 2225-2236.
- Brooker, E. W., Scott, J. S., and Ali, P., 1968. "A transducer piezometer for clay shales." Canadian Geotechnical Journal, 5, 256-264.
- Brooker and Associates, 1970. "Slope stability investigation, university river bank at 112th street". Report submitted to Campus Development Branch, University of Alberta.
- Casagrande, A., 1940. "Seepage through dams", in "Contributions to Soil Mechanics, 1925-1940". Boston Soc. Civ. Eng., 295-336.
- Casagrande, A., 1949. "Soil mechanics in the design and construction of the Logan Airport". J. Boston Soc. Civ. Eng., 36, 192-221.
- Conte, S. D., 1965. "Elementary numerical analysis". McGraw-Hill, New York.
- Davis, S. N. and Turk, L. J., 1964. "Optimum depth of wells in crystalline rocks". Groundwater, 2, 6-11.
- Duncan, J. M., Dunlop, P. and Seed, H. B., 1968. "Finite element analyses of slopes in soil". U.S. Army Waterways Experiment Station, Vicksburg, Contract Report S-68-6, University of California, Berkeley, 232 pp.

- Duncan, J. M. and Goodman, R. E., 1968. "Finite element analyses of slopes in jointed rock". U.S. Army Waterways Experiment Station, Vicksburg, Contract Report S-68-3, University of California, Berkeley, 276 pp.
- Eigenbrod, K. D. and Morgenstern, N. R., 1971. "A slide in cretaceous bedrock, Devon, Alberta". Presented at the 2nd Annual Symposium on Stability for Open Pit Mining, Vancouver, B.C., November, 1971.
- Fatt, I., and Davies, D. H., 1952. "Reduction in permeability with overburden pressure". Trans. AIME, 195, p. 329.
- Finn, W. D. Liam, 1967. "Finite element analysis of seepage through dams". Proc. ASCE, J. Soil Mechs. and Found. Div., 93, SM6, 41.
- Freeze, R. A., and Witherspoon, P. A., 1966. "Theoretical analysis of regional ground water flow: Analytical and numerical solutions to the mathematical model". Water Resources Res., 2, 4, 641-656.
- Freeze, R. A., and Witherspoon, P. A., 1967. "Theoretical analysis of regional ground water flow: Effect of water-table configuration and subsurface permeability variation". Water Resources Res., 3, 2, 623-634.
- Freeze, R.A., and Witherspoon, P. A., 1968. "Theoretical analysis of regional ground water flow: Quantitative interpretations." Water Resources Res., 4, 3, 581-590.
- Gibson, R. E., 1963. "An analysis of system flexibility and its effect on time lag in pore pressure measurements". Geotechnique, 13, 1, 1-9.
- Harr, M. E., 1962. "Groundwater and seepage". McGraw-Hill, New York.
- Hast, N., 1967. "The state of stresses in the upper part of the earth's crust". Engineering Geology (Elsevier), 2, 1, April, 5-17.
- Henkel, D. J., 1967. "Local geology and the stability of natural slopes". Proc. ASCE, J. Soil Mechs. and Found. Div., 93, SM4, 437-446.
- Holand, I., and Bell, K., 1970. "Finite element methods in stress analysis". Tapir, Trondheim, Norway, 500 pp.

- Hvorslev, M. J., 1951. "Time lag and soil permeability in ground-water measurements". U.S. Corps of Engineers, Waterways Experiment Station, Bull. No. 36.
- Kealy, C. D., and Busch, R. A., 1971. "Determining seepage characteristics of mill-tailings dams by the finite element method". U.S. Bureau of Mines, Report of Investigations, No. 7477.
- Khan, S. U., 1971. "Effect of changes in reservoir level on the stability of natural slopes". M.Sc. Thesis, Department of Civil Engineering, University of Alberta, Edmonton.
- Knutson, C. F., and Bohor, B. F., 1962. "Reservoir rock behaviour under moderate confining pressures." Proc. Fifth Symp. Rock Mech., Minnesota, 627-658.
- Lambe, T. W., 1960. "Directions for the installation of the modified Casagrande Piezometer". Chemical Grout Technical Data, Cyanamid of Canada Ltd.
- Lindberg, D. A., 1965. "Comparative aspects of piezometer designs". M.Sc. Thesis, Department of Civil Engineering, University of Alberta, Edmonton.
- Londe, P., 1971. "The flow of water in rock". Summer course on the Analysis and Design of Rock Slopes, University of Alberta, Edmonton.
- Lundgren, R., 1966. "Electrical piezometer for field installation". Civil Engineering, (New York), August.
- Lyell, K. A., 1970. "The interpretation of water pressure factors for use in slope theory". Symposium on Theoretical Background to the Planning of Open Pit Mines, p. 73-85. S. African J.M.M., Johannesburg.
- Meigh, A. C., and Greenland, S. W., 1965. "In situ testing of soft rocks". Proc. Sixth Int. Conf. Soil Mech. Found. Eng., Montreal, 1, 73-76.
- Mordecai, M., and Morris, L.H., 1971. "An investigation into the changes of permeability occurring in a sandstone when failed under triaxial stress conditions". Proc. Twelfth Symp. Rock Mech., Rolla, 221-239.
- Morgenstern, N. R., and Phukan, T. A. L., 1966. "Non-linear deformation of a sandstone". Proc. First Int. Cong. Rock Mechanics, Lisbon, 1, 543-548.

- Muskat, M., 1946. "The flow of homogeneous fluids through porous media". Edwards Brothers, Ann Arbor, Mich.
- Neuman, S. P. and Witherspoon, P. A., 1970. "Finite element method of analyzing steady seepage with free surface". Water Resources Research, 6, 3, 889-897.
- Parsons, R. W., 1966. "Permeability of idealized fractured rock". J. Soc. Pet. Eng., 6, 126-136.
- Patching, T. H., 1965. "Variations in permeability of coal". Proceedings of Rock Mechanics Symposium, Toronto, 185-199.
- Patching, T. H., 1970. "The retention and release of gas in coal--A review". Trans. CIM, 73, 328-334.
- Penman, A. D. M., 1961. "A study of the response times of various types of piezometer". Proc. Conf. on Pore Pressures and Suction in Soils, 53-58, Butterworths, London.
- Powers, T. C., Copeland, L. E., Hayes, J. C., and Mann, H. M., 1955. "Permeability of Portland cement paste". Research and Development Laboratories of the Portland Cement Association, Bulletin No. 53, Chicago.
- Scott, J. D. and Kilgour, J., 1967. "Experience with some vibrating wire instruments". Canadian Geotechnical Journal, 4, 100-123.
- Sharp, J. C., 1970. "Fluid flow through fissured media". Ph.D. Thesis, University of London.
- Sherman, W. C., and Banks, D. C., 1970. "Seepage characteristics of explosively produced craters in soil and rock". U.S. Waterways Expt. Station, NCG Technical Report No. 27, Vicksburg, Mississippi.
- Snow, D. T., 1967. "Anisotropic permeability of fractured rocks". Hydrology and Flow through Porous Media, R. J. M. DeWiest, ed., (Muskat Vol.), Academic Press, N.Y., 71 pp.
- Snow, D. T., 1968a. "Rock fracture spacings, openings and porosities." Proc. ASCE, J. Soil Mechs. and Found. Div., 94, 73-91.
- Snow, D. T., 1968b. "Fracture deformation and changes of permeability and storage upon changes of fluid pressure". Q. Colorado School of Mines, Pt.A, 63, 201-244.

- Steffen, O. K., and Klingman, H. L., 1966. "Slope stability at the open pit of Nchanga Consolidated Copper Mines Ltd." J. S. African I.M.M., 67, 140-171.
- Taylor, R. L. and Brown, C. B., 1967. "Darcy flow solutions with free surface". Proc. ASCE, J. Hydraul. Div., 93, HY2, 25-33.
- Terzaghi, K., 1960. "Discussion of 'Rockfill Dams: Wishon and Courtright Concrete Face Dams', by J. B. Cooke". Trans. ASCE, 125, part II.
- Terzaghi, K., 1962. "Stability of steep slopes in hard unweathered rock". Geotechnique, 12, 4, 251.
- Thomson, S., 1970. "Riverbank stability study at the University of Alberta, Edmonton". Canadian Geotechnical Journal, 7, 2, 157-168.
- Tomlin, G. R., 1966. "Seepage analysis through zoned anisotropic soils by computer". Geotechnique, 16, 3, 220-234.
- Toth, J., 1962. "A theoretical analysis of groundwater flow in small drainage basins". Proc. 3rd Hydrology Symposium, National Research Council of Canada, Queen's Printer, p. 75-96.
- Vaughan, P. R., 1969. "A note on sealing piezometers in boreholes". Geotechnique, 19, 405-413.
- Walsh, J. B., and Brace, W. F., 1966. "Cracks and pores in rocks". Proc. First Int. Cong. Rock Mechanics, Lisbon, 1, 643-646.
- Warlam, A. A., and Thomas, E. W., 1965. "Measurement of hydrostatic uplift pressure on spillway weir with air piezometer". ASTM, STP 392, p. 143.
- Zienkiewicz, O. and Cheung, Y. K., 1965. "Finite element in the solution of field problems". The Engineer, London, 220.
- Zienkiewicz, O., Mayer, P. and Cheung, Y. K., 1966. "Solution of anisotropic seepage by finite elements". Proc. ASCE J. Eng. Mech. Div., 92, EMI, 111-120.
- Zienkiewicz, O., and Stagg, K. G., 1967. "Cable method of in situ rock testing". Int. J. Rock Mech. Min. Sci., 4, 273-300.

APPENDIX A

BODY FORCE AND STRESS RELEASE

EQUATIONS

APPENDIX A

BODY FORCE EQUATIONS

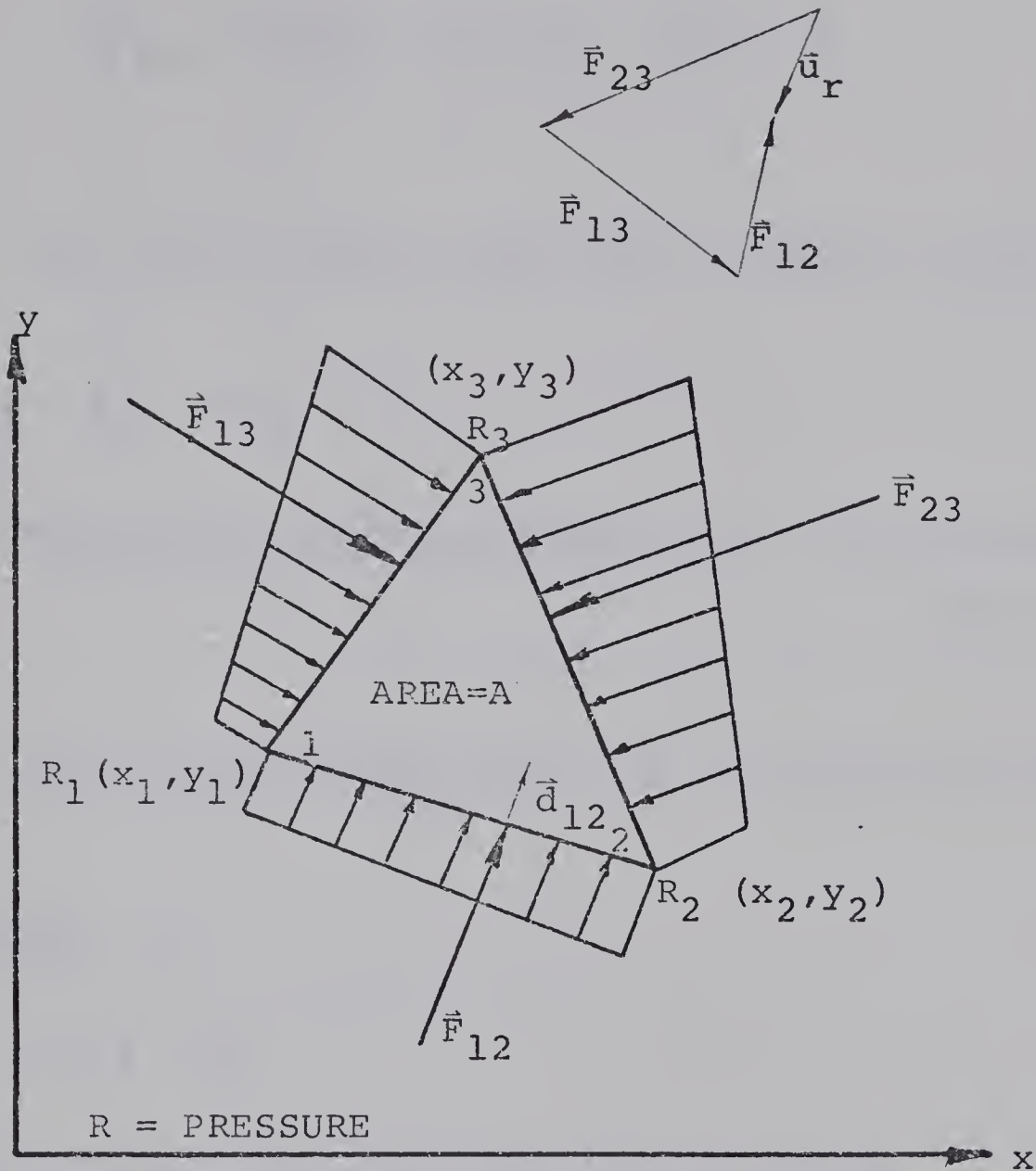


FIG. A1 ELEMENT PRESSURES AND RESULTANT FORCES

Considering the pressures on side 1-2 of the element shown in Fig. A1 the resultant force \vec{F}_{12} is given by

$$\vec{F}_{12} = \sqrt{(x_2 - x_1)^2 + (y_2 - y_1)^2} \left(\frac{R_1 + R_2}{2} \right) \vec{d}_{12}$$

where \vec{d}_{12} is a unit vector perpendicular to side 1-2 and pointing inward.

By vector algebra it may be shown that

$$\vec{F}_{12} = \frac{R_1 + R_2}{2} (y_1 - y_2) \vec{i} - (x_1 - x_2) \vec{j}$$

The sum of these three force vectors is \vec{u}_r .

$$\vec{u}_r = \vec{F}_{12} + \vec{F}_{23} + \vec{F}_{31}$$

$$= \frac{1}{2} \left[(-R_1 y_2 + R_2 y_1 - R_2 y_3 + R_3 y_2 - R_3 y_1 + R_1 y_3) \vec{i} - (-R_1 x_2 + R_2 x_1 - R_2 x_3 + R_3 x_2 - R_3 x_1 + R_1 x_3) \vec{j} \right]$$

The change in body force (R is in feet of water)

$$\Delta B.F. = A \vec{\gamma}_w + \vec{u}_r$$

$$= -A \gamma_w \vec{j} + \vec{u}_r$$

$$= \frac{1}{2} \gamma_w \left[(-R_1 y_2 + R_2 y_1 - R_2 y_3 + R_3 y_2 - R_3 y_1 + R_1 y_3) \vec{i} - (2A - R_1 x_2 + R_2 x_1 - R_2 x_3 + R_3 x_2 - R_3 x_1 + R_1 x_3) \vec{j} \right]$$

Check on Program Results

Since the change in body force is identical to the seepage force a check can be made on the program results. The following values are taken for a converged case using the weaker variation of permeability and $K_0 = 2.0$, and are shown in Fig. A2.

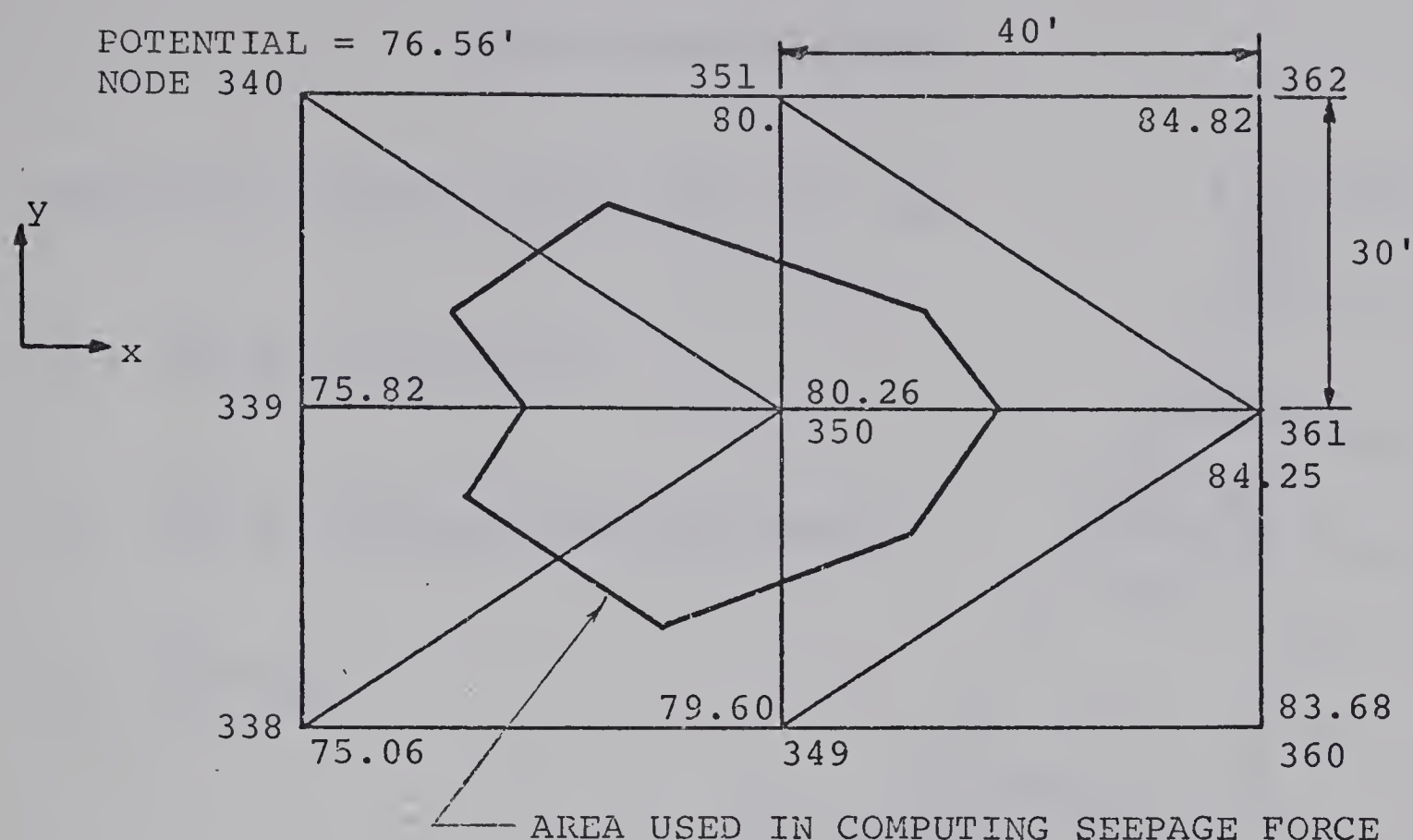


FIG. A2 ELEMENT CONFIGURATION AND PRESSURES IN THE VICINITY OF NODE 350

For node 350, the average gradient in the x direction = 1.083
in the y direction = .0225

$\frac{1}{3}$ of the area of each triangle which effects node 350 = 1200 FT²

The seepage force $F_x = A i_x \gamma_w = 62.4 \times 1200 \times 1.083 = 8120$ lb.

$F_y = A i_y \gamma_w = 62.4 \times .0225 \times 1200 = 1685$ lb.

The program gives a body force $F_x = 8033$ lb

$F_y = 1723$ lb.

STRESS RELEASE FORCES

HORIZONTAL RELEASE FORCES FROM FIG. A3a

$$F_b = \frac{\gamma K_O}{8} (3d_1^2 - 2d_1d_2 - d_2^2)$$

$$F_m = \frac{\gamma K_O}{8} (d_m^2 + 2d_md_{m+1} - 2d_{m+1}d_{m+2} - d_{m+2}^2)$$

$$F_t = \frac{\gamma K_O}{8} d_{t-1}^2$$

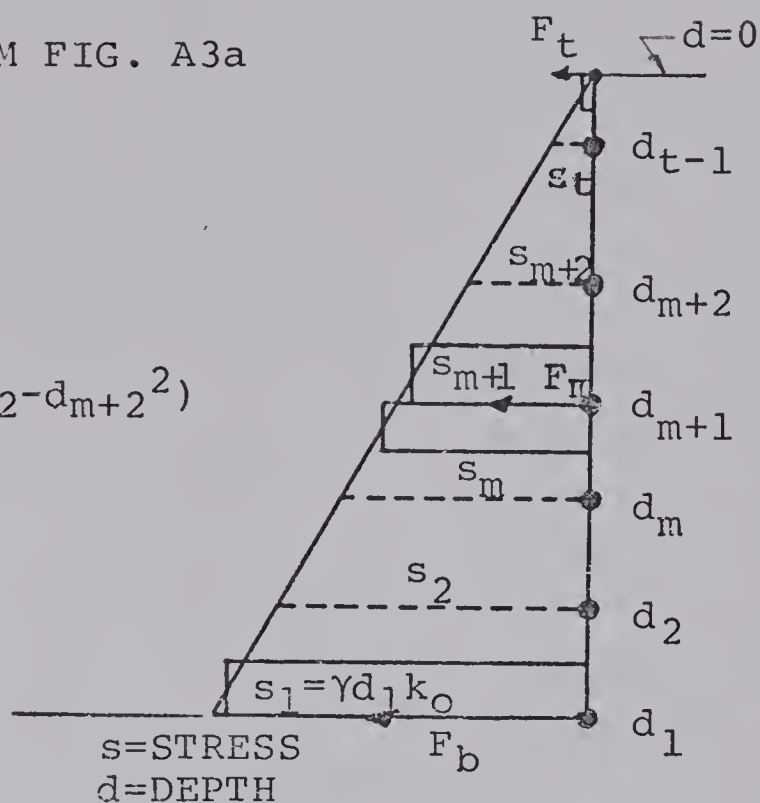


FIG. A3a

VERTICAL RELEASE FORCES FROM FIG. A3b

$$F_r = \gamma d_1 (x_r - x_{r-1})/2$$

$$F_\ell = \gamma d_1 (x_1 - x_0)/2$$

$$F_m = \gamma d_1 (x_{m+2} - x_m)/2$$

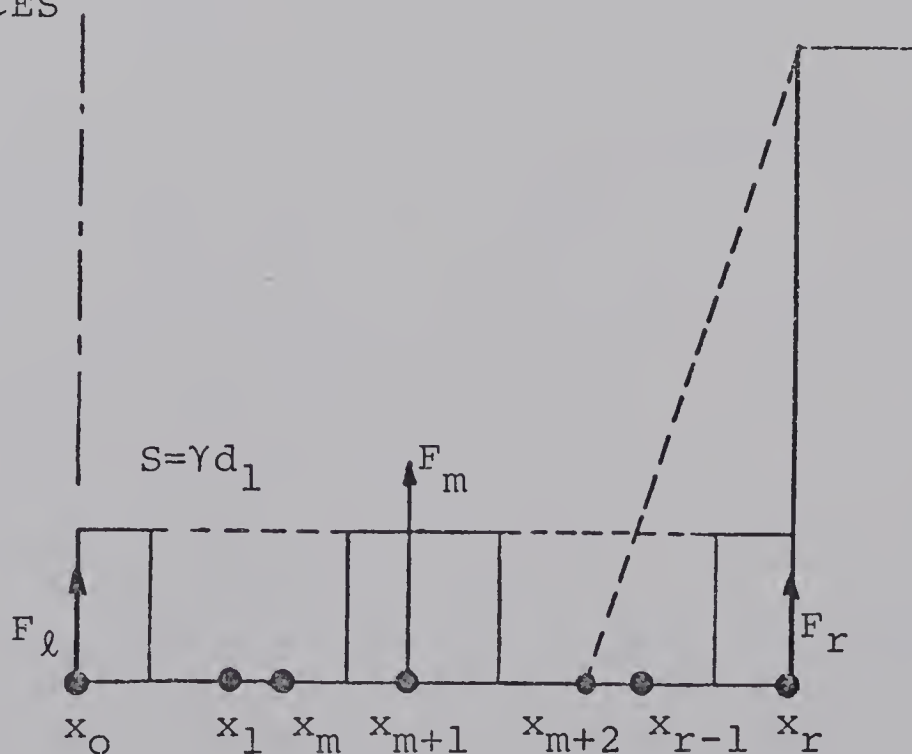


FIG. A3b

APPENDIX B

COMPUTER PROGRAM

APPENDIX B

COMPUTER PROGRAM

The following is a list of the important terms in the computer program. Occasionally two notations have been used for the same variable.

Seepage Section

C(L)	Initial total allocation of L storage locations for the seepage section.
NUMNP	Number of nodal points.
NUMEL	Number of elements.
NUMMAT	Number of materials (=number of elements).
NUMFSC	Number of free surface nodes.
RO	Density of fluid.
BETA	Free surface correction factor.
HTE,HEAD	Factors to normalize equipotential values.
TOL	Tolerance for free surface.
MAXIT	Maximum number of iterations per cycle.
X(),Y()	Nodal point co-ordinates.
NBC()	Nodal boundary condition.
FX()	Nodal flow or pressure.
NP(6,M)	Nodal points, material number and angle of the principal permeability axis associated with element M.
NPFS()	Free surface nodes.

Stress Section

JNUMNP, NUMNP	Number of nodal points.
JNUMEL, NUMNP	Number of elements.
NUMAT	Number of materials.
E()	Modulus of elasticity.
PR()	Poisson's ratio.
CO(), RO()	Density.
SX(), X() SY(), Y()	Nodal point co-ordinates.
KODE()	Nodal boundary condition.
NNP(3,I), NP(3,I)	Nodal points associated with element I.
MAT()	Element material.
NCORS(I)	Seepage element associated with stress element I.
NFSC	Number of free surface stress nodes.
MFP	Number of slope face nodes.
MBP	Number of base of excavation nodes.
NCYC	Number of cycles.
DEPG	Depth of grid.
DEPE	Depth of excavation.
XKO	Effective stress ratio.
IFSN()	Free surface stress nodes.
NFP()	Slope face nodes.
NBP()	Base of excavation nodes.

V IV G COMPILER

MAIN

03-29-72

22:59.31

PAGE 0001

```

C      THIS IS THE MAIN PROGRAM WHICH COUPLES THE FINITE ELEMENT
C      SEEPAGE PROGRAM WITH THE FINITE ELEMENT STRESS PROGRAM
C      AN EFFECTIVE STRESS ANALYSIS IS USED
C      PROVISION IS MADE FOR READING IN THE PERMEABILITIES OF A
C      PREVIOUS RUN IF POSITION OF FREE SURFACE NOT STABLE
C      THESE ARE READ IN FROM A TAPE FILE
C      THE SEEPAGE SECTION HAS A VARIABLE DIMENSIONING SCHEME WITH A
C      TOTAL STORAGE ALLOCATION OF C(21000)
C      THE STRESS SECTION HAS FIXED DIMENSION STATEMENTS WITH DIMENSIONS
C      FOR APPROXIMATELY 500 NODES AND 1000 ELEMENTS

```

```

C
COMMON/CONTRL/HED(18),NUMNP,NUMEL,NUMMAT,NUMFSC,NDMP,NTYPE,RO,
1 BETA,RITE,HEAD,TOL,MAXIT,MAXMSH,NFLCD,PI,CU(500),CV(500)
COMMON/COMING/ E(3),PR(3),CD(3),SX(500),SY(500),U(500),V(500),
1 TH(1000),STIF(1000,70),AP(1000),ESTIF(6,6),ECM(3,3),EBM(3,6),
1 ESM(3,6),WT, JNUMNP, JNUMEL, JNUMAT, KODE(500),NNP(3,1000),
1 MAT(1000),MBAND,NEQ,M,LM(6),IMXMSH,IMESH(500),NCORS(1000),
1 IFSN(20),NFP(20),NFSC,MFP,APS(1000),IHAR,INCOR(500)
1,XKO,NCYC,MBF,DEPG,DEFE,NBP(20)
COMMON C(21000)
COMMON/ETC/SIGP(1000,4)

```

```

C
READ(6,5) IHAR
5      FORMAT(15)
C

```

```

C      CALL CPLG(MAXBAN)

```

```

C      CALL READIN

```

```

C
C
N0=1
N1=N0+NUMMAT
N2=N1+NUMMAT
N3=N2+NUMFSC
N4=N3+NUMFSC
N5=N4+NUMNP
N6=N5+NUMNP
N7=N6+NUMNP
N8=N7+NUMNP
N9=N8+NUMNP
N10=N9+NUMEL
N11=N10+NUMEL*5
N12=N11+NUMNP

```

```

C
71      CALL FCRM(MAXBAN, C(N0),C(N1),C(N2),C(N3),C(N4),C(N5),C(N6),
1 C(N7),C(N8),C(N9), C(N10), C(N11), C(N12))

```

```

C      CALL CHANGE(C(N2),C(N5),C(N6),C(N10))

```

```

C      CALL ASTIF

```

```

C      CALL BAND1

```

```

C      CALL STRESS
GO TO 71
END

```

MEMORY REQUIREMENTS 000430 BYTES

J IV G COMPILER

CPLG

03-29-72

23:02.02

PAGE 0001

```

      SUBROUTINE CPLG(MAXBAN)
      COMMON/CONTRL/HED(18),NUMNP,NUMEL,NUMMAT,NUMFSC,NDMP,NTYPE,RO,
      1BETA,HITE,HEAD,TOL,MAXIT,MAXMSH,NFLCD,PI,CU(500),CV(500)
      COMMON C(21000)

```

```

      MMAX=21000

```

C

C

C

```

      READ INITIAL DATA

```

```

      30 REAC(5,1006) HED

```

```

      33 READ(5,1000) NUMNP,NUMEL,NUMMAT,NUMFSC,NTYPE,NFLCD,RO,HITE,HEAD

```

```

      X,BETA,MAXIT,TOL

```

```

      WRITE(6,1026)

```

```

      WRITE(6,2000) HED,NUMNP,NUMEL,

```

```

      NUMFSC,

```

```

      RO,HITE,HEAD,

```

```

      * BETA,MAXIT,TCL

```

```

      IF (NTYPE.EQ.0) WRITE(6,2001)

```

```

      IF (NTYPE.EQ.1) WRITE(6,2002)

```

C

```

C**** SET UP VARIABLE DIMENSIONING ADDRESSES

```

C

```

      N0=1

```

```

      N1=N0+NUMMAT

```

```

      N2=N1+NUMMAT

```

```

      N3=N2+NUMFSC

```

```

      N4=N3+NUMFSC

```

```

      N5=N4+NUMNP

```

```

      N6=N5+NUMNP

```

```

      N7=N6+NUMNP

```

```

      N8=N7+NUMNP

```

```

      N9=N8+NUMNP

```

```

      N10=N9+NUMEL

```

```

      N11=N10+NUMEL*5

```

```

      N12=N11+NUMNP

```

C

```

C***** INPUT MESH

```

C

```

      CALL MESHIN(MAXBAN,C(N0),C(N1),C(N2),C(N3),C(N4),C(N5),C(N6),

```

```

      X,C(N7),C(N8),C(N9),C(N10))

```

```

      IF(NDMP.NE.0) GO TO 30

```

C

```

C**** CHECK ON SIZE OF REQUIRED STORAGE FOR PROBLEM AND COMPARE TO AVAIL

```

C

```

      N13=N12+MAXBAN*NUMNP

```

```

      WRITE(6,3000) N13,MMAX

```

```

      IF(N13.GE.MMAX) CALL EXIT

```

C

```

C**** FORMATS

```

C

```

1026 FORMAT(1H1, '***** SEEPAGE INPUT *****
      1***'//)

```

```

1000 FORMAT(6I5,4F10.3,I5,F5.2)

```

```

1005 FORMAT(18A4)

```

```

2000 FORMAT ( 1PA4/

```

```

      1      30H0 NUMBER OF NODAL POINTS_____ I3/

```

```

      2      30H0 NUMBER OF ELEMENTS_____ I3/

```

```

      *      30H0 NUMBER OF FREE SURFACE CARDS, I3/

```


J IV G COMPILER CPLG 03-29-72 23:02.02 PAGE 0002

4 30H0 UNIT WEIGHT OF FLUID_____ E12.4/
4 30H0 REFERENCE FOR POTENTIALS_____ E12.4/
5 30H0 AVAILABLE HEAD_____ E12.4/
6 30H0 CORRECTION FACTOR_____ F10.5/
* 30H0 MAXIMUM NUMBER OF ITERATIONS, I3/
7 30H0 ERROR TOLERANCE_____ F10.5/)

2001 FORMAT (27H0 AXISYMMETRIC FLOW PROBLEM/)

2002 FORMAT (20H0 PLANE FLOW PROBLEM/)

3000 FORMAT(19H REQUIRED STORAGE = I10,

21H ALLOCATED STORAGE =

X I10)

RETURN

END

MEMORY REQUIREMENTS 000710 BYTES

IV G COMPILER

MESHIN

03-29-72

23:02.08

PAGE 0001

SUBROUTINE MESHIN(MAXBAN,XK1,XK2,NPFS,ALPHA,MESH,X,Y,NBC,FX,ANG,
X NP)

C

C****THIS SUBROUTINE INPUTS DATA FOR SEEPAGE MESH CONEIGURATION

C

COMMON/CONTRL/REC(18),NUMNP,NUMEL,NUMMAT,NUMFSC,NDMP,NTYPE,RO,
1BETA,HITE,HEAD,TOL,MAXIT,MAXMSH,NFLCD,P1,CU(500),CV(500)
DIMENSION XK1(1),XK2(1),X(1),Y(1),NBC(1),FX(1),ANG(1),NP(5,1)
DIMENSION MESH(1),ALPHA(1),NPFS(1)
NDMP=0

C

C

C**** READ AND PRINT NODAL INFORMATION

C

M=0

MMM=0

60 READ(5,1002) N,IN,NBC(N),X(N),Y(N),FX(N)

IF(N.LE.M) GO TO 64

MMM=MMM+1

MESH(MMM)=N

IF(N.LE.1) GO TO 161

XNMM=N-M

XNMM=XNMM

DX=(X(N)-X(M))/XNMM

DY=(Y(N)-Y(M))/XNMM

DF=(FX(N)-FX(M))/XNMM

MP1=M+1

IF(MP1.GE.N) GO TO 161

NM1=N-1

DO 61 NN=MP1,NM1

X(NN)=X(NN-1)+DX

Y(NN)=Y(NN-1)+DY

NBC(NN)=0

FX(NN)=0.0

IF (IM.EQ.0) GO TO 61

NBC(NN)=NBC(M)

FX(NN)=FX(NN-1)+DF

61 CONTINUE

161 IF (N.GE.NUMNP) GO TO 63

M=N

IM=IN

GO TO 60

64 WRITE(6,2012) N

NDMP=1

GO TO 60

63 CALL WRMESH(X,Y,NBC,FX)

MAXMSH=MMM

C

C**** READ ELEMENT CARDS

C

K=0

M=0

70 READ(5,1003) N,(NP(I,N),I=1,5),ANG(N)

NP(5,N)=N

IF(N.LE.M) GO TO 74

IV G COMPILER

MESHIN

03-29-72

23:02.08

PAGE 0002

```

      DO 440 I1=1,4
      DO 440 L1=11,4
      KK=IABS(NP(I1,N)-NP(L1,N))
      IF(KK.GT.K) K=KK
440  CONTINUE
      MPI=M+I
      IF (MPI.GE.N) GO TO 171
      NM1=N-I
      DO 71 NN=MPI,NMI
      DO 72 I=1,4
72  NP(I,NN)=NP(I,NN-1)+1
      NP(5,NN)=NN
      ANG(NN)=ANG(M)
71  CONTINUE
171  IF(N.GE.NUMEL) GO TO 73
      M=N
      GO TO 70
74  WRITE(6,2013) N
      NDMP=1
      GO TO 70
73  IF(NDMP.NE.0) RETURN
      IN=1
75  IM=IN+49
      IF(IM.GT.NUMEL) IM=NUMEL
C      WRITE(6,2005) HED,(N,(NP(I,N),I=1,5),ANG(N),N=IN,IM)
      IF(IM.GE.NUMEL) GO TO 76
      IN=IM+1
      GO TO 75
76  CONTINUE
C
C**** SET BANDWIDTH FOR PROBLEM
C
      MAXBAN=K+I
      WRITE(6,2600) HED,MAXBAN
      IF(NFLCD.LE.0) GO TO 78
C
C**** READ DISTRIBUTED FLOW INPUT CARDS
C
      WRITE(6,2601)
      DO 77 N=1,NFLCD
      READ(5,1004) I,J,QIJ
      SIJ=SQRT((X(J)-X(I))**2+(Y(J)-Y(I))**2)
      IF(NBC(I).NE.1) FX(I)=FX(I)+0.5*QIJ*SIJ
      IF(NBC(J).NE.1) FX(J)=FX(J)+0.5*QIJ*SIJ
      WRITE(6,2602) I,J,QIJ,FX(I),FX(J)
77  CONTINUE
C
C**** READ PHREATIC SURFACE DESCRIPTION
C
78  IF(NUMFSC.LE.0) RETURN
      WRITE(6,2603)
      READ(5,1005) (NPFS(I),ALPHA(I),I=1,NUMFSC)
      WRITE(6,2604) (NPFS(I),ALPHA(I),I=1,NUMFSC)
      RETURN
C

```


N IV G COMPILER

MESHIN

03-29-72

23:02.08

PAGE 0003

C**** FORMATS

C

1001 FORMAT (I5,2F10.0)

1002 FORMAT (I5,I2,I3,3F10.0)

1003 FORMAT (6I5,F10.0)

1004 FORMAT (2I5,F10.0)

1005 FORMAT (I5,F10.0)

2005 FORMAT(1H1,18A4//

2	65H ELMT	I	J	K	L	MAT
---	----------	---	---	---	---	-----

1	ANGLE//	(I5,5I10,F10.3)				
---	---------	-----------------	--	--	--	--

2600 FORMAT('1',18A4/,32H0BANDWIDTH FOR SEEPAGE PROBLEM =,I4//)

2601 FORMAT(17H DISTRIBUTED FLOW/,46H I J QIJ FX(I)

* FX(J) /)

2602 FORMAT(2I5,3F12.4)

2603 FORMAT(29H0PHREATIC SURFACE DESCRIPTION/,25H0 NODE CORR. AN
*GLE/)

2604 FORMAT(I10,F15.4)

2012 FORMAT(21H NODAL CARD ERROR, N= , I3/)

2013 FORMAT(23H ELEMENT CARD ERROR, N= , I3/)

END

MEMORY REQUIREMENTS 000CF8 BYTES

V IV G COMPILER

WRMESH

03-29-72

23:02.15

PAGE 0001

SUBROUTINE WRMESH(X,Y,NBC,FX)

C

C**** SUBROUTINE PRINTS NODAL POSITIONS

C

COMMON/CONTRL/HED(18),NUMNP,NUMEL,NUMMAT,NUMFSC,NDMP,NTYPE,RO,
 1 BETA,HTE,HEAD,TOL,MAXIT,MAXMSH,NFLCD,PI,CU(500),CV(500)
 DIMENSION X(1),Y(1),NBC(1),FX(1)

IN=1

75 IM=IN+49

IF(IM.GT.NUMNP) IM=NUMNP

WRITE(6,2004) HED,(N,NBC(N),X(N),Y(N),FX(N),N=IN,IM)

IF(IM.GE.NUMNP) RETURN

IN=IM+1

GO TO 75

2004 FORMAT(1H1,18A4//

	51H NODE	BC	X ORD	Y ORD	F//
1	(2I5,3F15.4)				

END

- MEMORY REQUIREMENTS 000294 BYTES

N IV G COMPILER

READIN

03-29-72

23:00.37

PAGE 0001

SUBROUTINE READIN

C

C STRESS GRID INPUT

C THIS SUBROUTINE READS AND PRINTS MATERIAL DATA, NODAL DATA, ELEMENT D

C IT GENERATES COORDINATES OF INTERMEDIATE NODAL POINTS AND CALCULATES

C THE BAND WIDTH AND NUMBER OF EQUATIONS

C

C

C

COMMON/COMMON/ E(3),PR(3),RO(3), X(500), Y(500),U(500),V(500),

1TH(1000),STIF(1000,70),AP(1000),ESTIF(6,6),ECM(3,3),EBM(3,6),

1 ESM(3,6),WT, NUMNP, NUMEL, NUMAT, KODE(500), NP(3,1000),

1 MAT(1000),MBAND, NEQ, M, LM(6), IMXMSH,IMESH(500), NCORS(1000),

1 IFSN(20),NFP(20), NFSC,MFP,APS(1000),IHAR,INCOR(500)

1,XKO,NCYC,MEF,DEPG,DEPE,NBP(20)

DIMENSION SHED(18)

WRITE(6,700)

C

C READ PRELIMINARY INFORMATION

C

READ(5,1000) SHED, NUMNP, NUMEL, NUMAT

WRITE(6,2000) SHED, NUMNP, NUMEL, NUMAT

C

C READ AND WRITE MATERIAL PROPERTIES

C

WRITE(6,2005)

DO 10 M=1,NUMAT

READ(5,1010) E(M),PR(M),RO(M)

10 WRITE(6,2010) M,E(M),PR(M),RO(M)

C

C READ AND WRITE NODAL DATA AND GENERATE INTERMEDIATE NODAL DATA

C

WRITE(6,2015)

MMM=1

L=1

READ(5,1020) N,KODE(N),X(N),Y(N)

IMESH(MMM)=N

GO TO 40

20 READ(5,1020) N,KODE(N),X(N),Y(N)

MMM=MMM+1

IMESH(MMM)=N

DN = N-L

DX =(X(N)-X(L))/DN

DY =(Y(N)-Y(L))/DN

25 L=L+1

IF(N-L) 50,40,30

30 X(L) = X(L-1)+DX

Y(L) = Y(L-1)+DY

KODE(L)= 0

WRITE(6,2020) L,KODE(L),X(L),Y(L)

GO TO 25

40 WRITE(6,2020) N,KODE(N),X(N),Y(N)

IF(NUMNP-N) 50,60,20

50 WRITE (6,2025) N

CALL EXIT

N IV G COMPILER

READIN

03-29-72

23:00.37

PAGE 0002

C

C READ AND WRITE ELEMENT DATA

C

50 IMXMSH=MMM

WRITE(6,2030)

DO 70 M=1,NUMEL

READ(5,1035) M,NP(1,M),NP(2,M),NP(3,M),MAT(M),TH(M),NCORS(M)

70 WRITE(6,2035) M,NP(1,M),NP(2,M),NP(3,M),MAT(M), NCORS(M)

C

C READ IN ADDITIONAL DATA

C

READ(5,1024) NFSC,MFP,MBP,NCYC,DEPG,DEPE,XKO

READ(5,1022) (IFSN(I),I=1,NFSC)

READ(5,1023) (NFP(I),I=1,MFP)

READ(5,1022) (NBP(I),I=1,MBP)

WRITE(6,1025) NFSC

WRITE(6,1026) (IFSN(I),I=1,NFSC)

WRITE(6,1027) MFP

WRITE(6,1026) (NFP(I),I=1,MFP)

WRITE(6,1028) MBP

WRITE(6,1026) (NBP(I),I=1,MBP)

WRITE(6,1029) DEPG

WRITE(6,1031) DEPE

WRITE(6,1032) XKO

WRITE(6,1033) NCYC

C

C DETERMINE BAND WIDTH AND NUMBER OF EQUATIONS

C

L=0

DO 80 M=1, NUMEL

DO 80 I=1,2

II=I+1

DO 80 J=II,3

K= IABS(NP(I,M)-NP(J,M))

IF (K.GT.L) L=K

80 CONTINUE

MBAND = 2*(L+1)

NEQ=2*NUMNP

WRITE(6,2040) MBAND,NEQ

WRITE(6,3000)

IF(MBAND.LE. 70.AND.NEQ.LE.1000) GO TO 90

WRITE(6,2050)

CALL EXIT

90 RETURN

C

C FORMAT STATEMENTS

C

700 FORMAT(1H1, '##### STRESS GRID INPUT #####'
1#####')

1025 FORMAT(///,34H NO. OF FREE SURFACE STRESS NODES=, 15/)

1026 FORMAT(10I10)

1027 FORMAT(///,25H NO. OF SLOPE FACE NODES=, 15/)

1028 FORMAT(///,19H NO. OF BASE NODES=,15/)

1029 FORMAT(//,15H DEPTH OF GRID=,F10.1)

1031 FORMAT(//,21H DEPTH OF EXCAVATION=,F10.1)

N IV G COMPILER READIN 03-29-72 23:00.37 PAGE 0003

```

1032  FORMAT(//,14H STRESS RATIO=, F6.1)
1033  FORMAT(//15H NO. OF CYCLES=,I3)
1022  FORMAT(8I10)
1023  FORMAT(8I10)
1024  FORMAT(4I5,3F10.1)
3000  FORMAT( ' STRESS READIN COMPLETED' ///)
1000  FORMAT(18A4/ 3I6)
2000  FORMAT( 10X,18A4,////
1 1H , 26H NUMBER OF NODAL POINTS = ,I6/
2 1H , 26H NUMBER OF ELEMENTS = ,I6/
3 1H , 26H NUMBER OF MATERIALS = ,I6)
2005  FORMAT(///,1H ,10X, 21H MATERIAL PROPERTIES //
11X, 8H MAT. NO.,4X, 9H MODULUS E,4X,14H POISSONS RATIO,4X,11H UNIT WEI
2GHT,/)
1010  FORMAT(6X,F12.0,2F6.0)
2010  FORMAT(1H ,15,F17.0,F15.3,F17.1)
2015  FORMAT(1H1,10X,18H NODAL POINT INPUT ,///
11H ,34H NODE CODE X COORD Y COORD //)
1020  FORMAT(15, 17, 4F12.0)
2020  FORMAT(14,I6,F13.3,1F12.3)
2025  FORMAT(1H0,28H ERROR IN NODAL DATA,NODE = ,I4)
2030  FORMAT(1H1,10X, 13H ELEMENT DATA ///,
1 44H ELEM I J K MAT SEEP ELEM //)
1035  FORMAT (5I5,F5.0,I5)
2035  FORMAT ( I4, 4I6, 5X,I6)
2040  FORMAT (///10X, 22H STRESS BAND WIDTH = ,I6/
1 10X, 22H NUMBER OF EQUATIONS = ,I6)
2050  FORMAT(///10X, 33H PROBLEM EXCEEDS SPECIFIED LIMITS )

```

C

END

L MEMORY REQUIREMENTS 000E62 BYTES

N IV G COMPILER

FORM

03-29-72

22:59.40

PAGE 0001

SUBROUTINE FORM(MAXBAN,XK1,XK2,NPFS,ALPHA,MESH,X,Y,NBC,FX,ANG,NP,
X R,C)

C

C**** SUBROUTINE FORMS FLOW MATRICES, MODIFIES FOR PRESCRIBED PRESSURES,

C**** SOLVES EQUATIONS AND COMPUTES ELEMENT FLOWS

C

COMMON/CONTRL/HED(18),NUMNP,NUMEL,NUMMAT,NUMFSC,NDMP,NTYPE,RO,
IBETA,HITE,HEAD,TOL,MAXIT,MAXMSH,NFLCD,PI,CU(500),CV(500)
COMMON/COMING/ E(3),PR(3),CO(3),SX(500),SY(500),U(500),V(500),
1TH(1000),STIF(1000,70),AP(1000),ESTIF(6,6),ECM(3,3),EBM(3,6),
1ESM(3,6),WT, JNUMNP, JNUMEL, JNUMAT, KODE(500),NNP(3,1000),
1MAT(1000),MBAND, NEQ, M, LM(6), IMXMSH,IMESH(500), NCORS(1000),
1IFSN(20),NFP(20), NFSC,MFP,APS(1000),IHAR,INCUR(500)
1,XKO,NCYC,MBF,DEPG,DEPE,NBP(20)
DIMENSION XK1(1),XK2(1),NPFS(1),ALPHA(1),MESH(1),X(1),Y(1),NBC(1)
X ,NP(5,1),P(1),C(MAXBAN,1)

COMMON/ETS/SIGP(1000,4)

DIMENSION ANG(1),FX(1)

DIMENSION ICAT(500)

C

C ROTATE NODAL VALUES SO THAT CORRESPONDANCE IS OBTAINED BETWEEN
C STRESS AND SEEPAGE NODES IN THE EVENT THAT THEY DO NOT

C CORRESPOND THE EXCHANGE WORKS PROPERLY IF ONE SIDE OF THE
C ELEMENT IS VERTICAL

C

DO 7111 IX=1,2

IF (IHAR.GT.0) GO TO 575

DO 576 JK=1,JNUMEL

KK=NCORS(JK)

IF(KK.EQ.0) GO TO 576

N1=NNP(1,JK)

N2=NNP(2,JK)

N3=NNP(3,JK)

I1=NP(1,KK)

I2=NP(2,KK)

I3=NP(3,KK)

IF((IABS(N1-N2).EQ.1).AND.(IABS(I1-I2).GT.1)) GO TO 577

IF((IABS(N2-N3).EQ.1).AND.(IABS(I2-I3).GT.1)) GO TO 577

IF((IABS(N3-N1).EQ.1).AND.(IABS(I3-I1).GT.1)) GO TO 577

GO TO 576

577 NNP(1,JK)=N3

NNP(2,JK)=N1

NNP(3,JK)=N2

576 CONTINUE

575 CONTINUE

7111 CONTINUE

C

C**** INITIALIZATION

C

DO 29 IZ=1,JNUMNP

29 ICAT(IZ)=0

PI=3.1415926/180.0

NUMIT=0

700 DO 80 II=1,NUMNP

DO 80 JJ=1,MAXBAN

N IV G COMPILER FORM 03-29-72 22:59.40 PAGE 0002

```

      80 C(JJ,II)=0.0
         DO 701 II=1,NUMNP
701      R(II)=0.0
81      CONTINUE
         IF(IHAR.EQ.-1) GO TO 2427
         GO TO 2428
C
C      IF IHAR=-1 READ PERMEABILITIES FROM TAPE FILE
C
2427     IHAR=1
         DO 2429 I=1,NUMEL
         READ(1,3319) XK1(I)
         XK2(I)=XK1(I)
2429     CONTINUE
         GO TO 2430
2428     CONTINUE
         IF(IHAR.EQ.0) GO TO 711
         IF(NUMIT.GT.0) GO TO 612
C
C      PERMEABILITY VALUES ASSIGNED
C
         DO 79 I=1,NUMEL
         M=NCCRS(I)
         IF(M.EQ.0) GO TO 79
C      PERMEABILITY FUNCTION
         XK1(M)=0.80/((-APS(I)/144.)+20.)*3.0
         XK2(M)=XK1(M)
79      CONTINUE
2430     CONTINUE
C
C      OUTPUT PERMEABILITY
C
         WRITE(6,1026) IHAR
         WRITE(6,2003) (XK1(I),I=1,NUMEL)
         GO TO 612
C
C      ASSIGN HOMO AND ISCTROPIC PERM TO FIRST ITERATION OF FIRST CYCLE
C
711      DO 712 ID=1,NUMEL
         XK1(ID)=1.0E-06
         XK2(ID)=1.0E-06
712      CONTINUE
612      CONTINUE
C
C**** FORM MATRICES FOR SOLUTION
C
         CALL QDFLOW(MAXBAN,XK1,XK2,X,Y,ANG,NP,R,C)
         IF(NDMP.NE.0) CALL WRMESH(X,Y,NBC,FX)
         IF(NDMP.NE.0) RETURN
C
C**** MODIFY FOR BOUNDARY CONDITIONS
C
         CALL MODIFY(MAXBAN,NBC,FX,R,C)
C
C**** SOLVE EQUATIONS

```


N IV G COMPILER

FORM

03-29-72

22:59.40

PAGE 0003

```

C      CALL SYMBC(C,R,NUMNP,MAXBAN,MAXBAN)
C
C      IF(NUMFSC.EQ.0) GO TO 2353
C
C      PRINT OUTPUT OF FREE SURFACE
C
C      JAC=NUMIT+1
C      WRITE(6,2349) IHAR,JAC
C      WRITE(6,2351)
C      DO 2353 NZ=1,NUMFSC
C      NZN=NPFS(NZ)
C      WRITE(6,2350) NZN, X(NZN), Y(NZN),R(NZN)
2353  CONTINUE
C      IF(IHAR.EQ.0) WRITE(6,713)
C
C**** CORRECT NODAL POSITIONS ALONG PHREATIC SURFACE
C
C      NUMIT=NUMIT+1
C      IF(NUMIT.GE.MAXIT) GO TO 203
C      ERROR=0.0
C      DO 800 II=1,NUMFSC
C      M=NPFS(II)
C      ALP=ALPHA(II)*PI
C      DX=BETA*R(M)*COS(ALP)/RO
C      DY=BETA*R(M)*SIN(ALP)/RO
C      ERROR=ERROR+DX*DX+DY*DY
C      X(M)=X(M)+DX
800  Y(M)=Y(M)+DY
C      ERROR=SQRT(ERROR)
C      IF(ERROR.LE.TOL) GO TO 203
C
C**** REGENERATE MESH
C
C      M=MESH(1)
C      DO 600 I=2,MAXMSH
C      N=MESH(I)
C      XNMM=X(N)-X(M)
C      DX=(X(N)-X(M))/XNMM
C      DY=(Y(N)-Y(M))/XNMM
C      MP1=M+1
C      DO 601 NN=MP1,N
C      X(NN)=X(NN-1)+DX
601  Y(NN)=Y(NN-1)+DY
C      M=N
600  CONTINUE
C      GO TO 700
203  CONTINUE
C      IF(IHAR.EQ.NCYC) GO TO 204
C
C      CALCULATE THE SEEPAGE BODY FORCES
C
C      DO 72 I=1,NUMNP
C      CV(I)=0.0
72  CU(I)=0.0

```


I V G COMPILER

FORM

03-29-72

22:59.40

PAGE 0004

```

      DO 50 I=1,NUMEL
        IA=NP(1,I)
        IB=NP(2,I)
        IC=NP(3,I)
        TA123=X(IC)*(Y(IA)-Y(IB)) +X(IB)*(Y(IC)-Y(IA))+X(IA)*(Y(IB)
1-Y(IC))
        BU=-31.2*(R(IA)*Y(IB)-R(IB)*Y(IA)+R(IB)*Y(IC)-R(IC)*Y(IB)
1 +R(IC)*Y(IA)-R(IA)*Y(IC))
        BV=-31.2*(+1.*TA123-R(IA)*X(IB)+R(IB)*X(IA)-R(IB)*X(IC)
1 +R(IC)*X(IB)-R(IC)*X(IA)+R(IA)*X(IC))
        CU(IA)=CU(IA)+0.3333*BU
        CU(IB)=CU(IB)+0.3333*BU
        CU(IC)=CU(IC)+0.3333*BU
        CV(IA)=CV(IA)+0.3333*BV
        CV(IB)=CV(IB)+0.3333*BV
        CV(IC)=CV(IC)+0.3333*BV
50      CONTINUE
        IHAR=IHAR+1
        RETURN
204     CONTINUE
200     CONTINUE
C
C      FIND THE CORRESPONDANCE BETWEEN STRESS AND SEEPAGE NODES
C
      DO 19 JJ=1,JNUMEL
        KK=NCORS(JJ)
        IF(KK.EQ.0) GO TO 24
        K1R=NP(1,KK)
        K2R=NP(2,KK)
        K3R=NP(3,KK)
        GO TO 25
24      K1R=0
        K2R=0
        K3R=0
25      CONTINUE
        K1S=NNP(1,JJ)
        K2S=NNP(2,JJ)
        K3S=NNP(3,JJ)
        IF(ICAT(K1S).EQ.1) GO TO 26
        INCOR(K1S)=K1R
26      IF(ICAT(K2S).EQ.1) GO TO 27
        INCOR(K2S)=K2R
27      IF(ICAT(K3S).EQ.1) GO TO 28
        INCOR(K3S)=K3R
28      ICAT(K1S)=1
        ICAT(K2S)=1
        ICAT(K3S)=1
19      CONTINUE
        MCOUNT=0
        DO 1119 JJ=1,JNUMNP
          KK=INCOR(JJ)
          IF(KK.EQ.0) GO TO 31
          PSI=0.
          IF(HEAD.NE.0.0) PSI=(R(KK)+RO*(Y(KK)-HITE))/HEAD
          RKK=R(KK)

```


V IV G COMPILER FORM 03-29-72 22:59.40 PAGE 0005

```

31      GO TO 329
      RKK=0.
      PSI=0.0
329     CONTINUE
C
C      PRINT AND PUNCH OUTPUT OF PRESSURES AND POTENTIALS AND OTHER DATA
C
      MCOUNT=MCOUNT-1
      IF(MCOUNT.GT.0) GO TO 119
      MCOUNT=50
      WRITE(6,2008) HED
119     WRITE(6,5) JJ, INCOR(JJ), SX(JJ), SY(JJ), U(JJ), V(JJ), RKK, PSI
      PUNCH 2377, JJ, INCOR(JJ), SX(JJ), SY(JJ), U(JJ), V(JJ), RKK, PSI,
1      X(KK), Y(KK)
1119    CONTINUE
      DO 120 JK=1, JNUMEL
      KK=NCORS(JK)
      N1=NNP(1, JK)
      N2=NNP(2, JK)
      N3=NNP(3, JK)
      I1=NP(1, KK)
      I2=NP(2, KK)
      I3=NP(3, KK)
      XAVE=(SX(N1)+SX(N2)+SX(N3))*0.3333
      YAVE=(SY(N1)+SY(N2)+SY(N3))*0.3333
      PUNCH 2376, JK, N1, N2, N3, KK, I1, I2, I3, XAVE, YAVE, XK1(KK), SIGP(JK,1),
      X SIGP(JK,2), SIGP(JK,3), SIGP(JK,4), APS(JK)
120     CONTINUE
C
C      READ PERMEABILITIES INTO TAPE FILE
C
      WRITE(1,3319) (XK1(I), I=1, NUMEL)
C
C**** SOLVE FOR ELEMENT FLOWS
C
      CALL ELFLOW(XK1, XK2, X, Y, ANG, NP, R)
C
32     WRITE(6,2015)
      STOP
C
C**** OUTPUT FORMATS
C
1026    FORMAT(/ 11H CYCLE NO. =, I3)
713     FORMAT(48H INITIAL ITERATION WITH HOMOGENEOUS PERMEABILITY)
2376    FORMAT(8I3, 2F6.1, E10.3, 3F7.0, F5.0, F8.0)
2377    FORMAT(2I3, 2F7.2, 2F10.1, 2F7.2, 2F8.2)
5       FORMAT(5X, I3, 13X, I3, 9X, F7.2, 4X, F7.2, 3X, F10.1, 3X, F10.1, 7X, F7.2,
1       8X, F7.2)
3319    FORMAT(E12.4)
2003    FORMAT (28HOMATERIAL PERMEABILITIES//
1       (10E11.3))
2349    FORMAT(1H1, 22H FREE SURFACE LOCATION, 20X, 11H CYCLE NO. =, I3,
1       15H ITERATION NO. =, I3/)
2351    FORMAT(5X, 5H NODE, 5X, 5HX-ORD, 5X, 5HY-ORD, 12X, 8HPRESSURE/)
2350    FORMAT(5X, 15, 2F10.4, E20.5)

```


V IV G COMPILER

FORM

03-29-72

22:59.40

PAGE 0006

2008 FORMAT(1H1,18A4//12H STRESS NODE,3X,13H SEEPAGE NODE,6X,
1 6H X-ORD,5X,6H Y-ORD,5X,8H X FORCE,5X,8H Y FORCE,5X,
1 9H PRESSURE,5X, 10H POTENTIAL)

2011 FORMAT(5X,15, 2E10,4, 2E20,5)

2012 FORMAT(15,4F10.2,F10.0,15)

2015 FORMAT (15H1END OF PROBLEM/)

2016 FORMAT (6I5, E15,5)

END

MEMORY REQUIREMENTS 002092 BYTES

N IV G COMPILER

CHANGE

03-29-72

23:01.15

PAGE 0001

```

      SUBROUTINE CHANGE(NPFS,X,Y,NP)
C      THIS SUBROUTINE TAKES THE BODY FORCES CALCULATED IN SUBROUTINE
C      FORM AND ASSIGNS THEM TO THE PROPER STRESS NODES
C      IT CHANGES THE INTERNAL NODAL POSITIONS TO THE POSITION OF
C      THE FREE SURFACE FOUND IN FORM AND GENERATES NEW POSITIONS
C      IT ALSO CALCULATES THE RELEASE FORCES FOR THE SLOPE FACE DUE TO
C      THE READJUSTMENT OF NODAL POSITIONS
C      IN ADDITION TO THE BASE NODE FORCES
C      THE SLOPE FACE NODES ARE READ IN GOING UP AND THE BASE NODES
C      ARE READ IN FROM THE LEFT TO THE SLOPE FACE
C
      COMMON/CONTRL/HED(18),NUMNP,NUMEL,NUMMAT,NUMFSC,NDMP,NTYPE,RO,
      1BETA,HITE,HEAD,TOL,MAXIT,MAXMSH,NFLCD,PI,CU(500),CV(500)
      COMMON/COMING/ E(3),PR(3),CO(3),SX(500),SY(500),U(500),V(500),
      1TH(1000),STIF(1000,70),AP(1000),ESTIF(6,6),ECM(3,3),EBM(3,6),
      1ESM(3,6),WT, JNUMNP, JNUMEL, JNUMAT, KUDE(500),NNP(3,1000),
      1MAT(1000),MBAND, NEQ, M, LM(6), IMXMSH, IMESH(500), NCURS(1000),
      1IFSN(20),NFP(20), NFSC,MFP,APS(1000),IHAR,INCOR(500)
      1,XKO,NCYC,MBP,DEPG,DEPE,NBP(20)
      DIMENSION ICAT(500)
      DIMENSION X(1),Y(1),NP(5,1),NPFS(1)
C
      DO 42 I=1,JNUMNP
      U(I)=0
42      V(I)=0
C
C      CHANGE THE POSITION OF THE FREE SURFACE STRESS NODES AND
C      REGENERATE NEW INTERMEDIATE LOCATIONS
C      MODIFY FOR BOUNDARY CONDITIONS WHERE REQUIRED
C
      DO 27 I=1,NUMFSC
      NA=NPFS(I)
      NB=IFSN(I)
      SX(NB)=X(NA)
      SY(NB)=Y(NA)
27      CONTINUE
      M=IMESH(1)
      DO 600 I=2,IMXMSH
      N=IMESH(I)
      XNMM=N-M
      DX=(SX(N)-SX(M))/XNMM
      DY=(SY(N)-SY(M))/XNMM
      MP1=M+1
      DO 601 NN=MP1,N
      SX(NN)=SX(NN-1)+DX
601      SY(NN)=SY(NN-1)+DY
      M=N
600      CONTINUE
C
C      CALCULATE RELEASE FORCES FOR HORIZONTAL STRESSES
C      MODIFY FOR BOUNDARY CONDITIONS WHERE REQUIRED
C
      DO 39 I=1,MFP
      IF(I.EQ.1) GO TO 20
      IF (I.EQ. MFP) GO TO 30

```


N IV G COMPILER

CHANGE

03-29-72

23:01.15

PAGE 0002

```

      GO TO 40
20    M1=NFP(I)
      M2=NFP(I+1)
      DM=DEPG-SY(M1)
      DMP1=DEPG-SY(M2)
      U(M1)=-C0(3)*XK0*0.125*(3.*(DM**2)-2.*DM*DMP1-DMP1**2)
      IF(KODE(M1).EQ.11) U(M1)=0.0
      GO TO 39
30    M1=NFP(I-1)
      M2=NFP(I)
      DMM1=DEPG-SY(M1)
      U(M2)=-C0(3)*XK0*0.125*(DMM1**2)
      IF(KODE(M2).EQ.11) U(M2)=0.0
      GO TO 39
40    M1=NFP(I-1)
      M2=NFP(I)
      M3=NFP(I+1)
      DMM1=DEPG-SY(M1)
      DM=DEPG-SY(M2)
      DMP1=DEPG-SY(M3)
      U(M2)=-C0(3)*XK0*0.125*(DMM1**2+2.*DMM1*DM-2.*DM*DMP1-DMP1**2)
      IF(KODE(M2).EQ.11) U(M2)=0.0
39    CONTINUE
C
C    CALCULATE RELEASE FORCES FOR VERTICAL STRESSES
C    MODIFY FOR BOUNDARY CONDITIONS WHERE REQUIRED
C
      DO 43 I=1,MBP
      IF(I.EQ.1) GO TO 44
      IF(I.EQ. MBP) GO TO 45
      GO TO 46
44    M1=NBP(I)
      M2=NBP(I+1)
      V(M1)=C0(3)*DEPE*(SX(M2)-SX(M1))*0.5
      IF(KODE(M1).EQ.11) V(M1)=0.0
      GO TO 43
45    M1=NBP(I)
      M2=NBP(I-1)
      V(M1)=C0(3)*DEPE*(SX(M1)-SX(M2))*0.5
      IF(KODE(M1).EQ.11) V(M1)=0.0
      GO TO 43
46    M1=NBP(I-1)
      M2=NBP(I)
      M3=NBP(I+1)
      V(M2)=C0(3)*DEPE*(SX(M3)-SX(M1))*0.5
      IF(KODE(M2).EQ.11) V(M2)=0.0
43    CONTINUE
      WRITE(6,130) IHAR
      WRITE(6,47)
      DO 53 I=1,MFP
      NI=NFP(I)
53    WRITE(6,48) NFP(I),U(NI)
      WRITE(6,49)
      DO 54 I=1,MBP
      MI=NBP(I)

```


N IV G COMPILER

CHANGE

03-29-72

23:01.15

PAGE 0003

```

54      WRITE(6,50)  NBP(I), V(MI)
C
C      ASSIGN BODY FORCES FOUND TO THE PROPER NODES
C      MODIFY FOR BOUNDARY CONDITIONS WHERE REQUIRED
C
      DO 36 I=1,JNUMNP
36      ICAT(I)=0
      DO 37 I=1,JNUMEL
      M=NCORS(I)
      IF(M.EQ.0) GO TO 37
      IA=NNP(1,I)
      IB=NNP(2,I)
      IC=NNP(3,I)
      IMA=NP(1,M)
      IMB=NP(2,M)
      IMC=NP(3,M)
      IF(ICAT(IA).EQ.1) GO TO 32
      IF(KODE(IA).EQ.11) GO TO 32
      IF(KODE(IA).EQ.10)  CU(IMA)=0.0
      IF(KODE(IA).EQ.01)  CV(IMA)=0.0
      U(IA)= U(IA)+CU(IMA)
      V(IA)=V(IA)+CV(IMA)
32      IF (ICAT(IB).EQ.1) GO TO 33
      IF(KODE(IB).EQ.11) GO TO 33
      IF(KODE(IB).EQ.10)  CU(IMB)=0.0
      IF(KODE(IB).EQ.01)  CV(IMB)=0.0
      U(IB)=U(IB)+CU(IMB)
      V(IB)=V(IB)+CV(IMB)
33      IF(ICAT(IC).EQ.1) GO TO 34
      IF(KODE(IC).EQ.11) GO TO 34
      IF(KODE(IC).EQ.10)  CU(IMC)=0.0
      IF(KODE(IC).EQ.01)  CV(IMC)=0.0
      U(IC)=U(IC)+CU(IMC)
      V(IC)=V(IC)+CV(IMC)
34      ICAT(IA)=1
      ICAT(IB)=1
      ICAT(IC)=1
37      CONTINUE
      RETURN
C
C      FORMAT STATEMENTS
C
130     FORMAT(1H1,11H CYCLE NO.=, I3/)
47      FORMAT(      18H SLOPE FACE FORCES/
1 5X, 5H NODE,10X,8H X FORCE/)
48      FORMAT(7X,I3,10X,F10.1)
49      FORMAT(//, 17H BASE NODE FORCES/
1 5X, 5H NODE,10X,8H Y FORCE/)
50      FORMAT(7X,I3,10X,F10.1)
      END

```

L MEMORY REQUIREMENTS 001484 BYTES

IV G COMPILER

QDFLOW

03-29-72

23:02.16

PAGE 0001

SUBROUTINE QDFLOW(MAXBAN,XK1,XK2,X,Y,ANG,NP,R,C)

C

C**** SUBROUTINE COMPUTES FLOW MATRICES FOR QUADRILATERAL OR TRIANGULAR

C**** ELEMENTS AND ADDS TO GLOBAL FLOW MATRICES

C

```

COMMON/CONTRL/HED(18),NUMNP,NUMEL,NUMMAT,NUMFSC,NDMP,NTYPE,RO,
1 BETA,HITE,HEAD,TOL,MAXIT,MAXMSH,NFLCD,PI,CU(500),CV(500)
COMMON/ELMT/ XX(5),YY(5),S(5,5),GG(5),XK11,XK22,XK12,NN
DIMENSION XK1(1),XK2(1),X(1),Y(1),ANG(1),NP(5,1),R(1),C(MAXBAN,1)
DO 300 NN=1,NUMEL

```

C

C**** INITIALIZE MATRICES

C

```

DO 201 II=1,5
  GG(II)=0.0
DO 201 JJ=1,5
  201 S(II,JJ)=0.0
  XK3=ANG(NN)*PI
  MAT=NP(5,NN)
  CC=COS(XK3)
  SS=SIN(XK3)
  XK11=XK1(MAT)*CC*CC+XK2(MAT)*SS*SS
  XK22=XK2(MAT)*CC*CC+XK1(MAT)*SS*SS
  XK12=SS*CC*(XK1(MAT)-XK2(MAT))
  D=4.0
  XX(5)=0.0
  YY(5)=0.0
  DO 100 J=1,4
    I=NP(J,NN)
    XX(J)=X(I)
    YY(J)=Y(I)
    XX(5)=XX(5)+X(I)/D
  100 YY(5)=YY(5)+Y(I)/D
  IF(NP(3,NN).EQ.NP(4,NN)) GO TO 110

```

C

C**** FORM QUADRILATERAL FLOW MATRICES FROM TRIANGLES

C

```

MM=4
CALL TRIFL(1,2,5)
CALL TRIFL(2,3,5)
CALL TRIFL(3,4,5)
CALL TRIFL(4,1,5)
IF(NDMP.NE.0) GO TO 300

```

C

C**** REDUCE CENTER NODE

C

```

DO 200 II=1,4
  COM=S(II,5)/S(5,5)
  GG(II)=GG(II)-COM*GG(5)
DO 200 JJ=1,4
  200 S(II,JJ)=S(II,JJ)-COM*S(5,JJ)
  GO TO 250
110 CONTINUE

```

C

C**** FORM MATRICES FOR SINGLE TRIANGLE

V IV G COMPILER

QDFLOW

03-29-72

23:02.16

PAGE 0002

C

MM=3

CALL TRIFL(1,2,3)

IF(NOMP.NE.0) GO TO 300

C

C**** ADD ELEMNT MATRICES TO GLCBAL MATRICES

C

250 CONTINUE

DO 202 II=1,MM

L1=NP(II,NN)

R(L1)=R(L1)+GG(II)

DO 202 JJ=1,MM

K2=NP(JJ,NN)-L1+1

IF(K2.LE.0) GO TO 202

C(K2,L1)=C(K2,L1)+S(II,JJ)

202 CONTINUE

300 CONTINUE

RETURN

END

_ MEMORY REQUIREMENTS 000680 BYTES

V IV G COMPILER

TRIFL

03-29-72

23:02.33

PAGE 0001

SLBRROUTINE TRIFL(I,J,K)

C

C**** SUBROUTINE COMPUTES FLOW MATRICES FOR TRIANGULAR ELEMENT

C

```

COMMON/CONTRL/HED(18),NUMNP,NUMEL,NUMMAT,NUMFSC,NDMP,NTYPE,RO,
1BETA,HITE,HEAD,TOL,MAXIT,MAXMSH,NFLCD,PI,CU(500),CV(500)
COMMON/ELMT/ XX(5),YY(5),S(5,5),GG(5),XK11,XK22,XK12,NN

```

A1=0.5

P21=YY(J)-YY(K)

P22=YY(K)-YY(I)

P23=YY(I)-YY(J)

P31=XX(K)-XX(J)

P32=XX(I)-XX(K)

P33=XX(J)-XX(I)

D=P33*P22-P23*P32

IF(NDMP.NE.0) RETURN

IF(D.LE.0.0) GO TO 500

IF(NTYPE.NE.1) A1=(XX(I)+XX(J)+XX(K))/6.0

T11=XK11*P21+XK12*P31

T12=XK11*P22+XK12*P32

T13=XK11*P23+XK12*P33

T21=XK12*P21+XK22*P31

T22=XK12*P22+XK22*P32

T23=XK12*P23+XK22*P33

COM=A1/D

S(I,I)=S(I,I)+COM*(P21*T11+P31*T21)

S(I,J)=S(I,J)+COM*(P21*T12+P31*T22)

S(I,K)=S(I,K)+COM*(P21*T13+P31*T23)

S(J,J)=S(J,J)+COM*(P22*T12+P32*T22)

S(J,K)=S(J,K)+COM*(P22*T13+P32*T23)

S(K,K)=S(K,K)+COM*(P23*T13+P33*T23)

S(J,I)=S(I,J)

S(K,I)=S(I,K)

S(K,J)=S(J,K)

COM=A1*RO

GG(I)=GG(I)-T21*COM

GG(J)=GG(J)-T22*COM

GG(K)=GG(K)-T23*COM

RETURN

500 WRITE(6,3000)NN

NDMP=1

RETURN

C

C**** ERROR MESSAGE

C

3000 FORMAT (30H ZERO OR NEGATIVE AREA ELEMENT, I3/)

END

L. MEMORY REQUIREMENTS 0006A4 BYTES

N IV G COMPILER

MODIFY

03-29-72

23:02.36

PAGE 0001

SUBROUTINE MODIFY(MM,NBC,FX,R,C)

C

C**** SUBROUTINE MODIFIES EQUATIONS OF NODES WITH PRESCRIBED PRESSURES

C**** OR FLOWS

C

COMMON/CONTRL/HED(18),NUMNP,NUMEL,NUMMAT,NUMFSC,NDMP,NTYPE,RO,

1 BETA,HITE,HEAD,TOL,MAXIT,MAXMSH,NFLCD,PI,CU(500),CV(500)

DIMENSION FX(1),R(1),C(MM,1),NBC(1)

DO 70 N=1,NUMNP

IF(NBC(N).GT.0) GO TO 72

R(N)=R(N)+FX(N)

GO TO 70

72 N1=N+1

DO 73 K=2,MM

N2=N1-K

IF (N2.LE.0) GO TO 74

R(N2)=R(N2)-C(K,N2)*FX(N)

C(K,N2)=0.0

74 M=N+K-1

IF (M.GT.NUMNP) GO TO 73

R(M)=R(M)-C(K,N)*FX(N)

C(K,N)=0.0

73 CONTINUE

C(1,N)=0.0

R(N)=FX(N)

70 CONTINUE

RETURN

END

MEMORY REQUIREMENTS 000376 BYTES

N IV G COMPILER

SYMB C

03-29-72

23:02.39

PAGE 0001

SUBROUTINE SYMB C(A,B,NN,MB,MMA X)

C

C**** SOLUTION OF SYMMETRIC BANDED EQUATIONS IN SINGLE SUBSCRIPT ARITH.

C**** SYMMETRIC. BAND MATRIC WITH DIMENSIONS K(MMA X,NN) IS STORED IN

C**** VECTOR A.

C

DIMENSION A(1),B(1)

MB1=MB-1

NNN=NN-1

C

C**** TRIANGULARIZE MATRIX BY GAUSS ELIMINATION WITHOUT PIVOTS

C

II=1

DO 300 N=1,NNN

CC=A(II)

IF(CC.EQ.0.0) GO TO 250

J1=II+1

J2=II+MB1

NE=NN-N

IF(NE.LT.MB1) J2=II+NE

M=II-1

DO 200 J=J1,J2

M=M+MMA X

C=A(J)/CC

IF(C.EQ.0.0) GO TO 200

K=M

DO 100 I=J,J2

K=K+1

100 A(K)=A(K)-C*A(I)

A(J)=C

200 CONTINUE

250 CONTINUE

II=II+MMA X

300 CONTINUE

C

C**** REDUCE FORCE VECTOR

C

II=1

DO 500 N=1,NNN

CC=A(II)

IF(CC.EQ.0.0) GO TO 450

J1=II+1

J2=II+MB1

NE=NN-N

IF(NE.LT.MB1) J2=II+NE

C=B(N)

L=N

DO 400 J=J1,J2

L=L+1

400 B(L)=B(L)-A(J)*C

B(N)=C/CC

450 CONTINUE

II=II+MMA X

500 CONTINUE

CC=A(II)

N IV G COMPILER

SYMB C

03-29-72

23:02.39

PAGE 0002

IF(CC.NE.0.0) B(NN)=B(NN)/CC

C

C**** BACKSUBSTITUTE EQUATIONX

C

N=NN

II=MMAX*(NN-2)+1

DO 700 I=2,NN

N=N-1

IF(A(II).EQ.0.0) GO TO 650

J1=II+1

J2=II+MB1

NE=NN-N

IF(NE.LT.MB1) J2=II+NE

C=B(N)

L=N

DO 600 J=J1,J2

L=L+1

600 C=C-A(J)*B(L)

B(N)=C

650 CONTINUE

II=II-MMAX

700 CONTINUE

RETURN

END

L MEMORY REQUIREMENTS 00062C BYTES

48.22 RC=0

IV G COMPILER

ELFLOW

03-29-72

23:01.58

PAGE 0001

```

      SUBROUTINE ELFLOW(XK1,XK2,X,Y,ANG,NP,R)
C**** SUBROUTINE COMPUTES FLOW VELOCITIES IN ELEMENTS
C

```

```

      COMMON/CONTRL/HED(18),NUMNP,NUMEL,NUMMAT,NUMFSC,NDMP,NTYPE,RO,
1 BETA,HTE,HEAD,TOL,MAXIT,MAXMSH,NFLCD,PI,CU(500),CV(500)
      DIMENSION XK1(1),XK2(1),X(1),Y(1),ANG(1),NP(5,1),R(1),YY(6)
      MCOUNT=0
      DO 400 N=1,NUMEL
      IF(NP(3,N).EQ.NP(4,N)) GOTO 200
      XM=0.
      YM=0.
      RM=0.0
      DO 100 J=1,4
      I=NP(J,N)
      RM=RM+0.25*R(I)
      XM=XM+0.25*X(I)
100  YM=YM+0.25*Y(I)
      MM=4
      GO TO 250
200  XM= 0.0
      YM = 0.0
      RM = 0.0
      DO 500 J=1,3
      I = NP(J,N)
      XM = XM + X(I) / 3.0
      RM = RM + R(I) / 3.0
500  YM = YM + Y(I) / 3.0
      MM = 3
250  CONTINUE
      MAT=NP(5,N)
      XK3=ANG(N)*PI
      CC=COS(XK3)
      SN=SIN(XK3)
      Y1K=CC*XM+SN*YM
      Y2K=CC*YM-SN*XM
      Q1=0.0
      Q2=0.0
      D1=0.0

```

C

C**** LOOP ON ELEMENTS FOR QUADRILATERAL ELEMENT

C

```

      J=NP(4,N)
      DO 300 NN=1,MM
      I=J
      J=NP(NN,N)
      Y1I=CC*X(I)+SN*Y(I)
      Y1J=CC*X(J)+SN*Y(J)
      Y2I=CC*Y(I)-SN*X(I)
      Y2J=CC*Y(J)-SN*X(J)
      YY(1) =Y2J-Y2K
      YY(2) =Y2K-Y2I
      YY(3) =Y2I-Y2J
      YY(4) =Y1K-Y1J
      YY(5) =Y1I-Y1K
      YY(6) =Y1J-Y1I

```


IV G COMPILER

ELFLOW

03-29-72

23:01.58

PAGE 0002

D=YY(6)*YY(2)-YY(3)*YY(5)

D1=D1+D

Q1=Q1-XK1(MAT)*(YY(1)*R(I)+YY(2)*R(J)+YY(3)*RM+SN*RO*D)

Q2=Q2-XK2(MAT)*(YY(4)*R(I)+YY(5)*R(J)+YY(6)*RM+CC*RO*D)

300 CONTINUE

C

C**** OUTPUT FLOWS

C

Q1=Q1/D1

Q2=Q2/D1

Q3=SQRT(Q1**2+Q2**2)

Q4=ATAN2(Q2,Q1)/PI+ANG(N)

MCOUNT=MCOUNT-1

IF(MCOUNT.GT.0) GO TO 350

MCOUNT=55

WRITE(6,2000) HED

350 WRITE(6,2001) N,XM,YM,Q1,Q2,ANG(N),Q3,Q4

400 CONTINUE

RETURN

C

C**** FORMATS

C

2000 FORMAT(1H1,18A4//5X,5H ELMT,5X,5HX-ORD,5X,5HY-ORD,14X,6H1-FLOW,
X 14X,6H2-FLOW,10X,5HANGLE,10X,10HTOTAL FLOW,6X,9HDIRECTION/)

2001 FORMAT(5X,I5, 2F10.4, 2E20.5, F15.4, E20.5, F15.4)

END

MEMORY REQUIREMENTS 000784 BYTES

I IV G COMPILER

ASTIF

03-29-72

23:00.58

PAGE 0001

SUBROUTINE ASTIF

```

C
C   THIS SUBROUTINE TAKES EACH ELEMENT IN TURN AND FORMS THE ELEMENT S
C   MATRIX (BY CALLING ELSTIF). IT ASSEMBLES THE ELEMENT STIFFNESSES IN
C   KSTIF, ASSEMBLES THE APPLIED LOAD VECTOR (AP), AND MODIFIES THE
C   ASSEMBLASES FOR DISPLACEMENT BOUNDARY CONDITIONS (BY CALLING MODIF
C
COMMON/COMING/ E(3),PR(3),RO(3), X(500), Y(500),U(500),V(500),
1TH(1000),STIF(1000,70),AP(1000),ESTIF(6,6),ECM(3,3),EBM(3,6),
1 FSM(3,6),WT, NUMNP, NUMEL, NUMAT, KODE(500), NP(3,1000),
1 MAT(1000),MBAND, NEQ, M, LM(6), IMXMSH,IMESH(500), NCORS(1000),
1 IFSN(20),NFP(20), NFSC,MFP,APS(1000),IHAR,INCOR(500)
1,XKO,NCYC,MBP,DEPG,DEPE,NBP(20)
C
C   INITIALIZE APPLIED LOAD VECTOR AND MASTER STIFFNESS MATRIX AND ECM
C
DO 10 I=1,NEQ
  AP(I)=0.0
DO 10 J=1,MBAND
  STIF(I,J)=0.0
DO 20 I=1,3
  DO 20 J=1,3
    ECM(I,J)=0.0
C
C   FORM ELEMENT CONSTITUTIVE MATRIX (ECM) IF NUMAT=1
C
IF(NUMAT.NE.1) GO TO 30
EPR=PR(1)
COM=E(1)/((1.+EPR)*(1.-2.*EPR))
COM1=COM*(1.-EPR)
COM2=COM*EPR
ECM(1,1)=COM1
ECM(2,2)=COM1
ECM(1,2)=COM2
ECM(2,1)=COM2
ECM(3,3)=E(1)/(2.*(1.+EPR))
C
30 DO 45 M=1,NUMEL
  CALL ELSTIF(1)
C
C   ASSEMBLE ELSTIF INTO MASTER STIFFNESS MATRIX
C
DO 35 I=1,3
  I2=2*I
  LM(I2)=2*NP(I,M)
35 LM(I2-1)=LM(I2)-1
DO 40 I=1,6
  II=LM(I)
DO 40 J=1,6
  JJ=LM(J)-II+1
  IF (JJ.LE.0) GO TO 40
  STIF(II,JJ)= STIF(II,JJ)+ESTIF(I,J)
40 CONTINUE
C

```


I IV G COMPILER

ASTIF

03-29-72

23:00.58

PAGE 0002

C ADD GRAVITY LOADS INTO AP VECTOR
C

DO 45 I=2,6,2

II=LM(I)

AP(II)=AP(II)-WT

45 CONTINUE

C

C ADD NODAL LOADS INTO AP VECTOR
C

DO 50 N=1,NUMNP

N2=2*N

AP(N2)=AP(N2)+V(N)

50 AP(N2-1)=AP(N2-1)+U(N)

C

C MODIFY STIFFNESS AND LOAD VECTOR FOR DISPLACEMENT BOUNDARY CONDITION:
C

DO 100 N=1,NUMNP

N2=2*N

IF (KODE(N)-10) 80,70,60

60 II=N2-1

CALL MODAFY(II,N)

CALL MODAFY(N2,N)

GO TO 100

70 II=N2-1

CALL MODAFY(II,N)

GO TO 100

80 IF(KODE(N).EQ.0) GO TO 100

CALL MODAFY(N2,N)

100 CONTINUE

C

C OUTPUT BODY FORCES FOR LAST CYCLE
C

IF(IHAR.NE.NCYC) RETURN

WRITE(6,51)

51 FORMAT(///24H TOTAL NODAL BODY FORCES/

1 5X, 5H NODE,10X, 8H X FORCE,10X, 8H Y FORCE/)

DO 2005 NZ=1,NUMNP

IY=2*NZ

IX=IY-1

XFORCE=AP(IX)

YFORCE=AP(IY)

WRITE(6,52) NZ,XFORCE, YFORCE

52 FORMAT(7X,I3,10X,F10.1,8X,F10.1)

2005 CONTINUE

RETURN

END

MEMORY REQUIREMENTS 000768 BYTES

IV G COMPILER

ELSTIF

03-29-72

23:01.44

PAGE 0001

SUBROUTINE ELSTIF(KCP)

C THIS SUBROUTINE FORMS THE ELEMENT STIFFNESS MATRIX (ESTIF) OR
 C ELEMENT STRESS MATRIX (ESM) FOR THE CONSTANT STRAIN TRIANGLE

C

COMMON/COMING/ E(3),PR(3),RO(3), X(500), Y(500),U(500),V(500),
 ITH(1000),STIF(1000,70),AP(1000),ESTIF(6,6),ECM(3,3),ERM(3,6),
 1 ESM(3,6),WT, NUMNP, NUMEL, NUMAT, KODE(500), NP(3,1000),
 1 MAT(1000),MBAND, NEQ, M, LM(6), IMXMSH,IMESH(500), NCORS(1000),
 1 IFSN(20),NFP(20), NFSC,MFP,APS(1000),IHAR,INCOR(500)
 1,XKO,NCYC,MBP,DEPG,DEPE,NBF(20)

C

DIMENSION AV(3),BV(3)

C

DO 10 I=1,3

DO 10 J=1,6

10

EBM(I,J)=0.0

I=NP(1,M)

J=NP(2,M)

K=NP(3,M)

C

C

FORM ELEMENT DIMENSIONS

C

AV(1)=X(K)-X(J)

AV(2)=X(I)-X(K)

AV(3)=X(J)-X(I)

BV(1)=Y(J)-Y(K)

BV(2)=Y(K)-Y(I)

BV(3)=Y(I)-Y(J)

AREA2=AV(3)*BV(2)-AV(2)*BV(3)

IF (TH(M).EQ.0.) TH(M)=1.

VOL=TH(M)*AREA2/2.

IF (VOL.LE.0.) GO TO 75

C

FORM CONSTITUTIVE MATRIX

C

IF (NUMAT.EQ.1) GO TO 30

NM=MAT(M)

EPR=PR(NM)

COM=E(NM)/((1.+EPR)*(1.-2.*EPR))

COM1=COM*(1.-EPR)

COM2=COM*EPR

ECM(1,1)=COM1

ECM(2,2)=COM1

ECM(1,2)=COM2

ECM(2,1)=COM2

ECM(3,3)=E(NM)/(2.*(1.+EPR))

C

C

FORM ELEMENT B MATRIX (EBM)

C

30

DO 40 I=1,3

I2=2*I

I2M=2*I-1

EBM(1,I2M)=BV(I)/AREA2

EBM(2,I2M)=AV(I)/AREA2

EBM(3,I2M)=EBM(2,I2)

40

EBM(3,I2)=EBM(1,I2M)

IV G COMPILER

ELSTIF

03-29-72

23:01.44

PAGE 0002

C

C FORM ELEMENT STRESS MATRIX (ESM)

C

DO 50 I=1,3

DO 50 J=1,6

ESM(I,J)=0.0

DO 50 K=1,3

50 ESM(I,J)=ESM(I,J)+ECM(I,K)*EBM(K,J)

C

IF(KOP.EQ.2) GO TO 80

IF(NUMAT.EQ.1) NM=1

WT=VOL*RC(NM)/3.

C

C FORM ELEMENT STIFFNESS MATRIX (ESTIF)

C

DO 70 I=1,6

DO 70 J=1,6

ESTIF(I,J)=0.0

DO 60 K=1,3

60 ESTIF(I,J)=ESTIF(I,J)+EBM(K,I)*ESM(K,J)

70 ESTIF(I,J)=ESTIF(I,J)*VOL

GO TO 80

75 WRITE(6,1000) M

CALL EXIT

80 RETURN

C

C

1000 FORMAT (1H1, 18H VOLUME OF ELEMENT ,I4, 18H IS LESS THAN ZERO)

C

END

MEMORY REQUIREMENTS 000736 BYTES

IV G COMPILER MODAFY 03-29-72 23:01.52 PAGE 0001

SUBROUTINE MODAFY (I,N)

C
C THIS SUBROUTINE MODIFIES KSTIF AND AP IF A DISPLACEMENT BOUNDARY COND.
C IS IMPOSED IN EQUATION I ASSOCIATED WITH NODAL POINT N

C
COMMON/COMING/ E(3),PR(3),RO(3), X(500), Y(500),U(500),V(500),
1TH(1000),STIF(1000,70),AP(1000),ESTIF(6,6),ECM(3,3),EBM(3,6),
1 ESM(3,6),WT, NUMNP, NUMEL, NUMAT, KODE(500), NP(3,1000),
1 MAT(1000),MBAND, NEQ, M, LM(6), IMXMSH,IMESH(500), NCORS(1000),
1 IFSN(20),NEP(20), NESC,MFP,APS(1000),IHAR,INCOR(500)
1,XKD,NCYC,MBP,DEPG,DEPE,NBP(20)

C
DISP=U(N)
IF((I-2*N).EQ.0) DISP=V(N)

C
DO 50 J=2,MBAND
IL=I+J-1
IU=I-J+1
IF(IU.LE.0)GO TO 10
AP(IU)=AP(IU) - STIF(IU,J)*DISP
STIF(IU ,J)=0.0
10 IF(IL.GT.NEQ) GO TO 50
AP(IL)= AP(IL)- STIF(I,J)*DISP
STIF(I,J)=0.0
50 CONTINUE
AP(I)=DISP
STIF(I,1)=1.0
RETURN
END

..MEMORY REQUIREMENTS 00020E BYTES

I IV G COMPILER

BAND1

03-29-72

23:01.54

PAGE 0001

SUBROUTINE BAND1

C

C THIS SUBROUTINE SOLVES FOR DISPLACEMENTS USING A GAUSSIAN ELIMINATION
C TECHNIQUE FOR SYMMETRIC BANDED MATRICES STORED IN CORE

C

CCMMCN/CCMING/ E(3),PR(3),RO(3), X(500), Y(500),U(500),V(500),
1TH(1000), A(1000,70), B(1000),ESTIF(6,6),ECM(3,3),EBM(3,6),
1 ESM(3,6),WT, NUMNP, NUMEL, NUMAT, KODE(500), NP(3,1000),
1 MAT(1000),MM , NN , M, LM(6), IMXMSH,IMESH(500), NCORS(1000),
1 IESN(20),NEP(20), NFSC,MFP,APS(1000),IHAR,INCOR(500)
1,XKO,NCYC,MSP,DEPG,DEPE,NBP(20)

C TRIANGULARIZE AND REDUCE RIGHT HAND SIDE

NL=NN-MM+1

NM=NN-1

MR=MM

C

DO 100 N=1,NM
IF (A(N,1).LE.0.) GO TO 700
BN=B(N)
B(N)=BN/A(N,1)
IF (N.GT.NL) MR=NN-N+1

C

DO 100 L=2,MR
IF (A(N,L).EQ.0.)GO TO 100
C= A(N,L)/A(N,1)
I= N+L-1
J= 0
DO 50 K=L,MR

50 A(I,J)= A(I,J)-C*A(N,K)
B(I)=B(I)-C*BN
A(N,L)=C
100 CONTINUE

C

C BACK SUBSTITUTE

C

I=NN
B(NN)=B(NN)/A(NN,1)
DO 600 N=1,NM
I=I-1
IF (N.LT.MM) MR= N+1
DO 600 J=2,MR
K=I+J-1

600 B(I) =B(I)- A(I,J)*B(K)
IF (IHAR.NE.NCYC) RETURN

C

C OUTPUT DISPLACEMENTS FOR LAST CYCLE

C

WRITE(6,2091) IHAR

WRITE(6,2001)

2091 FORMAT(1H1, 11H CYCLE NO.=, I3/)

2001 FORMAT(' ' NODAL DISPLACEMENTS '///' NODE X-DISPLACE
1MENT Y-DISPLACEMENT'//')

DO 2005 NZ=1,NUMNP

IY=2*NZ

IV G COMPILER

BAND1

03-29-72

23:01.54

PAGE 0002

```
      IX=IY-1
      XDISP=B(IX)
      YDISP=E(IY)
2005  WRITE(6,2006) NZ,XDISP,YDISP
2006  FORMAT (I9,E21.5,E20.5)
      RETURN
700  WRITE (6,2000) N
      CALL EXIT
2000  FORMAT(1H0, 81H ZERO OR NEGATIVE ELEMENT ON  MAIN DIAGONAL CF TRIA
      NGULARIZED MATRIX FOR EQUATION  ,IS)
C
      END
```

MEMORY REQUIREMENTS 00063A BYTES

I IV G COMPILER

STRESS

03-29-72

23:01.38

PAGE 0001

SUBROUTINE STRESS

C
 C THIS SUBROUTINE FORMS THE ELEMENT STRESS MATRIX (ESM), MULTIPLIES BY
 C THE ELEMENT DISPLACEMENT VECTOR (ELDISP) AND RECORDS THE STRESSES IN
 C SIGEL. IT THEN COMPUTES THE PRINCIPAL STRESSES AND DIRECTIONS (SIGP)
 C

COMMON/COMING/ E(3), PR(3), RO(3), X(500), Y(500), U(500), V(500),
 1TH(1000), STIF(1000,70), AP(1000), ESTIF(6,6), ECM(3,3), EBM(3,6),
 1 ESM(3,6), WT, NUMNP, NUMEL, NUMAT, KUDE(500), NP(3,1000),
 1 MAT(1000), MPAND, NEQ, M, LM(6), IMXMSH, IMESH(500), NCORS(1000),
 1 IFSN(20), NFP(20), NFSC, MFP, APS(1000), IHAR, INCOR(500)
 1, XKD, NCYC, MBP, DEPG, DEPE, NBP(20)
 DIMENSION SIGEL(1000,3), ELDISP(6), KOUNT(500)
 COMMON/ETS/SIGP(1000,4)

C
 DO 5 N=1, NUMNP
 KOUNT(N)=0

5 CONTINUE

C
 DO 100 M=1, NUMEL

C
 C COMPUTE ELEMENT DISPLACEMENTS

C
 DO 10 I=1,3
 I2=2+I
 LMI2 =2*NP(I,M)
 ELDISP(I2)=AP(LMI2)
 10 ELDISP(I2-1)=AP(LMI2-1)

C
 C COMPUTE ELEMENT STRESSES

C
 CALL ELSTIF(2)

C
 DO 20 I=1,3
 SIGEL(M,I)=0.0
 DO 20 J=1,6
 20 SIGEL(M,I)=SIGEL(M,I)+ESM(I,J)*ELDISP(J)
 C FIND AVERAGE X AND Y OF ELEMENT M
 J1=NP(1,M)
 J2=NP(2,M)
 J3=NP(3,M)
 XAVE=0.3333*(X(J1)+X(J2)+X(J3))
 YAVE=0.3333*(Y(J1)+Y(J2)+Y(J3))

C
 C CALCULATE THE AVERAGE PRINCIPLE STRESS

C
 APS(M)=0.3333*(-RO(3)*(DEPG-YAVE)*(1.+2.*XKD)+(SIGEL(M,1)+
 1 SIGEL(M,2))*(1.+PR(3)))
 SIGEL(M,1)=SIGEL(M,1)-((DEPG-YAVE)*RO(3)*XKD)
 SIGEL(M,2)= SIGEL(M,2)-((DEPG-YAVE)*RO(3))
 83 CONTINUE

C
 C COMPUTE ELEMENT PRINCIPAL STRESSES AND DIRECTIONS

C
 SIGM=(SIGEL(M,1)+SIGEL(M,2))/2.

IV G COMPILER

STRESS

03-29-72

23:01.38

PAGE 0002

```

      SIGD2=(SIGEL(M,1)-SIGEL(M,2))/2.
      RAD =SQRT(SIGD2**2 +SIGEL(M,3)**2)
      SIGP(M,1)=SIGM+RAD
      SIGP(M,2)= SIGM-RAD
      SIGP(M,3)= RAD
      SIGP(M,4)= 0.5*57.29578*ATAN2(SIGEL(M,3),SIGD2)
100  CONTINUE
      IF(IHAR.NE.NCYC) RETURN
C
C  FIND  MAXIMUM  ELEMENT  STRESSES
C  OUTPUT STRESSES FOR LAST CYCLE
C
      SIG1=0.0
      SIG2=0.0
      SIG3=0.0
      M1=0
      M2=0
      M3=0
      DO 130 M=1,NUMEL
      IF (SIGP(M,1).LT.SIG1) GO TO 115
      SIG1=SIGP(M,1)
      M1=M
115  IF (SIGP(M,2).GT.SIG2) GO TO 120
      SIG2=SIGP(M,2)
      M2=M
120  IF (SIGP(M,3).LT.SIG3) GO TO 130
      SIG3=SIGP(M,3)
      M3=M
130  CONTINUE
      WRITE(6,2019) IHAR
      WRITE(6,2020)
      WRITE(6,2030) (M,(SIGP(M,I) ,I=1,4),APS(M),M=1,NUMEL)
      WRITE(6,2040) (SIG1,M1,SIG2,M2,SIG3,M3)
1303  CONTINUE
C
C  FORMAT STATEMENTS
C
2019  FORMAT(1H1, 11H CYCLE NO.=, I3)
1306  FORMAT(15,3F10.3)
1304  FORMAT(14,F13.2,F12.2,F12.3)
2000  FORMAT(1H1,10X, 21H X-Y ELEMENT STRESSES /// 40H ELEM   SIGMA X
1  SIGMA Y      SIGMA XY //)
2010  FORMAT(14,F11.3,2F12.3)
2020  FORMAT( /10X,27H ELEMENT PRINCIPAL STRESSES ///
1 55H ELEM   SIGMA I      SIGMA II      MAX TAU      SIGMA I DEG ,
1 9X,5H APES //)
2030  FORMAT(14,F11.3,2F12.3, F14.3,F16.1)
2040  FORMAT(1H1,
1 27H MAXIMUM PRINCIPAL STRESS = ,F11.1,19H AND OCCURS IN ELEM,16//
2 27H MINIMUM PRINCIPAL STRESS = ,F11.1,19H AND OCCURS IN ELEM,16//
3 27H MAXIMUM SHEAR STRESS    = ,F11.1,19H AND OCCURS IN ELEM,16)
      END

```

MEMORY REQUIREMENTS 00408C BYTES

APPENDIX C

PLOT PROGRAM LISTING

PLOT PROGRAM LISTING

5 COMPILER MAIN 03-02-72 10:32.49 PAGE 0001

C
C FLOT PROGRAM
C
C

C THIS A PROGRAM WHICH TAKES PUNCHED OUTPUT FROM PROGRAM FPM5
C WHICH CONSISTS OF ELEMENT AND NODAL INFORMATION AND THE
C PCTENTIAL AT THE NODES AND USES IT TO OUTPUT AND PLOT THE DESIRED
C EQUIPOTENTIALS
C THESE EQUIPOTENTIALS CONSIST OF STRAIGHT LINE SEGMENTS BETWEEN
C THE INTERPOLATED POINTS

C
C THE FIRST CARD MUST CONTAIN INFORMATION TO IDENTIFY THE PLOT
C AND WILL BE THE ONLY IDENTIFYING INFORMATION WRITTEN ON THE PLOT

C CARD 2 MUST CONTAIN THE FOLLOWING INFORMATION: THE NUMBER OF
C EQUIPOTENTIALS TO BE FOUND, THE NUMBER OF NODAL POINTS, THE
C NUMBER OF ELEMENTS, THE MAXIMUM Y VALUE FOR THE F.E. GRID
C (THE PROGRAM CONVERTS THE GRID CO-ORDINATES INTO PAGE
C CO-ORDINATES--THE GRID SHOULD BE NEAR THE AXIS IN +X-Y QUADRANT)
C AND THE DESIRED HEIGHT OF THE PLOT (THIS SHOULD BE LESS
C THAN 25 INCHES)----FORMAT(3I5,2F10.2)

C CARD 3 MUST CONTAIN THE EQUIPOTENTIALS DESIRED
C -----FORMAT(F10.2)
C

C THE CARDS WHICH FOLLOW MUST CONTAIN INFORMATION FROM
C PROGRAM FPM5- ONE CARD FOR EACH NODE DESCRIBING ITS POSITION
C AND POTENTIAL FOLLOWED BY THE ELEMENT INFORMATION CARDS

C FOR EVERY EQUIPOTENTIAL THE PROGRAM TAKES EACH ELEMENT IN TURN
C AND CHECKS FOR THE DESIRED EQUIPOTENTIAL
C IT THEN INTERPOLATES AND STORES THESE VALUES
C A MAXIMUM Y VALUE IS FOUND AFTER WHICH THE CLOSEST POINT TO
C THIS MAXIMUM Y IS OBTAINED AND THEN THE CLOSEST POINT TO THE
C PRECEEDING POINT AND SO ON
C NOTE--- THIS PROCEDURE WILL NOT WORK IN ALL CASES

C THE PROGRAM HAS DIMENSION STATEMENTS FOR 25 CONTOURS,
C 500 NODES, 900 ELEMENTS AND 99 INTERPOLATED VALUES FOR EACH
C CONTOUR

C DIMENSION EPC(25),PSI(500),XP(99,25),YP(99,25),XPM(99,25),
1 YPM(99,25), X(500), Y(500), R(500),DATA(4000)
C DIMENSION IA(99),NP(4,900),ICLK(500,2)
C INTEGER HED(18)
C CALL PLCTS(DATA(1),16000)

C READ INPUT
C READ(5,4) HED
C READ(5,9) NEPC,NUMNP,NE,YMAX,DH
C READ(5,8)(EPC(I),I=1,NEPC)
C READ(5,7)(I,X(I),Y(I),R(I),PSI(I),I=1,NUMNP)
C DO 70 I=1,NE

7 FORMAT(3X,I3,T55,2F8.2,T41,2F7.2)

6 FORMAT(12X,5I3)

 READ(5,6)I,(NP(J,I),J=1,4)

3 COMPILER MAIN 03-02-72 10:32.49 PAGE 0002

```

70      CONTINUE
5       FORMAT(1H1,18A4)
8       FORMAT(8F10.1)
9       FORMAT(3I5,2F10.2)
4       FORMAT(18A4)
      WRITE(6,5) PED
      DO32 L=1,NEPC
      IA(L)=1
      MCT=0

      DO 10 I=1,NE
      DO 10 J=1,4
      K=NP(J,I)
      JP=J+1
      IF(NP(3,I).EQ.NP(4,I)) GO TO 81
      GO TO 80
81      IF(J.EQ.3) GO TO 10
80      IF(J.EQ.4) JP=1
      KK=NP(JP,I)
      A=PSI(K)-EPC(L)
      B=PSI(KK)-EPC(L)
      IF((A*B).GT.(0.0)) GO TO 10
C       CHECK TO SEE IF THE INTERPOLATION HAS ALREADY BEEN DONE
C       IN AN ADJACENT ELEMENT
      MCT=MCT+1
      ICHK(MCT,1)=K
      ICHK(MCT,2)=KK
      ICAT=0
      DO 77 JX=1,MCT
      IF(ICHK(JX,1).NE.KK) GO TO 77
      IF(ICHK(JX,2).EQ.K) ICAT=1
77      CONTINUE
      IF(ICAT.EQ.1) GO TO 10
      II=IA(L)
C       INTERPOLATE
      XP(II,L)=X(K)+(((X(KK)-X(K))*(PSI(K)-EPC(L)))/(PSI(K)-PSI(KK)))
      YP(II,L)=Y(K)+(((Y(KK)-Y(K))*(PSI(K)-EPC(L)))/(PSI(K)-PSI(KK)))
      IA(L)=IA(L)+1
10      CONTINUE
      IF(IA(L).LE.2) GO TO 39
      GO TO 38
39      WRITE(6,101) EPC(L)
      GO TO 32
38      CONTINUE
101     FORMAT('0',56HONE OR ZERO INTERPOLATED VALUES FOUND FOR EQUIPOTEN
      ITIAL=, F6.1)
C       FIND THE MAXIMUM Y OF THE EQUIPOTENTIAL VALUE IN QUESTION
      YPM(1,L)=-10000.
      II=IA(L)-1
      DO 20 I=1,II
      IF(YP(I,L).LT.YPM(1,L))GO TO 20
      YPM(1,L)=YP(I,L)
      XPM(1,L)=XP(I,L)
      IC=I
20      CONTINUE

```


3 COMPILER

MAIN

03-02-72

10:32.49

PAGE 0003

```

      II=II-1
      IF(IC.GT.II) GO TO 40
C     MOVE ALL VALUES FROM THE MAXIMUM FOUND TO THE LEFT ONE LOCATION
      DO 40 I=IC,II
      YP(I,L)=YP(I+1,L)
      XP(I,L)=XP(I+1,L)
40    CONTINUE
C     FIND NEXT CLOSEST POINT
      DO 31 IM=1,II
      J=II-IM+1
      EC=((YPM(IM ,L)-YP(I,L))**2+(XPM(IM ,L)-XP(I,L))**2)**0.5
      IC=I
      IF(J.LT. 2) GO TO 30
      DO 30 I=2,J
      BD=((YPM(IM ,L)-YP(I,L))**2+(XPM(IM ,L)-XP(I,L))**2)**0.5
      IF(BD.LT.BC) GO TO 28
      GO TO 30
28    IC=I
      BC=BD
30    CONTINUE
      YPM(IM+1,L)=YP(IC,L)
      XPM(IM+1,L)=XP(IC,L)
      IJ=II-IM
      IF(IC.GT.IJ) GO TO 50
C     MOVE ALL VALUES TO THE LEFT ONE LOCATION
      DO 50 I=IC,IJ
      YP(I,L)=YP(I+1,L)
      XP(I,L)=XP(I+1,L)
50    CONTINUE
31    CONTINUE
32    CONTINUE
      DO 15 I=1,NEPC
      II=IA(I)-1
      IF(II.LE.1) GO TO 15
      WRITE(6,66) EPC(I)
      WRITE(6,65)
      WRITE(6,67) (XPM(J,I),YPM(J,I),J=1,II)
15    CONTINUE
66    FORMAT('0', 32H CO-ORDINATES FOR EQUIPOTENTIAL=,F10.2)
65    FORMAT(15X,2H X,15X,2H Y)
67    FORMAT(9X,F10.2,7X,F10.2)
      YPOS=DH+3.0
      CALL SYMBCL(1.0,YPOS,0.20,HED,0.0,72)
C     PLOT GRID
      SF=YMAX/DH
      DO 23 I=1,NUMNP
      X(I)=X(I)/SF+1.0
      Y(I)=Y(I)/SF +1.0
23    CONTINUE
      DO 24 I=1,NEPC
      II=IA(I)-1
      IF(II.LE.1) GO TO 24
      DO 24 J=1,II
      XPM(J,I)=XPM(J,I)/SF+1.0
      YPM(J,I)=YPM(J,I)/SF+1.0

```


COMPILER MAIN 03-02-72 10:32.49 PAGE 0004

```

24      CCNTINUE
        DO 11 J=1,NE
          K=NP(1,J)
          CALL PLOT(X(K), Y(K),3)
        DO 1010 I=2,5
          L=I
          IF(NP(3,J).EQ.NP(4,J)) GO TO 91
          GO TO 811
91      IF(I.EQ.4) GO TO 1010
811     IF(I.EQ.5) L=1
          K=NP(L,J)
          CALL PLOT(X(K),Y(K),2)
1010    CONTINUE
11      CCNTINUE
        DO 16 I=1,NEPC
          II=IA(I)-1
          IF(II.LE.1) GO TO 16
          CALL PLOT(XPM(1,I),YPM(1,I),3)
          DO 100 J=1,II
            CALL PLOT(XPM(J,I),YPM(J,I),2)
100     CONTINUE
19      PX=XPM(II,I)-0.15
          PY=YPM(II,I)-0.30
          CALL NUMBER(PX,PY,0.15,EPC(I),0.0,1)
16      CONTINUE
          CALL PLOT(0.0,0.0,999)
        END

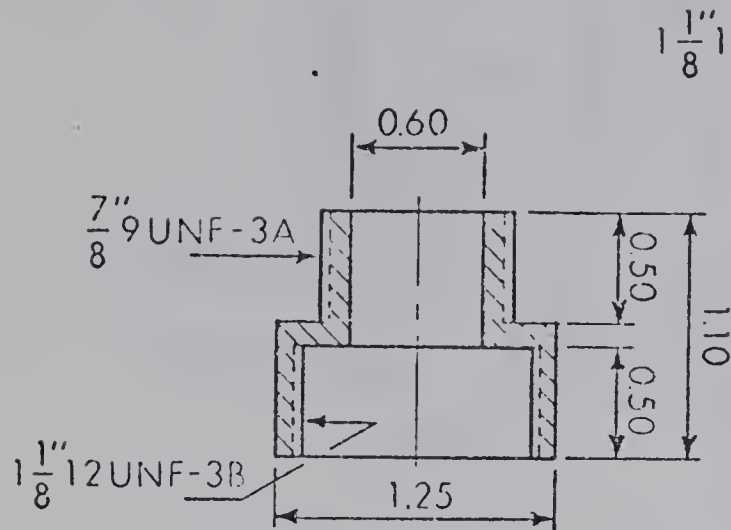
```

JOY REQUIREMENTS 015340 BYTES
RC=0

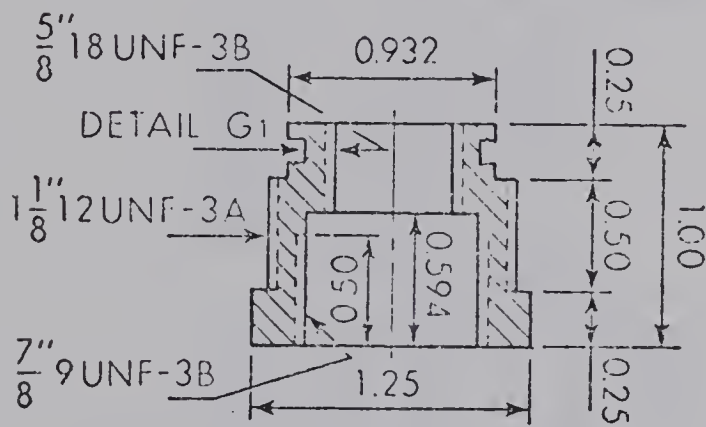
APPENDIX D

DETAILS OF PIEZOMETER PARTS

DETAILS OF PIEZOMETER PARTS



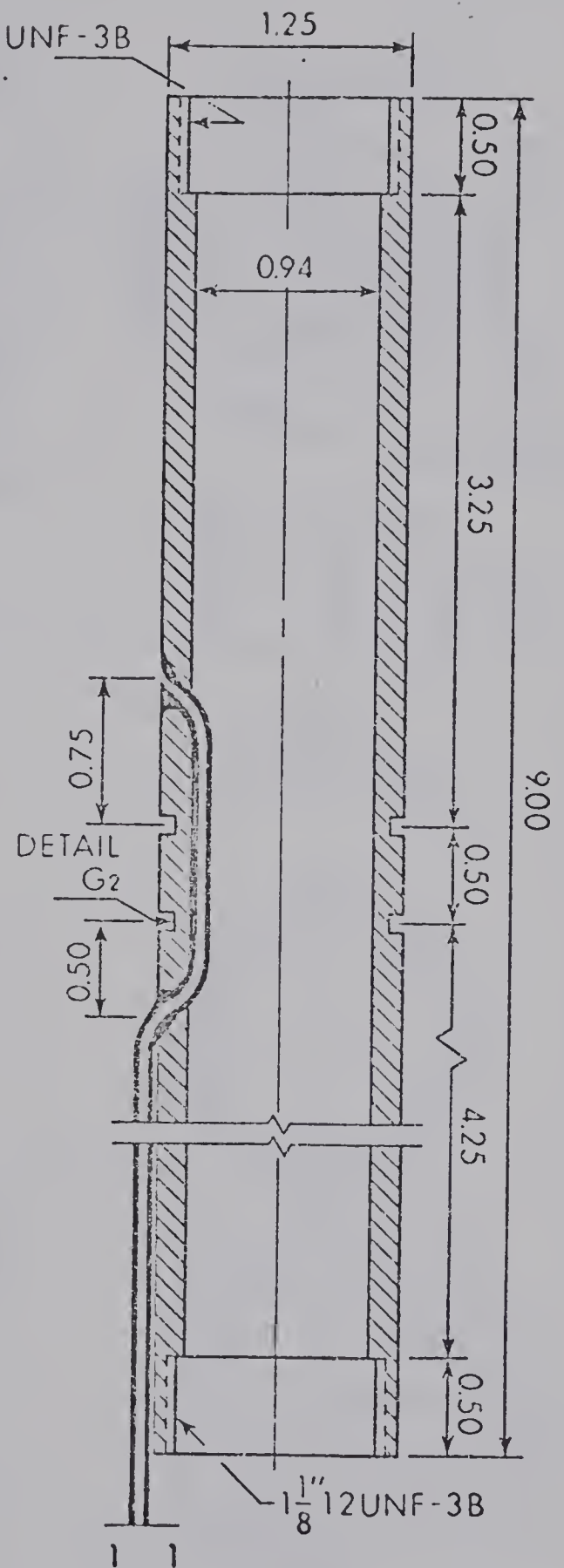
ITEM - 1
BARREL CONNECTOR
(Stainless Steel)



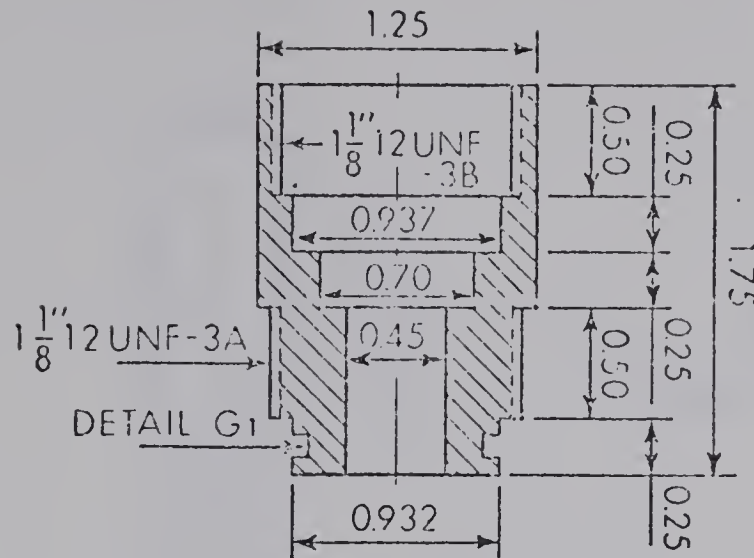
ITEM - 2
TRANSDUCER CONNECTOR
(Stainless Steel)



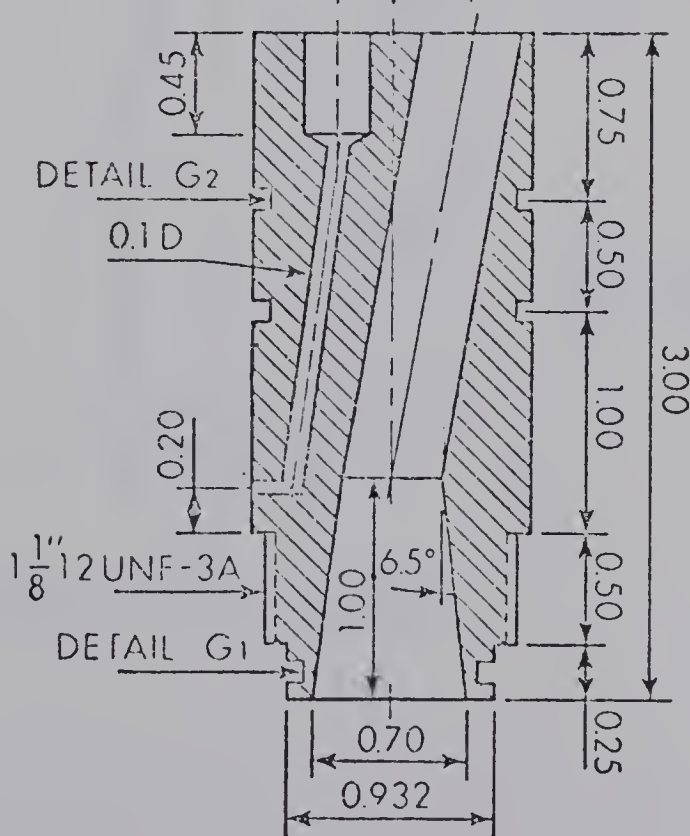
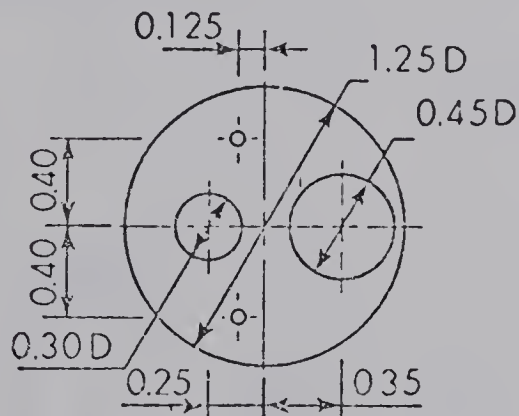
ITEM - 3 CONTINUED



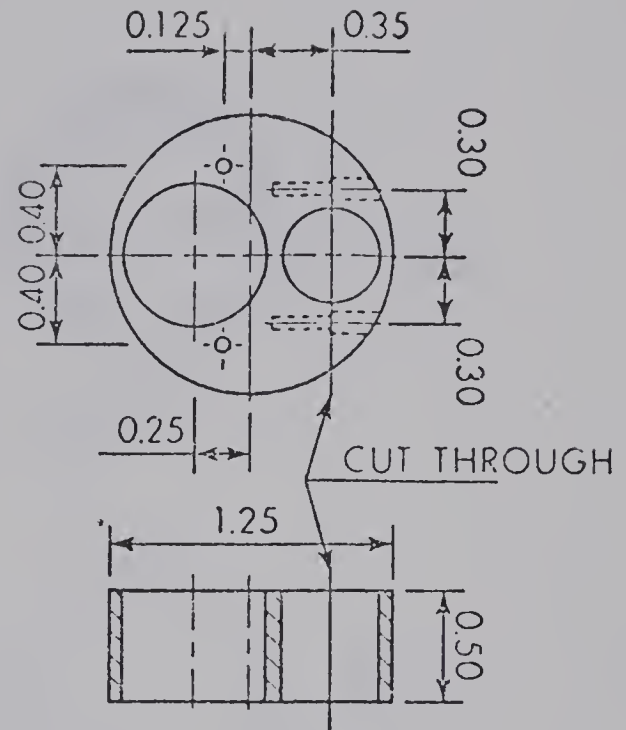
ITEM - 3
UPPER BARREL
(Stainless Steel)



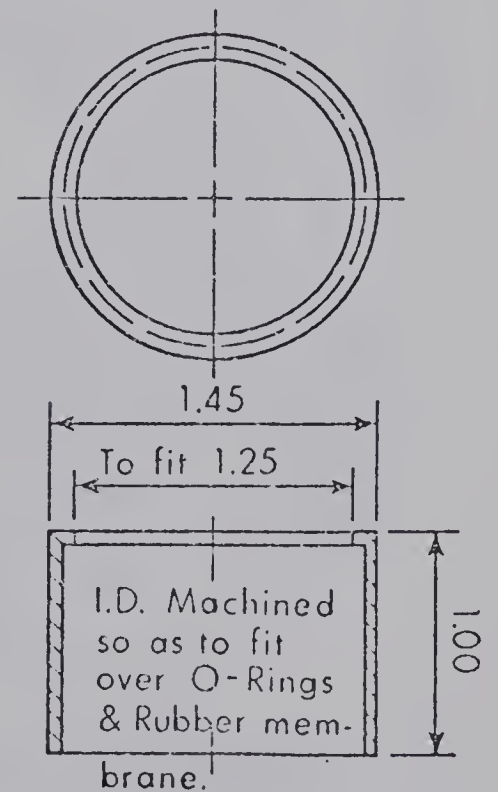
ITEM - 4
LOWER RUBBER PACKING RETAINER
(Stainless Steel)



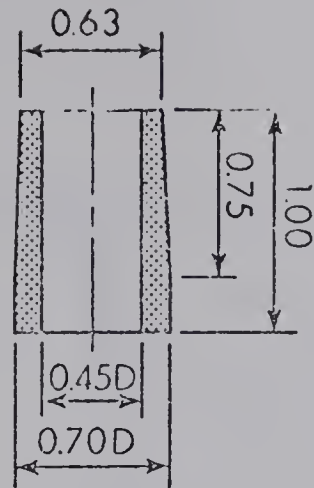
ITEM - 5
UPPER RUBBER PACKING RETAINER
(Stainless Steel)



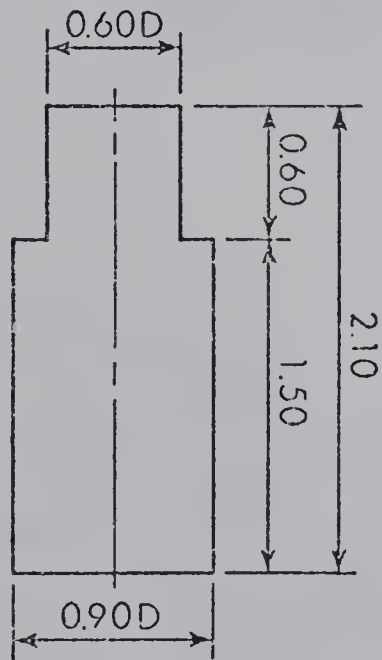
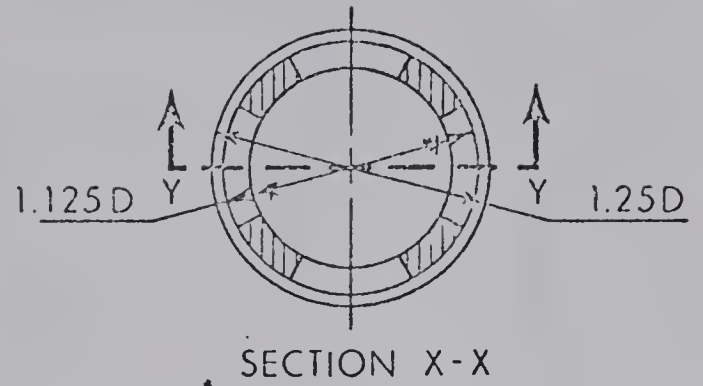
ITEM - 6
UPPER CAP
(Stainless Steel)



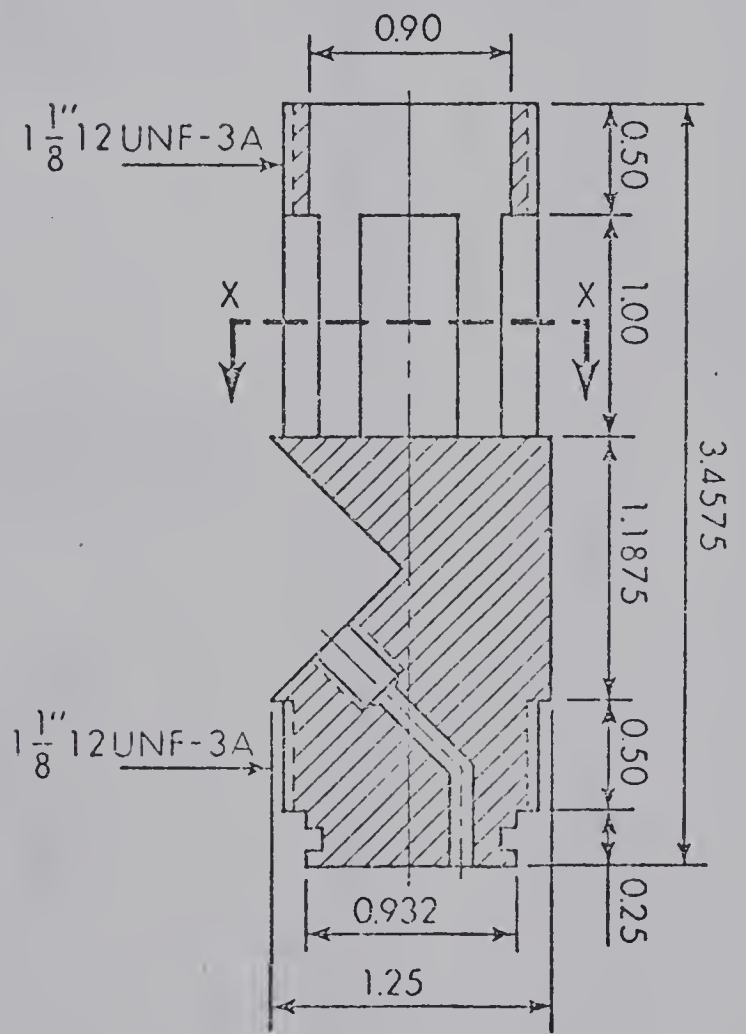
ITEM - 7
SEALING MEMBRANE RETAINER
(Stainless Steel)



ITEM - 8
RUBBER PACKING



ITEM - 9
POROUS NICKEL ELEMENT



ITEM - 10
PORUS TIP RETAINER
(Stainless Steel)

B30012